



**HAL**  
open science

**More transparency in bioanalysis of exocytosis :  
application of fluorescent false neurotransmitters in  
coupling methodology of electrochemistry with  
fluorescence microscopy at ITO microelectrodes**

Xiaoqing Liu

► **To cite this version:**

Xiaoqing Liu. More transparency in bioanalysis of exocytosis: application of fluorescent false neurotransmitters in coupling methodology of electrochemistry with fluorescence microscopy at ITO microelectrodes. Chemical Physics [physics.chem-ph]. Université Pierre et Marie Curie - Paris VI, 2016. English. NNT : 2016PA066415 . tel-02295570

**HAL Id: tel-02295570**

**<https://theses.hal.science/tel-02295570>**

Submitted on 24 Sep 2019

**HAL** is a multi-disciplinary open access archive for the deposit and dissemination of scientific research documents, whether they are published or not. The documents may come from teaching and research institutions in France or abroad, or from public or private research centers.

L'archive ouverte pluridisciplinaire **HAL**, est destinée au dépôt et à la diffusion de documents scientifiques de niveau recherche, publiés ou non, émanant des établissements d'enseignement et de recherche français ou étrangers, des laboratoires publics ou privés.

# Université Pierre et Marie Curie

Ecole doctorale de Chimie Physique et Chimie Analytique de Paris Centre

ED388

UMR8640

**More transparency in bioanalysis of exocytosis:  
application of fluorescent false neurotransmitters in  
coupling methodology of electrochemistry with  
fluorescence microscopy at ITO microelectrodes**

Par Xiaoqing LIU

Thèse de doctorat de PHYSICO-CHIMIE ANALYTIQUE

Dirigée par Christian AMATORE

Présentée et soutenue publiquement le 26/09/2016

Devant un jury composé de :

Prof. Petra HELLWIG (Université de Strasbourg)	Rapporteur
Prof. Fabien MIOMANDRE (ENS Cachan)	Rapporteur
Prof. Didier DEVILLIERS (UPMC)	Examineur
Prof. Pedro DE OLIVEIRA (Université Paris-Sud)	Examineur
Prof. Christian AMATORE (ENS)	Directeur de thèse
Dr. Manon GUILLE-COLLIGNON (UPMC)	Co-encadrante de thèse
Dr. Frédéric LEMAÎTRE (UPMC)	Co-encadrant membre invité



## **Acknowledgement**

With the financial support of China Scholarship Council, I underwent an exciting experience in ENS. It is sometimes hard to believe four years fly so fast. I would like to express my heartfelt gratitude to all those who helped me during this period, in one way or another.

My deepest gratitude goes first and foremost to Dr. Christian Amatore, my thesis director, who kindly accepted me as a PhD candidate in his wonderful lab. I am fortunate to have had the opportunity to learn from such an expert in science. His intelligence, rigorous scientific attitude and continuous curiosity about science are quite impressive and benefit me greatly. Many thanks for his constant encouragement and guidance.

I would like to sincerely acknowledge my committee members: Dr. Petra Hellwig and Dr. Fabien Miomandre for having graciously accepted to evaluate this work and compose a relevant report to UPMC; Dr. Didier Devilliers and Dr. Pedro De Oliveira for acceding to examine this thesis.

Many thanks to Dr. Manon Guille-Collignon and Dr. Frédéric Lemaître for their valuable guidance of my work, indispensable advices on the research strategies, consistent and illuminating instruction on the writing/correction of this thesis and invaluable help in my daily life. Without your patient instruction, insightful criticism and expert guidance, the completion of this thesis would not have been possible.

I owe a special debt of gratitude to Dr. Jérôme Delacotte who devotes continuously to make the TIRFM work correctly. I am greatly touched by his innovative scientific viewpoint, impressive problem-solving ability as well as his kindness. The equivalent appreciation owes to Dr. Laurence Grimaud, Alexandra Savy and Sylvie Maurin, who dedicated a lot for the synthesis of our magic fluorescent molecules. I extend my thanks to Dr. Eric Labbé and Dr. Olivier Buriez for interesting discussions and fruitful collaborations. I also feel grateful to Dr. Laurent Thouin and Dr. Catherine Sella, for offering me a decent office during the renovation work and for their friendly help.

Thanks to my adorable colleagues/friends who create such a harmonious atmosphere in the lab: Adnan (for organizing lots of interesting activities and being super patient to my awful French), Ana (for always being there to share my joy and sorrow, like my older sister), Cong (for greatly helping me to get adapted to the new life in Paris and for being my model in learning new things), Damien (for teaching me many things in both science and daily life; for being always optimistic and friendly), Lihui (for giving me many useful suggestions and accompanying me in some difficult moments), Lylian (for taking care of me in a 'tranquille' way), Marie-Aude (for your helpful guide in cell culture

and your effort in improving my poor French), Marine (for sharing time in the cell culture room and a lot of funny talks), Margherita (for creating many sweet memories), Baptist, Eric, Guillaume, Hakim, Lucas, Pierluca, Pierre, Raquel, Thomas, Yun, etc... Thank you for interesting scientific discussions, fun social activities and delicious birthday cakes. I really cherish every sweet moment with you and our wonderful time together will be forever embedded in my memory.

Great thanks to Dr. Ana-Maria Lennon-Duménil and Dr. Marine Bretou, for their work in dendritic cells and for giving me a lot of perceptive advice in this work.

Thanks to Dr. Yong Chen and his students: Junjun Li, Jian Shi, Wentao He, Yu Zhang, Li Wang, Yadong Tang, Weikang Wang, Bin Wang, Jin Wei and Xiaolong Tu, for allowing me working in the white room and for their helpful suggestions in microfabrication. I also give my sincere thanks to M. José Palomo, for kindly letting me work in their white room during the renovation work in chemistry department.

I shall extend my thanks to Dominique Ho Tin Noe, Anne Halloppe, Frédéric Bataille, Auguste Filippi in ENS; Soobrayen Koonavadee and Hélène Gérard in UPMC. They are always so nice to help me arrange the multifarious student affairs.

Special thanks go to Dr. Yaoqun Li, my previous supervisor in Xiamen University. It is your great/enduring passion in science and your high moral/scientific integrity that keep on encouraging me on my way.

Thanks to my Chinese friends: Hui Chen, Hancheng Hu, Lihui Hu, Chenge Li, Qiong Qi, Yadong Tang, Yueyi Wang, Lei Zhang, Xia Zhang, Zhubao Zhang, Shenglan Zheng, Li Zhou, Xiaoyan Zhu... Thanks a lot, girls, for your generous friendship and gracious love.

Many thanks to my parents and dear sister who always let me make important decisions following my heart in my life. I would not have made it here without your selfless/endless love and unconditional support. I also would like to thank my little niece, Xiaoli, for making my life so much happier by just existing.

Final thanks go to my fiancée, Xiubin, whose love and support are the foundation for everything since our arrival in France. Thank you for being my best friend, for your understanding and for your confidence and hard-working for our future. All the trips from Lyon to Paris will become our precious memories in our happy and bright future.

## Table of contents

<b>Table of contents.....</b>	<b>5</b>
<b>Abbreviations.....</b>	<b>9</b>
<b>Résumé de la thèse en Français.....</b>	<b>40</b>
<b>General introduction.....</b>	<b>36</b>
<b>1 Introduction .....</b>	<b>40</b>
<b>1.1 Vesicular exocytosis.....</b>	<b>40</b>
<i>1.1.1 Principle of exocytosis.....</i>	<i>40</i>
<i>1.1.2 SNAREs proteins in exocytosis.....</i>	<i>42</i>
<i>1.1.3 Cell models for exocytosis investigation .....</i>	<i>43</i>
<b>1.2 Microelectrodes in electrochemistry.....</b>	<b>46</b>
<i>1.2.1 Microelectrode geometry.....</i>	<i>46</i>
<i>1.2.2 Properties of microelectrodes .....</i>	<i>47</i>
<b>1.3 Techniques for exocytosis investigation.....</b>	<b>49</b>
<i>1.3.1 Electrical methodology.....</i>	<i>49</i>
<i>1.3.2 Optical methodology .....</i>	<i>66</i>
<i>1.3.3 Coupling methodology.....</i>	<i>73</i>
<b>1.4 Fluorescent analogs of monoamine neurotransmitters.....</b>	<b>78</b>
<i>1.4.1 Monoamine neurotransmitters .....</i>	<i>79</i>
<i>1.4.2 Fluorescent false neurotransmitters for optical imaging .....</i>	<i>83</i>
<i>1.4.3 Are fluorescent false neurotransmitters electroactive?.....</i>	<i>87</i>
<b>1.5 Goals and research interests.....</b>	<b>87</b>
<b>2 Photophysical and electrochemical properties characterization of 4-(2-aminoethyl)-6-chloro-7-hydroxy-2H-1-benzopyran-2-one hydrochloride.....</b>	<b>88</b>

<b>2.1 Synthesis of a fluorescent false neurotransmitter .....</b>	<b>88</b>
<b>2.2 Photophysical properties characterization of 1 .....</b>	<b>89</b>
2.2.1 Spectral characterization .....	89
2.2.2 pH-dependent optical properties.....	89
<b>2.3 Electrochemical characterization.....</b>	<b>94</b>
2.3.1 Electrochemical test of 4-(2-chloroethyl)-6-chloro-7-hydroxy-2H-1-benzopyran-2-one and <b>1</b> on glassy carbon electrode.....	95
2.3.2 Electrochemical test of <b>1</b> on CFE.....	98
2.3.3 Electrochemical test of <b>1</b> on ITO microelectrodes .....	102
2.3.4 Electrochemical oxidation mechanism of <b>1</b> .....	109
<b>2.4 Conclusions .....</b>	<b>111</b>
<b>3 TIRFM observation of exocytosis in 1-stained BON N13 cells .....</b>	<b>112</b>
<b>3.1 Introduction .....</b>	<b>112</b>
<b>3.2 Penetration of 1 into PC-12 cells and BON N13 cells.....</b>	<b>113</b>
3.2.1 PC-12 cells .....	113
3.2.2 BON N13 cells.....	117
<b>3.3 Exocytosis observed by epi-fluorescence and TIRFM .....</b>	<b>119</b>
3.3.1 Epi-fluorescence versus TIRFM.....	119
3.3.2 Incident angle dependence of TIRFM signals.....	121
3.3.3 Behaviors of <b>1</b> -labeled vesicles assessed by TIRFM .....	122
3.3.4 Fluorescence intensity investigation of different types of exocytosis .....	129
<b>3.4 Conclusions .....</b>	<b>134</b>
<b>4 Amperometric detection of exocytosis in 1-stained BON N13 cells.....</b>	<b>136</b>
<b>4.1 Introduction .....</b>	<b>136</b>
<b>4.2 ITO microchips for amperometric measurement.....</b>	<b>138</b>

4.2.1 ITO microdevice preparation .....	138
4.2.2 Characterization of ITO microdevices .....	141
4.2.3 Electrical characterization of MD-C.....	147
<b>4.3 Amperometric test of exocytosis in 1-stained BON N13 cells in MD-C.....</b>	<b>149</b>
4.3.1 Cellular exocytosis assessed by amperometric measurement .....	149
4.3.2 Characterization of exocytotic process .....	155
<b>4.4 Comparison of apex and bottom secretion in BON N13 cells.....</b>	<b>157</b>
4.4.1 Amperometric detection of vesicular exocytosis by CFE .....	157
4.4.2 Comparison of exocytotic release detected by CFE and ITO microelectrode .....	159
<b>4.5 Reuse of ITO microdevice.....</b>	<b>165</b>
<b>4.6 Conclusions .....</b>	<b>166</b>
<b>5 TIRFM/amperometry coupling measurement of exocytosis in 1-stained BON N13 cells</b> <b>.....</b>	<b>168</b>
<b>5.1 Introduction .....</b>	<b>168</b>
<b>5.2 TIRFM/amperometry coupling measurement in one set-up .....</b>	<b>169</b>
5.2.1 Vesicular release tracked by TIRFM in MD-C .....	170
5.2.2 Set-up for TIRFM/amperometry coupling measurement.....	170
5.2.3 Influence of 405 nm laser irradiation on amperometric detection.....	172
<b>5.3 TIRFM/amperometry coupling measurement of vesicular exocytosis .....</b>	<b>176</b>
5.3.1 Effect of exposure time in TIRFM imaging .....	176
5.3.2 TIRFM/amperometry coupling test of vesicular exocytosis .....	177
<b>5.4 Fluorescent/amperometric coupled signals of exocytotic events.....</b>	<b>180</b>
5.4.1 Three different modes of exocytotic release .....	180
5.4.2 Continuous secretions monitoring with high temporal/spatial resolution .....	185
5.4.3 Tracking of ITO microelectrode surface passivation by electrooxidation of <b>I</b> .....	188

<b>5.5 Conclusions .....</b>	<b>191</b>
<b>General conclusions and perspectives .....</b>	<b>194</b>
<b>Experimental section .....</b>	<b>198</b>
<b>I Cell culture .....</b>	<b>198</b>
<i>I.1 BON N13 cells culture .....</i>	<i>198</i>
<i>I.2 PC-12 cells culture.....</i>	<i>199</i>
<b>II Fabrication of microelectrodes and microsystems .....</b>	<b>201</b>
<i>II.1 CFE construction.....</i>	<i>201</i>
<i>II.2 Fabrication of ITO microelectrodes.....</i>	<i>202</i>
<i>II.3 Construction of other electrodes.....</i>	<i>206</i>
<b>III Analytical methods .....</b>	<b>207</b>
<i>III.1 Electrochemical techniques.....</i>	<i>207</i>
<i>III.2 TIRFM .....</i>	<i>210</i>
<i>III.3 Time-lapse imaging .....</i>	<i>211</i>
<b>IV Solution preparation .....</b>	<b>211</b>
<i>IV.1 Buffer solutions.....</i>	<i>211</i>
<i>IV.2 Solutions for experiments in vitro.....</i>	<i>212</i>
<b>V Sample preparation and measurement.....</b>	<b>213</b>
<i>V. 1 Synthesis of I.....</i>	<i>213</i>
<i>V. 2 Optical and electrochemical characterization of I.....</i>	<i>213</i>
<i>V. 3 Experiments on living cells .....</i>	<i>215</i>
<b>Appendix .....</b>	<b>220</b>
<b>References .....</b>	<b>230</b>

## **Abbreviations**

**1:** 4-(2-aminoethyl)-6-chloro-7-hydroxy-2H-1-benzopyran-2-one hydrochloride

**2:** 6-chloro-7-hydroxychromen-2-one

**3:** serotonin

**4:** dopamine

**5:** norepinephrine

**6:** epinephrine

**7:** umbelliferone

**8:** benzoic acid

**9:** 4-(2-chloroethyl)-6-chloro-7-hydroxy-2H-1-benzopyran-2-one

**Ag/AgCl:** silver-silver chloride reference electrode

**CFE:** carbon fiber microelectrode

**CNT:** carbon nanotubes

**CVs :** cyclic voltammograms

**EMCCD:** electron multiplying charge coupled device

**F-actin:** filamentous actin

**FFNs:** fluorescent false neurotransmitters

**GCE:** glassy carbon working electrode

**IPA:** isopropyl alcohol

**ITO:** indium tin oxide

**MD-A:** microdevice A

**MD-B:** microdevice B

**MD-C:** microdevice C

**MEA:** microelectrode arrays

**NA:** numerical aperture

**NGF:** nerve growth factor

**NPY-GFP:** green fluorescent protein-tagged neuropeptide-Y

**NSF:** N-ethylmaleimide-sensitive factor

**PBS:** phosphate buffer saline

**PSF:** pre-spike feature

**SCE:** saturated calomel reference electrode

**SNAP-25:** synaptosome-associated protein of 25 kDa

**SNAREs:** soluble N-ethylmaleimide sensitive fusion protein attachment receptors

**TIR:** total internal reflection

**TIRFM:** total internal reflection fluorescence microscopy

**t-SNAREs:** target proteins in the membrane

**v-SNAREs:** vesicular membrane proteins

**UMEs:** ultramicroelectrodes

**VMAT:** vesicular monoamine transporters

**UV-vis:** ultraviolet-visible

*Résumé de la thèse (French version)*

# Résumé de la thèse en Français

## 1. L'exocytose vésiculaire

### 1.1 Mécanisme d'exocytose

La communication intercellulaire est une fonction vitale des êtres vivants. Elle est normalement réalisée par l'expulsion des molécules biochimiques ou chimiques à partir d'une cellule émettrice à une cellule cible qui est capable de détecter ces messagers spécifiques, conduisant à diverses réponses physiologiques en fonction des différents stimuli. L'exocytose est le mécanisme par lequel les cellules eucaryotes sécrètent des molécules actives dans le milieu extracellulaire. Ce mécanisme est la base de nombreux processus physiologiques comme la communication intracellulaire dans le système nerveux, la défense immunitaire et la régulation hormonale. Les molécules libérées sont initialement contenues dans des vésicules synaptiques (dans le cas des neurotransmetteurs) ou dans des granules ou vésicules de sécrétion (pour ce qui est des hormones) qui fusionnent avec la membrane plasmique pour déverser leur contenu dans le milieu extracellulaire. Il a été démontré que l'exocytose vésiculaire présente une grande importance dans la régulation des événements normaux et pathologiques dans les cellules. Les études concernant ce phénomène biologique représentent un champ de recherche d'intérêt depuis plusieurs dizaines d'années, date de sa première découverte, à la fin du 19<sup>ème</sup> siècle, par Ilya Mechnikov. Comme exemple notable de cet intérêt, le prix Nobel de physiologie et médecine de 2013 a été décerné conjointement à trois scientifiques (James E. Rothman, Randy W. Schekman et Thomas C. Südhof) pour leurs contributions aux découvertes des machines de régulation du trafic vésiculaire.

#### 1.1.1 Principe de l'exocytose

Durant l'exocytose, des messagers chimiques/biochimiques stockés dans les vésicules de sécrétion sont expulsés par la cellule émettrice et leur diffusion vers les cellules voisines conduit à diverses communications intercellulaires. Pour une vésicule sécrétoire individuelle, quatre étapes sont principalement impliquées dans l'ensemble du processus d'exocytose, tel qu'il apparaît dans Fig. Résumé-1.

Tout d'abord, des messagers biochimiques (neurotransmetteurs, hormones ...) qui sont essentielles pour la transmission de signaux intercellulaires, sont internalisés pour remplir le cœur de la vésicule sécrétoire située dans le cytoplasme de la cellule émettrice (Fig. Résumé-1, étape a). Ces messagers sont compactés dans la matrice vésiculaire par le biais d'interactions ioniques attractives, celle-ci se comportant comme un polymère. Lors d'une stimulation physiologique appropriée (qui provoque une entrée de  $Ca^{2+}$  ou l'augmentation de sa concentration), la vésicule disponible est transportée à travers le cytoplasme vers la membrane cellulaire où elle accoste via des interactions spécifiques entre protéines,

à savoir la formation du complexe SNAREs (soluble N-ethylmaleimide sensitive fusion protein attachment receptors) (Fig.Résumé-1, étape b). Un pore de fusion nanométrique est ensuite formé dans les membranes fusionnées, ce qui induit la libération spontanée et initiale du contenu vésiculaire dans le milieu extracellulaire (Fig.Résumé-1, étape c). Dans cette étape, l'échange des messagers cationiques de la matrice avec de petits cations ( $\text{Na}^+$ ,  $\text{H}_3\text{O}^+$ ) du milieu extracellulaire conduisent à une déstructuration du gel matriciel polyélectrolytique en raison de nouvelles interactions moléculaires et supramoléculaires répulsives. Enfin, l'expansion du pore de fusion a lieu, ce qui entraîne l'expulsion d'un plus grand flux de messagers chimiques/biochimiques, suivie par la suite d'une fusion plus complète de la vésicule avec la membrane cellulaire (Fig.Résumé-1, étape d).

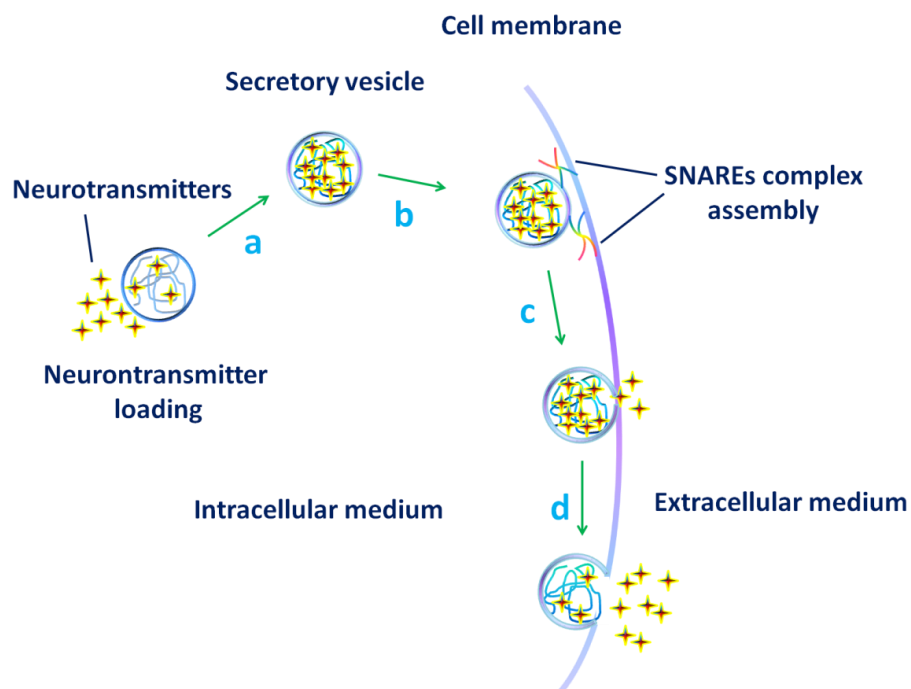


**Figure Résumé-1:** Représentation schématique des principales phases de l'exocytose vésiculaire. Les vésicules de sécrétion qui vont subir l'exocytose sont tout d'abord remplies dans leur lumière par des molécules messagères (étape a); lors d'une stimulation appropriée, elles accostent à la membrane cellulaire grâce à des protéines complexes (étape b); les membranes cellulaire et vésiculaire se mélangent et évoluent vers la formation d'un pore de fusion à travers lequel le contenu vésiculaire commence à diffuser hors de la matrice vésiculaire (étape c); l'expansion du pore de fusion se produit conduisant au relargage massif des biomolécules.

## 1.2 Couplage de l'ampérométrie et de la microscopie de fluorescence par réflexion totale interne pour l'étude de l'exocytose

Au cours des 25 dernières années, l'étude de l'exocytose vésiculaire a attiré de plus en plus d'attention en raison de sa grande importance dans la communications cellulaire et de diverses approches analytiques électrochimiques et optiques qui ont pu être mises au point pour ces recherches. Parmi celles-ci, l'ampérométrie et la microscopie de fluorescence par réflexion totale interne (TIRFM) sont généralement considérés comme deux des outils les plus puissants pour étudier le processus de libération exocytotique. En ce qui concerne l'analyse de l'exocytose, les principaux avantages de l'enregistrement électrochimique par ampérométrie (mesure de bas courants à potentiel constant, celui-ci correspondant au potentiel d'oxydation ou de réduction des molécules d'intérêt) sont l'excellente résolution temporelle ( $\sim < \text{ms}$ ), ainsi que sa grande sensibilité (rapport S/B élevé), ce qui permet des études quantitatives de la dynamique d'ouverture du pore de fusion et ce, au niveau de la vésicule unique. Cependant, un inconvénient intrinsèque de cette technique, décrit ci-après, limite son application dans le suivi du processus de libération. En effet, elle est tout à fait «aveugle» à la dynamique de la sécrétion vésiculaire dans le cytoplasme ou toute protéine régulatrice marquée **avant** la formation du pore de fusion car les signaux électrochimiques ne peuvent être détectés que lorsque les biomessagers électroactifs arrivent à la surface de l'électrode et donc au stade de l'ouverture du pore de fusion. Au contraire, dans le TIRFM, l'ensemble du processus d'exocytose (avant et pendant la libération) est en mesure d'être entièrement visualisé en raison de la fluorescence des molécules suivies et marquées au préalable, même si sa résolution temporelle est loin d'être aussi bonne ( $\sim$  dizaines de ms) que celle de la détection ampérométrique. En outre, en raison de la fluorescence, le TIRFM présente une résolution spatiale remarquable, de l'ordre de 120 nm pour les équipements standard, ce qui permet une identification précise des comportements des vésicules illuminées, tels que leurs déplacements, les lieux d'accueil ainsi que les zones géométriques de fusion. Cette caractéristique spécifique du TIRFM joue un rôle significatif pour distinguer les libérations exocytotiques provenant de deux / plusieurs vésicules déchargeant simultanément leur contenu, ce qui serait représenté comme 2 pics de courant superposés difficilement analysables par la seule mesure ampérométrique.

En contrepartie de natures complémentaires du TIRFM et de l'ampérométrie, nous pensons que la combinaison de ces deux techniques deviendrait une approche prometteuse pour l'analyse complète et précise de l'ensemble de l'événement exocytose (de l'amarrage de la vésicule, puis la formation du pore de fusion jusqu'à la libération vésiculaire complète) avec de hautes résolutions temporelle (par ampérométrie) et spatiale (via le TIRFM).

La mise au point du couplage de l'ampérométrie et de la microscopie de fluorescence pour l'étude de l'exocytose dépend fortement des propriétés spécifiques de l'électrode de mesure qui doit permettre à la fois la détection électrochimique et l'imagerie par fluorescence (Fig.Résumé-2). Autrement dit, le matériau pour la fabrication de l'électrode de travail doit non seulement être transparent, mais aussi conducteur de l'électricité de manière à enregistrer les signaux optiques et ampérométriques résultant des mêmes vésicules individuelles en même temps.

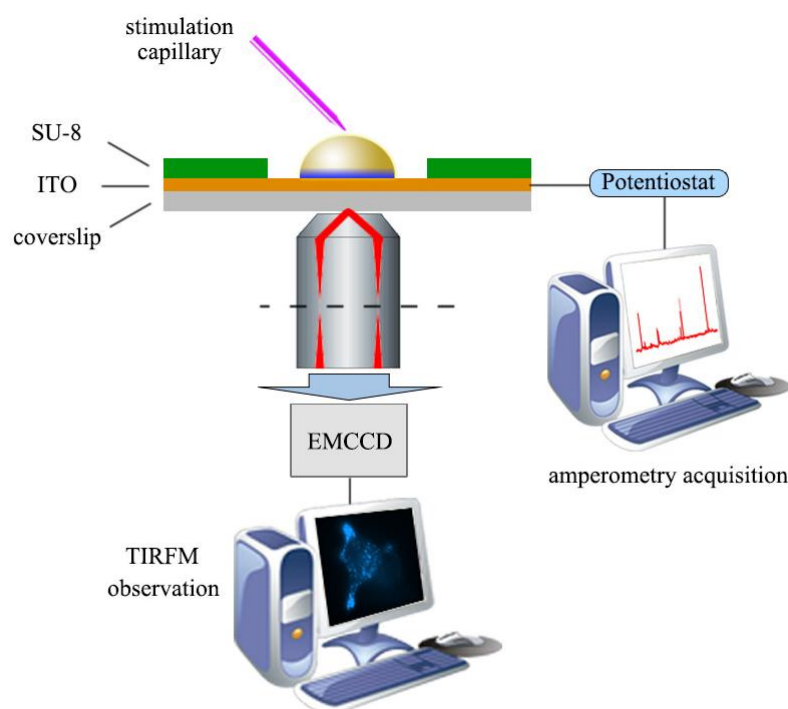


**Figure Résumé-2** Configuration requise pour les mesures de couplage TIRFM/ampérométrie; les signaux fluorescents/électrochimiques ont été simultanément recueillis ici par l'ITO (indium tin oxide ou oxyde d'indium dopé à l'étain) usinés sous forme de microélectrodes transparentes.

En 2006, notre groupe a démontré que l'emploi de microélectrodes d'ITO (oxyde d'indium dopé à l'étain), via des microdispositifs, permet l'acquisition de signaux fluorescents en configuration d'épi-fluorescence ainsi que le suivi des événements ampérométriques d'exocytose sur cellule chromaffine unique. Cependant, à ce stade, plutôt que de combiner l'enregistrement, la détection des signaux indépendants était non simultanée. En effet, la première mise au point du couplage de l'ampérométrie et du TIRFM basée sur ITO a été réalisée en 2011, dans le cadre de la thèse d'Anne Meunier dans notre équipe, en recueillant simultanément la fluorescence (par TIRFM) et des courants d'oxydation (par ampérométrie) de signaux d'exocytose des cellules BON BC21 transfectées par GFP (green fluorescent protein) et chargées avec de la sérotonine.

Au cours des dernières années, grâce au développement rapide de la fabrication de puces microfluidiques, en plus des microsystèmes à base d'ITO développés par quelques équipes dont la notre, quelques autres microdispositifs basés sur film d'or fin (épaisseur de 12~17 nm, semi-transparent) ou de carbone amorphe adamantin ("nitrogen-doped diamond-like carbon" ou dépôt DLC dopé à l'azote) ont également été utilisés pour l'analyse combinée de la fluorescence et de l'électrochimie pour l'étude de l'exocytose. Dans ce travail, la faisabilité du microdispositif avec plusieurs électrodes d'ITO pour la détection TIRFM/ampérométrique sera testée dans le cadre de son utilisation avec une sonde unique fluorescente et électrochimique pour la mesure couplée, contrairement à ce qui avait été fait dans la thèse de Anne Meunier en 2011 où deux sondes découplées (sérotonine et GFP) en proportions relative et absolue non connues et non contrôlées, avaient été internalisées dans les vésicules de sécrétion.

### 1.3 Faux neurotransmetteurs fluorescents

De nos jours, l'une des avancées les plus intéressantes dans le domaine du développement d'une nouvelle sonde fluorescente pour le processus de suivi de l'exocytose est la synthèse réussie de divers monoamines analogues de neurotransmetteurs, à savoir les faux neurotransmetteurs fluorescents (FFNs), ces derniers permettant la visualisation directe de l'absorption, la redistribution et la libération des molécules sécrétées (Fig. Résumé-3).

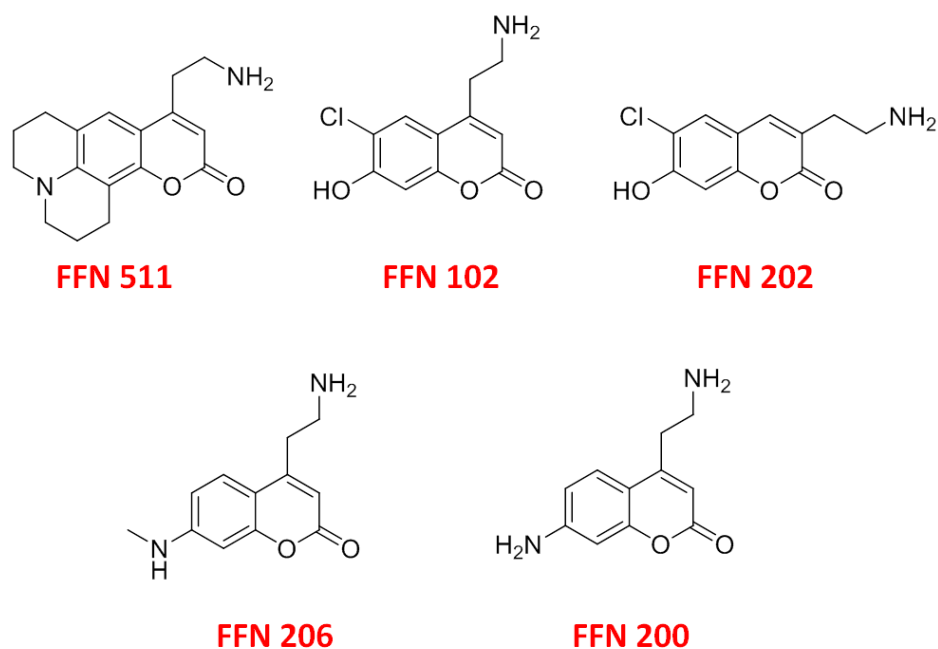


**Figure Résumé-3** Formules moléculaires des cinq molécules rapportées dans la famille des FFNs.

L'idée sous-jacente à l'utilisation des FFNs est de synthétiser des molécules organiques fonctionnelles dont la structure globale est très similaire à celle des neurotransmetteurs monoamines biogènes. La Figure Résumé-3 présente cinq molécules rapportées dans la littérature dans la famille des FFNS. Elles présentent le groupe amino-éthyle intact comme site de reconnaissance cellulaire, mais la fonctionnalité aromatique supplémentaire est ajoutée à la structure pour obtenir des propriétés de fluorescence améliorées. Lorsque les cellules ont été exposées à des milieux extracellulaires supplémentés avec des FFNs, les transporteurs de monoamines vésiculaires (VMAT) seront, en quelque sorte, "induits en erreur" par la structure des FFNs présentant une similitude élevée avec les neurotransmetteurs monoamines endogènes. Autrement dit, VMAT considère les FFNs comme neurotransmetteurs monoamines endogènes et les transportent par conséquent dans les lumières vésiculaires. De cette façon, les FFNs semblent être un candidat de choix comme sonde optique pour le suivi spécifique des comportements des vésicules sécrétoires fluorescentes.

Les mesures ampérométriques d'événements d'exocytose dans les cellules vivantes sont principalement basées sur l'oxydation électrochimique des neurotransmetteurs monoamines endogènes à la surface de l'électrode. L'électroactivité de ces neurotransmetteurs monoamines biogènes doit être attribuée à l'oxydation des groupes hydroxyle sur le cycle benzène.

Fait intéressant en ce qui concerne les FFNs (Fig.Résumé-3), nous avons remarqué que deux d'entre eux (FFN102 et FFN202) possèdent également un tel groupe hydroxyle sur le noyau benzénique, ce qui pourrait conférer à ces deux molécules une électroactivité appropriée. En contrepartie de leur excellente propriété de fluorescence, nous nous demandons donc de savoir s'il est possible d'utiliser les FFNs comme sonde unique optique et électrochimique pour le suivi de l'exocytose par technique de couplage TIRFM/ampérométrie.

L'objectif de ce travail de thèse est donc de tester la faisabilité d'utilisation de certaines molécules de FFNs comme sonde duale pour le couplage TIRFM/ampérométrie afin de suivre l'ensemble du processus d'exocytose dans les cellules vivantes. Plus précisément, pour mieux élucider les mécanismes sécrétoires au niveau d'une seule vésicule, notre questionnement dans cette thèse porte sur les trois aspects présentés ci-bas:

- I. Y a-t-il certaines molécules dans la famille des FFNs qui soient électroactives? Si oui, est-ce qu'elles peuvent être utilisées comme sondes électroactives pour la détection ampérométrique de l'exocytose?
- II. Est-il possible de suivre spécifiquement l'exocytose en TIRFM avec des cellules chargées avec des FFNs ? Dans ce cas, quelle lignée cellulaire est un meilleur modèle d'investigation de l'exocytose par la méthode de couplage TIRFM/ampérométrie : les cellules PC-12 ou celles BON N13?

- III. Est-il faisable d'employer ces FFNs choisies comme une double sonde (optique et électrochimique) pour simultanément mesurer la libération d'exocytose avec deux techniques TIRFM et ampérométrie? Quelles sont les nouvelles informations que nous pourrions acquérir grâce à l'application de la sonde duale en technique de couplage TIRFM/ampérométrie?

## 2. Suivi d'exocytose des cellules marquées par 4-(2-aminoéthyl)-6-chloro-7-hydroxy-2H-1-benzopyran-2-one hydrochloride

La Fig. Résumé-4 présente la formule moléculaire d'un membre de la famille des FFNs, 4-(2-aminoéthyl)-6-chloro-7-hydroxy-2H-1-benzopyran-2-one, que nous avons synthétisé selon la procédure précédente rapportée par Sames et ses collègues et nommé **1** dans cette thèse.

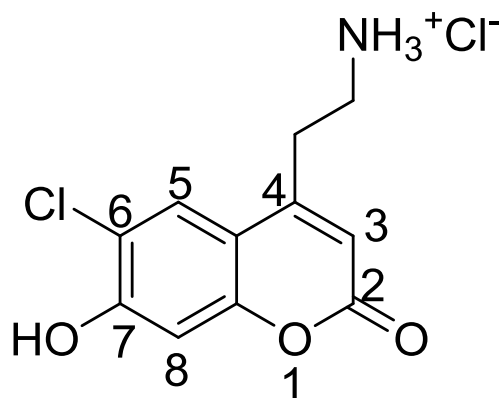


**Figure Résumé-4** La formule moléculaire d'un membre de la famille des FFNs, 4-(2-aminoéthyl)-6-chloro-7-hydroxy-2H-1-benzopyran-2-one, nommé **1** dans cette thèse

Pour l'étude de l'exocytose au moyen de la technique de couplage TIRFM/ampérométrie, **1** peut être une sonde prometteuse grâce aux trois raisons suivantes. Tout d'abord, il a été rapporté que cette molécule présente des propriétés photophysiques dépendantes du pH en raison de l'équilibre entre le phénol et la forme phénolate. En outre, du fait de l'introduction d'un groupe attracteur d'électrons (-Cl) à la position 6 de la coumarine, la valeur du pKa du groupe hydroxyle phénolique est abaissée à environ 6, se situant dans la gamme de pH à l'intérieur des vésicules de sécrétion (ca 5~6). Par conséquent, si une diffusion de **1** hors de la vésicule (pH interne = 5~6) dans le milieu extracellulaire (pH = 7,4) a lieu, une augmentation de la fluorescence devrait être observée en TIRFM. D'autre part, le groupe aminoéthyle peut être reconnu sélectivement par les cellules exprimant VMAT, ce qui rend possible le suivi des vésicules par microscopie à fluorescence depuis leur déplacement dans le cytoplasme jusqu'à la libération. Enfin, et de façon intéressante, il a déjà été signalé qu'une série de coumarines hydroxylés sont électroactives avec une capacité à être oxydées à des valeurs de potentiel comparables à celles utilisées pour la détection électrochimique de l'exocytose. En conséquence, **1**,

une coumarine hydroxylée avec un groupe hydroxyle phénolique à la position 7 de la coumarine, pourrait présenter des caractéristiques électrochimiques prometteuses, ainsi qu'une sonde difonctionnelle (fluorescente et électrochimique) prometteuse pour la mesure de couplage TIRFM/ampérométrique.

## 2.1 Propriétés photophysiques et électrochimiques de 1

### 2.1.1 Propriétés photophysiques

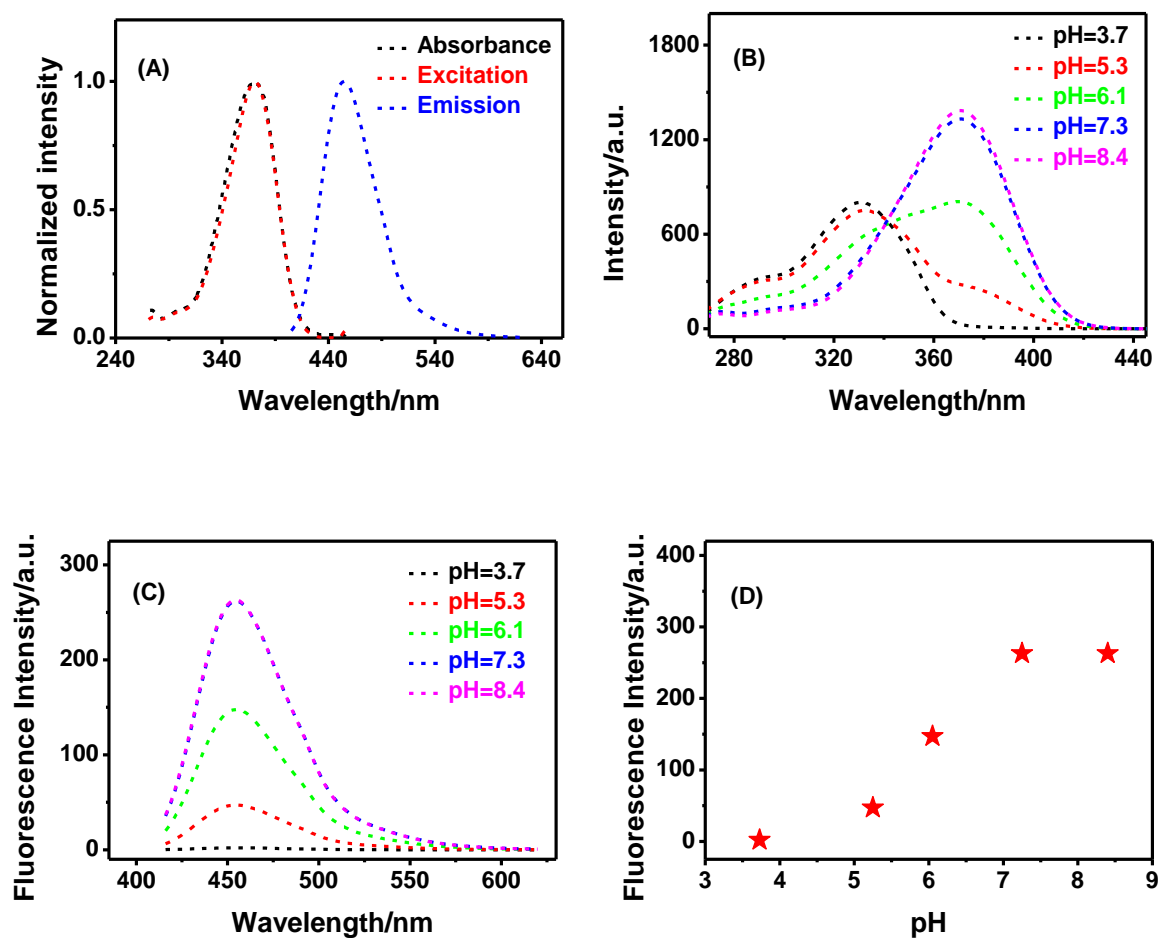


**Figure Résumé-5** (A) Spectres d'absorption (blanc), d'excitation (rouge,  $\lambda_{em} = 456 \text{ nm}$ ) et d'émission (bleu,  $\lambda_{ex} = 371 \text{ nm}$ ) de 10  $\mu\text{M}$  de 1 dissous dans du PBS ( $\text{pH} = 7,4$ ); (B) et (C) les spectres d'excitation ( $\lambda_{em} = 456 \text{ nm}$ ) et d'émission ( $\lambda_{ex} = 405 \text{ nm}$ ) de 1 obtenus dans le PBS à différentes valeurs de pH; (D) les intensités maximales d'émission extraites de (C); les intensités de fluorescence ont été représentées en unités arbitraires.

Nous avons tout d'abord mesuré le rayonnement ultraviolet-visible (UV-vis) d'absorption, d'excitation et d'émission des spectres de **1** dans une solution tampon (PBS, pH = 7,4). Comme représenté sur la Fig. Résumé-5(A), **1** absorbe à une longueur d'onde de 300~420 nm, avec un maximum d'absorption à 371 nm et émet dans la plage de 405~620 nm, avec un maximum d'émission à 456 nm, présentant ainsi d'excellentes propriétés optiques. La Fig. Résumé-5(B) présente les spectres d'excitation de **1** en fonction du pH et révèle que les propriétés optiques de cette sonde sont fortement dépendantes du pH. En particulier, **1** a montré deux longueurs d'onde d'excitation maximale à 330 nm et 370 nm, respectivement, et le spectre d'excitation est apparu sous forme de mélange de ces deux longueurs d'onde à un pH de 6,1. La dépendance en pH de **1** est due à l'équilibre bien connu entre le phénol et la forme phénolate protonnée/déprotonnée du groupe hydroxyle phénolique à la position 7 de la coumarine, plutôt que le groupe amino. Plus précisément, l'ancien pic d'absorption à 330 nm correspond à la forme phénolique protonnée tandis que le second à 370 nm à la forme phénolate déprotonnée. À un pH de 6,1, ces deux formes existent, ce qui entraîne un spectre mixte, tel que présenté dans la Fig. Résumé-5(B).

Notre dispositif expérimental de TIRFM est équipé d'une source laser à 405 nm. Nous avons donc mesuré les intensités de fluorescence de **1** à 10  $\mu$ M (dans le PBS) sur une plage de pH de 3,7 à 8,4 et à une longueur d'onde d'excitation de 405 nm, tel que présenté dans la Fig. Résumé-5(C). **1** pourra donc être éclairé à 405 nm, longueur d'onde à laquelle sa fluorescence est stable, même si une partie des signaux fluorescents y est perdue. De plus, nous avons comparé les intensités de fluorescence excitées à 405 nm à différentes valeurs de pH, ce qui montre que l'intensité de la fluorescence a été presque doublé de pH 5 à 7. Par conséquent, si cette molécule est utilisée comme sonde fluorescente pour marquer les vésicules, nous nous attendons à voir une augmentation des signaux fluorescents causée par un gradient de pH pour **1** diffusant à partir des vésicules acides (pH = 5 à 6) vers le milieu extracellulaire physiologique neutre (pH = 7,4).

Sur la base des études rapportées ci-dessus, nous proposons que **1**, un analogue de synthèse des neurotransmetteurs monoamines, pourrait être utilisé pour le suivi des vésicules durant l'exocytose en raison de sa fluorescence stable et pH-dépendante. Si **1** est libéré d'une vésicule acide vers le milieu extracellulaire neutre, le signal fluorescent sera intense transitoirement, puis disparaîtra en raison de sa diffusion. Autrement dit, les événements d'exocytose simples devraient être visualisés comme des «flashes» de lumière accompagnés par la disparition de la tache fluorescente, comme d'autres sondes fluorescentes dépendantes du pH de même type.

### **2.1.2 Propriétés électrochimiques**

La Fig. Résumé-6 (A) présente les voltammogrammes cycliques (CVs) de **1** dissous dans une solution de PBS à différentes valeurs de pH et enregistrés sur électrode à fibre de carbone (CFE). **1** commence à

être oxydé à +0.60 V vs. Ag/AgCl, montrant un pic d'oxydation à environ +0,76 V vs. Ag/AgCl, donc présentant une bonne électroactivité. En outre, le pic d'oxydation de **1** est décalé vers des valeurs plus négatives lorsque le pH croît de 5 à 8. Plus précisément, à un pH de 8, **1** existe principalement sous la forme phénolate déprotonnée qui pourrait être oxydée à +0,86 V vs. Ag/AgCl sur CFE alors qu'à pH 5, **1** existe principalement sous la forme non dissociée qui est oxydée à partir de +0,90 V vs. Ag/AgCl. Des résultats similaires ont été acquis sur microélectrodes ITO (cf Fig.Résumé-6 (B)), ce qui confirme que l'oxydation de **1** doit avoir lieu sur le site hydroxyle et que la forme phénolate déprotonnée tend à être oxydée à un potentiel inférieur.

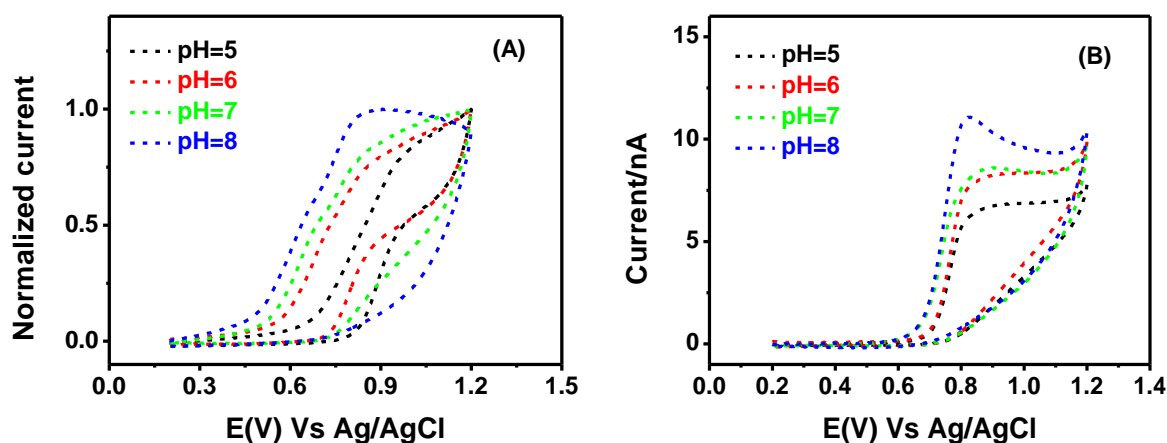


**Figure Résumé-6** Voltammogrammes cycliques (CVs) normalisés obtenus sur CFE (A) et ITO (B) de 100 µM de **1** dans du PBS à différentes valeurs de pH variant de 5 à 8. Potentiel initial: +0,2 V (vs Ag /AgCl); vitesse de balayage de 100 mV/s. On a soustrait le blanc à tous les CVs présentés.

## 2.2 TIRFM pour l'étude de l'exocytose des cellules marquées par la sonde **1**

**1** a pu être reconnu et transféré de manière sélective dans les vésicules acides par les deux lignées cellulaires testées ici dans ce travail de thèse (PC-12 et BON N13). Néanmoins, nous avons finalement utilisé des cellules BON N13 marquées par **1** pour mesurer des sécrétions d'exocytose par TIRFM car les cellules PC-12 ont montré une trop petite taille de vésicules pour être suivies correctement en TIRFM (limitation de la résolution spatiale)..

Nous avons étudié par TIRFM l'exocytose, déclenchée par l'ion calcium, de vésicules individuelles (marquées par **1**) dans les cellules BON N13. Comme cela est illustré sur la Fig.Résumé-7, les vésicules marquées par **1** sont apparues sous forme de petites taches bleues lors de la configuration TIRFM et la plupart de ces vésicules fluorescentes ont disparu en raison certainement de leur exocytose après l'application d'un stimulus déclenchant la sécrétion (10 µM d'ionomycine). En outre, trois formes d'événements exocytose ont été observés à partir de cellules BON N13 marquées par **1**: «flash normal», «extinction de fluorescence» ainsi que «flash soudain» (voir Fig.Résumé-8). Dans ce

travail, nous démontrons que lors de la configuration de TIRFM, **1** est une excellente sonde optique pour visualiser et quantifier la libération de neurotransmetteurs au cours de l'exocytose directement au niveau de la vésicule unique.

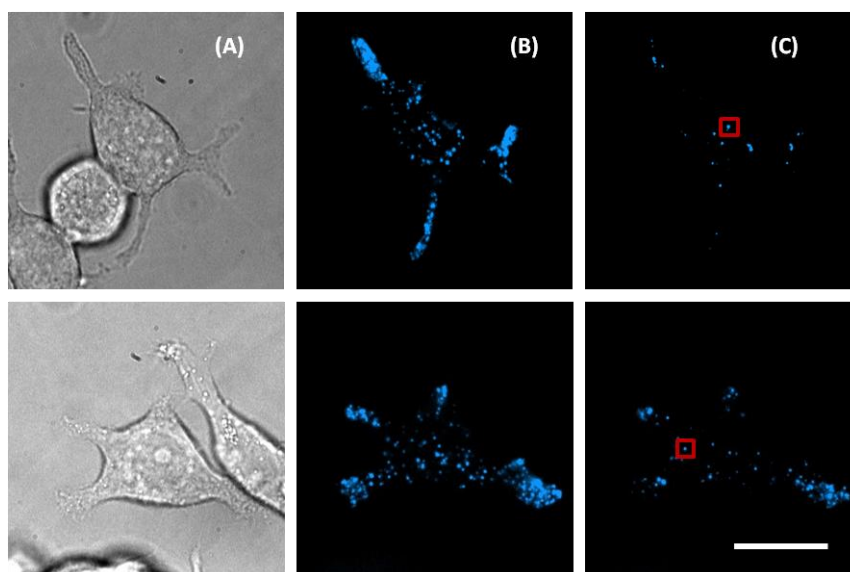


**Figure Résumé-7** Deux exemples typiques de cellules individuelles de BON N13 marquées par **1** observées en lumière visible (A) et en TIRFM (B et C); (B) et (C) montrent les images de la cellule cible avant et après l'application de 10  $\mu\text{M}$  d'ionomycine, respectivement; les taches bleues représentent des vésicules fluorescentes marqués par **1** et un exemple de telles vésicules est indiqué dans le rectangle rouge; barre d'échelle: 10  $\mu\text{m}$ .

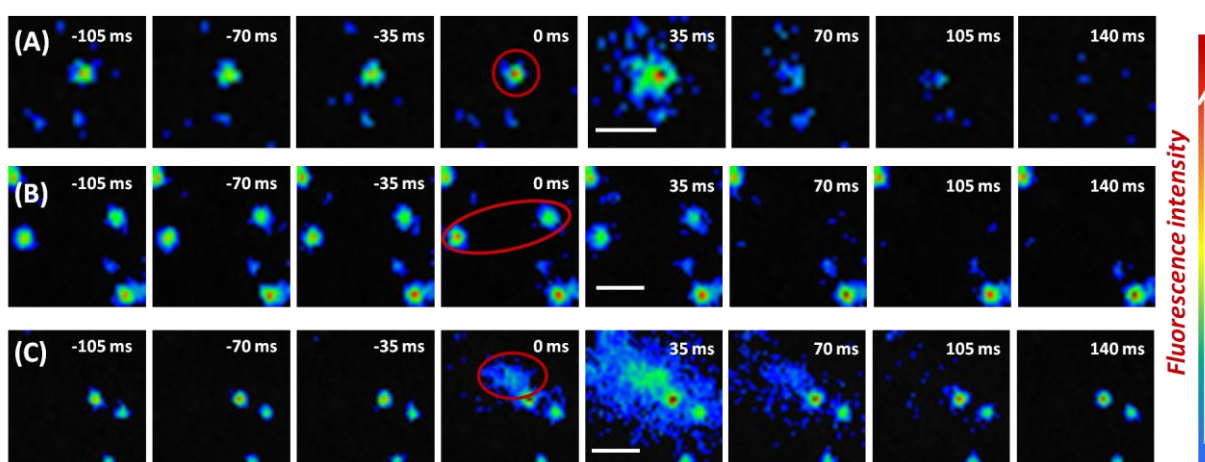
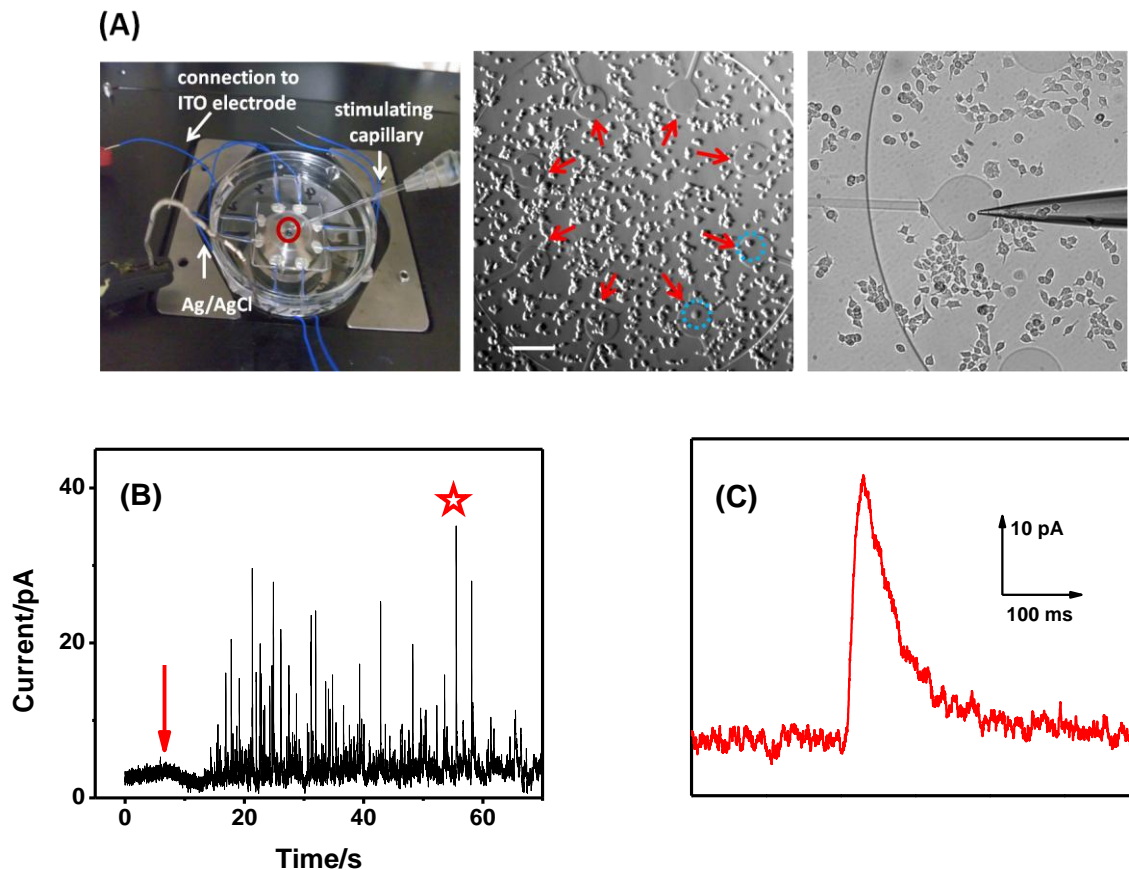


**Figure Résumé-8** Trois formes d'événements exocytose observés à partir de cellules BON N13 marquées par **1**: (A) 'flash normal', (B) 'extinction de fluorescence' ainsi que (C) 'flash soudain'.

## 2.3 Ampérométrie pour l'étude de l'exocytose des cellules marquées par la sonde 1

### 2.3.1 L'exocytose suivie par ampérométrie

Les résultats de cette série d'expérience montrent que lors d'une stimulation par un ionophore de calcium ( $10 \mu\text{M}$  d'ionomycine), une fraction de **1** internalisée a été expulsée de la vésicule vers l'espace extracellulaire à travers le pore de fusion, conduisant à une diminution évidente de l'intensité de fluorescence.



Pour les cellules situées sur la microélectrode ITO, l'événement d'exocytose détecté à la surface d'électrode est enregistré comme un pic de courant d'oxydation brutal et le processus d'exocytose d'une cellule individuelle apparaît comme une succession de ces pics de courant appelée ampérogramme. Ainsi **1** est bien une sonde électrochimique de choix pour étudier les sécrétions vésiculaires par ampérométrie, comme espéré et envisagé au début de cette thèse.

Au cours du test ampérométrique, un potentiel constant de +900 mV par rapport à Ag/AgCl a été appliqué à l'électrode de travail d'ITO (Fig.Résumé-9(A)). Le courant a été enregistré en fonction du temps et l'injection d'un ionophore de calcium (10  $\mu$ M d'ionomycine) a été utilisé. Il est nécessaire de noter que la sélection de cellules cibles a été réalisée à l'aide de la microscopie optique en utilisant le marquage par fluorescence des cellules chargées avec **1** pour repérer les bonnes cellules.

La Fig.Résumé-9(B) est une trace ampérométrique typique représentant la libération d'exocytose des cellules BON N13 marquées par **1** et la flèche rouge à l'intérieur du chiffre indique le moment où la solution d'ionomycine a été injectée par le micro-injecteur. Comme prévu, aucun signal d'oxydation n'a été observé avant l'application de 10  $\mu$ M d'ionomycine (avant la flèche rouge). Une succession de pics individuels ampérométriques est apparu par la suite (quelques secondes après l'injection de la solution de stimulation), qui est attribuée à la libération de **1** suivie par son oxydation rapide sur la surface des microélectrodes d'ITO. Dans la trace ampérométrique, chaque pic a été attribué à un événement exocytotique individuel d'une seule vésicule de sécrétion (Fig.Résumé-9(C)). Il est notable que la technique d'ampérométrie présente une résolution temporelle extrêmement élevée puisque les pics de courant durent habituellement en moyenne moins de 100 ms. Des paramètres cinétiques et quantitatifs significatifs (largeur à mi-hauteur, temps de montée, temps de décroissance, fréquence, aire ou charge du pic, intensité maximale) sont extraits à partir des pics individuels isolés d'une trace ampérométrique et permettent d'illustrer les étapes spécifiques de l'ensemble de l'événement d'exocytose au niveau de la vésicule unique, ce qui sera discuté en détails plus loin dans ce résumé.

### ***2.3.2 Ampérométrie sur électrodes d'ITO et ou à fibre de carbone (CFE)***

Le suivi de l'exocytose vésiculaire est susceptible d'être obtenu en effectuant des expériences avec une configuration expérimentale soit en positionnant une électrode à fibre de carbone (CFE) sur le sommet des cellules au contact étroit de la surface cellulaire à une centaine de nms environ (Fig.Résumé-10, image de gauche) ou soit sur la base de la cellule par ensemencement des cellules sur un substrat conducteur, tel que des microélectrodes de Pt, d' Au ou d'ITO (Fig.Résumé-10, image de droite).

Dans les deux cas, dès que les biomolécules électroactives sont libérées des vésicules et diffusent à la surface des électrodes, elles seront immédiatement oxydées formant une succession de pics sur l'ampérogramme (Fig.Résumé-10, courbe en rouge). Toutefois, en raison des conditions physiologiques sans doute différentes aux deux pôles (sommet et base) des cellules, ainsi que peut être

des différences intrinsèques caractéristiques des microélectrodes CFE ou ITO, il existe une légère variation des paramètres quantitatifs et temporels extraits pour la caractérisation de l'exocytose des cellules BON N13 à partir de l'analyse au sommet ou à la base. Ceci a déjà été observé par le passé au laboratoire lors de la thèse de Anne Meunier (2011) et dans la littérature.

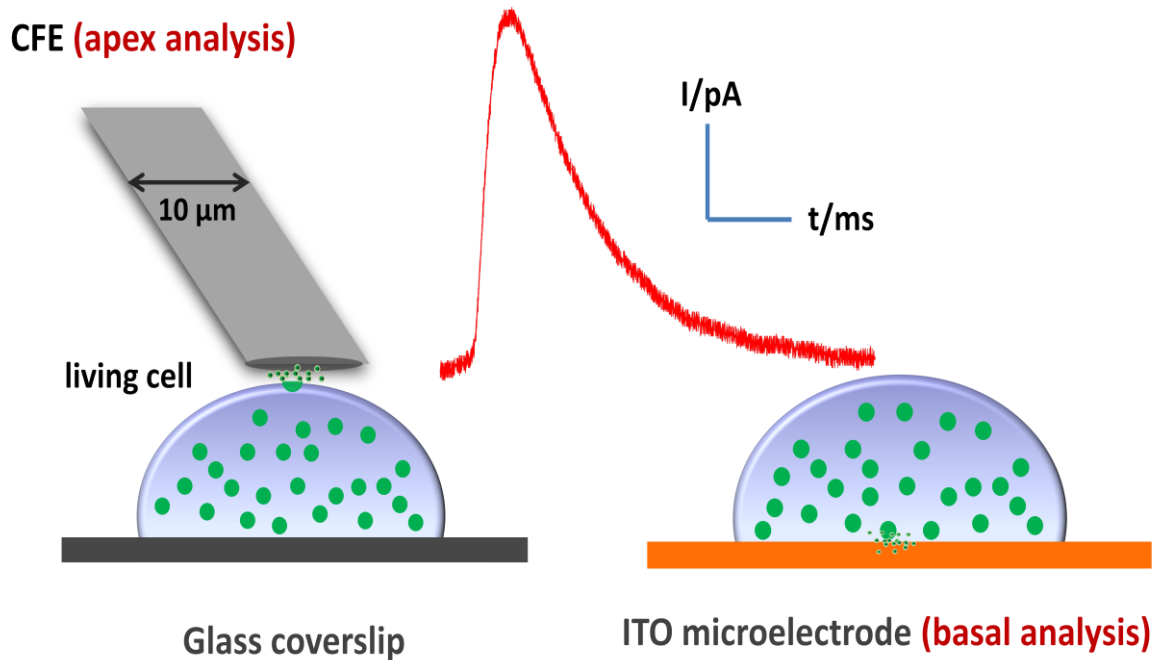


**Figure Résumé-10** Illustration schématique de la détection électrochimique de l'exocytose vésiculaire sur une cellule BON N13 au pôle apical (au moyen d'une CFE) ou au pôle basal (avec une électrode d'ITO). A noter que la microélectrode plane d'ITO est utilisée comme substrat pour l'adhésion cellulaire et pour détecter les signaux d'oxydation.

La comparaison de la libération vésiculaire détectée à différentes configurations, à savoir par CFE au sommet de la cellule et par ITO au fond de la cellule, montre qu'il y a une disparité en termes de dynamique de libération et des quantités relarguées sur cellules BON N13 (Fig. Résumé-11). Pour être plus précis, par rapport aux événements exocytose enregistrés sur CFE, ceux détectés sur ITO présentent une plus grande quantité de contenu en charge ( $\sim 2,6$  fois plus élevé que ceux obtenus sur CFE) et leur cinétique est également plus rapide. Compte tenu de cette observation, il est donc extrêmement important d'enregistrer les signaux au même pôle lorsque deux techniques complémentaires, comme dans le couplage de la fluorescence et de l'ampérométrie, sont utilisées.

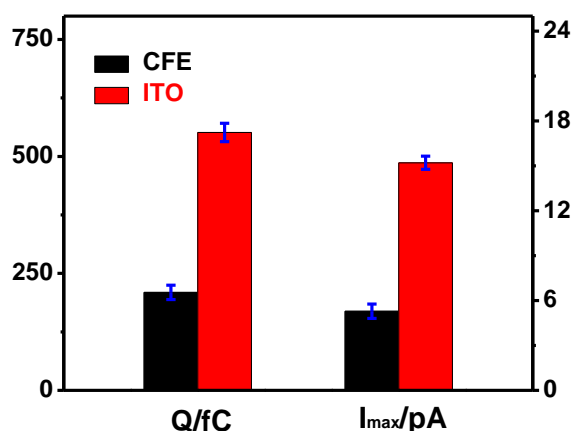
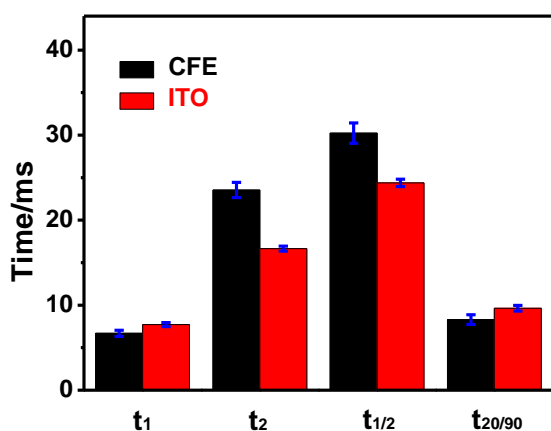
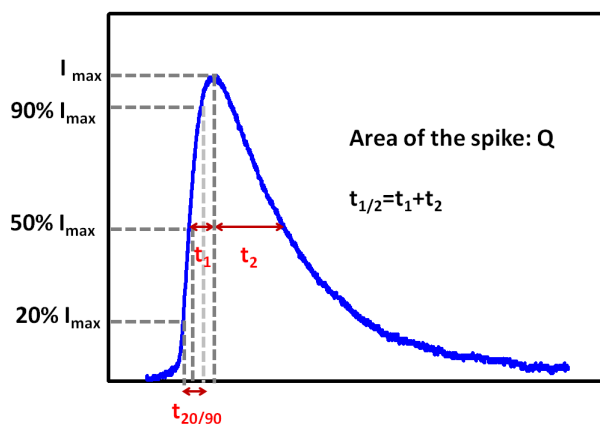


**Figure Résumé-11** Comparaison des événements d'exocytose vésiculaire de cellules BON N13 marquées par *I* se produisant au sommet (détecté par CFE) et à la base (obtenus sur microélectrodes d'ITO) cellulaire par ampérométrie.

## 2.4 Couplage de l'ampérométrie et du TIRFM pour l'étude de l'exocytose des cellules marquées par la sonde FFN 1

L'ampérométrie est complètement «aveugle» aux mouvements 3D des vésicules car les signaux électriques ne peuvent être détectés qu'après que les biomessagers électroactifs arrivent à la surface de l'électrode. En dépit de sa haute résolution temporelle et de sa sensibilité, sa faible résolution spatiale devient le principal défaut de la méthodologie électrochimique pour les suivis de sécrétions vésiculaires. Cependant, la combinaison de l'ampérométrie avec le TIRFM est susceptible de résoudre ce problème, compte tenu de la résolution spatiale de cette technique (centaine de nm soit, peu ou prou, la dimension des vésicules de sécrétion selon les types cellulaires). Autrement

dit, le couplage de ces deux techniques d'analyse de nature complémentaire permettra le suivi précisément de l'exocytose à la fois avec une haute résolution spatiale et temporelle. Dans ce travail, la combinaison du TIRFM avec l'ampérométrie est atteinte grâce à des microdispositifs basés sur la fabrication de microélectrodes d'ITO qui permettent à la fois l'imagerie par fluorescence et l'enregistrement ampérométrique en raison de la transparence optique spécifique, ainsi qu'une excellente conductivité électrique de l'ITO.

#### ***2.4.1 Signaux fluorescents et ampérométriques couplés d'évènements d'exocytose***

Le couplage TIRFM/ampérométrie a été réalisé avec succès sur les cellules BON N13 cultivées dans un microdispositif d'ITO et chargées au préalable avec la sonde duelle optique et électrochimique **1** de la famille des FFNs. Lors de la stimulation, **1** a commencé à diffuser de la vésicule vers l'espace extracellulaire, ce qui conduit à la mesure de fluorescence et des signaux ampérométriques ont pu être recueillis simultanément à la surface transparente de l'électrode d'ITO. En outre, il existe trois formes d'évènements exocytose lors de la détection couplée en vertu des propriétés optiques et électrochimiques de **1**: «flash normal », «extinction de fluorescence» ainsi que « flash soudain». Par exemple, la Fig.Résumé-12 représente un événement d'exocytose classique défini comme étant «un « flash normal» et qui a été détecté par la technique de couplage TIRFM/ampérométrie.

En ce qui concerne l'imagerie de séquence (Fig.Résumé-12, en bas), la libération exocytotique a été indiquée via le flash lumineux. Autrement dit, le signal fluorescent transitoire est dû à la libération de **1** de la vésicule acide vers le milieu extracellulaire à pH neutre, puis disparaît complètement en environ 100 ms quand les fluorophores diffusent et se diluent, en accord avec notre résultat précédent indiqué dans la Fig.Résumé-8(A). A cause de la résolution temporelle limitée des signaux fluorescents (acquisition à 35 ms/image), il n'est pas possible d'effectuer un suivi de la fluorescence à chaque étape de l'exocytose en « temps réel » comme avec l'ampérométrie (acquisition à un point/25 us soit 40 kHz). C'est la raison pour laquelle il est très important de faire une détection couplée où l'ampérométrie apportera la résolution temporelle nécessaire. Dans la détection ampérométrique correspondante (Fig.5-8, en haut), le pic de courant d'oxydation a duré moins de 100 ms, ce qui est comparable à la durée de fluorescence du « flash normal» enregistrée par TIRFM, mais la résolution temporelle a été grandement améliorée (~ 25 ms pour chaque acquisition).

La combinaison du TIRFM avec la détection électrochimique permet donc d'éclairer de manière inédite les mécanismes d'exocytose. La corrélation des signaux optiques et ampérométriques démontre (Fig. Résumé-12) que le délai ( $t = 181.910$  s) pendant lequel l'augmentation de la fluorescence initiale a eu lieu a été accompagné par la forte hausse du courant en ampérométrie, indiquant un flux maximal de la sonde double fluorescente/électrochimique **1** en quelques ms. Ensuite, la dispersion de **1** conduit à une concentration plus faible des fluorophores, la fluorescence étant plus faible ( $t = 181.945$  s) à la

surface de l'ITO et étant aussi associée à une diminution lente du courant détecté. Enfin, la disparition de la fluorescence ( $t = 181.980$  s) est corrélée avec par le retour du courant à la ligne de base.

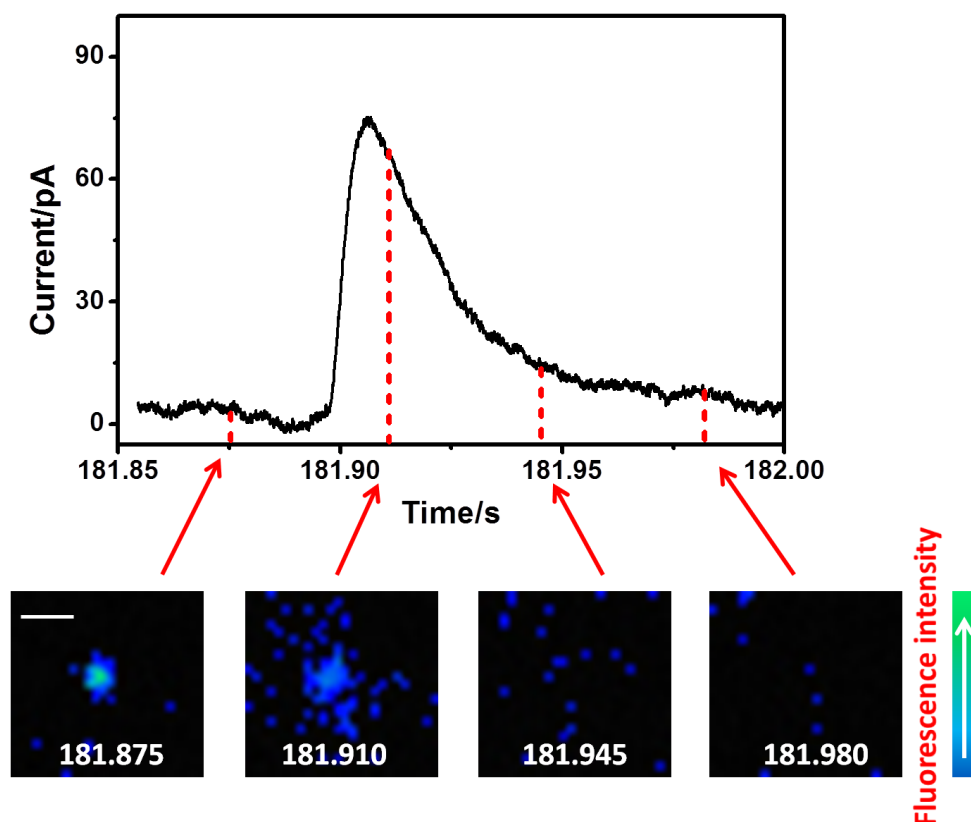


**Figure Résumé-12** Corrélation des informations ampérométrique et fluorescente pour un événement de libération unique de cellules BON N13 marquées par **1** sur une microélectrode d'ITO; haut: un événement d'exocytose suivi sur ITO est apparu comme un pic de courant dans la détection électrochimique; bas: images en « pseudo-couleur » obtenues en TIRFM d'un seul événement d'exocytose défini comme un « flash normal »; excitation laser à 405 nm, temps d'exposition à 35 ms. Les instants correspondants aux signaux fluorescents et ampérométrique sont précisément indiqués par des flèches rouges et les lignes pointillées rouges; barre d'échelle: 500 nm.

Outre les informations couplées, nous avons également observé des signaux «uniquement fluorescents» et «uniquement électrochimiques» qui ont été définis comme des événements «orphelins optiques» ou «orphelins ampérométriques» dans la littérature passée. Nous avons ensuite comparé les taux de signaux couplés obtenus à partir des cellules BON N13 marquées par **1** avec ceux obtenus à partir de cellules BON BC21. Ces dernières étaient marquées par un marqueur fluorescent des granules sécrétoires (NPY-GFP, neuropeptide NPY greffé avec une protéine verte fluorescente et

internalisé dans les cellules BC21 de manière endogène) et un marqueur électroactif : la sérotonine qui ont été employés conjointement comme, respectivement, sondes fluorescente et électrochimique dans le travail de thèse de Anne Meunier au laboratoire en 2011.

Comme le montre le Tableau Résumé-1, dans des conditions similaires, l'efficacité du couplage optique/ampérométrique obtenu est optimisée de 12% grâce à l'emploi de la sonde double **1** pour marquer les vésicules des cellules BON N13. Pour la mesure du couplage sur cellules BON BC21 avec deux sondes indépendantes (NPY-GFP et sérotonine), 57% des événements ne sont que des signaux TIRFM et 21% sont uniquement des pics ampérométriques. En outre, les amplitudes des pics ampérométriques dans ce cas variaient de 0,2 à 3,5 pA en amplitude en raison de la faible quantité de sérotonine accumulée à l'intérieur des vésicules transfectées par la GFP. Le courant ampérométrique est si faible qu'il est difficile de mesurer les signaux et un traitement de données supplémentaires tel qu'un filtrage adapté ou un lissage des points était parfois nécessaire. En revanche, les signaux électrochimiques résultant d'une oxydation de **1** semblent bien meilleurs ( $I_{\max} = 19,2 \pm 0,7$  pA, Fig.Résumé-11) en raison de son chargement réussi et meilleur dans les vésicules que dans le cas de la sérotonine.

	<b>1</b> (cette thèse 2016)	<b>GFP + sérotonine</b> (thèse Anne Meunier 2011)
<b>Evènements couplés</b>	34%	22%
<b>Orphelins optiques</b>	42%	57%
<b>Orphelins ampérométriques</b>	24%	21%

**Tableau Résumé-1** Comparaison des proportions de trois types de signaux ('évènements couplés', 'Orphelins optiques' et 'Orphelins ampérométriques') détectés à partir de cellules BON lignée N13 marquées par **1** ou les cellules BON lignée BC21 (marquées par la GFP et la sérotonine).

Une autre comparaison peut être faite avec le travail de Kisler et coll. qui a analysé par TIRFM/ampérométrie l'exocytose de cellules chromaffines (les sondes étant l'adrénaline électroactive endogène et l'acridine orange fluorescente) sur électrodes fines d' Au ou d'ITO. Bien que l'analyse des données ait été partielle, il a été établi que 20% des pics ampérométriques ont été accompagnés d'un événement de fluorescence sur électrodes d'ITO et 38% des pics d'ampérométriques ont été combinés

à un événement de fluorescence détectable au niveau des électrodes d' Au. Dans notre cas, concernant **1**, 59% des signaux électrochimiques ont été couplés à leur événement optique correspondant (42% dans les précédents travaux sur les cellules BON BC21 chargées avec GFP et la sérotonine de la thèse de Anne Meunier en 2011), ce qui constitue une amélioration notable et significative ainsi que très encourageante et fructueuse en ce qui concerne l'utilisation de sonde unique duelle optique et électrochimique pour le suivi de l'exocytose.

L'analyse en détails des pourcentages obtenus dans Tableau Résumé-1 nous permet de conclure que le chargement unique avec la double sonde **1** permet une amélioration de la qualité et de l'efficacité de la charge électrochimique. En effet, par rapport aux cellules BON BC21 (GFP + sérotonine), le pourcentage d'événements couplés obtenus sur cellules BON N13 (double sonde **1**) augmente de 22% à 34%. De plus, le pourcentage d'événements «orphelins optiques» diminue de 57% à 42%. Le fait que les événements «orphelins optiques» sont définis comme des événements sans pics ampérométriques conduit à la conclusion que la molécule **1** a une affinité plus favorable de passage à l'intérieur des vésicules que la sérotonine seul et que le travail avec une sonde duale unique est plus efficace qu'avec deux sondes séparées optique et électrochimique (cas de la GFP et de la sérotonine dans les cellules BON N13). En outre, le pourcentage d'événements «ampérométriques orphelins» reste constant. Par rapport au travail précédent au laboratoire avec «GFP + sérotonine», cela signifie que l'amélioration est due uniquement un meilleur chargement de la sonde électrochimique puisque la résolution temporelle de la caméra est fixée à niveau comparable dans les deux cas. (Si la caméra allait « plus vite » il serait normal d'enregistrer davantage d'événements fluorescents, manqués dans le cas d'une caméra trop « lente »).

Par conséquent, la stratégie qui consiste à utiliser une sonde unique (électrochimique et fluorescente) pour la détection de la libération exocytotique au niveau d'événements individuels semble plus adaptée que tous les travaux antérieurs impliquant des sondes indépendantes et différentes pour l'optique et l'électrochimie.

#### ***2.4.2 Enregistrement en continu de la sécrétion exocytotique avec une haute résolution spatiale et temporelle***

La technique TIRFM/ampérométrie combinant deux puissants outils d'analyse, de nature complémentaire : visualisation par TIRFM et quantification par ampérométrie, et ce, pour l'analyse de l'exocytose au niveau de la vésicule unique dans une cellule isolée, permet d'assurer à la fois une haute résolution spatiale (centaine de nms) et temporelle (temps de réponse inférieur à la ms et fréquence d'acquisition à 25 us). L'application de cette technique de couplage a été démontrée dans ce travail de thèse à l'aide de la double sonde **1** à la fois électrochimique et optique, issue de la famille des faux neurotransmetteurs fluorescents (FFNs).

La Fig.Résumé-13 montre un exemple de deux événements d'exocytose de cellules BON N13 marquées par **1** et suivies par la combinaison fluorescence/électrochimie dans un microdispositif à base de microélectrodes d'ITO.

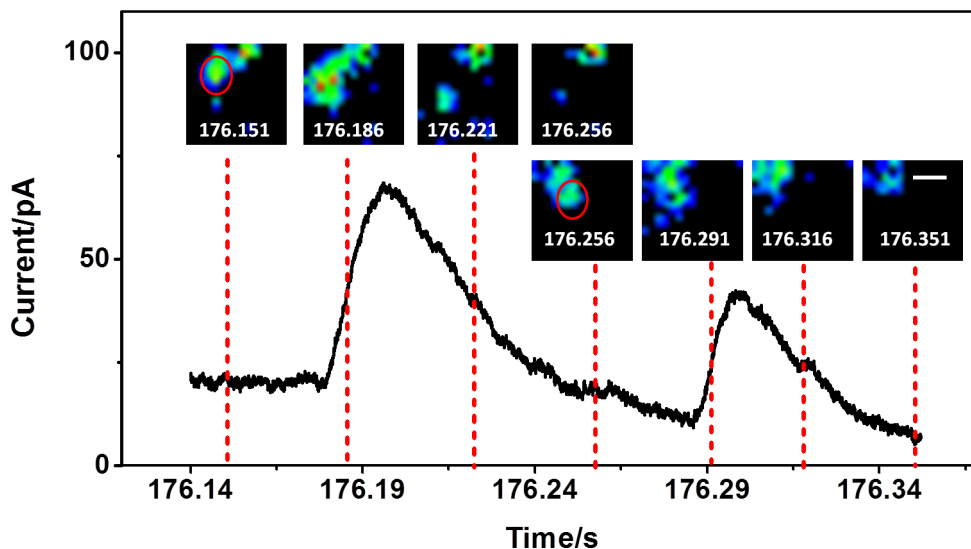


**Figure Résumé-13** Un exemple de deux sécrétions d'exocytose consécutives de cellules BON N13 marquées par **1**, images de TIRFM de deux vésicules individuelles (marquées par l'ellipse rouge) temporellement corrélées avec les pics ampérométriques correspondants simultanément comme indiqué par la ligne pointillée rouge. Excitation laser à 405 nm, temps d'exposition à 35 ms; barre d'échelle: 500 nm.

	$t_1$ (ms)	$t_2$ (ms)	$t_{20/90}$ (ms)	$t_{1/2}$ (ms)	$I_{\max}$ (pA)	Q (fC)
<b>vesicle 1</b>	10.6	23.4	12.3	34.1	52.5	1920
<b>vesicle 2</b>	6.9	17.0	7.5	24.0	35.2	980

**Table Résumé-2** Paramètres cinétiques et quantitatifs de deux évènements d'exocytose de vésicules indépendantes (numérotées 1 et 2, cf. Fig.Résumé-13) et extraits sur les pics ampérométriques correspondants,

Selon les pics ampérométriques détectés, il est évident que deux sécrétions d'exocytose indépendantes ont successivement lieu dans un très court laps de temps, ~ 200 ms. Leurs paramètres cinétiques et quantitatifs peuvent être extraits sur la base des pics de courant qui sont bien séparés donc isolables, tel que présenté dans le Tableau Résumé-2. La figure Résumé-13 présente deux vésicules relarguant la sonde **1** et suivies par la méthode couplée. Par comparaison avec la vésicule 2 ( $t = 176.256$  s sur l'enregistrement par fluorescence), la vésicule 1 ( $t = 176.151$  s sur le suivi fluorescent) présente une libération relativement plus lente mais avec plus grande quantité de **1**. En outre, dans cette mesure de couplage, grâce aux signaux optiques par TIRFM, les emplacements et les comportements de ces deux vésicules ont été identifiés avec précision, comme le montrent les ellipses rouges dans la Fig. Résumé-13.

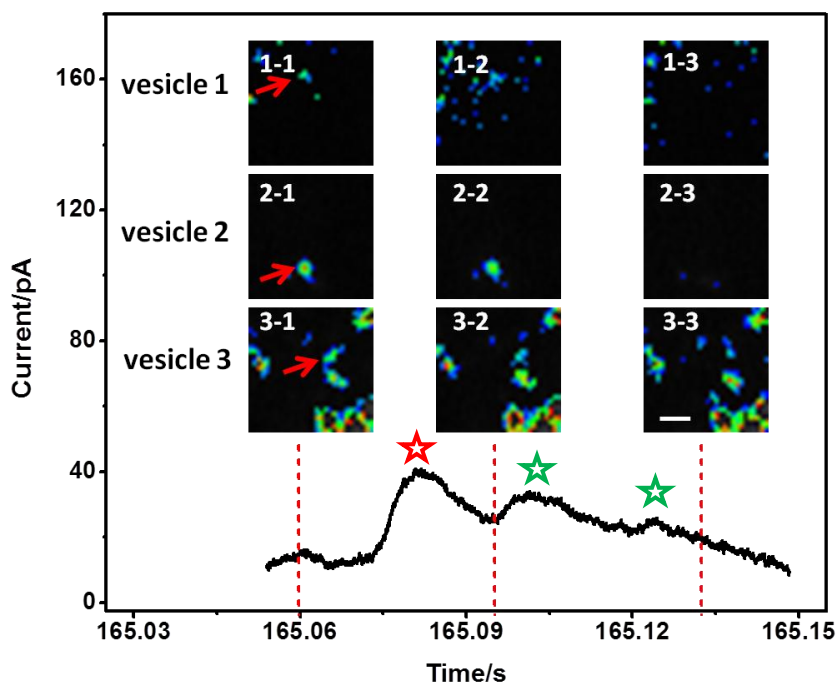


**Figure Résumé-14** Un exemple de la faisabilité de la technique TIRFM / ampérométrie pour l'analyse des événements exocytotiques superposés de cellules BON N13 marquées par **1**. Suivi TIRFM de trois vésicules individuelles (vésicules 1, 2 et 3, indiquées par les flèches rouges) et corrélé aux pics ampérométriques superposés correspondants (les pics de courant sont marqués par des étoiles rouge / vertes). Excitation laser à 405 nm, temps d'exposition à 35 ms; barre d'échelle: 500 nm.

Un autre avantage remarquable de la technique de couplage TIRFM/ampérométrie est son application pour l'analyse de sécrétions superposées temporellement qui se traduisent par des pics qui se chevauchent dans la détection électrochimique. La Fig. Résumé-14 montre un exemple représentatif de

pics ampérométriques qui se chevauchent et détectés par couplage. En corrélant la trace ampérométrique aux images séquentielles de TIRFM, on voit que la superposition est due à une libération vésiculaire de 3 granules qui se déroulent dans un petit intervalle de temps (~ ms). La vésicule 1 décharge la sonde **1** un peu plus tôt que les deux dernières vésicules (vésicules 2 et 3).

La corrélation des signaux complémentaires optiques/électrochimiques avec une sonde unique et duelle montre la possibilité du suivi direct et en temps réel par la technique de couplage de la libération d'exocytose, révélant ainsi des détails quantitatifs et temporels de la sécrétion inaccessibles jusque lors par des méthodes découplées ou des sondes indépendantes optique et électrique.

### **3. Conclusions et perspectives**

L'exocytose vésiculaire est une voie physiologique majeure de la communication intercellulaire. Dans ce contexte, le TIRFM et l'ampérométrie sont aujourd'hui les deux méthodes analytiques les plus fréquemment utilisées dans l'étude de l'exocytose. En raison de la complémentarité de ces deux techniques d'analyse pour le suivi de la sécrétion exocytotique, leur combinaison pour suivre la sécrétion par exocytose a d'abord été réalisée par notre groupe en 2011 dans le cadre de la thèse de Anne Meunier. Ce couplage a permis un enregistrement simultané des signaux fluorescents et ampérométriques avec une bonne résolution spatiale et temporelle. L'inconvénient majeur de ce travail reste le chargement indépendant des sondes optique et électrochimique dans les vésicules de sécrétion, ce qui entraîne la détection d'évènements « orphelins » ampérométriques ou « orphelins » optiques ainsi que la faible efficacité de détection des évènements couplés. Par conséquent, dans cette thèse, nous avons tenté de mettre à profit une sonde unique à la fois fluorescente et électroactive pour suivre l'exocytose par la méthodologie couplée TIRFM/ampérométrie. Ainsi, un analogue de neurotransmetteurs monoamine primaire, la 4-(2-amino-éthyl)-6-chloro-7-hydroxy-2H-1-benzopyran-2-one (nommé **1** dans ce travail), a été synthétisé.

**1** présente une fluorescence forte, stable et pH-dépendante. Lorsque cette entité est excitée à 405 nm, son intensité de fluorescence est presque doublée de pH 5 (valeur intra-vésiculaire) à 7 (valeur du milieu extracellulaire). De plus, des études en voltammétrie ont pu mettre en évidence que **1** est oxydable sur électrode de carbone vitreux, microélectrode à fibre de carbone et ITO (oxyde d'indium dopé à l'étain), montrant ainsi une bonne électroactivité. La pénétration cellulaire dans les vésicules de cellules BON N13 a également été démontrée, prouvant la spécificité de l'interaction entre **1** et ces vésicules équipées d'un transporteur de monoamines primaires (VMAT). L'utilisation de **1** comme sonde unique optique et électrochimique pour le suivi de l'exocytose a ensuite été validée séparément dans des cellules BON N13 par les deux techniques de TIRFM et d'ampérométrie, donc d'abord utilisées indépendamment. L'enregistrement simultané par fluorescence et électrochimie en utilisant **1**

comme sonde double a ensuite été réalisé dans un microdispositif constitué d'électrodes ITO conductrices et transparentes. Nos résultats basés sur la sonde unique **1** montrent qu'elle semble plus adaptée que toutes les stratégies antérieures impliquant deux sondes indépendantes. Les résolutions spatiale et temporelle de cette méthode combinée ont permis d'analyser des sécrétions d'exocytose consécutives ainsi que des événements qui se chevauchent dans des cellules BON lignée N13 marquées par **1**. Une analyse ultérieure de ces signaux couplés optique et électrochimique sera à même d'étudier la corrélation entre le comportement du pore de fusion (dynamique d'ouverture/de fermeture, stabilité..) détecté par ampérométrie et le mouvement d'une vésicule en trois dimensions (ancrage, amarrage, fusion puis retrait dans le cytoplasme) détecté par TIRFM.

Ce travail représente une étape fondatrice pour développer d'autres sondes nouvelles capables de fonctionner comme double sonde électrochimique et fluorescente pour le suivi des événements vésiculaires par la méthode de couplage, en particulier d'autres molécules avec des structures similaires à **1** mais avec des longueurs d'onde d'excitation/émission plus hautes. De cette façon, l'efficacité du couplage devrait être encore améliorée. Cette piste est actuellement à l'étude au laboratoire.

La combinaison de deux sondes en une, nommée ici **1**, avec la méthode de couplage TIRFM/ampérométrie fournit des informations qui ne pouvaient pas être obtenues par ampérométrie ou l'imagerie de fluorescence seul. Ceci indique ainsi une perspective prometteuse pour la recherche sur d'autres processus physiologiques liés à l'exocytose. (i) D'autres études peuvent consister par exemple à faire la lumière sur les rôles spécifiques de certaines protéines régulatrices (comme les protéines SNAREs, l'actine et d'autres protéines fonctionnelles qui interagissent avec elles) et impliqués dans le mécanisme de fusion avant, pendant et après la fusion. (ii) Les sondes duelles permettront sans doute également d'observer le recrutement de molécules marquées par fluorescence dans des vésicules sécrétoires (en utilisant le TIRFM en mode deux couleurs). (iii) Elles seront aussi certainement capables de contribuer à révéler si le contenu et la taille vésiculaire (mesuré par ampérométrie) dépend de la surface de la sécrétion de la membrane plasmique (visualisée par TIRFM) ou s'il y a des zones spatiales spécifiques nommées 'points chauds' pour la sécrétion d'exocytose au niveau de la cellule unique. (iiii) Enfin elles permettront l'étude de la libération différentielle de différents marqueurs vésiculaires fluorescents non électroactifs par rapport à la libération ampérométrique détectée, ce qui contribuera beaucoup à la compréhension des différents facteurs de régulation de la sécrétion d'exocytose en raison de la spécificité de ces marqueurs fluorescents.



## **General introduction**

Vesicular exocytosis, an intracellular membrane trafficking pathway, is a ubiquitous process for intercellular communication in living things. It occurs when an intracellular vesicle fuses with the cell membrane and subsequently releases its contents (an infinitely minute number of chemical or biochemical messengers) to the extracellular space within a brief fraction of time (milliseconds to seconds), resulting in various physiological responses (insertion of particular receptors at defined areas of the plasma membrane, release of chemical/biochemical messengers, removal of waste products from the cell...). This specific exocytotic process is found to be involved in plenty of normal and pathologic events in living cells and its investigation thus attracts increasing research attentions.

So far, patch clamp, amperometry and total internal reflection fluorescence microscopy (TIRFM) are the three most frequently used techniques in exocytotic secretion studies. Nevertheless, the employment of one of these analytical methods solely seems not enough to fully illustrate the complex exocytotic process since each technique suffers from some shortcomings, like no information about the vesicular content (patch-clamp), the lack of spatial resolution (patch-clamp and amperometry) or the deficiency of temporal resolution (TIRFM).

In order to integrate the complementary advantages of these techniques for exocytosis detection, our group (thesis work of Anne Meunier, a former PhD in our group, 2008-2011) established a novel method in combination of TIRFM and amperometry which is capable of simultaneously monitoring the optical and electrochemical signals resulting from exocytotic secretions at the bottom of a single cell with excellent temporal (thanks to amperometry, ~ms) and spatial (owing to TIRFM, ~100 nm in the x-y plane and 10 nm in the z plane) resolutions. Such TIRFM/amperometry coupling test was achieved on BON BC21 cells (which stably expressed fluorescent GFP in the vesicles as optical probes and were loaded with electroactive serotonin as electrochemical probes) in an indium tin oxide (ITO, both transparent and electrically conductive) microchip. However, among all the exocytotic events recorded, only 22% clearly corresponded to simultaneous detection by amperometry and TIRFM, which ought to be mainly ascribed to the independent loading of these two probes. In this case, serotonin was poorly loaded inside the GFP-transfected vesicles because the resulting current spikes were quite low (ranging from 0.2 to 3.5 pA in magnitude), making it difficult to really 'see' these spikes without further data treating process. Therefore, in this thesis, we attempt to develop a unique probe exhibiting both fluorescent and electroactive characteristics so as to overcome the shortcomings caused by the separate loading of fluorescent and electrochemical reporters.

Fluorescent false neurotransmitters (FFNs), a group of new emerging optical and biocompatible probes, have successfully been applied to specifically stain secretory vesicles in various cell types, to visualize the neurotransmitter release, and to unveil functional parameters by optical imaging. In

consideration of the existence of hydroxyl groups on the benzene ring of some FFNs molecules which might endow them with decent electroactivities as well, they are thus highly probable to function as a dual probe (fluorescent/electrochemical) in the TIRFM/amperometry coupling technique.

The main goal of this work is to test the feasibility of using certain molecules in the FFNs family as optical/electrochemical difunctional probes to track exocytotic process in living cells by TIRFM/amperometry coupling technique. The coupling efficiency of optical and amperometric signals is expected to be improved since they origin from the same dual probe stored inside the secretory vesicles in the combined method. The manuscript is organized in the following way:

In **Chapter 1**, we report the state-of-the-art of research advances in this domain. The principle of vesicular exocytosis and their significant roles in life process are first recalled. Various detection methods and their analytical performances are then summarized and discussed. Particular attention is paid to amperometry and TIRFM. Methodologies for detecting single-cell events or population of cells are presented. Recent developments of FFNs in optical imaging are subsequently summarized and their potential electroactivity is finally discussed.

In **Chapter 2**, an analog of monoamine neurotransmitters (belonging to FFN family), 4-(2-aminoethyl)-6-chloro-7-hydroxy-2H-1-benzopyran-2-one hydrochloride (named as **1** in this thesis) is synthesized and the possibility of using this molecule as functional dual probes (fluorescent and electrochemical) is discussed. To be specific, the photophysical properties of **1** are firstly characterized (UV-vis absorption, excitation and emission spectra) and then the electrochemical detection of **1** in voltammetry is carried out on glassy carbon electrode, carbon fiber electrode and ITO microelectrode separately. The pH and concentration influences on the photophysical/electroactive characteristics of **1** are also studied in details.

In **Chapter 3**, we introduce **1** as a novel fluorescent probe to directly visualize and quantify the exocytotic secretions during the calcium-triggered exocytosis at single vesicle level. Two cell lines, PC-12 cells and BON N13 cells, will be employed and compared to characterize the kinetics of uptake and release of **1** by secretory vesicles. Furthermore, behaviors of **1**-stained vesicles adjacent to the plasma membrane before and during exocytotic release are also going to be visualized by virtue of bright fluorescence of **1** at TIRFM configuration.

In **Chapter 4**, we attempt to testify the capability of **1** functioning as an electrochemical probe for vesicular exocytosis tracking in BON N13 cells. Firstly, the design, fabrication, characterization and comparison of three ITO microdevices will be presented and discussed in detail. Then, the exocytotic release of **1**-stained BON N13 cells is going to be amperometrically measured in the microfabricated ITO chips. Finally, the comparison of the vesicular release detected at different configurations

(exocytosis at the cell apex recorded by CFE and those at the cell bottom monitored by ITO microelectrode) is carried out.

In **Chapter 5**, we present a microfabricated ITO device that allows coupling of two complementary analytical techniques for the direct and real-time analysis of exocytotic phenomena. Optical (TIRFM observation) and electrochemical (amperometric detection) signals resulting from exocytotic events of **1**-stained BON N13 cells are simultaneously detected in this ITO microdevice for the first time. The influence of 405 nm laser irradiation in TIRFM on amperometric recording as well as on exocytotic release process are studied and discussed as well.



# 1 Introduction

## 1.1 Vesicular exocytosis

Intercellular communication is a vital function of living things. It is normally achieved by the expulsion of biochemical or chemical molecules from an emitting cell to a target cell which is capable of detecting these specific messengers, resulting in various physiological responses depending on different stimulus. Vesicular exocytosis, an intracellular membrane trafficking pathway consisting of an outward flux of vesicular contents to the plasma membrane, represents a fundamental process of intercellular communications such as synaptic transmission and hormone secretion. It has been demonstrated that vesicular exocytosis shows significant importance in plenty of normal and pathologic events in cells, its investigation has thus attracted extensively research interest for several decades since its first discovery in the late 19th century by Ilya Mechnikov.<sup>[1]</sup> As a notable example, the Nobel Prize in Physiology or Medicine 2013 was awarded jointly to three scientists (James E. Rothman, Randy W. Schekman and Thomas C. Südhof) for their contributes to the discoveries of machinery regulating vesicle traffic.

### 1.1.1 Principle of exocytosis

In exocytosis, chemical/biochemical messengers stored inside the secretory vesicles are expelled by the emitting cell and their further diffusion toward the neighboring cells leads to various intercellular communications. For an individual secretory vesicle, four steps are mainly involved in the whole exocytotic process, as displayed in Fig.1-1.<sup>[2]</sup> First of all, for preparation, chemical/biochemical messengers (neurotransmitters, hormones...) that are essential for intercellular signal transmission, are internalized to fill the secretory vesicle core located in the emitting cell cytoplasm (Fig.1-1, step a). These messengers are cationically compacted in the vesicular matrix, behaving like a polyelectrolytic gel and are likely to participate in constitution of polyanionic proteins such as chromogranins. Secondly, upon an appropriate physiological stimulation (which provokes a  $\text{Ca}^{2+}$  entry or increase), the available vesicle is transported through cytoplasm towards the cell membrane where its contents will be fully eliminated. Then the secretory vesicle attempts to dock to the cell membrane with the help of specific protein-protein interactions, namely, the formation of SNAREs (soluble N-ethylmaleimide sensitive fusion protein attachment receptors, see section 1.1.2 for details) complex (Fig.1-1, step b). A small fusion pore is subsequently formed in the merged membranes, inducing the initial spontaneous release of vesicular contents to the extracellular medium (Fig.1-1, step c). In this step, exchanges of the cationic messengers in the matrix with small cations ( $\text{Na}^+$ ,  $\text{H}_3\text{O}^+$ ) in the extracellular medium lead to a destructure of the polyelectrolytic gel due to different molecular

and supramolecular interactions. Finally, the expansion of the fusion pore takes place, resulting in the expulsion of a larger flux of the chemical/biochemical messengers followed by an eventually ‘full fusion’ of the vesicle with the cell membrane (Fig.1-1, step d).

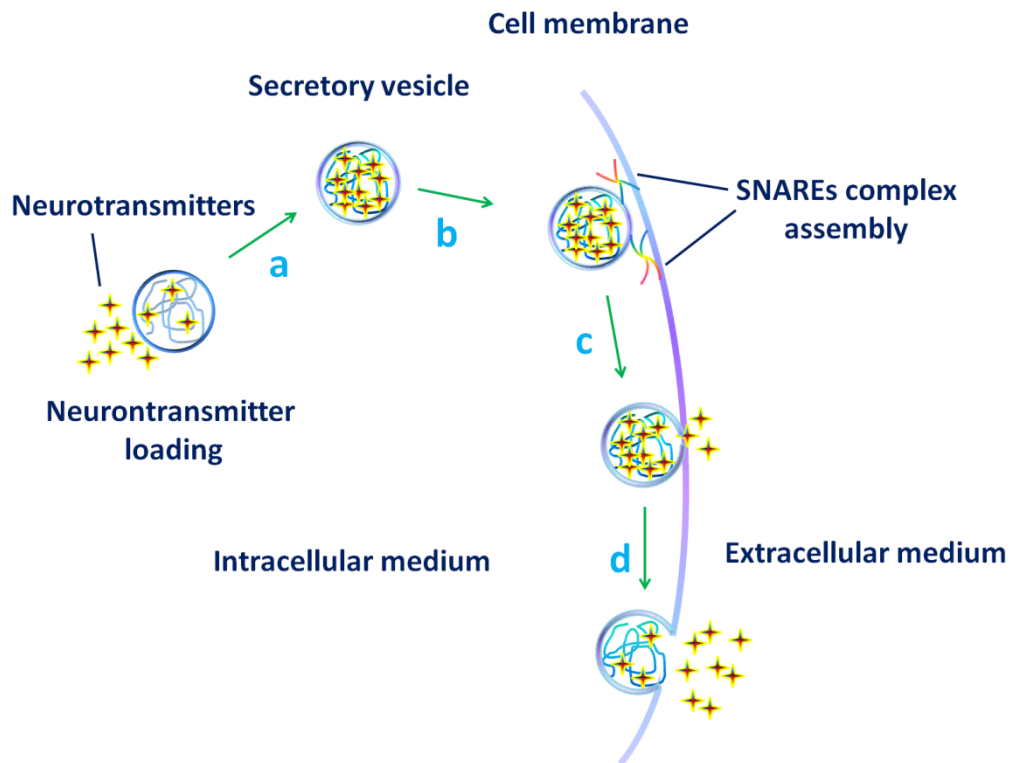


**Figure 1-1** Schematic representation of the main phases of vesicular exocytosis. Secretory vesicles that are primed to undergo exocytosis firstly fill their vesicular lumen with messenger molecules (step a); upon appropriate stimulation, they dock to the cell membrane by virtue of SNAREs proteins complex (step b); the cell and vesicular membranes mix and evolve to the formation of a fusion pore, through which vesicular contents begin to diffuse out the vesicular matrix (step c); fusion pore expansion occurs because of the cargo exchange between the intravesicular and the extracellular media, leading to the full fusion.

It is necessary to mention that besides ‘full fusion’ mode, there is another type of exocytotic release defined as ‘kiss-and-run’.<sup>[3]</sup> The major difference between ‘full fusion’ and ‘kiss-and-run’ appears in the last step of exocytosis where the nanometric fusion pore can either ‘expand’ or ‘close’ again, as illustrated in Fig.1-2. That is, in ‘kiss-and-run’ mode, the vesicle docks and transiently fuses with cell membrane forming a fusion pore through which vesicular contents are initiated to release. Instead of full fusion, the fusing vesicle closes the fusion pore, retains its gross shape, precludes full integration

into the cell membrane, and keeps enough molecular components for rapid retrieval, reacidification, and reuse. It must be emphasized that the increase of the intracellular  $\text{Ca}^{2+}$  concentration has been evidenced to play concomitantly an important role during all steps of the whole exocytotic process.

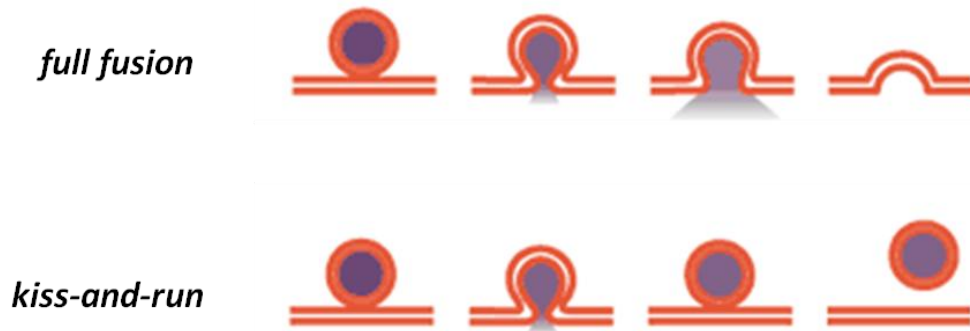


**Figure 1-2** Schematic drawing of two modes of exocytosis: full fusion (wherein the fusion pore rapidly expands to fully expel its contents, allowing the vesicle to fully flatten into the planar surface of the target) and 'kiss-and-run' (in which the vesicle releases part of its contents through a transient, narrow fusion pore while retaining its gross morphological shape). Image adapted from reference <sup>[4]</sup>.

### 1.1.2 SNAREs proteins in exocytosis

Before fusing with cell membrane, secretory vesicles must first become docked to the plasma membrane through the assembly of SNAREs protein complex at the docking site (Fig.1-b).<sup>[5, 6]</sup> Indeed, according to their locations, SNAREs proteins are usually divided into two categories: vesicular membrane proteins (v-SNAREs) which are incorporated into the membranes of transport vesicles, and target proteins or t-SNAREs which are anchored in the cell membrane.

As displayed in Fig.1-3, SNAP-25 (synaptosome-associated protein of 25 kDa) and syntaxin are two typical t-SNAREs located in the cell membrane while synaptobrevin is the v-SNAREs attached to vesicle membrane. When a secretory vesicle approaches to the cell membrane, these three proteins interact with each other to form a loose SNAREs complex with four helix coiled-coil motif at the docking site. The progressive tightening of the resulting SNAREs complex then generates energy through protein-lipid and protein-protein interactions and this energy allows overcoming the natural electrostatic repulsions between the cell and vesicular membranes, acting as a driving force to pull these two membranes within angstromic distances of each other prior to fusion.<sup>[7, 8]</sup> All these three

proteins involved in this significant process are essential during exocytosis and cleavage of any of these proteins severely impairs or abolishes exocytosis.<sup>[9]</sup>

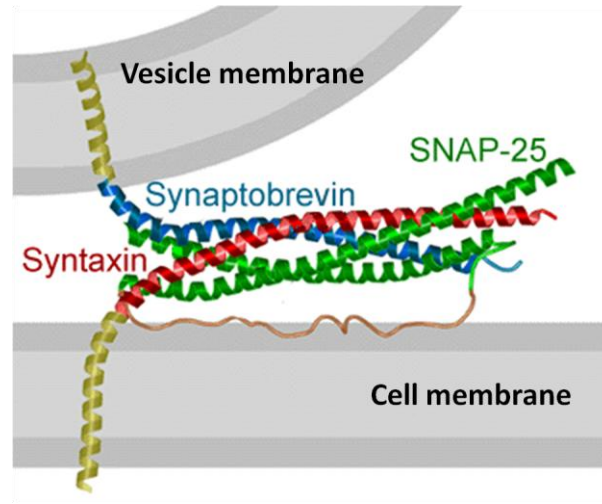


**Figure 1-3** The SNAREs complex is composed of three proteins: syntaxin (red), synaptobrevin (blue), and SNAP-25 (green). The transmembrane domains of syntaxin and synaptobrevin are shown in yellow. When the vesicle is close to the cell membrane, the three proteins coil into a helical structure, drawing the two membranes together. Image adapted from reference <sup>[7]</sup>.

### 1.1.3 Cell models for exocytosis investigation

For the sake of working as a decent model for exocytosis investigation, a suitable cell line must meet several criteria: firstly, cells ought to be relatively pure (containing little or no contaminants) and simple to prepare (allowing multiply subcultures); secondly, secretory vesicles in cells have to be sufficiently large and numerous so that exocytotic secretions are easy to observe; finally, the cells should be able to satisfy different requirements for various biochemical studies related to exocytosis such as the exocytotic mechanism, the specific role of some regulation proteins, drug delivery and the resulting effect, environmental factors influence and so on. Nowadays, many types of secretory cells have been employed as models to investigate the mechanisms of regulated vesicular exocytosis. In this section, we will introduce some cell lines which have been most frequently used to date.

#### 1.1.3.1 Neurons

Vesicular exocytosis is an essential biological process involved in the chemical synapse transmission occurring in neural communications. Neurons are thus employed as cell models for exocytosis

investigations. However, as primary culture cells, studies based on neurons indeed pose a number of problems. For instance, sufficiently pure neuronal preparations are difficult to obtain from nerve tissues. Furthermore, synaptic vesicles in neurons are usually few and small, and their exocytotic release is extremely limited, making it difficult to track the exocytotic secretion, either by optical or electrochemical techniques. Therefore, exocytosis studies are usually carried out with other cell models rather than neurons unless necessary.

### ***1.1.3.2 Neuroendocrine cells***

Among many cell models that have provides insights into exocytotic release, endocrine cells have taken a prominent place owing to their remarkable secretion ability as well as the diversity of available cell types.

- **Chromaffin cells**

Chromaffin cells are neuroendocrine cells found mostly in the medulla of the adrenal glands in mammals and they are generally derived from laboratory animals, mainly rats and mice, or from slaughterhouses in the case of bovine chromaffin cells. So far, most work on single vesicle exocytosis in living cells has been accomplished with the adrenal chromaffin cell model.<sup>[10]</sup> This ought to be greatly assigned to its favorable properties such as possession of relatively large vesicles (~170 nm radius in mean),<sup>[11]</sup> secretion of electroactive catecholamines, which facilitate their applications in optical imaging and electrochemical detections. Moreover, numerous knock-out animals are nowadays available. The comparison of present results with these further obtained by ‘knock-out’ chromaffin cells is considered to offer deeper insights into the exocytotic process. For this cell line, the major shortcoming is that chromaffin cells are quiescent. They therefore cannot divide and only a primary cell culture can be envisaged. This is why they have to be freshly derived from laboratory animals which is not convenient and increases cell variations.

- **PC-12 cells**

The PC-12 cell line was firstly isolated from a transplantable rat pheochromocytoma in 1976 by Greene and his colleagues.<sup>[12]</sup> PC-12 cells were found to be able to release electroactive monoamine neurotransmitters (dopamine) via exocytosis. Nowadays, this cell line has become popular choices in exocytosis studies owing to their extreme versatility for pharmacological manipulation, their ease of culture and the large amount of background knowledge on their proliferation.<sup>[13]</sup>

Notably, under the effect of NGF (nerve growth factor) treatment, PC-12 cells are differentiated, developing neurites which resemble the phenotype of sympathetic ganglion neurons. This specific

characteristic of PC-12 cells offers the opportunity to study the effect of cell differentiation as well as to use this cell line as a model of neurons.

However, there are today not one but multiple PC-12 cell lines that differ significantly from each other. In particular, some lines still secrete when others have lost this ability. Additionally, the size of secretory vesicles in PC-12 cells is relatively small (75~120 nm radius).<sup>[13]</sup> On one hand, the small size of vesicles makes it difficult to clearly visualize their behaviors by optical imaging. On the other hand, their rather low vesicular monoamine content leads to amperometric spikes with short time course and low current magnitudes in electrochemical monitoring of exocytosis.

- **Pancreatic  $\beta$  cells**

Pancreatic  $\beta$  cells are another type of neuroendocrine cells of which the primary function is to store and secrete a hormone called 'insulin' so as to reduce blood glucose concentration.<sup>[14]</sup> Researches on pancreatic  $\beta$  cells thus contribute a lot to the understanding of the role of exocytosis in diabetes disease. Because it is still difficult to work on primary culture cells, most of the work is therefore performed on tumor lines derived from  $\beta$ -pancreatic cells, such as cell line INS and MIN6.

- **BON cells**

BON cell line is an enterochromaffin line derived from a metastatic human carcinoid tumor of the pancreas. BON cells display morphological and biochemical characteristics consistent with the enterochromaffin cell phenotype, including the presence of numerous large secretory vesicles (100~150 nm radius)<sup>[15]</sup> and the expression and secretion of a variety of bioactive substances such as serotonin, histamine, prostaglandins, as well as neurotensin and other regulatory peptides.<sup>[16, 17]</sup> In addition, BON cells are easy to culture and transfect compared with chromaffin cells or other primary culture cells, and thus constitute a convenient model for exocytosis investigation.

Two stable clones of this cell line, BON BC21 and BON N13, have been successfully developed in order to satisfy different research requirements.<sup>[18]</sup> BON BC21 cells stably express green fluorescent protein-tagged neuropeptide-Y (NPY-GFP), a soluble luminal marker of secretory granule, making it an adapted model for optical visualization of exocytotic secretions.<sup>[19]</sup> In contrast, BON N13 cells do not express NPY-GFP. In addition, both cell lines have been demonstrated to have lost the ability to synthesize endogenous monoamine neurotransmitter serotonin.<sup>[18]</sup> That is, vesicular contents of BON N13 cells are neither fluorescent nor electroactive, making it a suitable cell line to load the fluorescent/electrochemical dual probe for exocytosis studies in this thesis.

Besides the neuron cells and neuroendocrine cells mentioned above, some hematopoietic cells including mast cells, basophil, eosinophils and neutrophil are also employed to study the exocytotic release from time to time.

## 1.2 Microelectrodes in electrochemistry

Microelectrodes, also commonly known as ultramicroelectrodes (UMEs), have been defined as electrodes of which at least one dimension (called critical dimension) is in the micrometre range, although some nanometric electrodes have also been fabricated. Compared with the conventional electrodes which generally have millimetric or even larger dimensions, UMEs possess several typical advantages in electrochemical detection, including efficient mass transport, short response time and high sensitivity.<sup>[20, 21]</sup> Their introduction to exocytosis investigation has led to unprecedented advances in this field.

### 1.2.1 Microelectrode geometry

For UMEs, only one critical dimension is necessary to be confined to micrometer range and thus various shapes have been developed to meet various requirements for practical uses. Fig.1-4 presents the five most popular UME geometries to date, including disks, rings, ring-disks, hemispherical/spherical electrodes and finite conical electrodes. Each type of these microelectrodes possesses peculiar features in mass transport while experiencing several essential rules in common (i.e. a voltammetric steady-state and show a short response time). We thus take the microdisk geometry as an example to illustrate the specific properties of UMEs compared with conventional electrodes with millimetric dimension in section 1.2.2.

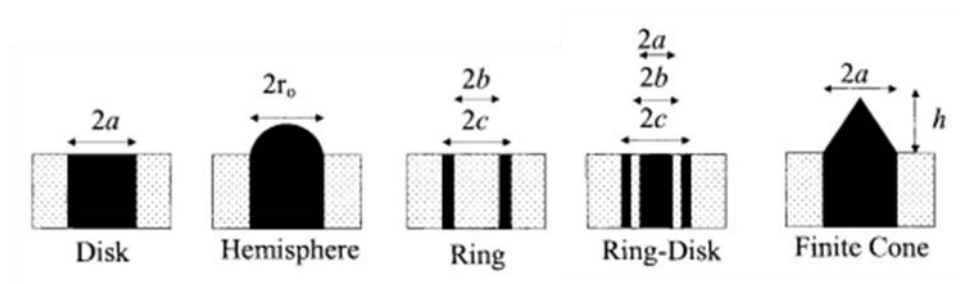


**Figure 1-4** Several typical UME geometries. *a*: radius of disk or finite conical electrode; *r*: radius of hemispherical electrode; *b*: inner radius of ring electrode; *c*: outer radius of ring electrode. Image adapted from reference<sup>[20]</sup>.

## 1.2.2 Properties of microelectrodes

- **Mass transport**

In electrochemical detection, when a heterogenous charge transfer is taking place at the electrode/liquid interface, electroactive substances at the interface will be rapidly depleted, generating concentration gradient between the interface and bulk solution, and thus setting off diffusive mass transport to and from the electrode. With respect to millimetric electrodes, the mass transport is dominated by linear diffusion to the electrode surface and the thickness of diffusion layer is at micrometric dimensions, as illustrated in Fig.1-5.

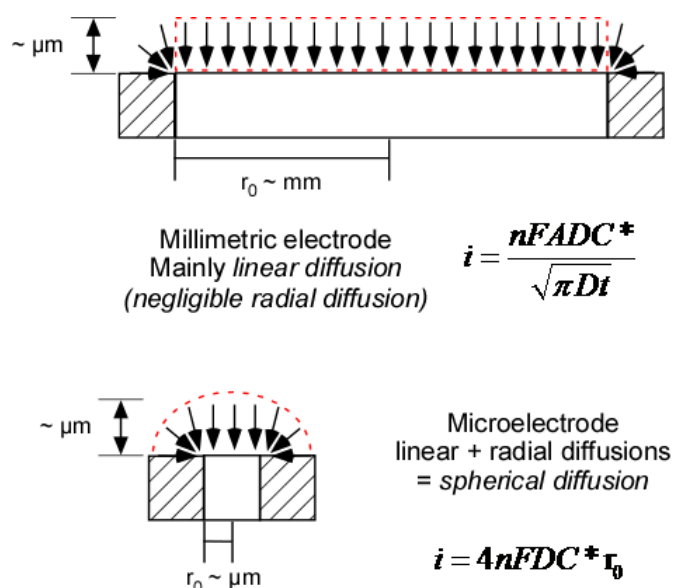


**Figure 1-5** Illustrations of the differences of diffusion fields of UMEs and conventional electrodes at millimetric dimension.

When the electrode size is decreased to UMEs level, which is comparable to the thickness of diffusion layer mentioned above, the usual linear diffusion is fastly ( $t > (r_0)^2/D \sim \text{ms}$ , where  $r_0$  is the radius of the disk electrode and  $D$  the diffusion coefficient) replaced by a spherical diffusion. This convergent diffusional regime thus leads to a steady state with a constant diffusion layer (a few  $r_0$ ) and a constant faradic current recorded at the electrode ( $4nFDC^*r_0$  for a disk microelectrode where  $F$  is the Faraday's number and  $C^*$  the bulk concentration of the electroactive species).

Electrochemical analysis using UMEs are similar to those employing conventional millimetric electrodes. That is, the current recorded with a microelectrode is directly proportional to the concentration without any temporal distortion as usually observed with millimetric electrodes.

- **Reduced response time**

When a potential is applied to the electrical cell, an electrochemical double layer is formed at the interface, behaving like an electrolytic capacitor. If the applied potential changes, a current flow through the solution resistance ( $R$ ) to charge the double layer capacitance ( $C$ ) is obligatory. Therefore, the potential at the interface could not attain the applied value unless the capacitance charging process is accomplished. Moreover, the capacitive and faradic currents are difficult to distinguish at short time.

Indeed, the double layer capacitance ( $C$ ) is found to be proportional to the electrode area ( $r_0^2$ ) and  $RC$  ( $R \propto 1/r_0$ ) is defined as the time constant ( $\tau$ ) that governs the exponential decay of the capacitive current. Therefore, the employment of UMEs with smaller sizes is a good choice to reduce the capacitance ( $C \propto r_0^2$ ) as well as the time constant ( $\tau \propto r_0$ ). The capacitive distortion with a UME is less limited for short time scales by comparison with millimetric electrodes. In other words, UMEs respond more rapidly to potential variations, making them very attractive for investigation of high speed electron-transfer reactions.

- **Improved sensitivity**

The signal-to-noise ratio is expected to be better with UMEs because the intrinsic capacitive noise depends on the electrode size (i.e. to  $(r_0)^2$ ) while the faradic current is proportional to the electrode radius ( $r_0$ ). The signal-to-noise ratio is thus proportional to  $1/r_0$ , thus making UMEs much appropriate for highly sensitive electroanalytical measurements.

- **Neglectable ohmic drop**

When faradic and capacitive currents pass through the solution resistance  $R$ , an ohmic drop ( $Ri$ ,  $R$  is the resistance while  $i$  is the total current) that can possibly alter the potential value of the working electrode is generated. With conventional millimetric electrodes, this might lead to severe distortions of experimental responses. In contrast, the ohmic drop effect seems to be negligible with UMEs because the detected faradic current is usually small and the capacitive current is minimized as well. In consequence, for experiments with UMEs, the counter-electrode is no longer required and a very basic two-electrodes configuration may be used thus facilitating the manipulations during the experiments.

## 1.3 Techniques for exocytosis investigation

As described in section 1.1, for intercellular communications, especially in the case of the chemical synapse transmission occurring in the neural communication, the chemical/biochemical messengers (neurotransmitters, proteins, hormones...) stored inside the secretory vesicles are expelled by the emitting cell to initiate the corresponding physiological responses of target cells. In the past several decades, the development of various analytical methods for the investigation of regulated secretory exocytosis is mainly based on two powerful routes, namely, optical and electrical techniques.<sup>[22]</sup> In this section, we will focus on the illustrations and comparisons of three analytical methods which have been mostly implemented in the past twenty years. That is, total internal reflection fluorescence microscopy (TIRFM) as well as the electrical techniques including patch-clamp and amperometry.

### 1.3.1 Electrical methodology

On account of the small size of individual secretory vesicles (usually 25~500 nm, depending on various cell lines),<sup>[23]</sup> the relatively low amount of molecules released, and the high speed at which vesicular content is extruded (usually  $\leq 100$  ms per event), analytical techniques for exocytosis investigation ought to possess some advantageous characteristics such as high sensitivity/signal-to-noise ratio, high spatial/temporal resolution so as to achieve a fundamental understanding of secretion process taking place in ultra small environments. That is why electrical methods based on microelectrodes with comparable sizes of cells have emerged as increasingly important techniques for studies of intercellular communications via vesicular exocytosis.

#### 1.3.1.1 Electrophysiological technique: patch clamp

Patch clamp has been firstly developed by Erwin Neher and Bert Sakmann (Nobel Prize in 1991) in 1976 for the detection of single ion channel currents across a membrane patch of a frog skeletal muscle.<sup>[24]</sup> It is an electrophysiological technique based on the measurements of electrical conductance and electrical capacitance which are closely related to the surface area of cell membranes. This approach has been proven to show distinct temporal resolution as well as high sensitivity to small variations of surface area of cell membrane, making it an appropriate tool to monitor membrane associated processes, such as the functions of ion channels and vesicular exocytosis.

- **Different detection configurations**

Patch clamp is usually carried out with a glass micropipette called a patch pipette as a recording electrode, and another electrode in the bath around the cell plays the role of the reference electrode. It is important to emphasize that, the recording electrode in patch clamp is sealed onto the

surface of the cell membrane so as to collect the resulting signals, rather than inserted through it. Moreover, the small size of the electrode at micrometer level ensures its ability to enclose/patch a membrane surface area containing just one or a few ion channels.

In fact, patch clamp is not only a technique used to study the functions of membrane channels but also an evolution allowing analysis of cellular transmissions at single cell level. Depending on different research interests, four patch clamp configurations have been mainly developed to date, including ‘cell-attached’, ‘whole-cell’, ‘inside-out’ and ‘outside-out’ recordings, as displayed in Fig.1-6.

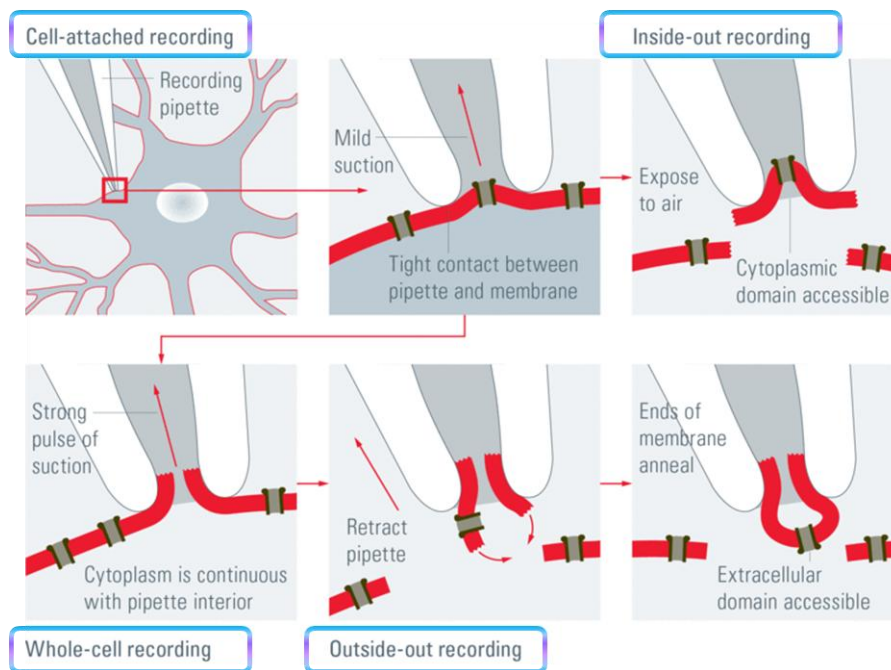


**Figure 1-6** The four recording configurations of patch-clamp. ‘Cell-attached’: when the pipette is in closest proximity to the cell membrane, mild suction is applied to gain a tight seal between the pipette and the membrane; ‘whole-cell’: by applying another brief but strong suction, the cell membrane is ruptured and the pipette gains access to the cytoplasm; ‘inside-out’: in the cell-attached mode, the pipette is retracted and the patch is separated from the rest of the membrane and exposed to air; the cytosolic surface of the membrane is thus exposed; ‘Outside-out’: in the ‘whole-cell’ mode, the pipette is retracted resulting in two small pieces of membrane that reconnect and form a small vesicular structure with the cytosolic side facing the pipette solution. Images adapted from: <http://www.leica-microsystems.com/science-lab/the-patch-clamp-technique/>.

'Cell-attached' is the patch clamp mode which allows the tracking of the ion channel conductivity as well as its ionic selectivity. In this configuration, the pipette is positioned in closest proximity to the cell membrane and mild suction is applied to achieve a tight seal between the pipette and the membrane. Owing to the small size of the pipette, the activity of only a few ion channels contained in the isolated membrane portion is recorded in this configuration. The study of the chemical and electrical properties of these isolated ion channels is thus possible.

'Whole-cell' is a recording configuration derived from the 'cell-attached' mode. Instead of a mild suction, a stronger suction is applied to achieve the seal between the pipette and the cell membrane. As a consequence, the membrane patch is disrupted and the interior of the pipette becomes continuous with the cytoplasm. This method is usually used to record the electrical potentials and currents from the entire cell.

Actually, both 'cell-attached' and 'whole cell' configurations aim at detection of electrical signals at single cell level. However, it is also possible to record signals only from a small patch instead of the entire cell which raises the chances of recording information from single ion channels. The patch can be orientated in two different directions inside the patch pipette. To achieve the 'inside-out' configuration, the patch pipette is attached to the cell membrane and is then retracted to break off a patch of membrane. In this case, the cytosolic surface of the membrane is exposed. This is often applied to investigate single channel activity with the advantage that the medium exposed to the intracellular surface can be modified.

If the aim is to study the influence of extracellular impact factors, the 'outside-out' configuration should be chosen. In this case, the pipette is retracted during the 'whole-cell' configuration, causing a rupture and rearrangement of the membrane. As a consequence, single/several ion channels are isolated from the cell and exposed successively to different solutions on the extracellular surface of the membrane, enabling to investigate effects of a variety of solutions in a relatively short time.

- **Exocytosis investigation by patch clamp**

The temporal resolution of patch clamp is in the order of milliseconds, comparable to the time course of rapid exocytotic process. It was firstly introduced to the investigation of vesicular secretions in chromaffin cells in the early 1980s<sup>[25, 26]</sup> and is then applied to various cell lines such as pancreatic  $\beta$  cells, neutrophils, and mast cells.

In patch clamp, the cell membrane serves as an electrical capacitor of which the capacitance is proportional to cell surface area. For an individual exocytotic event, the vesicular membrane is fully or partly incorporated to the cell membrane, resulting in an increase in the total cell surface. Consecutive fusions of individual secretory vesicles with the cell membrane are thus expected to be depicted as continuous increases of capacitance detected in patch clamp. This viewpoint has been demonstrated by

studies on chromaffin cells in ‘whole-cell’ configuration. That is, an increase in the overall membrane capacitance was detected because of exocytotic response upon extensive stimulation.<sup>[25]</sup> However, no available information was obtained at single vesicle level because the high secretion frequency and the small size of secretory vesicles make it difficult to distinguish the exocytotic events concurrently taking place. On the contrary, for mast cells with bigger secretory granules (~2.5  $\mu\text{m}$  diameter), individual exocytotic secretions appeared as ‘stepwise’ increases in capacitance at the same detection configuration, owing to larger vesicular size resulting in more apparent surface area variations.<sup>[27]</sup>

Indeed, remarkable progress for exocytosis investigation has been achieved by conducting the capacitance measurement at ‘cell-attached’ configuration. Such recording configuration presents a higher signal-to-noise ratio than whole-cell recordings, allowing the tracking of small changes of membrane surface caused by exocytosis. For instance, for a single secretory cell, continuous fusions of individual secretory vesicles with the cell membrane were depicted as a series of ‘stepwise’ increases in capacitance and each ‘stepwise’ increase represented a single exocytotic event, as shown in Fig.1-7. Moreover, researches based on patch clamp also reveal a lot of information regarding to the details of exocytotic process such as the specific role of calcium in the regulation of the membrane fusion.<sup>[28, 29]</sup>

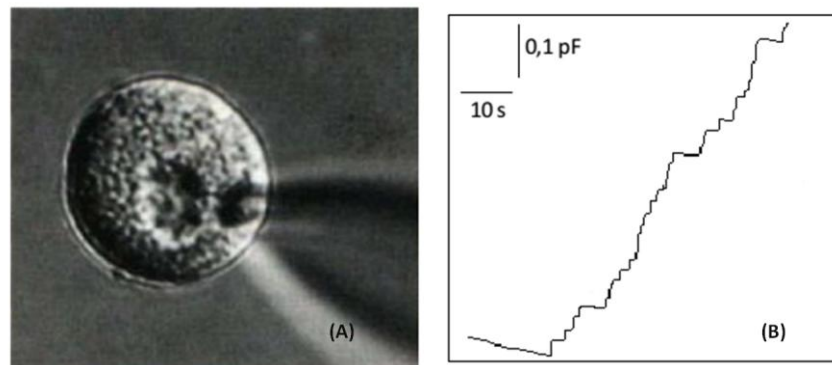


**Figure 1-7** (A) a single secretory mast cell measured by patch clamp at ‘cell-attached’ configuration; (B) A series of capacitance changes resulting from the fusion of secretory vesicles with the cell membrane and each ‘stepwise’ increase is caused by an individual exocytotic event; images adapted from reference <sup>[30]</sup>.

Among different analytical methods for exocytosis investigation, patch-clamp has demonstrated its particular importance in examining and characterizing exocytotic fusion pores and synaptic membrane events. However, beyond the mechanical stress it imposes on the cell studied, this method is not able to provide chemical or kinetic information about granular content released from the vesicle following complete opening of fusion pores. Furthermore, it lacks the spatial information of the locations where

secretory vesicles undergo exocytosis. Moreover, this technique is also sensitive to endocytotic events, a phenomenon of membrane internalization and the overlapping of endocytotic and exocytotic signals can then trigger the underestimation of the contribution of exocytosis.

Nevertheless, in the context of exocytosis analysis, patch-clamp is a powerful research tool that is readily coupled to several complementary methods such as amperometry or fluorescent microscopy. For instance, coupled with amperometry, this technique not only confirms the existence of the fusion pore, but also allows the observation of the exocytotic dynamics as well as the determination of the fusion pore size (see section 1.3.3.1). While being combined with fluorescence microscopy, it permits distinguishing different granular populations differentiated by their fusion kinetics (see section 1.3.3.2).

### ***1.3.1.2 Electrochemical technique: Amperometry***

The release of monoamine neurotransmitter through exocytosis is one of the most common ways for intercellular communications.<sup>[31, 32]</sup> A unique feature of some well-known monoamine neurotransmitters is their electroactive property which promises the possibility of using an electrochemical technique to quantitatively detect these molecules secreted in exocytosis.<sup>[33-35]</sup> In the 1990s, owing to the electroactivity of catecholamine, their quantal secretion was electrochemically monitored for the first time by amperometry and cyclic voltammetry with a carbon fiber microelectrode (CFE) placed adjacent to a single chromaffin cell by Wightman and his colleagues.<sup>[36, 37]</sup> After two decades of development, amperometry has become the most widely used electrochemical technique for exocytosis investigation because of its remarkable advantages such as facility to implement, high temporal resolution as well as high sensitivity.<sup>[2, 35, 38]</sup>

- **Basic principle of amperometry**

Amperometric tracking of vesicular exocytosis is commonly based on the oxidation of electroactive chemical/biochemical messengers on the electrode surface when they are released from vesicular lumens to extracellular spaces upon proper stimulation (Fig.1-8).

To perform the amperometric measurement, a microelectrode with comparable size of cells is directly in contact with the membrane of target cells, either on the top or at the bottom (depending on the research interest). A constant potential at which electroactive molecules extruded during exocytosis is able to be oxidized (in a diffusion controlled way) is then applied to the microelectrode and the resulting electrochemical current is monitored with time. In this configuration, the diffusion layer is the separation between the cell and electrode, leading to very steep concentration gradients to which the electrode will be very sensitive. Such an experimental configuration mimics the chemical synapse,

the working electrode here corresponding to the receiving neuron. This is why it is sometimes called the ‘artificial synapse’ configuration.

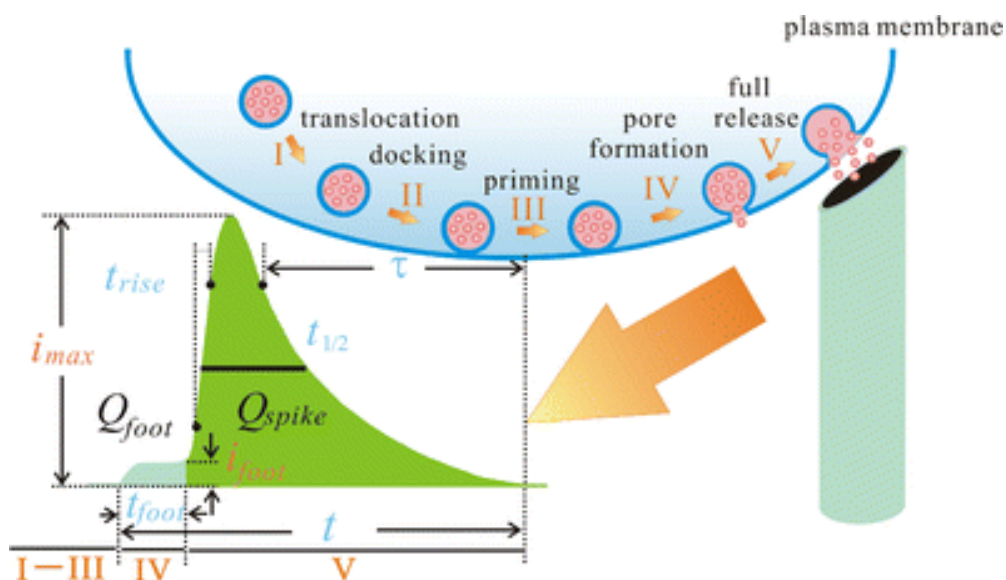


**Figure 1-8** Schematic representation of the experimental configuration (‘artificial synapse’ configuration) involving amperometric measurements. The late phases of fusion pore opening and the full release can be respectively revealed by a smaller foot/pre-spike feature (PSF) and the main current spikes resulting from oxidation of the discharged transmitters at a CFE positioned against to the cell membrane. Major relevant quantitative and kinetic information can be extracted from an amperometric spike to investigate a single exocytotic event. Image adapted from reference <sup>[39]</sup>.

As shown in Fig.1-8, for an individual exocytotic event, the late phases of fusion pore opening and the full release can be respectively revealed by a pre-spike feature (PSF) known as the amperometric foot and the main current spikes. To be specific, in response to an appropriate stimulation, a nanometric fusion pore is formed to transport electroactive contents (usually monoamine neurotransmitters) to the extracellular space (i.e. tightly attached microelectrode surface), creating a known as an amperometric foot. With expansion of the fusion pore, there is a rapid flux of transmitter onto the electrode surface, which generally leads to a sharp current transient with a shape characterized by a fast but not instantaneous rise to a peak amplitude and a more gradual decay to baseline.<sup>[40]</sup> It is necessary to note that, in many cases, current spikes resulting from vesicular exocytosis do not possess an amperometric foot and this is mainly considered to be caused by their too fast time course beyond the temporal resolution of amperometry.

- **Specific characteristics of amperometry**

The first and most important exquisite property of amperometry for exocytosis monitoring is its excellent temporal resolution at milliseconds level which allows detailed real-time analysis of the kinetic processes involved in extrusion of vesicular contents into the extracellular space. Another advantageous characteristic of amperometry is its favorable ability for quantitative characterization of exact exocytotic release at single vesicle level. For each amperometric spike, the integral of the current with respect to time yields the measured charge (Q) which is related to the number of moles of material detected (N) by Faraday's law,

$$Q = nFN,$$

where n is the number of electrons involved in the electrochemical reaction (n = 2 for catecholamines) and F is Faraday's constant (96,485 C/mol).

- **Contributions of amperometry for exocytosis investigation**

- (a) **Evidences of multiple vesicular populations**

The co-existence of multiple populations of granules in the same cell line has been demonstrated by statistic analysis of the histogram distributions of integral charge (Q) per amperometric spike, which is closely related to the vesicular radius by combining the Faraday's law and the formula of the spherical volume:

$$r = \left( \frac{3Q}{8\pi F C_{ves}} \right)^{1/3}$$

Assuming that the concentration of oxidized molecules ( $C_{ves}$ ) stored inside secretory vesicles is a constant value, it is thus the vesicle size (r) which plays a decisive role in the resulting integral charge (Q) detected on the surface:

$$r \propto Q^{1/3}$$

According to the equation above, the radius of an individual secretory vesicle (r) is proportional to the cube root of the corresponding amperometric charge ( $Q^{1/3}$ ).

For instance, in chromaffin cells, distributions of their vesicular radius were depicted as the sum of two Gaussians distributions by amperometry (by the mean of  $Q^{1/3}$ ), as shown in Fig.1-9(B). Since vesicle radius of the same population usually distribute as a Gaussian, the amperometric results in the given example suggest that chromaffin cells possess at least two populations of dense-core vesicles

with specific secretory properties. This viewpoint is further confirmed by the similar vesicular radius distributions obtained by electron microscopy, as presented Fig.1-9(A).<sup>[41]</sup>

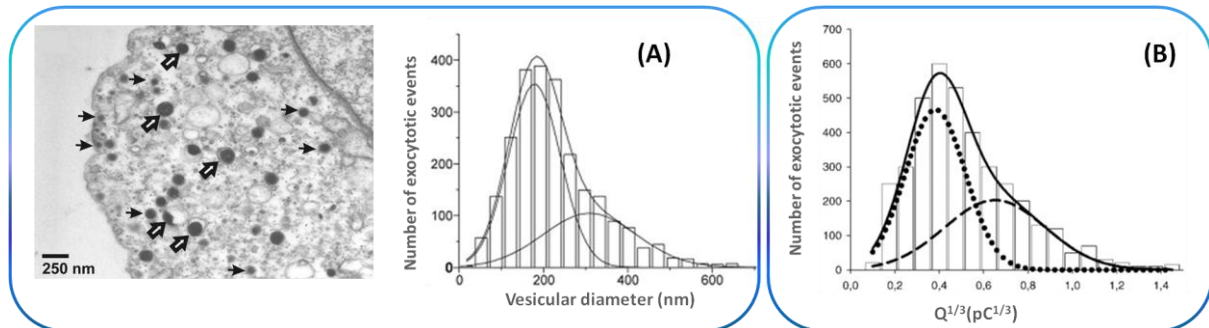


**Figure 1-9** (A) Direct analysis of dense-core vesicle diameter obtained by electron microscopic measurements and two vesicular populations were observed; (B) Example of quantitative analysis of dense-core vesicle size provided by amperometric measurements (the vesicle diameter is assumed to be proportional to  $Q^{1/3}$ ). Two vesicular populations can be fitted with the sum of two Gaussian distributions, showing the same statistical distributions as that visualized by electron microscopy. Figure adapted from reference <sup>[41]</sup>.

By performing a more accurate analysis of the charge  $Q$  from amperometric detection, Tang et al. found that the  $Q^{1/3}$  distribution of chromaffin cells could be reasonably described by the summation of at least three Gaussians, suggesting that they contained at least three distinct populations of granules, with a small, medium or large modal  $Q$  whereas the proportion of each vesicular population was not constant.<sup>[42]</sup> Interestingly, the detected charge  $Q$  and the relative proportion of the vesicular populations, were likely to be modulated by various parameters such as the duration of the cell culture before experiments, specific chemical stimulation as well as the extracellular environment properties like osmolarity.<sup>[42, 43]</sup> This interesting discovery raises the possibility that distinct populations of granules in chromaffin cells can be regulated either differentially or uniformly with proper treatment.

By virtue of amperometric measurement, the fact that at least two vesicular populations participate concurrently in exocytosis has been extended to other cell lines such as PC-12 cells,<sup>[13, 44]</sup> Retzius cells of the leech,<sup>[45-47]</sup> and neuron of *Planorbis corneus*.<sup>[48-51]</sup>

## **(b) Investigations of influences of the physico-chemical parameters**

Vesicular exocytosis is a physiological process which is closely related to plenty of physico-chemical parameters. To date, the effects of pH,<sup>[52-55]</sup> temperature<sup>[56-58]</sup> and osmolarity<sup>[43, 59, 60]</sup> have been largely investigated by amperometric measurements.

### **pH effect**

In physiological conditions, the pH gradient between the acidic vesicular lumen and the neutral extracellular medium is responsible for the accumulation of amines, ATP because their transporters use H<sup>+</sup> as the counter ion.<sup>[52, 61, 62]</sup> Similarly, it ought to also play an important role in the regulation of exocytosis through which these contents are expelled to the extracellular space in the reverse way. To elucidate the pH effect on exocytotic release, amperometric detections were usually carried out in two ways: by adjusting the intravesicular pH values or by modifying the pH of the extracellular medium, respectively.

Here, we take chromaffin cells as an example to illustrate the pH effect observed by electrochemical detections. The comparison of amperometric results obtained at different extracellular pH shows that the decrease of pH value of extracellular medium from 7.4 to 5.5 was accompanied by the slower kinetics of release as well as the less amount of secreted catecholamines.<sup>[63, 64]</sup> In contrast, regarding to the pH inside the secretory vesicles, their alkalization by using drugs to block vesicle proton pumps induced a deceleration in the dynamics and a fall in the released quantities, whereas acidification of the vesicular lumens caused the opposite effect.<sup>[54]</sup>

Notably, the impact of pH on exocytosis is complicated and strongly relies on the cell models and the compounds stored inside the acidic vesicular lumens.<sup>[65]</sup> It is thus difficult to draw a general conclusion adapted to different cell lines. For instance, in PC-12 cells, the vesicular dopamine automatically diffused to extracellular space without the application of any secretagogue by declining the external pH to 6.8.<sup>[66]</sup> With respect to another cell line, pancreatic  $\beta$  cells, which release both insulin and serotonin during exocytosis at proper conditions, the increase of extracellular pH from 6.9 to 7.9 accelerated the release of insulin (confirmed by a narrower amperometric spikes resulting from insulin oxidation), whereas the same treatments did not impact the secretion of serotonin.<sup>[55]</sup> Moreover, when extracellular pH was quite low, at 6.4, no insulin extrusion could be detected, proving that proper extracellular pH was essential to insulin release via vesicular exocytosis.<sup>[67]</sup>

### **Temperature influence**

The influence of temperature on exocytosis was evaluated from several cell models by amperometry. From a physiochemical viewpoint, temperature augmentation would not only increase the expansion

of vesicular matrix but also change the viscosity of the membrane while these conditions would favor the achievement of exocytosis events. As expected, in both chromaffin cells and mast cells,<sup>[56, 57]</sup> increasing the temperature from room temperature to physiological temperature (37°C) was accompanied by increases in the frequency of exocytotic events, the quantity of molecules released by individual vesicles and an acceleration of the release kinetics. In the case of platelets, the exocytotic frequency seemed to be higher but the amount of molecules released from each event does not change at higher temperature (37°C).<sup>[58]</sup>

### Osmolarity effect

External osmolarity modulation is likely to alter the tension in the cell membrane and thus impact the rate, duration and amount of transmitter release during exocytosis. For instance, when chromaffin cells were incubated in a hypotonic medium of low osmolarity (200 mOsm) during amperometric measurement, the frequency of the exocytotic events was significantly increased compared with that obtained from cells under physiological conditions (315 mOsm).<sup>[43]</sup> In contrast, a progressive decrease of the amperometric peak frequency was observed when cells were exposed to hyperosmotic media of which the osmolarity increasing from 630 mOsm to 970 mOsm. Additionally, the mean decreases of exocytosis frequency at 630 mOsm to 970 mOsm were around 50% and 90%, respectively.<sup>[60]</sup> Moreover, an increase in the number of release events displaying an amperometric foot (see Fig.1-8) was observed when PC-12 cells were stimulated in high osmolarity saline solutions (700 mOsm) during amperometric measurement of vesicular dopamine releases.<sup>[59]</sup>

### **(c) Studies of effects of biological parameters**

SNAREs proteins, the cytoskeleton (especially actin), membrane curvature, vesicular contents as well as some other biological parameters are likely to participate in and affect vesicular exocytosis. Amperometry seems to be capable of revealing their roles in this complex process to some extent.

### SNAREs proteins function

The formation of SNAREs protein complex by v-SNAREs linked to t-SNAREs is commonly considered to play a crucial role in vesicular exocytosis, especially in the recognition of exocytotic locations on the cell membrane (see section 1.1.2). This viewpoint has been electrochemically confirmed by the fact that the frequency of amperometric spikes dramatically decreased when SNAREs proteins were modified or cleaved by specific neurotoxins.<sup>[68, 69]</sup> Moreover, functions of some other biological factors which affect the exocytotic process through their interactions with SNAREs protein complex have also been investigated by amperometry. For instance, N-ethylmaleimide-sensitive factor (NSF) and soluble NSF attachment protein (alpha-SNAP), two proteins required for SNARE complex disassembly, were found to play a role in priming granules for

release at an early step.<sup>[70]</sup> Additionally, the overexpression of complexin (a protein binding specifically to the assembled SNAREs complex) in chromaffin cells modified the kinetics of vesicle release events. The resulting amperometric spikes showed a shorter time course, indicating this protein regulated the closure of the fusion pore in exocytosis.<sup>[71]</sup> The functions of Munc18-1, a protein essential to neurotransmitter release, have also been more and more characterized by amperometric measurement.<sup>[72-74]</sup> Burgoyne and his colleagues found that this protein influenced all of the steps (vesicle recruitment, tethering, docking, priming, and membrane fusion) leading to exocytosis through its multiple interactions with SNAREs complex.<sup>[72]</sup>

### Actin effect

In early studies, actin was mainly considered as a physical barrier for exocytotic secretion because transient depolymerization of cortical actin filaments was obligatory and energy-consuming for secretory vesicles to fuse with cell membrane. If secretory cells are treated with special drugs such as Latrunculin A that causes the disassembly of filamentous actin (F-actin)<sup>[75, 76]</sup>, the vesicular exocytosis is thus expected to be promoted.<sup>[75-77]</sup> For instance, amperometric measurements on single taipoxin-treated cells (note that taipoxin is a neurotoxin leading to fragmentation of F-actin cytoskeleton) proved that the number of released vesicles was increased because of taipoxin treatment whereas kinetic parameters of individual vesicle fusions were not altered.<sup>[77]</sup> Similar results were obtained in platelet dense-body secretion.<sup>[76]</sup> These results support the previous viewpoint that actin impeded of the exocytotic release, serving as a physical barrier.

However, experimental evidence has been accumulated in recent years suggesting that the actin cytoskeleton is likely to be also involved in regulating vesicular exocytosis, playing a relative active role in this complex process.<sup>[78, 79]</sup> For instance, the group of Lindau discovered that, in chromaffin cells, actin and myosin II facilitated exocytotic release from individual granules by accelerating dissociation of catecholamines from the vesicular matrix possibly through generation of mechanical forces.<sup>[80]</sup> Moreover, it was evidenced in PC-12 cells that the actin cytoskeleton probably mediated the constriction of the fusion pore and was able to control the fraction of neurotransmitters released in an extended 'kiss-and-run' release mode.<sup>[81]</sup> Another recent finding supporting the active role of actin in exocytosis was that F-actin contributed to the formation of granule docking sites in nicotine-stimulated chromaffin cells.<sup>[82]</sup>

In consideration of the amperometric results related to actin influence on exocytosis, it is more reasonable to believe that actin plays a dual role in exocytosis but how it coordinates these two contrary functions needs to be further figured out with more deeper studies or in combination of additional results obtained by other analytical methods with complementary feature.

#### (d) Mapping the cell surface

The lack of spatial resolution is the major constraint of amperometry. In order to improve spatial resolution of this technique, people mainly make efforts on two ways (minimization of the dimension of individual microelectrodes and fabrication of multiple microelectrode arrays (MEA) of subcellular size) to collect electrochemical information regarding to exocytotic zones on the surface of individual cells.

By simultaneously positioning two independent CFE (~5  $\mu\text{m}$  diameter) on the single cell surface, Wightman and his coworkers discovered for the first time that exocytosis seemed not to be homogeneous at the cell membrane and there were active and passive zones of exocytotic activity in chromaffin cells.<sup>[83]</sup>

Further improvement of the electrochemical ‘mapping’ of heterogeneous secretions were achieved by the employment of various MEA based on microfabrication. For instance, Fig.1-10(A) presented a microdevice embedded with four independent platinum microelectrodes capable of testing the heterogeneity of exocytosis in chromaffin cells. The single target cell was placed at the device center by a patch pipette and subsequent amperometric measurement was carried out by simultaneously monitoring current variations from different cellular compartments lying on the electrode surfaces. The resulting four amperometric traces in the four channels revealed the different secretion activities of these four detected zones on the electrodes (Fig.1-10(B)).

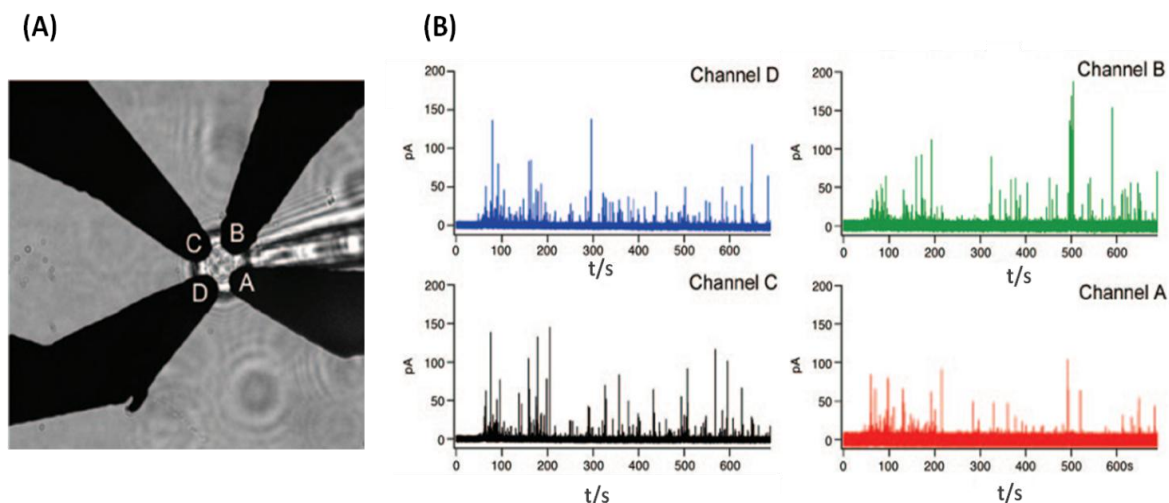


**Figure 1-10** (A) Microscope image of a chromaffin cell placed on top of MEA, with four electrodes labeled A through D; (B) Amperometric traces of the single cell recorded by the four independent microelectrodes. Figure adapted from reference<sup>[84]</sup>.

In recent years, owing to the rapid development of microfabrication technique, plenty of MEA devices were validated for the application of spatially mapping of exocytotic activity at single or clusters of secretory cells.<sup>[85-88]</sup> Nevertheless, to date, the progress of electrochemically mapping of exocytosis at the single cell level is not satisfying because the spatial resolution is still not good enough, especially compared with that of TIRFM (~nm).

#### **(e) Study of the initial fusion pore**

In cellular exocytosis, fusion of a secretory vesicle with the cell membrane is commonly considered to begin with the SNAREs complex-coordinated formation of 'fusion pore', a nanometric channel connecting vesicular lumens and extracellular spaces.<sup>[89, 90]</sup> The PSF detected in amperometry is usually ascribed to the oxidation of a small amount of electroactive vesicular contents released through such a 'fusion pore' to the electrode surface, which was firstly reported by Chow and his colleagues,<sup>[91, 92]</sup> and subsequently confirmed by the correlation of simultaneous patch-clamp and amperometric measurements in beige mouse mast cells.<sup>[93]</sup> Actually, not all the current spikes possess a PSF. For instance, in chromaffin cells, only 30% of the exocytotic events have a sufficiently long-lived fusion pore to be electrochemically detectable whereas the other 70% becomes sightless in amperometry because of their short life.<sup>[94]</sup>

As displayed in Fig.1-11, an individual PSF is usually characterized by three main parameters, namely,  $t_{foot}$ ,  $I_{foot}$ , as well as  $Q_{foot}$ , so their variations are expected to reflect those of the pore and of the intravesicular media. Notably, the integrated area of PSF ( $Q_{foot}$ ) represents precisely the amount of molecules released through the fusion pore, prior to full fusion and the duration of such release ( $t_{foot}$ ) reflects the lifetime/stability of the fusion pore structure.<sup>[35]</sup> The analysis of PSF thus allows precise characterization of the dynamics of fusion pore formation and pore stability.

In addition, the influence of external physico-chemical parameters and pharmacological/genetic manipulations on exocytosis can be studied according to single PSF feature in combination of PSF frequency (the ratio of spikes with PSF among all the detected events). For example, in chromaffin cells, various modulations on cell membrane properties (the insertion of exogenous lipids to modify the membrane curvature<sup>[95]</sup>, temperature or external osmolarity regulations<sup>[94]</sup> to interfere with the membrane tension and viscosity...) did not alter the PSF frequency and the amount of catecholamines released during PSF whereas the kinetics of the fusion pore was greatly modified, suggesting that the presence of a PSF was related to the internal structure of the secretory vesicles. In contrast, the modification of the vesicular internal contents (L-dopamine or reserpine treatments)<sup>[94, 96]</sup> was demonstrated to have strong effects on both the PSF frequency and its kinetics.

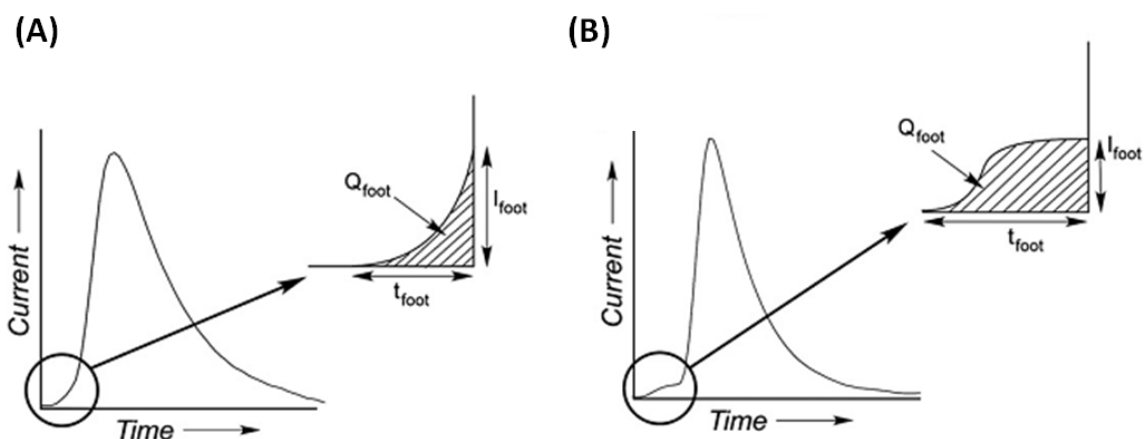


**Figure 1-11** Two shapes of amperometric events with a PSF. (A) Only a ramp is achieved before the spike onsets; (B) The foot current is stabilized as a plateau after its initial rising phase. In both cases, a zoom of a PSF and a representation of the quantitative ( $Q_{\text{foot}}$ ) and kinetic ( $t_{\text{foot}}$ ,  $I_{\text{foot}}$ ) parameters for PSF characterization is provided for clarity. Figure adapted from reference <sup>[94]</sup>.

- **Developments of microdevices in amperometry**

In the past twenty-five years, amperometric detection with CFE significantly contributed to the understanding of the exocytotic mechanism itself as well as various physico-chemical/biological parameters affecting the vesicular release. Nevertheless, this method itself owns several intrinsic limitations. The first one concerns the fact that in this method, only a single cell could be tested each time. People thus have to perform a large number of repeated experiments in order to acquire enough data for statistical analysis as well as to overcome the cell variability. The second constraint of this method is that only about a maximum of 15% of the total exocytotic events can be recorded by CFE because not all the cell surface secretion is probed,<sup>[97-99]</sup> and all these detected electrochemical signals come from the exocytotic releases occurring at the apical pole whereas those events taking place at other locations, especially at the basal pole, are usually neglected. Moreover, this approach does not show spatial resolution at the subcellular scale. In other words, we can never locate the corresponding secretory vesicles of the detected amperometric spikes solely by this technique. To conquer these drawbacks mentioned above, nowadays, people developed plenty of other microdevices/microsystems for real-time amperometric determination of cellular exocytosis to satisfy different research requirements.

Indeed, in recent years, owing to the blooming microfabrication procedures, various electrically conductive materials (carbon<sup>[100, 101]</sup>, Pt<sup>[84, 102]</sup>, Au<sup>[103, 104]</sup>, ITO<sup>[95, 105-107]</sup>, conductive polymers<sup>[108]</sup>...)

have been employed to fabricate UMEs for exocytosis investigation by amperometry. A particular advantage of these microfabricated electrodes is that they can be designed and fabricated with virtually any size and geometry. Moreover, microelectrodes in arrays allow multiple single cell measurements or recordings from multiple sites of a single cell.

**(a) Microdevices for analysis at the single cell level within a cell population**

In order to avoid the numerous independent experiments performed by CFE, some novel microdevices allowing rapid and high through-out detections are therefore developed so as to increase the number of release events detected during each performance. It is worth mentioning that the high through-out property of these microfabricated devices are usually achieved by the embedded multiple microelectrode arrays (MEA) and the resulting amperometric spikes come from multiple cells rather than a single cell. The three main designs of microchips suitable for ‘cell populations’ investigations are displayed in Fig.1-12. Typical examples are going to be presented and discussed in this section.

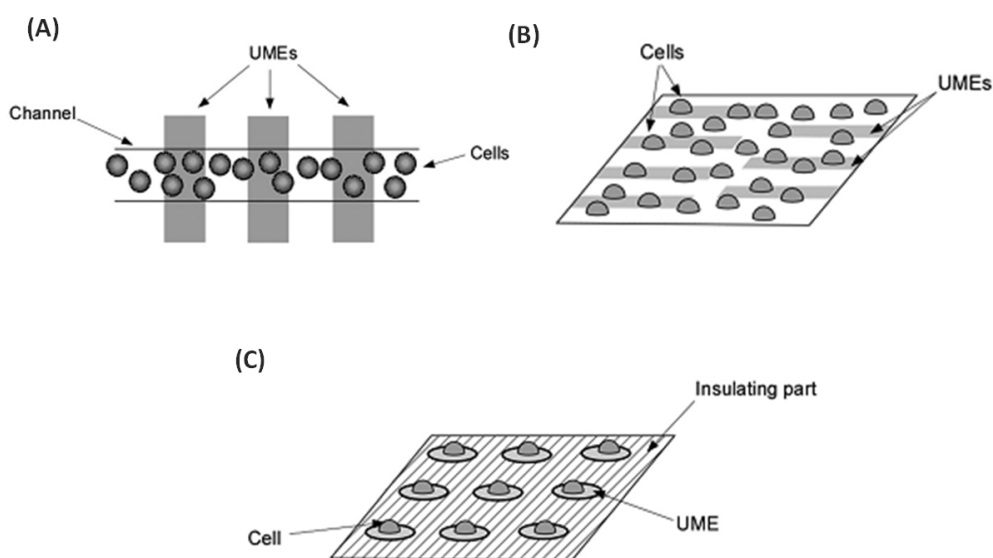


**Figure 1-12** Schematic views of the main strategies for the investigation of cell population using MEA: (A) within a microchannel; (B) with a cell population randomly adhered on MEA; (C) with a cell population selectively adhered on the UME surfaces. Figure adapted from reference <sup>[109]</sup>.

The first application of MEA-integrated biochip for the temporal detection of vesicular exocytosis was accomplished by Cui and his colleagues.<sup>[103]</sup> Their biochip consisted of a  $5 \times 5$  array of Au disk

microelectrodes (25 UMEs in total) of which the diameters ranged from 10 to 90  $\mu\text{m}$  and the distance between the centers of two neighbor electrodes was 250  $\mu\text{m}$ . A mouse mesencephalic dopaminergic cell line, MN9D cells, was able to grow in the microchip and some of them located right on the Au UMEs surfaces. Then, upon the application of high KCl concentration, vesicular exocytosis was triggered, resulting in the secretion of electroactive dopamine. For those cells lying on the MEA surfaces, their exocytotic processes were thus simultaneously recorded by amperometry as the oxidation of released dopamine on MEA surface.<sup>[103]</sup> Similar results were also obtained in PC-12 cells with the same microdevice.<sup>[104]</sup>

For the given example, secretory cells were distributed randomly on the MEA surface. However, thanks to the rapid development of ‘lab-on-a-chip’, nowadays, it is also possible to fabricate various microdevices allowing positioning cells onto the electrode surface or confining cells in the microfluidic channels/wells as expected.<sup>[110-112]</sup>

### **(b) Microdevices for analysis at the single cell or subcellular level**

Exocytosis activity in a single cell is confirmed to be inhomogeneous and secretions are concentrated at specific zones termed as ‘hotspots’. The existence of ‘hotspots’ makes it important to correlate the kinetic and quantitative information obtained by amperometry to the corresponded release sites. In recent years, microfabricated device allowing amperometric measurement at single cell or subcellular level appears to be a promising way to unveil the spatial information of cellular exocytosis which is sightless by CFE detection.

As illustrated in Fig.1-13, to optimize the spatial resolution, the dimension of UMEs in the MEA is usually limited at subcellular level. In this way, the recognition of exocytotic ‘hotspots’ seems to be feasible. Actually, the amperometric tracking of exocytosis with these MEAs is able to be carried out either on the top or at the bottom of cells, depending on the research interest.

For instance, two independent MEAs composed by multiple CFEs at subcellular size scale (~several  $\mu\text{m}$ ) have been employed to detect dopamine releases from the apex of PC-12 cells.<sup>[100, 101]</sup> Subcellular heterogeneity (hot and cold spots) of exocytotic secretions in single cells was evidenced according to the amperometric results detected by these two MEAs.

An obvious disparity of the exocytotic secretion at the two poles (cell apex and cell bottom) of a single cell has been demonstrated both in chromaffin cells<sup>[113]</sup> and BON cells<sup>[118]</sup> through the comparison of the temporal and quantitative parameters collected in different geometric configurations. Therefore, it is significative to electrochemically detection/mapping the exocytotic events at the bottom of single cell by introducing MEAs to cell culture, deposition or trapping.<sup>[114]</sup> For example, Wang and his colleagues developed several microwell-based MEAs consisting of UMEs with different sizes (ranging

from 2  $\mu\text{m}$  to 4  $\mu\text{m}$ ).<sup>[86]</sup> Exocytotic release of dopamine from a single PC-12 cell was successfully recorded by eight independent 2  $\mu\text{m}$ -wide UMEs. Analysis of the amperometric results showed that the subcellular heterogeneity appeared at the cell bottom as well, similar as that observed previously at cell apex.

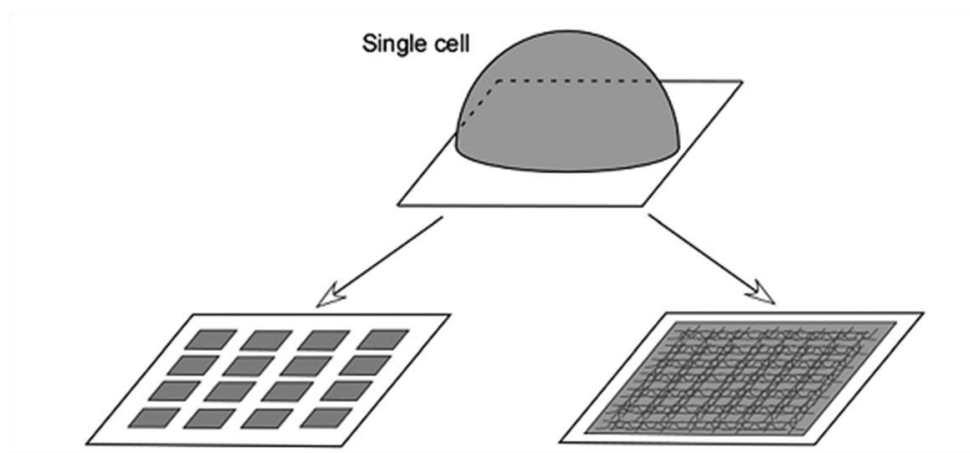


**Figure 1-13** Two strategies related to single cell analysis with microelectrode arrays. Left: MEAs with subcellular UME dimensions should help to perform the electrochemical mapping of the cell release; right: MEAs with electrode material other than carbon and with surface modifications (CNT etc.) for improving the electrode sensitivity. figure adapted from reference <sup>[109]</sup>.

To further improve the properties of UMEs in MEAs, one can either change the original materials for electrode fabrication or attempt to modify the electrode characteristics by using some nano-materials such as single walled carbon nanotubes (CNTs).<sup>[106, 115]</sup>

### **(c) Transparent microdevices for coupling analytical techniques**

Optical and electrochemical techniques are two complementary analytical methods for exocytosis investigation and the combination of these two approaches will illuminate the exocytotic process with high spatial (by fluorescence) and temporal resolutions (by amperometry). (See section 1.3.3.3) To implement the dual measurements mentioned above, the microfabricated devices should consist of electrodes showing both excellent optical (transparency) and electrochemical properties (conductivity and electroactivity).

With the development of microfabrication process, some microchips based on different electrode materials (Pt<sup>[116]</sup>, Au<sup>[117]</sup>, ITO<sup>[19, 117, 118]</sup>, CNT-modified ITO<sup>[106]</sup>...) have already been used for coupling

of electrochemistry and fluorescence for the analysis of single exocytotic events considering their optical transparency or semi-transparency. However, it is ITO that has attracted increasing attention since it was introduced to the fluorescence/amperometry combined observation of vesicular exocytosis for the first time by our group in 2006.<sup>[118]</sup> Several ITO microsystems have been reported for independent electroanalysis<sup>[113, 119, 120]</sup> or fluorescence/amperometry coupling measurements<sup>[19, 105, 116, 117]</sup> in the last ten years. TIRFM/amperometry coupling technique on the basis of ITO microsystems seems to be a promising tool for quantitative, temporally and spatially resolved monitoring of single-vesicle motions and exocytosis.

For instance, in our group, a microdevice composed of four independent ITO bands was fabricated and successfully applied for the simultaneously optical and electrochemical tracking of exocytotic events of BON BC21 cells by TIRFM (employing NPY-GFP as fluorescent probes) and amperometry (using serotonin as electroactive probes) coupling measurement at single cell level, as illustrated in Fig.1-14.<sup>[19]</sup> In these experiments, the precise location of releasing points at the cell bottom was achieved by the temporal correlation of fluorescence images and amperometric current spikes.

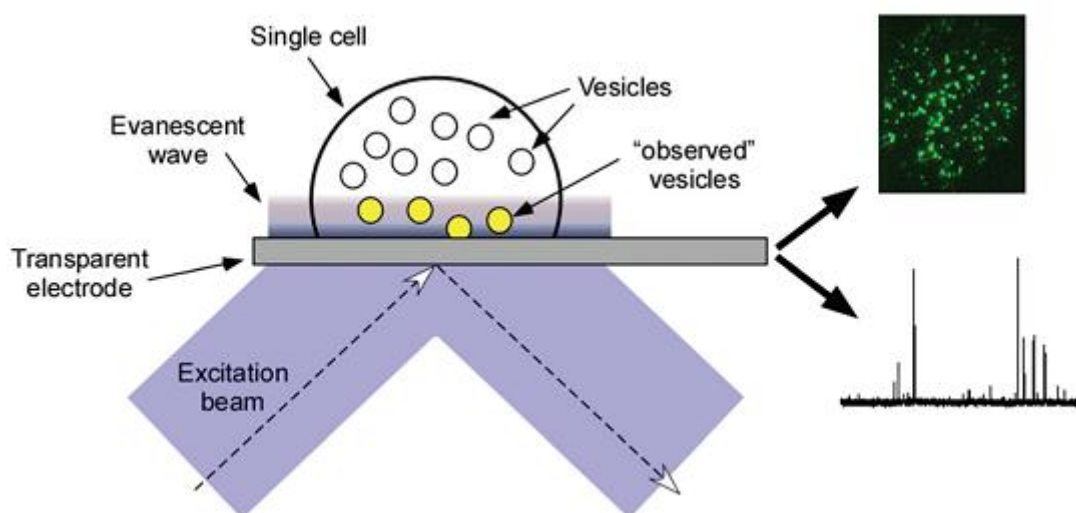


**Figure 1-14** Scheme of the fluorescence/amperometry combination which involves a transparent electrode. Figure adapted from reference <sup>[109]</sup>.

### 1.3.2 Optical methodology

The study of exocytosis poses great challenges to analytical methods because of these nano-scale vesicles (~nm). Optical microscopy with inherent spatial resolution provides reliable pathways for

elucidating the molecular and cellular mechanisms of exocytosis since the whole exocytotic process is directly visualized. So far, optical observation of exocytotic release has been achieved by plenty of microscopy techniques such as two/multiple-photon excitation microscopy,<sup>[121-123]</sup> confocal microscopy<sup>[124-126]</sup> as well as TIRFM<sup>[127-129]</sup>. It is necessary to mention that the spread of the first two techniques for exocytosis tracking is limited by their low temporal resolution and few studies have been reported so far.

In recent years, some new emerging microscopy techniques providing super resolution (stimulated emission depletion microscopy (STED),<sup>[130, 131]</sup> structured illumination microscopy (3D-SIM),<sup>[132]</sup> photoactivation localization microscopy (PALM),<sup>[133]</sup> and stochastic optical reconstruction microscopy (STORM)<sup>[134]</sup>) have also started to be adapted to exocytosis investigation in order to enhance the optical resolution, the sensitivity and recording speed.<sup>[135-137]</sup> Indeed, among all these approaches mentioned above, TIRFM accounts for a predominant position for exocytosis tracking at present owing to its specific characteristics.

### ***1.3.2.1 Total internal reflection fluorescence microscopy***

TIRFM is a special technique developed by Daniel Axelrod in the early 1980s<sup>[138]</sup> and is widely used in cell biological applications nowadays.<sup>[139-141]</sup> This technology is based on a physical phenomenon called ‘total internal reflection’ (TIR) which only occurs when a wave is propagating from an optically denser medium (higher refractive index,  $n_1$ ) to an optically less dense medium (lower refractive index,  $n_2$ ) at an angle beyond a particular critical value with respect to the normal to the surface.

- **Basic principle of TIRFM**

In general, when an incident light arrives at a boundary between different materials with different refractive indices ( $n_1$  and  $n_2$  with  $n_1 > n_2$ ) at a certain angle, it will be partially refracted and partially reflected (Fig.1-15(A)).

Moreover, the angle of refraction augments with the increase of incident angle. As a result, when we increase the angle of incidence, it will finally arrive at a critical value ( $\theta_c$ ) where the angle of refraction reaches  $90^\circ$  and the refracted light travels along the surface of the medium, depicted as the dashed line in Fig.1-15(A). This specific angle of incidence is defined as the well-known ‘critical angle’ and it could be calculated by virtue of Snell’s law:

$$\theta_c = \sin^{-1} n_2/n_1$$

Interestingly, if the incidence light strikes the interface from an angle beyond the critical angle  $\theta_c$  (Fig.1-15(B)), TIR will take place, generating a very thin electromagnetic field, namely, an evanescent

wave, at the interface with the same frequency as the incident light. The intensity of the evanescent wave decays exponentially with the perpendicular distance from the interface and its propagation distance is limited to hundreds of nanometers. Therefore, this field is feasible to excite fluorescent molecules that present adjacent to the interface and is employed to develop the TIRFM with an outstandingly high axial resolution below 10 nm.<sup>[142, 143]</sup>

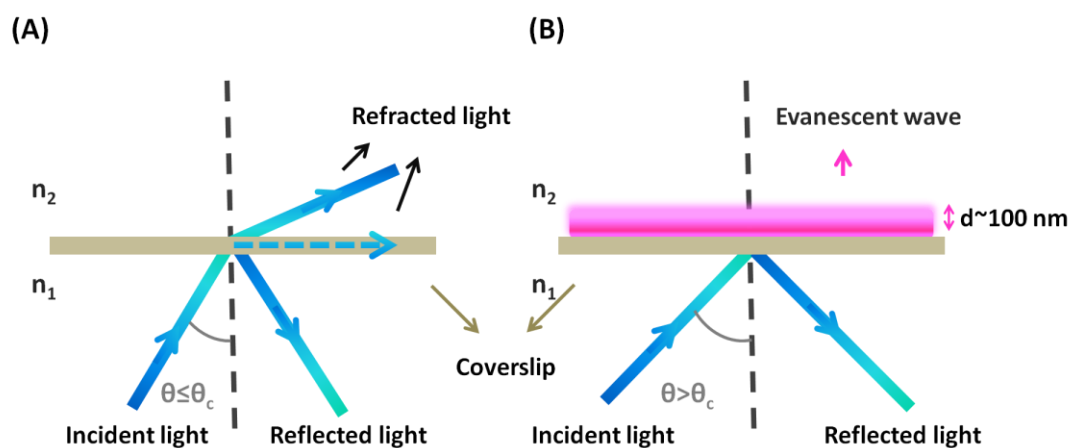


**Figure 1-15** Refraction at the interface:  $n_1$  and  $n_2$  are the refractive indices of the cover slip and the sample, respectively ( $n_1 > n_2$ ). (A) For an incident angle smaller than the critical angle, the incident light is partially refracted. (B) For an incident angle greater than the critical angle, the beam is totally reflected and an evanescent wave is created at the interface.

As previously described, in TIRFM, a thin evanescent field could be initiated in the close vicinity of the coverslip-sample interface if the incident angle of the excitation beam surpasses the critical angle  $\theta_c$ . The intensity of the evanescent field at any position  $z$  is described by:

$$I_z = I_0 e^{-z/d},$$

where  $I_0$  is the intensity of the evanescent field at  $z = 0$ .  $I_0$  is related to the intensity of the incident beam by a complex function of  $\theta$  and polarization while  $d$  represents the depth of the resulting evanescent wave field. It refers to the distance from the cover slip at which the excitation intensity decays to  $1/e$  of  $I_0$ . The excitation field depth  $d$  is dependent on several parameters, including the wavelength of the excitation light  $\lambda_0$ , incidence angle  $\theta$  as well as the refractive indices of the sample ( $n_1$ ) and the cover slip ( $n_2$ ), as defined in the following equation:

$$d = \frac{\lambda_0}{4\pi} (n_1^2 \sin^2 \theta - n_2^2)^{-1/2}$$

For a given system (i.e. system with fixed excitation wavelength as well as refractive indices), the depth is only decided by the incidence angle  $\theta$ : the higher the angle value, the narrower the excitation field depth. Typical values of  $d$  are in the range 60-100 nm. It indicates that only fluorophores locating within this depth could be illuminated while those outside this depth range shall dim, leading to the highlight of the signal in a defined distance.

- **Two configurations of TIRFM**

There are two basic configurations to set up a TIRFM instrument: the prism-based configuration and the objective-based configuration, as displayed in Fig.1-16.

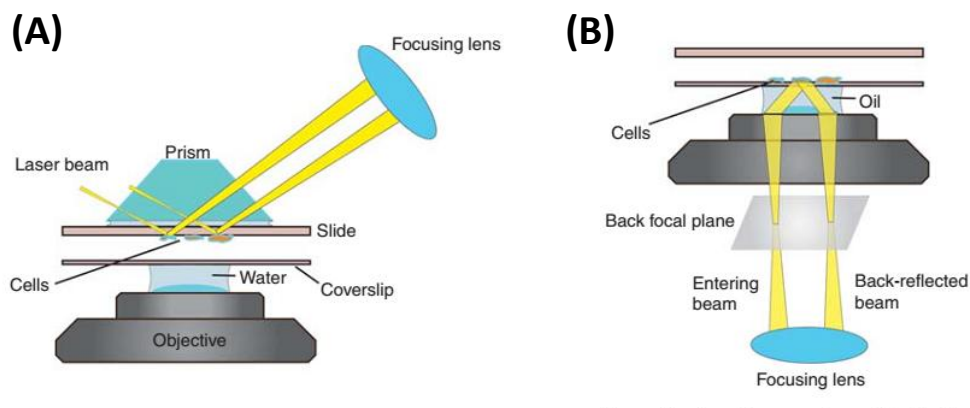


**Figure 1-16** The prism-based (A) and objective-based (B) configurations of TIRFM set-up. Figure adapted from reference <sup>[144]</sup>.

In the prism-based method (Fig.1-16(A)), a prism is attached to the coverslip surface to enable the achievement of critical angle when a focused laser beam is introduced to excite the fluorophores. The sample is therefore located in a narrow space between the objective and the prism, making it difficult to carry out manipulations on the cell specimen such as medium injection and physiological measurements. In addition, the prism has to be removed to exchange the sample, which necessitates realignment of the prism for each experiment.

Another TIRFM set-up (Fig.1-16(B)) is developed by using an objective with a high numerical aperture (NA) to simultaneously refract incident light beyond critical angle for illumination and collect

fluorescence emission. In this way, evanescent field excitation is accomplished through the use of high-aperture objectives. It thus offers greater flexibility in specimen manipulation and measurement options compared with the prism-based configuration. This objective-based configuration has become a general choice of many labs.

- **TIRFM versus epi-fluorescence**

For the application of cell biological imaging, especially analysis of the localization and dynamics of molecules and events near the plasma membrane, TIRFM exhibits great advantages in spatial resolution compared with the traditional fluorescence microscopy based on epifluorescence.

For instance, if we excite the cell specimen with a laser perpendicular to the normal, described as epi-fluorescence, all the fluorescent vesicles of the entire sample are illuminated (Fig.1-17(A)). However, when we increase the incident angle to achieve TIRFM condition ( $\theta > \theta_c$ ), the excitation beam is reflected off the coverslip-sample interface and an evanescent field is generated at the interface in the low-reflective-index medium. Due to the limited evanescent field penetration depth, only fluorophores within a defined distance ( $d \sim 100$  nm) are excited, as indicated by the green color in Fig.1-17(B), leading to a high signal-to-noise ratio and an axial resolution of about 10 nm.<sup>[142, 143]</sup>

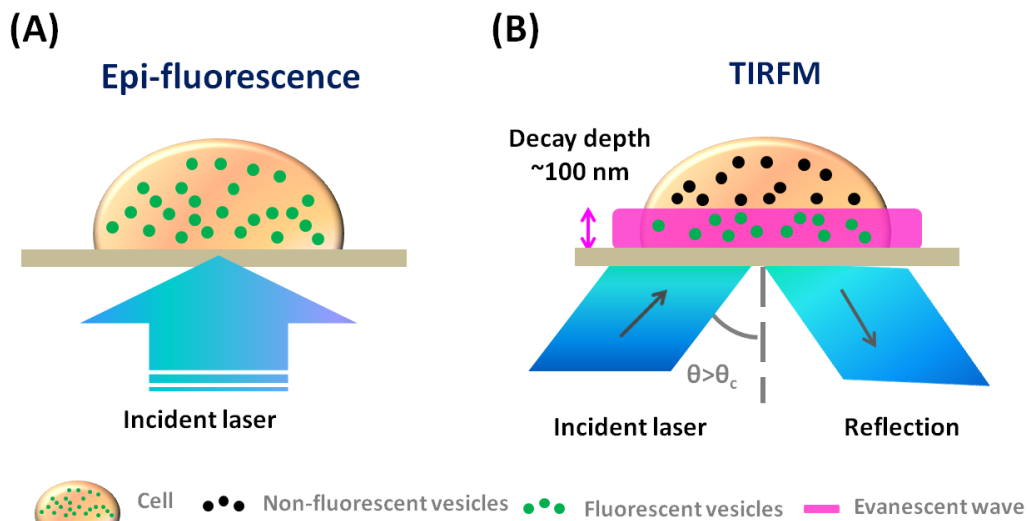


**Figure 1-17** Cell specimen with fluorescent vesicles excited by epi-fluorescence (A) and TIRFM (B) configurations, respectively.

- **Exocytosis investigation by TIRFM**

Thanks to its high spatial resolution as well as its low fluorescence background, TIRFM is a useful and accessible imaging technique used in cell biology for selective excitation of fluorophores at or near the cell membrane. In the late 1990s, this approach was firstly applied to the observation of the fusion of secretory vesicles with the plasma membrane in chromaffin cells<sup>[145-147]</sup> and in this method, the whole exocytotic process (including the behaviors of vesicular membrane before and after contents release) are able to be directly visualized with proper fluorescent staining. Nowadays, TIRFM has become the most widely used optical approach not only for the investigation of the exocytotic process itself, but also for study of some biological parameters impacting exocytosis.

- (a) **Tracking of vesicle behaviors and exocytotic release**

In 1997, TIRFM observation of exocytotic release was achieved for the first time in chromaffin cells by Steyer and his coworkers by staining cellular vesicles with the fluorescent probe called acridine orange.<sup>[145]</sup> According to the sequential TIRFM images, they found that (1) there was a large pool of docked granules with slow motility; (2) fresh granules kept on moving actively to reach their docking sites; (3) vesicle docking was reversible; (4) single docked granules underwent exocytosis upon stimulation. This work successfully demonstrated the feasibility of TIRFM to study the transport, docking and release of single secretory vesicle with high spatial resolution. From then on, the investigation of exocytosis by TIRFM in different cell lines (chromaffin cells, PC-12 cells, BON cells, neurons,...) blossoms and this is accompanied by the development of various types of biocompatible fluorescent probes for vesicle labeling (styryl dye molecules<sup>[148, 149]</sup>, pH-sensitive fluorescent proteins,<sup>[150]</sup> nanometre-sized fluorescent quantum dots<sup>[151]</sup> and false fluorescent neurotransmitters<sup>[152]</sup>).

TIRFM in combination with fluorescent probes contributes a lot to the better understanding of exocytotic mechanism. For instance, the behaviors of vesicles have been assessed by TIRFM in many studies.<sup>[127, 136, 153]</sup> Generally, there are two different vesicles pools with different release properties in a single secretory cell: one pool includes secretory vesicles highly dynamic and normally lying in the cell interior while the other represents immobile vesicles at the plasma membrane. For those secretory vesicles lying at the plasma membrane and ‘ready to release’, they do not exhibit free motility but instead demonstrate a ‘caged’ or ‘tethered’ behavior, termed morphological docking. Upon stimulation, only a proportion of these morphologically docked vesicles fuse rapidly with the plasma membrane to discharge their cargo. Moreover, TIRFM observation confirms the existence of the fusion pore through which the fluorescent vesicular contents are released. The expansion of fusion pore corresponds to a fluorescence intensity increase due to the release of vesicular probe into the extracellular medium, followed by fluorescence extinction as the dyes diffuse away.<sup>[154, 155]</sup>

Another important contribution by TIRFM is the discovery of incomplete or multi-step release of fluorescent content stored inside the vesicles during exocytosis. To distinguish this class of exocytotic processes from ‘full fusion’ of which vesicular contents are completely released, accompanied by full fusion of the vesicular and cellular membranes, it is thus generally termed ‘kiss-and-run’.<sup>[156, 157]</sup> For instance, in chromaffin cells and PC-12 cells, partial melting seems to be predominant<sup>[158]</sup> whereas in pancreas  $\beta$  cells, the majority of exocytotic events occur via ‘full fusion’, mainly resulting in complete release.<sup>[159]</sup>

## **(b) Influences of biological parameters**

### **SNAREs protein influence**

Before fusing with cell membrane, secretory vesicles must first become docked to the plasma membrane through the formation of SNAREs complex. At present, the molecular mechanisms that underlie the docking/fusion of secretory vesicles remain poorly understood. However, SNAREs proteins are hypothesized to play significant roles at different stages (docking and fusion) of secretory cycle. Actually, some of these roles have already been confirmed by TIRFM.

To investigate functions of two SNAREs proteins, SNAP-25 and synaptobrevin, Johns and his colleagues<sup>[160]</sup> transiently transfected chromaffin cells to express the light chains of tetanus toxin and botulinum toxin A so as to cleave the SNAREs proteins and then monitored their exocytotic process by TIRFM. Their results suggested that SNAREs proteins were not necessary for the decreased mobility at the docking sites. However, they may influence the interaction between the secretory vesicles with corresponding docking sites as the lack of these proteins on the cellular/vesicular membranes led to the decreased time course that some vesicles spent adjacent to the cell membrane. This work opens the door to mechanistic studies of how SNAREs proteins regulate fusion processes in different cell lines in vivo. In pancreas  $\beta$  cells,<sup>[161]</sup> it is established by TIRFM that SNAREs proteins were essential for the docking and fusion of insulin granules and there was a close correlation between the number of syntaxin and SNAP-25 clusters and the number of docked insulin vesicles, in accordance with the results obtained from another cell line (MIN6  $\beta$  cells) which also discharge insulin during exocytosis<sup>[162]</sup>. Moreover, in PC-12 cells<sup>[163]</sup>, all three components of the SNAREs complex (synaptobrevin, syntaxin and SNAP-25) contributed to promote secretory vesicle docking according to the TIRFM imaging results.

### **Role of actin in exocytosis**

Actin participates the whole exocytotic process from vesicle transport, docking and fusion. For instance, before releasing their contents to extracellular space, secretory vesicles have to be delivered and tethered to the plasma membrane, which highly relies on the actin. Moreover, exocytotic secretion

is always accompanied by a fine reorganization of the peripheral F-actin. The actin behavior is thus able to affect the transport and secretion of cellular vesicles.

Many earlier findings based on TIRFM mainly support the viewpoint that actin exists as a physical barrier to exocytotic secretion and transient depolymerization of cortical F-actin permits vesicles to gain access to their appropriate docking and fusion sites at the plasma membrane. For example, Oheim and his colleagues<sup>[164]</sup> studied the relationship between actin organization and vesicular exocytosis by perturbing actin dynamics with specific drugs. They firstly treated chromaffin cells with two drugs showing contrary effects on actin behavior, namely, latrunculin (a drug that can depolymerize F-actin) and jasplakinolide (a drug that can stabilize the actin cortex by inducing polymerization) respectively. Relying on TIRFM imaging to track the secretory vesicles behaviors, they discovered that in both cases, the rate of exocytotic release was reduced whereas the 3D diffusion efficiency of these vesicles was changed in different ways. Specifically, the application of jasplakinolide caused almost complete immobilization of secretory vesicles while contrary results were obtained from cells treated by latrunculin, demonstrating that movement of granules are mediated as well as constrained by the actin cortex. Similar results were also obtained in PC-12 cells.<sup>[165]</sup>

However, in 2006, Malacombe and co-workers<sup>[78]</sup> proposed that actin polymerization plays a dual role in exocytotic release. That is, despite their ‘physical barrier’ function, they might show positive effects on exocytotic process as well. This viewpoint becomes more and more acceptable taking account to the recent discoveries by TIRFM. For instance, recent study in neurosecretory cells proved that, in response to secretagogue stimulation, actin interplays with myosin II so as to establish new release sites for secretory vesicles.<sup>[166]</sup>

### **1.3.3 Coupling methodology**

The three analytical techniques described above (patch clamp, amperometry and TIRFM) provide extensive information of exocytotic secretion in different and complementary aspects. However, the employment of one of these analytical methods solely seems not enough to fully illustrate the complex exocytotic process since each technique suffers from some shortcomings, either the lack of spatial resolution (patch clamp and amperometry) or the deficiency of temporal resolution (TIRFM). In order to improve the understanding of this complex mechanism, people start to combine two analytical methods together for exocytosis observation.

#### ***1.3.3.1 Combination of patch clamp with amperometry***

In the 1990s, a technique called ‘patch-amperometry’ emerged as a novel choice for the tracking of exocytotic secretions in living cells.<sup>[167-169]</sup> As displayed in Fig.1-18, the combination of ‘patch clamp’ and ‘amperometry’ is achieved by introducing a CFE into a patch pipette. In this way, as the vesicular

contents are secreted from vesicular lumens to extracellular spaces, the resulting electrophysiological (electrical capacitance) and amperometric (oxidation current) signals are able to be simultaneously recorded at single cell or single vesicle level, depending on the employed patch configuration.

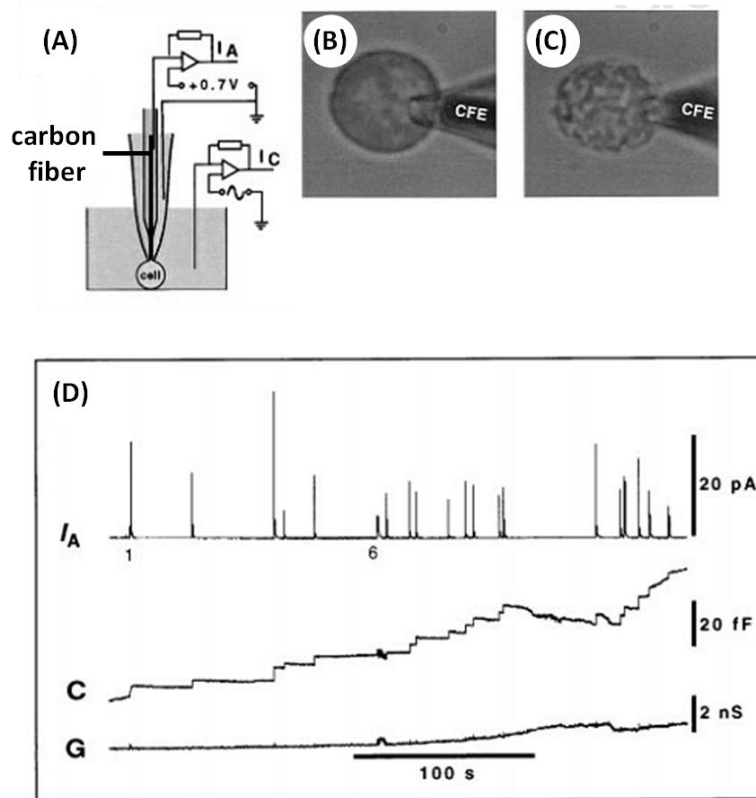


**Fig.1-18** (A) Arrangement of a CFE inside a patch pipette; chromaffin cell with attached patch pipette containing CFE at the beginning (B) and end (C) of the experiment; (D) Recording from this cell shows amperometric transients (top), associated capacitance steps (middle), and conductance trace (bottom). Figure adapted from reference <sup>[167]</sup>.

Patch-amperometry possesses all the advantages of the two complementary analytical methods, providing quantitative information with excellent temporal resolution and high sensitivity. Its application for exocytosis observations greatly increased our understanding of different aspects of secretion process, especially the part related to the formation/evolution of fusion pore. For instance, using this technique (cell-attached patch configuration), Lindau and his coworkers confirmed the transient formation of small fusion pore (~3 nm) through which electroactive neurotransmitter started to be released to the CFE surface, resulting in a ‘foot’ signal in amperometry.<sup>[167]</sup> Another interesting

finding by this method (cell-attached patch configuration) was that a high  $\text{Ca}^{2+}$  concentration on the extracellular side of the membrane promotes the ‘kiss-and-run’ mode of exocytosis.<sup>[170]</sup>

Despite its distinct advantages, patch-amperometry has some inherent drawbacks. Firstly, only one single cell could be detected each time and a lot of experiments need to be performed in order to avoid the cell viability. Secondly, distortion of recorded amperometric spikes were seen from time to time because of diffusional broadening while electroactive molecules covered the distance between the patched cell membrane and the CFE tip, which is hard to control and minimize precisely.<sup>[65]</sup> Finally, this technique does not give actual spatial information from where biochemical messengers are released, still being ‘blind’ to the behaviors of secretory vesicles before release.

### 1.3.3.2 Combination of patch clamp and TIRFM

To test whether exocytosis measured with TIRFM is representative for global secretions of a single chromaffin cell, Becherer and his colleagues proposed a new method combining patch clamp (whole-cell configuration) and TIRFM which was capable of simultaneously recording the capacitance changes and fluorescence extinctions resulting from vesicular exocytosis, as displayed in Fig.1-19.<sup>[171]</sup>

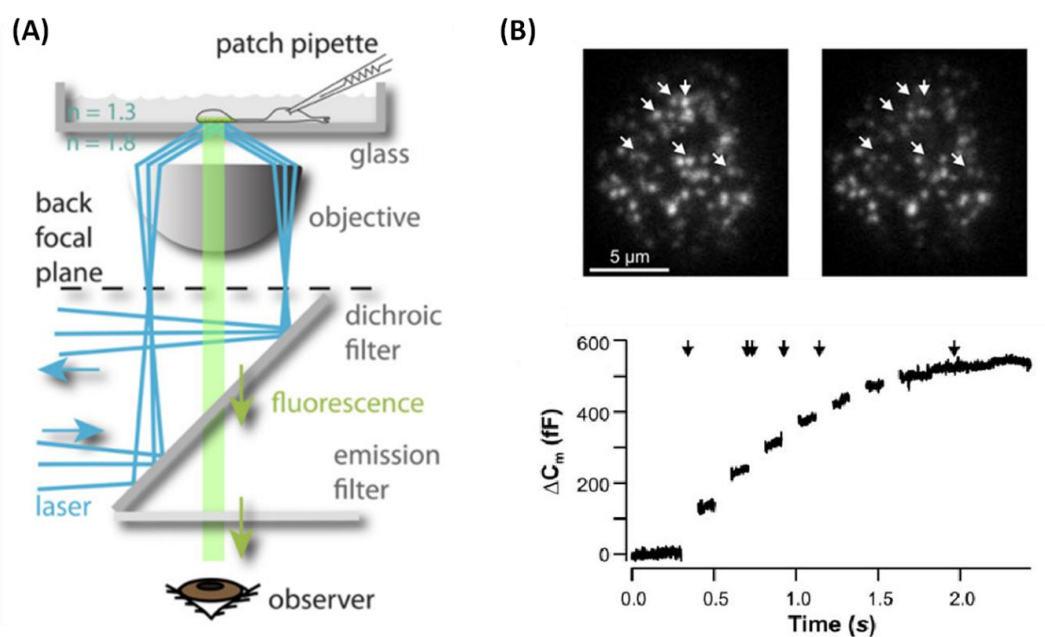


**Figure 1-19** (A) Set-up for patch clamp/TIRFM coupling measurements of exocytosis; (B) An example of such combined detection in a single chromaffin cell transfected with NPY-Mrfp. Upper: TIRFM image of the cell taken prior to (left) and immediately after (right) depolarization and white arrows indicate vesicles that were secreted during stimulation; Bottom: corresponding membrane capacitance and the black arrows indicate the approximate time of secretion in TIRFM. Figure adapted from reference <sup>[172]</sup> and reference <sup>[171]</sup>, respectively.

By correlating these two kinds of signals qualitatively and quantitatively, they found secretion visualized by TIRFM was ten times lower than secretion measured by membrane capacitance recording. Nevertheless, secretion at the bottom of the cell (detected by TIRFM) was a reliable index of the secretion over the entire cell surface (detected by patch clamp) considering that the time course of exocytotic release was identical in both methods and that PMA treatment (a drug promotes exocytotic secretion) resulted in a similar increase of global secretion and of secretion at bottom of the cell. In this work, TIRFM was confirmed to be an appropriate tool to study the exocytotic process. In addition, this novel coupling technique with high temporal (because of patch clamp) and spatial resolution (because of TIRFM) provides a new tool for deeply investigating the exocytotic mechanism with combined electrophysiological and imaging information. Investigation of adiponectin effect on insulin secretion in pancreatic  $\beta$  cells<sup>[173]</sup> and the size measurement of fusing vesicles<sup>[174]</sup> were achieved by employing this combined method. The exocytotic detail that docking of secretory vesicles was modulated by lower intracellular  $\text{Ca}^{2+}$  than priming in chromaffin cells, was also revealed by this novel technique.<sup>[175]</sup>

Compared with the exocytosis investigation by patch clamp alone, this coupling method makes great progress in the tracking of secretory vesicle behaviors before release as well as in the location of release sites owing to the inherent high spatial resolution of TIRFM. However, this method shows a major constraint that information about the granular content released is still missed.

#### ***1.3.3.3 Combination of TIRFM and amperometry***

As previously described, the great advantage of amperometry is its inherent high temporal resolution (~ms), which allows studies of the dynamics of the fusion pore itself. However, in this technique, the dynamics of the secretory vesicle itself prior to the fusion event is completely missed because electrochemical signals appear only after fusion has commenced. In contrast, by using TIRFM, behaviors of secretory vesicles prior to their fusion are directly visualized with distinct spatial resolution (100 nm in the x-y plane and 10 nm in the z plane)<sup>[38]</sup> but with a relatively low temporal resolution which is not fast enough to follow the dynamics of the fusion pore. In order to integrate the complementary advantages of these two techniques for exocytosis detection, our group (thesis work of Anne Meunier, a former PhD in our group, 2008-2011) established a novel method in combination of TIRFM and amperometry which is capable of simultaneously monitoring the optical and electrochemical signals resulting from exocytotic secretions at the bottom of a single cell.<sup>[19]</sup> Such TIRFM/amperometry coupling test is based on an adequate microchip embedded with microelectrodes which are both transparent and electrically conductive, as an example displayed in Fig.1-20.

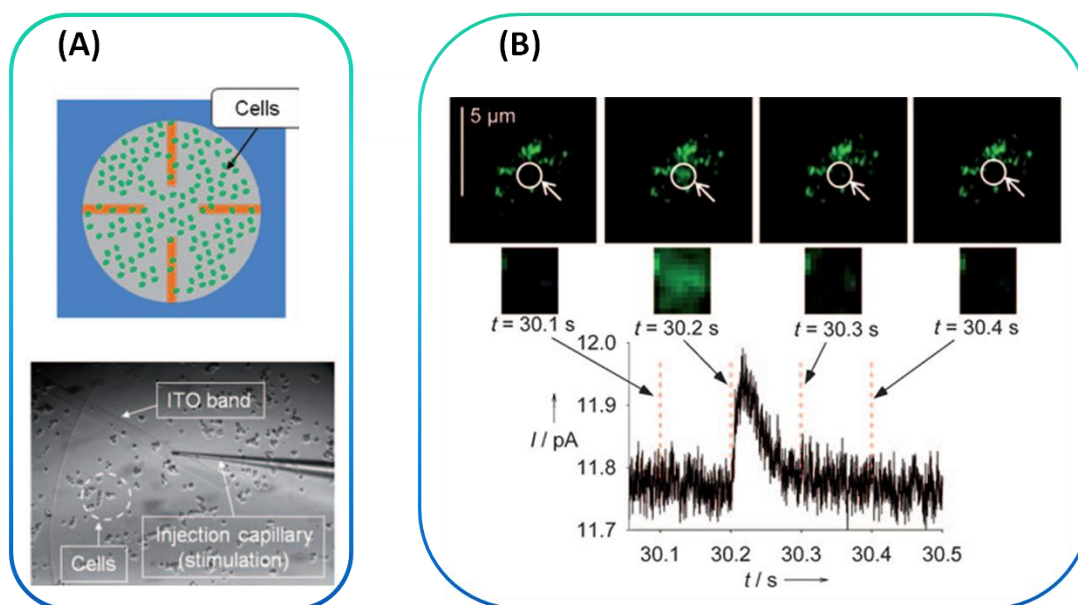


**Figure 1-20** (A) Top: scheme of cells adhered on the microdevice with four independent ITO electrodes (in orange); bottom: inverted microscopy image of BC21 BON cells adhering to the well containing the ITO microelectrodes; (B) A representative examples of combined analyses of an exocytotic event (top: TIRFM; bottom: amperometry) obtained with the ITO microdevice. Images adapted from reference <sup>[19]</sup>.

In the first analysis of exocytosis by TIRFM/amperometry coupling measurement, BON BC21 cells was employed as the cell model because it stably expressed GFP working as optical probes during TIRFM observation and its secretory vesicles were capable of being loaded with serotonin working as electrochemical reporters in amperometric detection. Such cells were seeded into a microsystem embedded with four independent ITO microelectrodes and TIRFM imaging and amperometric test were then carried out at the same time.(Fig.1-20(A)) Upon stimulation, exocytotic release concurrently appeared as ‘fluorescent flash’ and ‘oxidation current spike’ in some cases during the coupling test.(Fig.1-20(B)) In this way, the exocytotic release from single vesicles was directly visualized with high spatial and temporal resolution, associated with additionally quantitative information about the release amount. However, because of the independent loading of these two probes, among all the exocytotic events recorded, only 22% clearly corresponded to simultaneous detection by amperometry and TIRFM.

Similar results have been obtained in chromaffin cells by Kisler and her colleagues by using other different microsystems with transparent/semi-transparent ITO or Au microelectrodes.<sup>[117]</sup> To perform coupling detection, secretory vesicles of chromaffin cells (possessing endogenous electroactive

catecholamines) were preloaded with one of the fluorescent markers lysotracker green or acridine orange which were both able to be accumulated into acidic vesicles. In their cases, ~20% of amperometric spikes were accompanied by a detectable fluorescence event on Au microelectrodes while with ITO electrodes 38% of amperometric spikes were associated by a detectable fluorescence event. Interestingly, they found the employment of different fluorescent probes for vesicle staining led to disparities of the observed coupling events. To be specific, when lysotracker green was used to label the secretory vesicles, the main fluorescence intensity decrease was observed in TIRFM when the steep rising phase of the amperometric spike occurred. In contrast, when acridine orange was employed, the initial fluorescence variation often occurred after the amperometric spike peak appeared. They attributed the delay of fluorescence signals to the extra time needed for acridine orange to deaggregate and dequench.

This coupling technique shows great advantages in some applications which are not able to be achieved by amperometry or fluorescence imaging alone. For instance, the coupling method enable to study differential release of various fluorescent vesicle markers in relation to the amperometrically detected electroactive probes release, as previously observed with lysotracker green and acridine orange. Moreover, the relationship between various fluorescently labeled proteins involved in exocytosis and the exocytotic release are also able to be revealed in this method. Because of complementary natures of these two analytical methods, TIRFM/amperometry coupling technique is considered as a powerful tool allowing a comprehensive and precise analysis of the whole exocytotic event, from predocking through fusion steps up to the dynamics of vesicular release.

As discussed in this section, the correlation of two signals obtained by two complementary techniques in coupling detection reveals more information (the locations of vesicles undergoing exocytosis, the dynamics of the fusion pore, the parameters modulating the secretion, the amount of release....) related to the exocytotic process. However, experimental development is a great challenge since constraints of two different techniques can be contradictory. In this thesis, the combination of TIRFM with amperometry is achieved by virtue of ITO microdevices which allow simultaneously fluorescence imaging and amperometric recording owing to the specific optical transparency as well as excellent electrical conductivity of ITO.

#### **1.4 Fluorescent analogs of monoamine neurotransmitters**

Fluorescent probes have been extensively used for the detection and study of the dynamics of vesicular exocytosis in living cells and the five main strategies to labeling vesicular membranes or vesicular contents have been summarized in a recent review<sup>[176]</sup>. An ideal fluorescent probe for exocytosis investigation ought to have a high quantum yield, a relatively longer excitation wavelength, and must

be able to mark the secretory vesicles in a specific way.<sup>[177]</sup> Actually, in recent years, one of the most exciting advances in the area of novel fluorescent probe development for the monitoring exocytotic process is the successful synthesis of various neurotransmitter analogs, namely fluorescent false neurotransmitters (FFNs),<sup>[152, 178, 179]</sup> which allow direct visualization of monoamine uptake, redistribution and release. It is well-known that compared with other chemical probes, fluorescent analogs of biomolecules are more ideal/friendly probes to study the structure, conformations and dynamics of cellular processes as they retain the shape, size, conformation, and recognition element of the natural substrate. Therefore, FFNs seem to be an ideal probe for fluorescently tracking the exocytotic process of secretory cells.

#### **1.4.1 Monoamine neurotransmitters**

##### ***1.4.1.1 Monoamine neurotransmitters and their transporters***

In 1921, Otto Loewi predicted that one neuron transmitted chemical signals to another neuron through the synaptic cleft by releasing chemicals and the first chemical neurotransmitter that he found was 'acetylcholine' in the frog heart.<sup>[180, 181]</sup> To date, a multitude of neurotransmitters participating in neural communications have been identified whereas more are being still unveiled. In general, known neurotransmitters are mainly divided into three classes: amino acids, peptides, and biogenic monoamines. In this section, we will mainly focus on monoamine neurotransmitters which have been demonstrated to closely related to different psychiatric and neurological diseases such as depression, anxiety, chronic pain, sleep disorders, schizophrenia, various aspects of drug abuse, Parkinson's disease and Alzheimer's disease.<sup>[177]</sup> Additionally, some electroactive monoamine neurotransmitters such as serotonin, dopamine, norepinephrine as well as epinephrine have widely been employed as electrochemical probes in exocytosis investigation by amperometry, which will be discussed later in this thesis.

To achieve intercellular communications via vesicular exocytosis, active transport of neurotransmitters into vesicles of secretory cells is essential for their subsequent exocytotic release. With respect to monoamine neurotransmitters including dopamine, serotonin, norepinephrine, epinephrine, and histamine, this process is generally carried out by specific functional proteins known as vesicular monoamine transporters (VMAT). Indeed, there are two kinds of VMAT isoforms (VMAT1 and VMAT2) expressed in humans, of which pharmacological properties and tissue distributions are found to be distinctly different.<sup>[182-185]</sup> Studies indicate that VMAT1 is preferentially expressed in secretory vesicles of various neuroendocrine cells, including chromaffin and enterochromaffin cells whereas VMAT2 is primarily expressed in multiple monoaminergic cells in the brain, sympathetic nervous system, mast cells, histamine containing cells in the gut, pancreas  $\beta$  cells and blood platelets.<sup>[186]</sup>

In addition, VMAT1 and VMAT2 exhibit different abilities for specific biogenic monoamine recognition and affinity. For instance, catecholamines (dopamine, norepinephrine, and epinephrine) and histamine have three-fold and thirty-fold higher affinity for VMAT2 binding compared to VMAT1 binding, respectively. However, the two VMAT isoforms show a similar ability for serotonin transport.<sup>[185, 186]</sup>

Interestingly, previous studies demonstrate that both VMAT isoforms seem not to be absolutely specific to biogenic monoamines recognition since synthetic monoamines such as tyramine, amphetamine, and other phenylethylamines are also found to be able to be accumulated into vesicular lumens via VMAT-mediated transport process.<sup>[187, 188]</sup> It is thus probable to design various functional VMAT substrates as neurotransmitter analogs that closely mimic biogenic amino neurotransmitters with respect to structure and properties (to improve their biocompatibility so as to result in less or no perturbation in the cellular process) but in contrast show special characteristics such as fluorescence characteristic or electroactivity. (See section 1.4.2)

#### ***1.4.1.2 Electrochemical analysis of monoamine neurotransmitters***

To date, all the reported biogenic monoamines are non-fluorescent or weak fluorescent, so visualization of their uptake and release via optical imaging is difficult to realize. So far, there are few reports about the application of dopamine<sup>[189]</sup> or serotonin<sup>[190-192]</sup> as fluorescent probes to study the exocytotic process taking advantages of their native fluorescence. Optical imaging of biogenic monoamines activities in exocytosis is mainly carried out by staining target cells with various exogenous optical probes.<sup>[176, 190]</sup>

On the contrary, some well-known monoamine neurotransmitters are easily to be electrically oxidized or reduced on the electrode surface at certain potential, showing good electroactivity which makes it possible to directly investigate vesicular exocytosis by tracking the oxidation process of released monoamine neurotransmitters themselves.<sup>[33, 193, 194]</sup>

As previously described (see section 1.3.1.2), amperometry is a powerful tool to monitor exocytotic process relying on the electrochemical oxidation/reduction of redox molecules. Here, we will present several monoamine neurotransmitters which have been frequently used as electroactive probes for exocytosis investigation in amperometry.

- **Catecholamines**

Catecholamines are a series of monoamines which possess the special structure of a benzene ring with two hydroxyl side groups, an intermediate ethyl chain and a terminal amine group.

As presented in Fig.1-21(A), epinephrine, norepinephrine and dopamine are three biogenic monoamine neurotransmitters known as catecholamines. All of these three molecules have been proven to show good electroactivities and be able to work as electrochemical reporters for exocytosis studies. For instance, the first amperometric measurement of exocytosis in chromaffin cells was achieved by monitoring the current spikes resulting from oxidation of released catecholamines on the CFE surface<sup>[36]</sup> while dopamine has been extensively used as electrochemical probes for exocytosis studies in neuron cells or PC-12 cells to date.<sup>[13]</sup>

In addition, electroactivities of catecholamines are ascribed to their easily oxidizable hydroxyl groups on the benzene ring and here we take dopamine as an example to illustrate the electrooxidation process of catecholamines on electrode surface. As illustrated in Fig.1-21(B), dopamine oxidation involves a multi-step two-electron, two-proton transfer process through which another chemical product dopamine o-quinone is generated and this is definitely owing to the electroactivities of the two hydroxyl groups on the benzene ring.

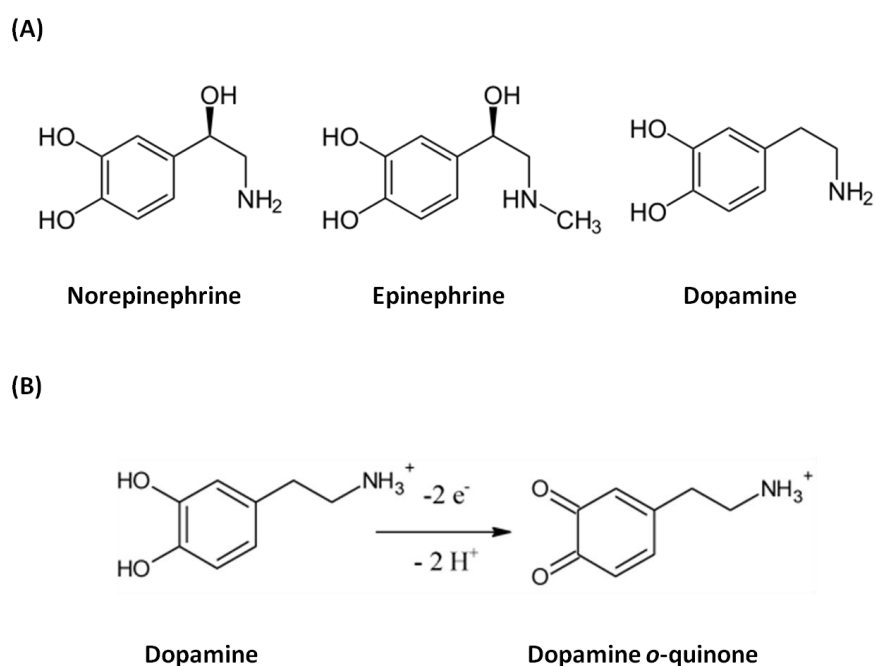


**Figure 1-21** (A) Molecular formulas of three well-known electroactive catecholamines: norepinephrine, epinephrine and dopamine; (B) Scheme for the two proton, two electron oxidation of dopamine released during vesicular exocytosis.

- Serotonin

Serotonin is another functional monoamine neurotransmitter which plays a significant role in numerous physiological processes, such as depression, thermoregulation, liver regeneration, cardiovascular function and irritable bowel syndrome.<sup>[195, 196]</sup> As serotonin is easily oxidizable, its application as electrochemical probe for exocytosis investigation by amperometry has received considerable attentions.<sup>[18, 168, 197]</sup>

As shown in Fig.1-22, similar with dopamine, serotonin oxidation also involves a multi-step two-electron, two-proton transfer process and its electroactivity is attributed to the hydroxyl group on the benzene ring as well. However, it is necessary to figure out that fouling of electrode surface is commonly observed during the oxidation process of serotonin, which is usually considered to be caused by the formation of an insoluble polymer-like by-product on the electrode surface.

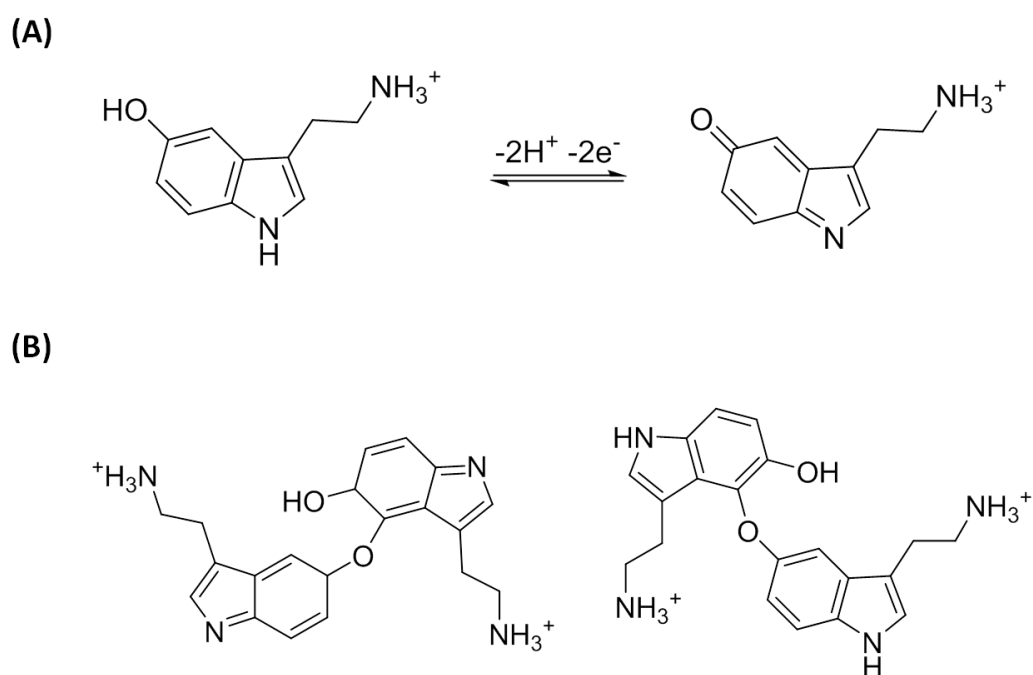


**Figure 1-22** (A) Scheme for the two proton, two electron oxidation of serotonin released during vesicular exocytosis; (B) Two examples of the major dimers formed in side reactions that are thought to lead to formation of insoluble polymer-like by-products.<sup>[196]</sup>

So far, the direct tracking of monoamine neurotransmitter behaviors in exocytosis is commonly based on electrochemical analytical techniques such as amperometry in which monoamine neurotransmitters

themselves work as the electroactive reporters. Interestingly, the electroactivities of these monoamine neurotransmitters are all attributed to the oxidation of the phenolic hydroxyl group, which raises the possibility to design analogs with similar structures to function as electrochemical reporters in amperometry.

#### 1.4.2 Fluorescent false neurotransmitters for optical imaging

VMAT2 plays a significant role in the monoaminergic transmission system as it selectively transports monoamine neurotransmitters from the cytosol into the secretory vesicles. However, this protein is reported to be relatively nonspecific and capable of transporting both biogenic monoamines (such as dopamine, serotonin, and norepinephrine) and synthetic amines (such as amphetamine, 3,4-methylenedioxymethamphetamine, and 1-methyl-4-phenylpyridinium) from cytoplasm to the secretory vesicles. Inspired by this fact, in 2009, the group of Dalibor Sames and David Sulzer designed and synthesized the first fluorescent probe in the FFNs family (compound FFN511, chemical structure shown in Fig.1-23(A)), for the sake of directly visualizing neurotransmitter uptake and release from individual presynaptic terminals by optical imaging.

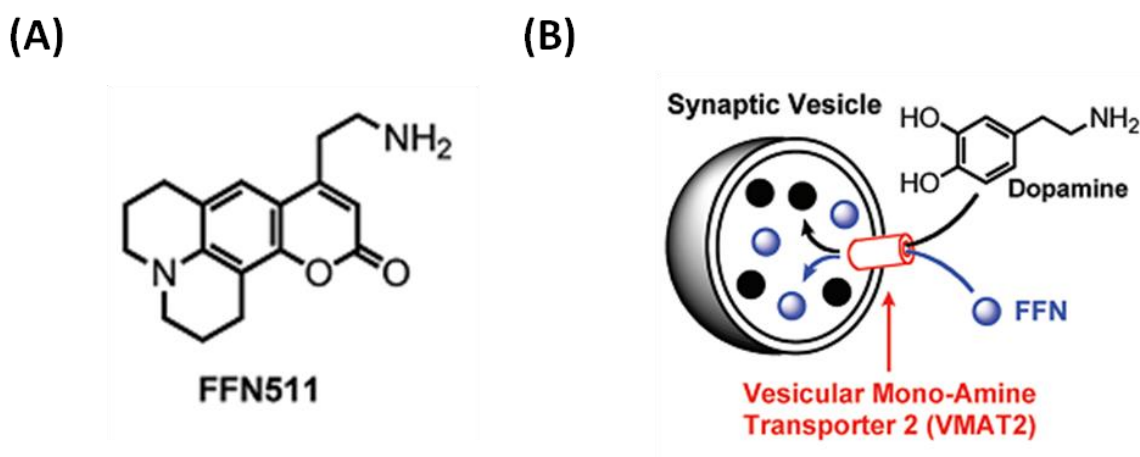


**Figure 1-23** (A) Molecular formula of compound FFN511; (B) FFNs function as fluorescent substrates of VMAT2, the protein that accumulates dopamine into synaptic vesicles. In this manner, FFNs act as optical tracers of the neurotransmitter, allowing for imaging of both location (accumulation of fluorescence signal) and activity of presynaptic terminals (loss of fluorescence signal). Figure adapted from reference <sup>[198]</sup>.

As shown in Fig.1-23, the general concept of FFNs designs is to synthesize functional organic molecules (such as FFN511) of which overall structure is highly similar to that of biogenic monoamine neurotransmitters. That is, they maintain the aminoethyl group intact to work as a cellular recognition site, but additional aromatic functionality is added to the structure to achieve enhanced fluorescent properties. When cells were exposed to extracellular media supplemented with FFNs, VMAT will be misled by the high structure similarity of FFNs and biogenic monoamine neurotransmitters and thus cannot discriminate their differences. In other words, VMAT is about to consider FFNs as the biogenic monoamine neurotransmitters and subsequently transport them into the vesicular lumens. In this way, FFNs such as FFN511 seem to be capable of working as an optical probe to specifically monitor the uptake and release of neurotransmitters related to the secretory vesicles.

As expected, FFN511, acting as VMAT2 substrates, was selectively accumulated into the secretory vesicles and released by evoked activity or drugs such as amphetamine. In this work, the fraction of synaptic vesicles releasing neurotransmitter per stimulus was found to be dependent on the stimulus frequency. Moreover, this new probe seemed compatible with other fluorescent probes such as GFP and FM1-43, allowing the construction of fine-resolution maps of synaptic microcircuitry and presynaptic activity.<sup>[152, 199]</sup>

Modeled on the former probe FFN511, they then developed ratiometric pH-responsive FFN probes (FFN102 and FFN202, chemical structures shown in Fig.1-24) of which the fluorescence are bright, stable and highly dependent on the pH values. Using two-photon fluorescence microscopy, pH value of catecholamine secretory vesicles was found to be  $5.88 \pm 0.08$  by measuring the fluorescence intensity changes of FFN probe. Effect of drug treatment (methamphetamine) on pH variations of cellular vesicles was also achieved by in situ measurement of the fluorescence intensity of FFN202 accumulated inside the acidic vesicular lumens.<sup>[178]</sup> Furthermore, besides its ability to work as a pH sensor, FFN102 was demonstrated to be suitable for not only the identification of cells releasing dopamine and their processes in brain tissue, but also for the optical measurement of exocytotic release of dopamine at the level of individual synapses.<sup>[200-202]</sup>

Another important optical probe in the FFN family is FFN206 (an excellent fluorescent substrate of VMAT2, chemical structures shown in Fig.1-24) designed for optical examination of the physiological function of VMAT2 which has attracted increasing research interest as a drug target in recent years.<sup>[203]</sup> Firstly, subcellular location of VMAT2-expressing organelles was accomplished by fluorescence microscopy using FFN206 as an optical reporter.<sup>[203]</sup> Secondly, this molecule was also capable of reporting on VMAT2 activity variations resulting from the VMAT2 modulators (inhibitors, substrates, or enhancers) in a fluorometric format highly amenable to high-throughput screening.<sup>[203, 204]</sup> This special characteristic enables this molecule to investigate the process of pharmacological modulation

on neurotransmitter release and its consequences on brain function. For instance, lately, FFN206 combined with genetic manipulations was employed to investigate the role of VMAT2 in mediating amphetamine (a widely prescribed and abused drug elevating extracellular dopamine) action in dopamine neurons of *Drosophila*. It was found that inhibition of VMAT2 blocked amphetamine-induced locomotion and self administration, indicating that amphetamines must be actively transported by VMAT2 in tandem to produce psychostimulant effects.<sup>[204]</sup>

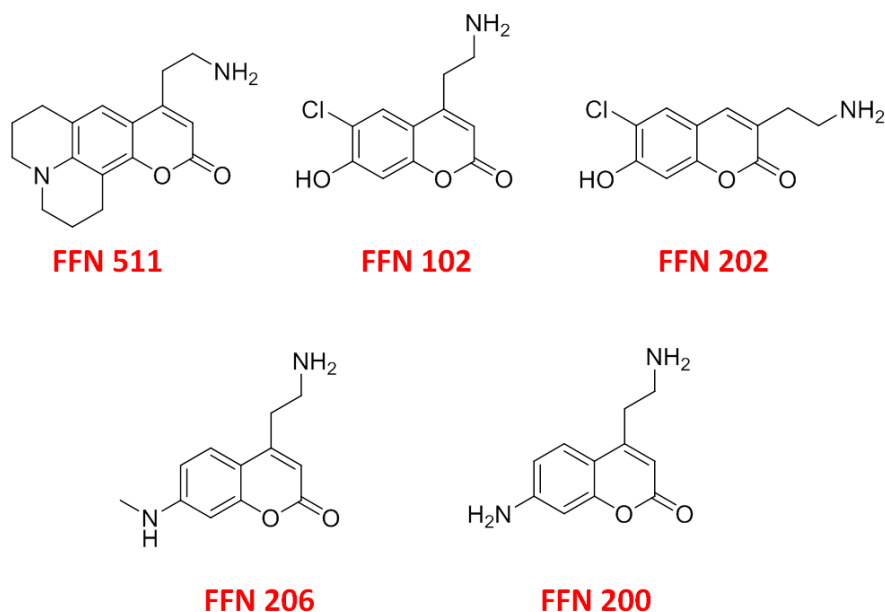


**Figure 1-24** Molecular formulas of the five reported molecules in the FFNs family.

The latest reported member in the FFNs family is FFN 200 (as shown in Fig.1-24) which represents a fluorescent VMAT2 substrate capable of being selectively loaded into VMAT2 containing vesicles and tracking monoamine exocytosis in both neuronal cell culture and brain tissue.<sup>[205]</sup> Interestingly, most of FFN 200-labeled axonal sites exhibited electrically evoked Ca<sup>2+</sup> transients with GCaMP3 whereas only a small fraction of these vesicles underwent exocytosis in response to local electrical stimulation, suggesting that the majority of vesicles capable of accumulating neurotransmitter are functionally ‘silent’ in dopaminergic axons.

In conclusion, FFNs, new emerging optical probes, have successfully been applied to fluorescent staining of various cells (Fig.1-25) as well as to the tracking of neurotransmitter release at individual release sites and the related functional parameters by optical imaging. They possess some distinct characteristics for exocytosis investigation. First of all, the staining process is easy to operate by

simply incubating target cells into solutions supplemented with the probes, without additional chemical or genetic manipulation. Secondly, as substrates of VMAT, FFNs enable purposefully staining of secretory vesicles rather than other cellular compartments in the target cells, displaying high specificity. Moreover, molecules in the FFNs family show good compatibility with other common fluorescent vesicular marker for exocytosis tracking such as FM1-43 and various fluorescent protein-based markers, making it possible to simultaneously monitor several parameters with respect to the exocytotic release in one experiment. In addition to these strengths, FFNs also suffer from some shortcomings. For instance, the optimal excitation wavelengths of the reported molecules in the FFNs family (Fig.1-24) to date are mainly around 370 nm, making them difficult to be adapted to some powerful optical techniques such as TIRFM and confocal microscopy at present. Most notably, FFNs as synaptic vesicle content markers are not capable of quantitatively detecting the actual concentration of neurotransmitters in the synaptic cleft or in the extrasynaptic areas.<sup>[202]</sup>

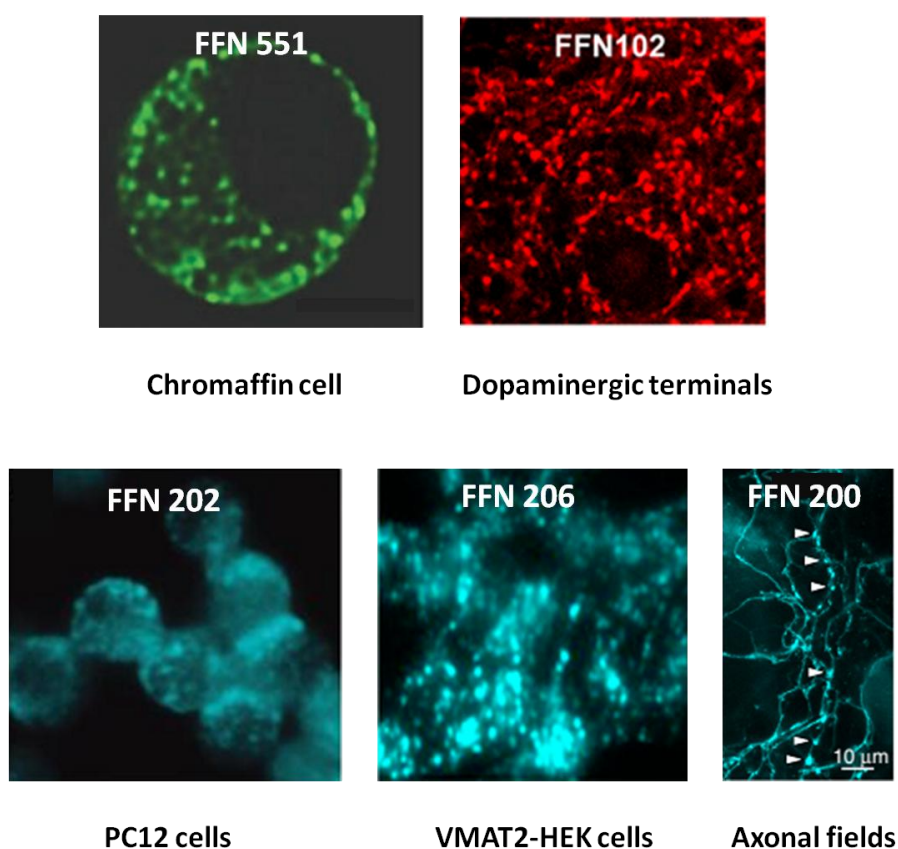


**Figure 1-25** Optical imaging examples of various cells stained by different FFNs molecules. Images adapted from references <sup>[152, 178, 200, 203, 205]</sup>. Note that the colors in the images do not represent the fluorescence emission colors.

### **1.4.3 Are fluorescent false neurotransmitters electroactive?**

As described in section 1.4.1.1, amperometric measurements of exocytotic events in living cells are mainly on the basis of electrochemically oxidation of endogenous monoamine neurotransmitters on the electrode surface. More importantly, the electroactivities of these biogenic monoamine neurotransmitters ought to be assigned to the oxidation of hydroxyl groups on the benzene ring. Interestingly, when it comes to the reported FFNs molecules (Fig.1-24), we found two of them (FFN102 and FFN202) also possess such hydroxyl group on the benzene ring, which might endow these two molecules with proper electroactivities. In consideration of their fluorescence property (section 1.4.2), we thus wonder whether it is possible to use FFNs as dual electrochemical and fluorescent probes for exocytosis studies by TIRFM/amperometry coupling technique.

### **1.5 Goals and research interests**

Amperometric detection enables studies of single vesicle fusion and transmitter release at millisecond time resolution while TIRFM has the advantage of permitting direct observation of secretory vesicles in the stages prior to fusion with distinct spatial resolution. As presented in section 1.3.3.3, the combination of these two analytical methods with complementary features allows a comprehensive and precise analysis of the whole exocytotic event. The correlation of optical and electrochemical signals will reveal more information from predocking through fusion steps up to the dynamics of vesicular release (the locations of vesicles undergoing exocytosis, the dynamics of the fusion pore, the parameters modulating the secretion, the amount of release....). The objective of this work is to test the feasibility of employing certain FFNs molecules to function as dual probes in TIRFM/amperometry coupling technique in order to track the entire exocytotic process in living cells. Specifically, to better elucidate secretory mechanisms at the single-vesicle level, our research interest in this thesis resorts to the three aspects presented as follows:

- I. Are there some FFN molecules electroactive? (Chapter 2) Whether they can work as proper electroactive reporters in amperometric detection of exocytosis? (Chapter 4)
- II. Is it possible to fluorescently track the exocytosis with specific FFNs molecules at TIRFM configuration? Which cell line is a better cell model for exocytosis investigation by the TIRFM/amperometry coupling method, PC-12 or BON N13 cells? (Chapter 3)
- III. Is it feasible to employ these FFNs molecules as a dual probe for simultaneously electrochemical/fluorescent measurement of exocytotic release? Which new information we are able to acquire owing to the application of the difunctional probe in TIRFM/amperometry coupling technique? (Chapter 5)

## 2 Photophysical and electrochemical properties characterization of 4-(2-aminoethyl)-6-chloro-7-hydroxy-2H-1-benzopyran-2-one hydrochloride

### 2.1 Synthesis of a fluorescent false neurotransmitter

Fig.2-1 presents the molecular formula of 4-(2-aminoethyl)-6-chloro-7-hydroxy-2H-1-benzopyran-2-one hydrochloride, a molecule in the FFNs family, which was synthesized according to previous procedure reported by Sames and co-workers<sup>[178, 200]</sup> and named **1** in this thesis.

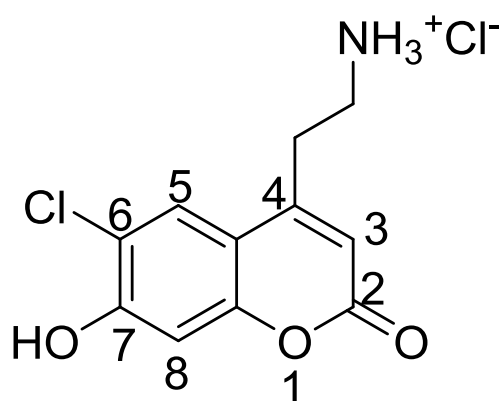


**Figure 2-1** Molecular formula of a fluorescent false neurotransmitter (FFN): 4-(2-aminoethyl)-6-chloro-7-hydroxy-2H-1-benzopyran-2-one hydrochloride, named **1** in this thesis.

For exocytosis investigation by TIRFM/amperometry coupling technique, **1** may be a promising probe due to the following three reasons. First of all, it has been reported that this molecule exhibits pH-dependent photophysical properties because of the equilibrium between the protonated phenol and the deprotonated phenolate forms.<sup>[178]</sup> Moreover, owing to the introduction of an electron-withdrawing group (-Cl) to the 6-position of coumarin, the pKa value of the phenolic hydroxyl group is decreased to around 6, lying in the relevant pH range of acidic secretory vesicles (c.a. 5~6).<sup>[206, 207]</sup> In consequence, if **1** diffuses out from the cellular vesicle (pH=5~6) to the extracellular medium (pH=7.4), a fluorescence augmentation should be observed. Secondly, its aminoethyl group could be selectively recognized by cells expressing VMAT, making it feasible for vesicle tracking by fluorescence microscopy. Finally and interestingly, it has been previously reported that a series of hydroxylated coumarins are electroactive with an ability to be oxidized at potential values comparable to those used in electrochemical detection of exocytosis.<sup>[208-210]</sup> As a consequence, **1**, a hydroxylated coumarin with a phenolic hydroxyl group at the 7-position of coumarin, could present a promising

electrochemical characteristic, predicting its potential application as a potential difunctional probe (fluorescent and electrochemical) for TIRFM/amperometry coupling measurement. Indeed, **1** used in this work was kindly synthesized by Alexandra Savy, Sylvie Maurin and Laurence Grimaud in our group (see experimental part V.1).

## 2.2 Photophysical properties characterization of **1**

### 2.2.1 Spectral characterization

We firstly measured the Ultraviolet-visible (UV-vis) absorption, excitation and emission spectra of **1** in phosphate buffer solution (PBS, pH=7.4). As shown in Fig.2-2, **1** absorbed at wavelength 300 ~ 420 nm with absorption maximum at 371 nm and emitted in the range 405 ~ 620 nm with emission maximum at 456 nm, exhibiting fluorescent properties.

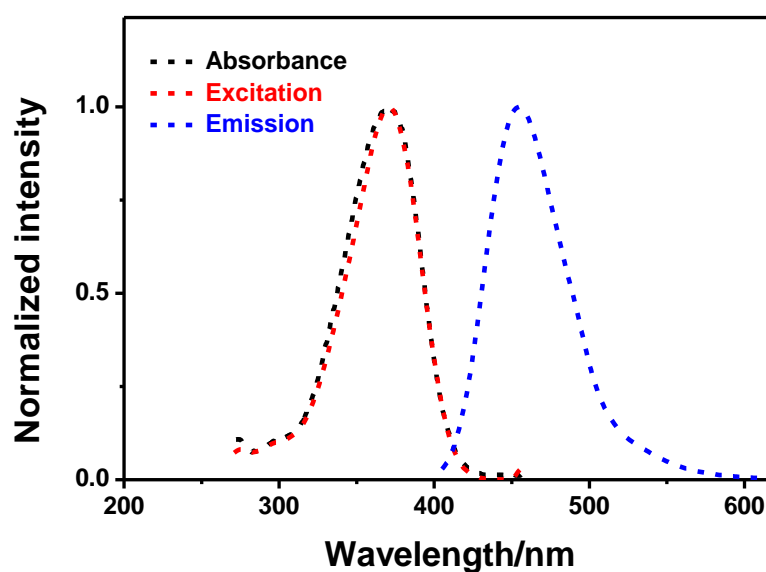


**Figure 2-2** Absorption (black dashed line), excitation (red dashed line,  $\lambda_{em} = 456$  nm), and emission (blue dashed line,  $\lambda_{ex} = 371$  nm) spectra of 10  $\mu$ M **1** dissolved in PBS solution (pH=7.4).

### 2.2.2 pH-dependent optical properties

Fig.2-3 presents the excitation spectra of **1** as a function of pH and reveals that the optical properties of this probe were strongly pH-dependent. Particularly, **1** showed two fully resolved maximum excitation

wavelengths at 330 nm and 370 nm respectively, and the excitation spectrum appeared as a mixture at pH 6.1.

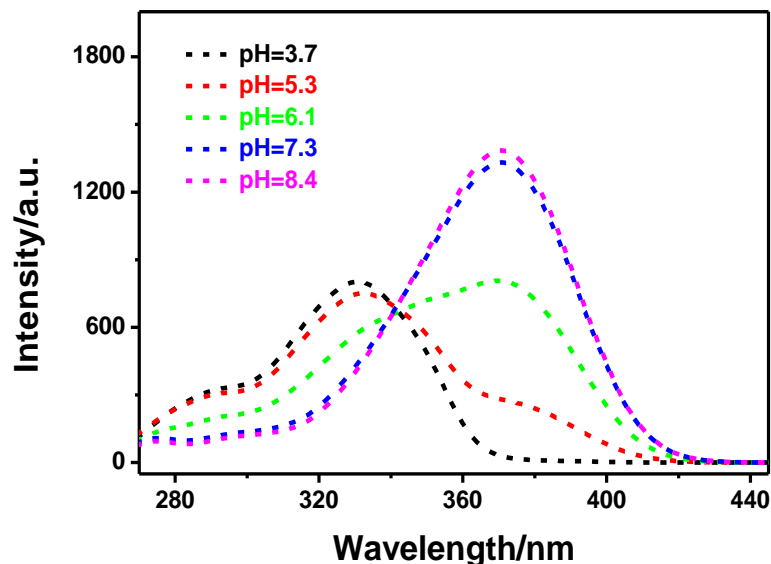


**Figure 2-3** Excitation spectra ( $\lambda_{em} = 456 \text{ nm}$ , intensities shown in arbitrary units) of  $10 \mu\text{M}$  **1** dissolved in PBS solution at different pH values: pH 3.7, pH 5.3, pH 6.1, pH 7.3, and pH 8.4.

As expected, when recording the emission spectra excited at the optimal excitation wavelength (i.e. 330 nm and 370 nm, respectively), we found that fluorescence intensity of **1** was also strongly dependent on pH values, as shown in Fig.2-4. Specifically, it exhibited higher emission intensity in basic conditions ( $\text{pH} > 7$ ) compared with that obtained in acidic environment ( $\text{pH} < 7$ ), indicating that deprotonated phenolate form of **1** was more fluorescent.

The effect of the aminoethyl group can be investigated by comparing the photophysical properties of **1** with another commercial product, 6-chloro-7-hydroxychromen-2-one (named **2** in this work), of which the chemical structure is similar to **1** (Fig.2-5). Taking account to the high similarity of pH-dependant UV-vis spectra obtained from **2** and **1** (Fig.2-6), we confirmed that the pH-dependent photophysical character of **1** was owing to the well-known equilibrium between the protonated phenol and the deprotonated phenolate forms of phenolic hydroxyl group at the 7-position of coumarin, rather than the amino group. More specifically, the former absorption peak at 330 nm corresponded to the protonated phenolic form while the latter at 370 nm to the deprotonated phenolate form. At pH 6.1, both these two forms existed, resulting in a mixed spectrum, as presented in Fig.2-6.

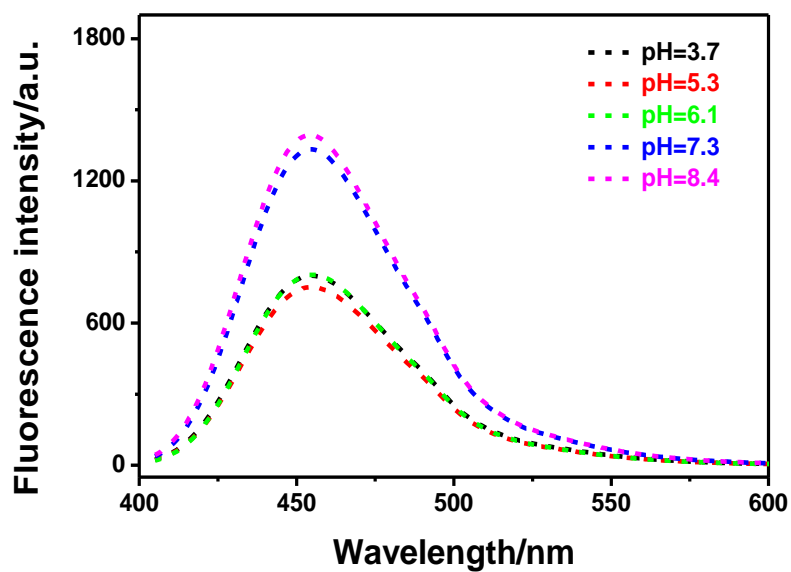


**Figure 2-4** Emission spectra (intensities shown in arbitrary units) of 10  $\mu\text{M}$  **1** dissolved in PBS solution at different pH values: pH 3.7 ( $\lambda_{ex} = 330 \text{ nm}$ ), pH 5.3 ( $\lambda_{ex} = 330 \text{ nm}$ ), pH 6.1 ( $\lambda_{ex} = 330 \text{ nm}$ ), pH 7.3 ( $\lambda_{ex} = 370 \text{ nm}$ ), and pH 8.4 ( $\lambda_{ex} = 370 \text{ nm}$ ).

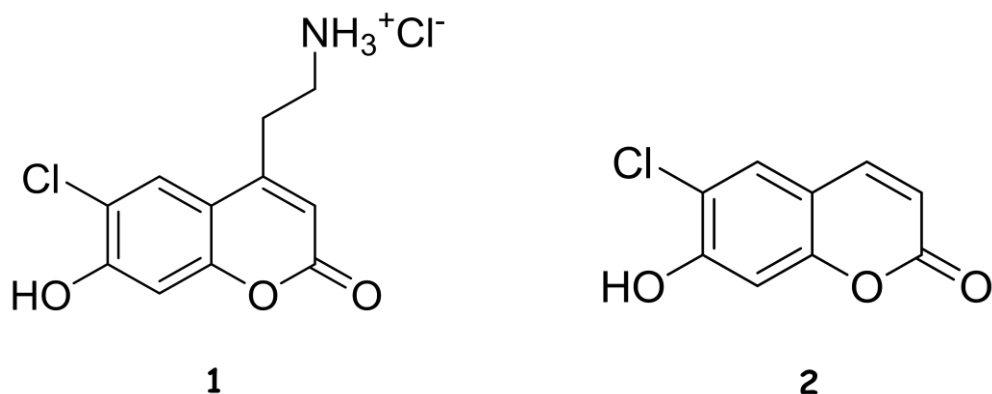


**Figure 2-5** Molecular formulas of **1** and 6-chloro-7-hydroxychromen-2-one (named **2** in this work).

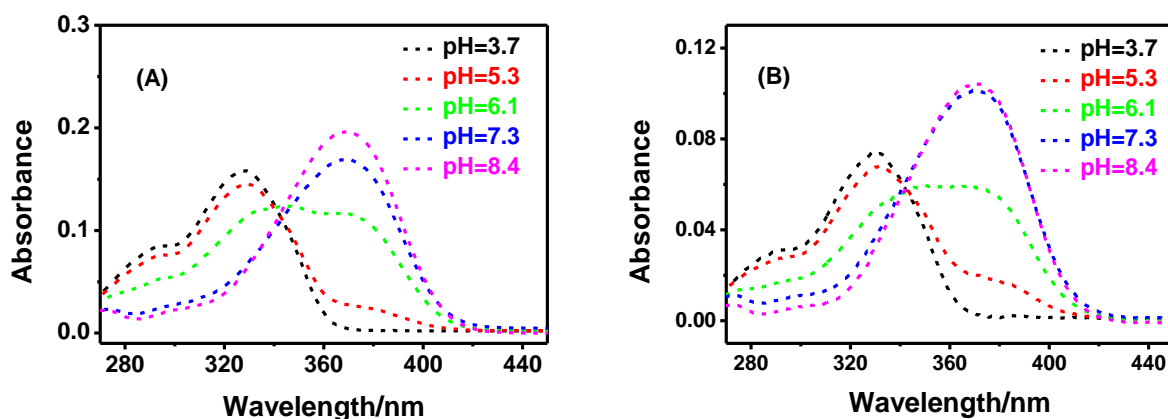


**Figure 2-6** Absorption spectra of 10  $\mu\text{M}$  **2** (A) and 10  $\mu\text{M}$  **1** (B) in PBS solution at different pH values: pH 3.7, pH 5.3, pH 6.1, pH 7.3, and pH 8.4.

As mentioned in the experimental part, our TIRFM set-up used in the laboratory is equipped with 405 nm laser source. We thus measured fluorescence intensities of 10  $\mu\text{M}$  **1** dissolved in PBS solution over a pH range from 3.7 to 8.4 with an excitation wavelength of 405 nm, as presented in Fig.2-7. We can see that **1** could be illuminated at 405 nm, showing stable fluorescence even though we lost part of fluorescent signals.

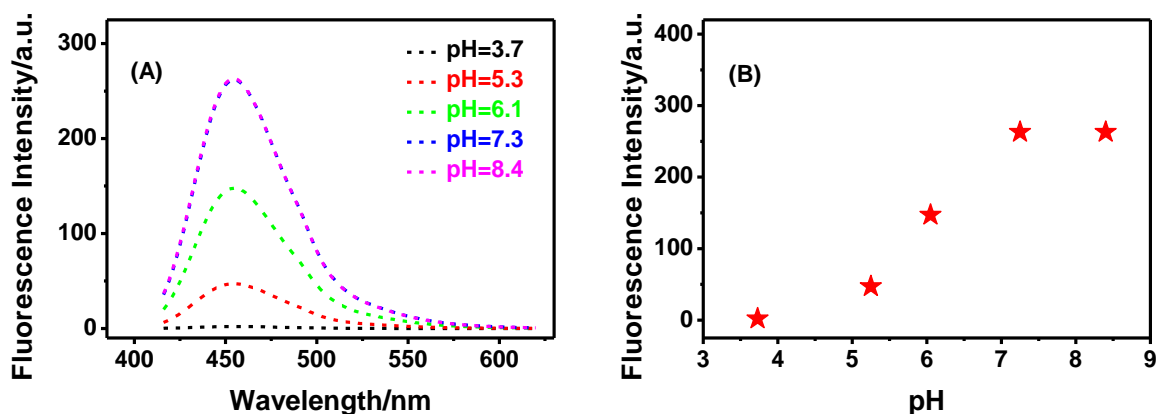


**Figure 2-7** Emission spectra ( $\lambda_{ex} = 405 \text{ nm}$ ) (A) and maximum emission intensities (B) of 10  $\mu\text{M}$  **1** in PBS solution at different pH values: pH 3.7, pH 5.3, pH 6.1, pH 7.3, and pH 8.4. Fluorescence intensities were shown in arbitrary units.

Moreover, we compared the fluorescence intensities excited at 405 nm at various pH values, demonstrating that the fluorescence intensity was almost doubled from pH 5 to pH 7. As a result, if this molecule is employed as fluorescent probes to mark the cellular vesicles, we are expecting to see an augmentation of fluorescent signals caused by pH gradient when **1** diffusing out from the acidic vesicles (pH=5~6) to neutral extracellular medium (pH=7.4).

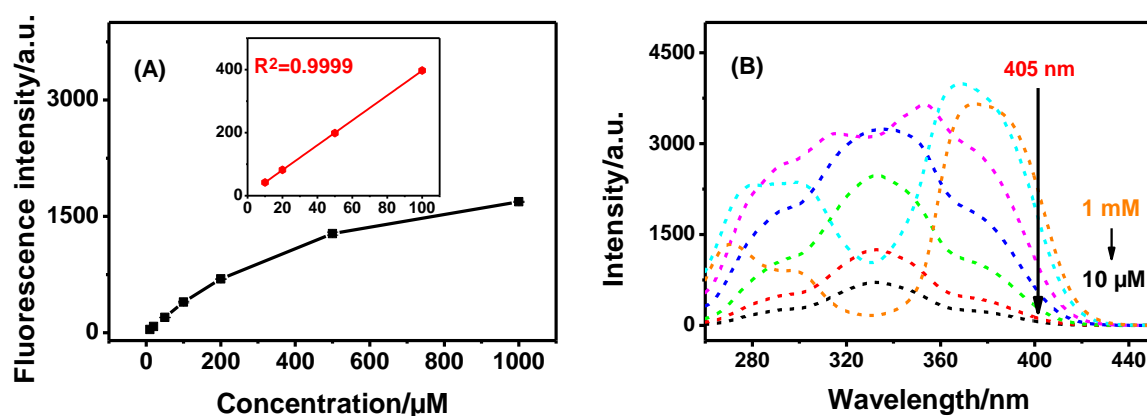


**Figure 2-8** Maximum emission intensities ( $\lambda_{ex} = 405 \text{ nm}$ ) (A) and excitation spectra ( $\lambda_{em} = 456 \text{ nm}$ ) (B) of **1** in PBS (pH = 5.3) at different concentrations: 10  $\mu\text{M}$ , 20  $\mu\text{M}$ , 50  $\mu\text{M}$ , 100  $\mu\text{M}$ , 200  $\mu\text{M}$ , 0.5 mM and 1 mM. Intensities were shown in arbitrary units.

We then investigated the effect of concentrations of **1** by measuring maximum emissions illuminated at 405 nm from **1** at various concentrations from 10  $\mu\text{M}$  to 1 mM. As shown in Fig.2-8, at acidic condition (pH = 5.3) which is similar to the microenvironment inside cellular vesicles, a good linear relationship was observed between the emission intensity and the concentration of **1** from 10  $\mu\text{M}$  to 100  $\mu\text{M}$  ( $R^2=0.9999$ ), as illustrated in the inset of Fig.2-8(A). However, when the concentration of **1** became higher, exceeding 100  $\mu\text{M}$ , an effect of fluorescence self-quenching was taking place (Fig.2-8(B)), causing a slower growth of fluorescence emission intensities.

Based on the investigations reported above, we propose that **1**, a synthesized analog of monoamine neurotransmitters, could be applied for the vesicular tracking during exocytosis owing to its stable, pH-dependent fluorescence. If **1** is released from an individual acidic vesicle to neutral extracellular medium, the fluorescent signal transiently brightens and then disappears due to its diffusion, that is, single exocytotic events are expected to be visualized as ‘puffs’ of light which is accompanied by the disappearance of fluorescent spot, as other reported pH-dependent fluorescent probes.<sup>[19, 211]</sup>

## 2.3 Electrochemical characterization

Nowadays, electrochemical techniques such as chronoamperometry and fast-scan cyclic voltammetry are powerful tools for the study of neurotransmission thanks to some easily oxidizable monoamine neurotransmitters.<sup>[2, 33, 35, 38, 65]</sup>

Serotonin (molecule **3**)<sup>[118, 168, 197]</sup> and catecholamines such as dopamine (molecule **4**)<sup>[212, 213]</sup>, norepinephrine (molecule **5**)<sup>[214, 215]</sup> as well as epinephrine (molecule **6**)<sup>[216, 217]</sup> are the most commonly employed electroactive reporters for electrochemical test of cellular secretions via exocytosis. Interestingly, the electroactivities of these neurotransmitters are all attributed to the oxidation of the phenolic hydroxyl group, as shown in Fig.2-9.

In addition, umbelliferone (molecule **7**) and benzotertonic acid (molecule **8**), two representative and widely used coumarins, were also reported to be electroactive.<sup>[208]</sup> Since the chemical structure of **1** is similar to umbelliferone, possessing both one phenolic hydroxyl group and the pyrone ring, we thus start to consider its ability of functioning as an electroactive probe for exocytosis investigation.

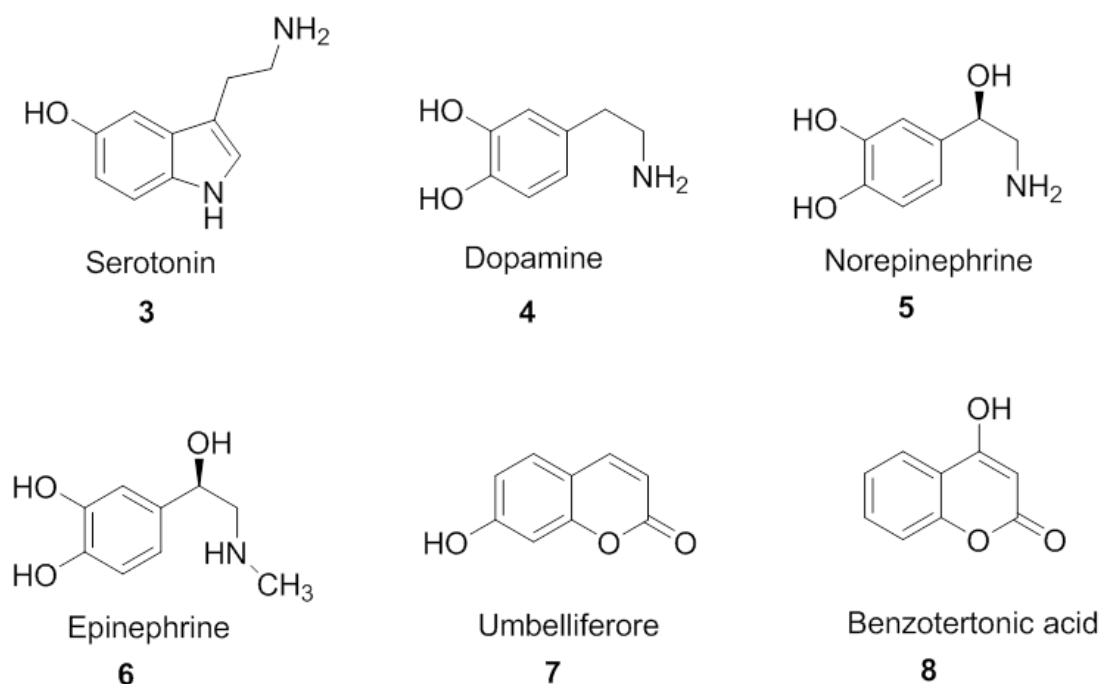


*Figure 2-9 Molecular formulas of well-known electroactive molecules.*

### 2.3.1 Electrochemical test of 4-(2-chloroethyl)-6-chloro-7-hydroxy-2H-1-benzopyran-2-one and **1** on glassy carbon electrode

To confirm the electroactivity of the phenolic hydroxyl group at the 7-position of coumarin, electrochemical detection was firstly carried out with a precursor of **1** synthesis, 4-(2-chloromethyl)-6-chloro-7-hydroxy-2H-1-benzopyran-2-one, which also owns a phenolic hydroxyl group and the pyrone ring (molecule **9** shown in Fig.2-10, synthesized by Alexandra Savy, Sylvie Maurin and Laurence Grimaud in our group). A three-electrode system (Fig.2-11(A)) with a 1 mm diameter glassy carbon working electrode (GCE), a platinum net auxiliary electrode, and a saturated calomel reference electrode (SCE), was used to conduct the cyclic voltammetric measurements. The potential was cycled from +0.1 V to +1.2 V and back to +0.1 V (vs. Ag/AgCl) at a scan rate of 20 mV/s. Moreover, GCE was polished between each test to get a reproducible working surface. Fig.2-11(B) presents the cyclic voltammograms (CVs) of 0.5 mM **9** obtained from the 1 mm diameter GCE. We can see that only one anodic peak appeared at around +0.76 V for **9** without the corresponding cathodic peak, indicating its irreversible oxidation process. Moreover, according to the six well overlapped CVs of **9**, the 1-mm GCE shows good reproducibility after the polishment between each test.

Furthermore, the effect of scan rate on the anodic peak was also evaluated. As shown in Fig.2-12, a plot of peak current versus square root of the potential scan rate (from 10 mV/s to 200 mV/s) for 0.5 mM **9** solution (pH=7.5) resulted in a linear response ( $y=0.136 X-0.067$ ,  $R^2 = 0.998$ ), suggesting a planar diffusion controlled electrochemical process of **9** oxidation.

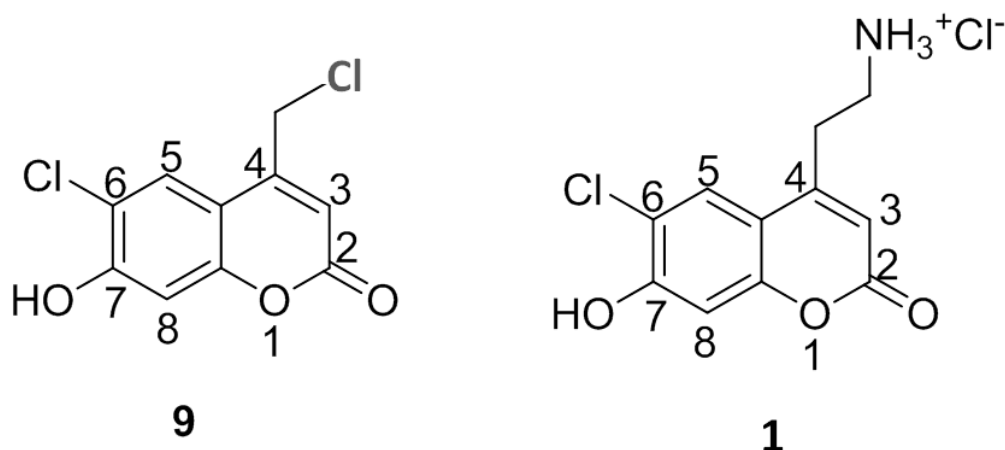


**Figure 2-10** Molecular formulas of 4-(2-chloromethyl)-6-chloro-7-hydroxy-2H-1-benzopyran-2-one (**9**) and **1**.

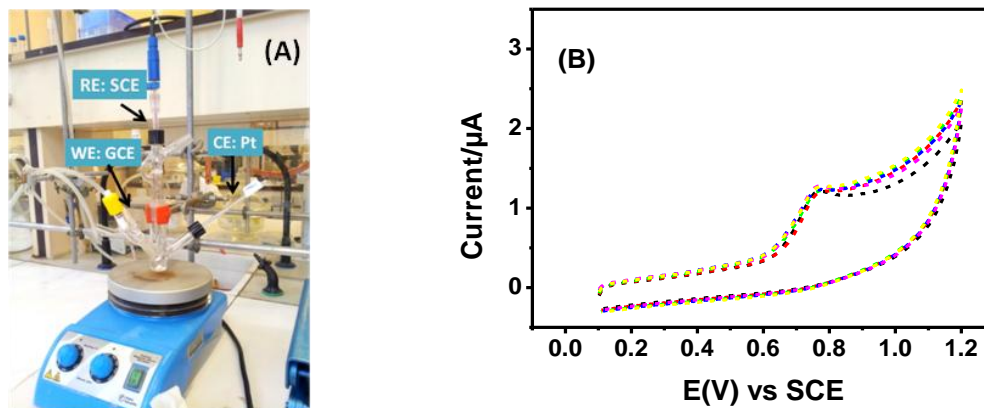


**Figure 2-11** (A) Experimental setup for cyclic voltammetric measurement with 1-mm GCE electrode; (B) Six consecutive cyclic voltammograms (CVs) of 0.5 mM **9** in PBS/MeOH solution (pH=7.5). Initial potential: +0.1 V (vs. Ag/AgCl); scan rate: 100 mV/s.

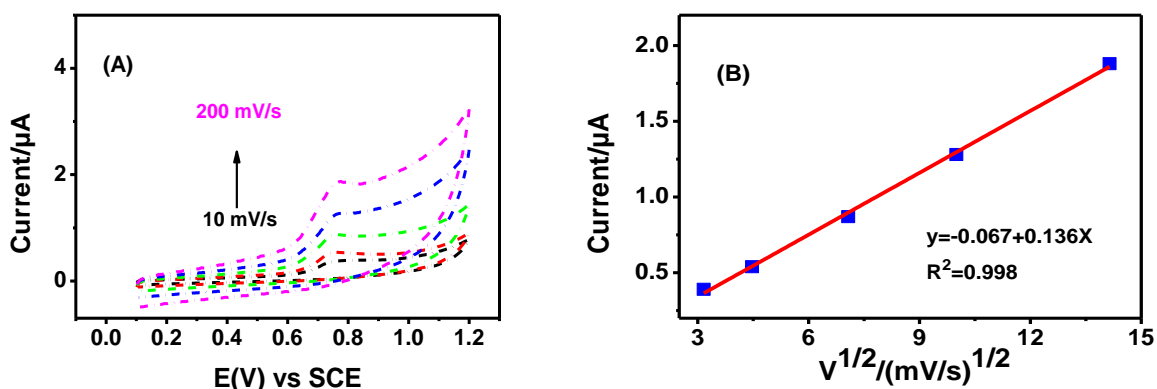


**Figure 2-12** (A) CVs of 0.5 mM **9** in PBS/MeOH solution (pH=7.5) obtained at different scan rates: 10 mV/s, 20 mV/s, 50 mV/s, 100 mV/s, and 200 mV/s. Initial potential: +0.1 V (vs. Ag/AgCl); (B) A plot of peak current versus square root of scan rate (from 10 mV/s to 200 mV/s).

Similar results were obtained during CV studies of 1 mM **1** in PBS/DMSO solution (pH=7.4). Fig.2-13 illustrates that **1** started to be oxidized at +0.60 V, showing an oxidation peak at about +0.76 V. According to current electrochemical results, both **1** and **9** could be oxidized on GCE surface with the same oxidation peak at around +0.76 V, exhibiting good electroactivity.

Taking account to the highly similarity of their molecular structures, we affirm that the electroactivity of **1** arises from the oxidation of its phenolic hydroxyl group at the 7-position of coumarin, rather than

its aminoethyl group. Additionally, a good linear relationship ( $y=0.125x-0.2$ ,  $R^2 = 0.995$ ) was observed between the oxidation peak current and the square root of the potential scan rate (from 10 mV/s to 200 mV/s) at the acidic environment (pH=5), demonstrating the planar diffusion controlled electrochemical process of FFN oxidation (Fig.2-14).

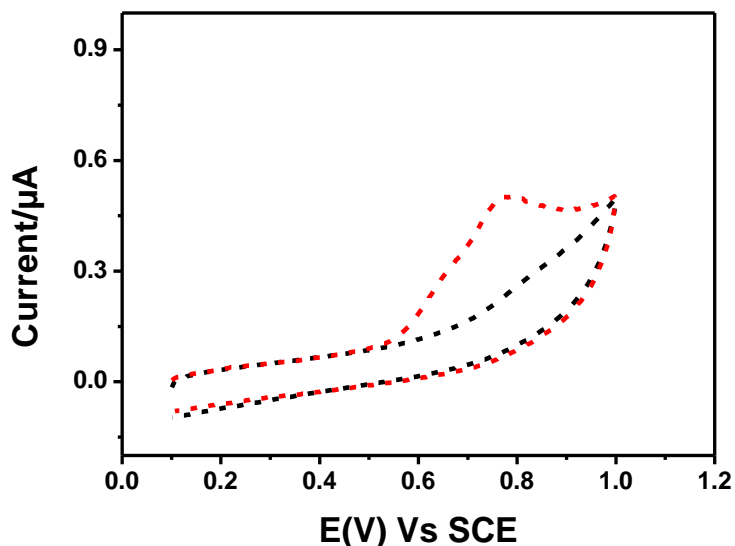


**Figure 2-13** CVs of 1 mM **1** (pH=7.4) in PBS/DMSO solution (red dashed line) and the blank (black dashed line). Initial potential: +0.1 V (vs. Ag/AgCl); scan rate 10 mV/s.

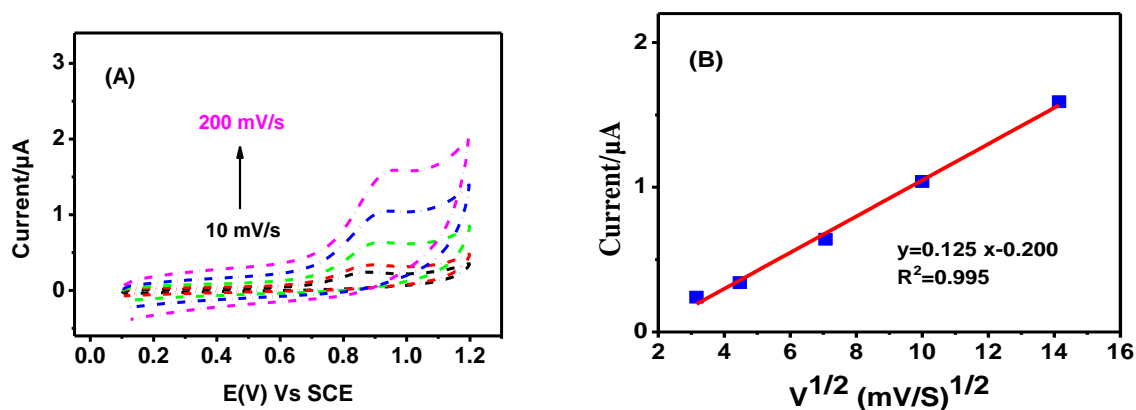


**Figure 2-14** (A) CVs of 1 mM **1** in PBS/DMSO solution (pH=5) obtained at different scan rates: 10 mV/s, 20 mV/s, 50 mV/s, 100 mV/s, and 200 mV/s. Initial potential: +0.1 V (vs. Ag/AgCl); (B) A plot of peak current versus square root of scan rates (from 10 mV/s to 200 mV/s) for 1 mM **1**.

In order to investigate the effect of the predominant species (pKa of **1** is about 6), we tested the pH behavior of **1** oxidation in PBS over a pH range of 5.1 to 8.5 by using GCE. As illustrated in Fig.2-15, the CVs of **1** were pH-dependant and its oxidation peak potential shifted to more negative values with the increasing of pH values. In addition, the oxidation peak current was higher at basic condition compared with that obtained at acidic environment, suggesting that a deprotonated phenolate form of **1** was easier to be oxidized.

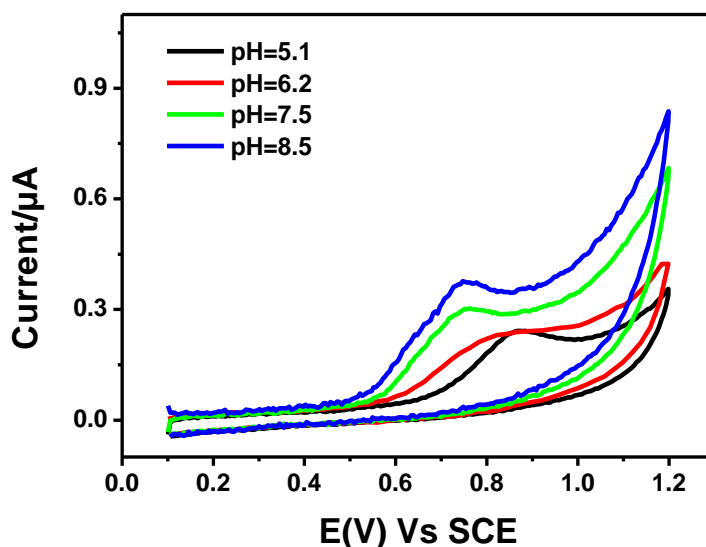


**Figure 2-15** CVs of 1 mM **1** in PBS/DMSO solution at different pH values (pH=5.1, 6.2, 7.5 and 8.5). Initial potential: +0.1 V (vs. Ag/AgCl); scan rate 10 mV/s.

Briefly, so far, we have demonstrated that **1** undergoes a pH-dependent, irreversible electrooxidation on GCE and the phenolic hydroxyl group in the 7-position of the coumarin nucleus contributes to its electroactivity. Because **1** is supposed to be involved in amperometric measurements of exocytosis at the single cell level, we have to firstly verify if the electrochemical behavior observed at vitreous carbon can be extended to CFE.

### 2.3.2 Electrochemical test of **1** on CFE

- **Cyclic voltammetry of **1** on CFE**

Fig.2-16(A) displays single CVs of 0.5 mM **1** (pH=7.5) and 0.5 mM **9** (pH=7.5) obtained from 10-μm CFE. The potential was cycled from +0.1 V to +1.0 V and back to +0.1 V (vs. Ag/AgCl) at a scan rate of 50 mV/s. Similarly to the results mentioned above, both **1** and **9** exhibited an irreversible oxidation

peak at +0.76 V for the oxidation of the phenolic hydroxyl group and the irreversibility was testified by the lack of any corresponding reduction peak on the reverse cycle, in agreement with the results we obtained by GCE, as previously described. Nevertheless, an additional passivation of CFE surface due to electrooxidation of **1** was seen according to the sudden decrease of oxidation current from the second cycle on, as shown in Fig.2-16(B). A non-conductive polymer film formation or product adsorption onto electrode was thus supposed to have taken place during the electrooxidation process of **1**.

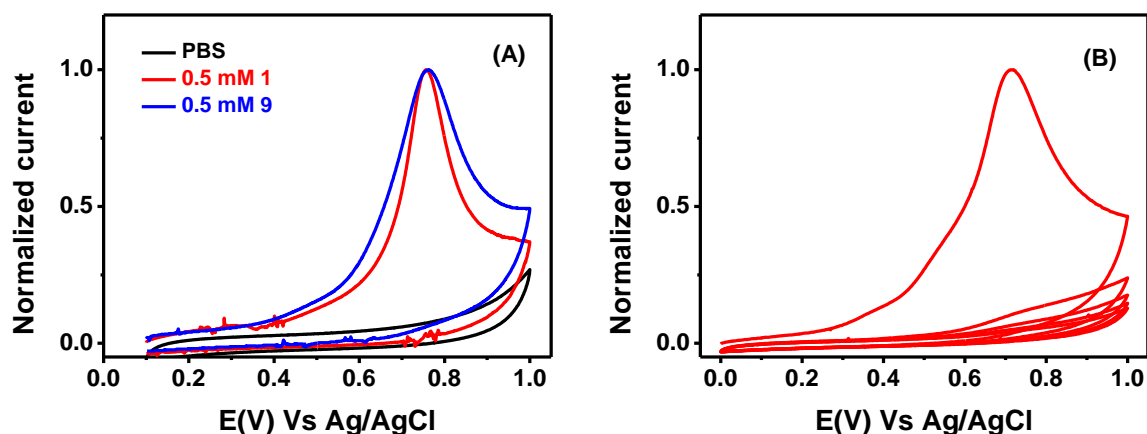


**Figure 2-16** (A) CVs of 0.5 mM **1** (red line), 0.5 mM **9** (blue line) as well as the blank solution (PBS/DMSO (v/v) = 4/1, black line) obtained by CFE (pH=7.5); scan rate: 50 mV/s. (B) five consecutive CVs of 1 mM **1** in PBS/DMSO solution. Initial potential: 0 V (vs. Ag/AgCl); scan rate: 100 mV/s.

- **pH-dependence of cyclic voltammograms of **1****

Investigation of pH influence on CVs of **1** (pKa~6) was also carried out with 100  $\mu$ M **1** dissolved in PBS over a pH range of 5 to 8, as presented in Fig.2-17. We can observe that the oxidation current peak of **1** shifted to more negative values with the increase of pH value from 5 to 8, as indicated by the dashed arrow in the figure. More specifically, at pH 8, **1** existed mainly as the deprotonated phenolate form which could be oxidized at +0.86 V by CFE while at pH 5, **1** existed mainly as the undissociated molecules which started to be oxidized at +0.90 V. This result confirms our previous viewpoint that the oxidation of **1** ought to take place at the hydroxyl site and the deprotonated phenolate form tends to be oxidized at lower potential.

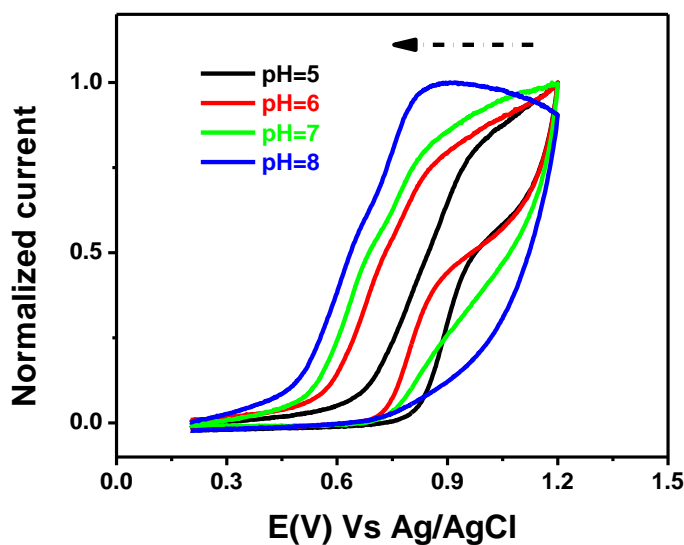


**Figure 2-17** Normalized CVs (obtained by CFE) of  $100 \mu\text{M}$  **I** in PBS solution at different pH values of 5, 6, 7, and 8. Initial potential:  $+0.2 \text{ V}$  (vs. Ag/AgCl); scan rate  $100 \text{ mV/s}$ . All the CVs presented were background-subtracted.

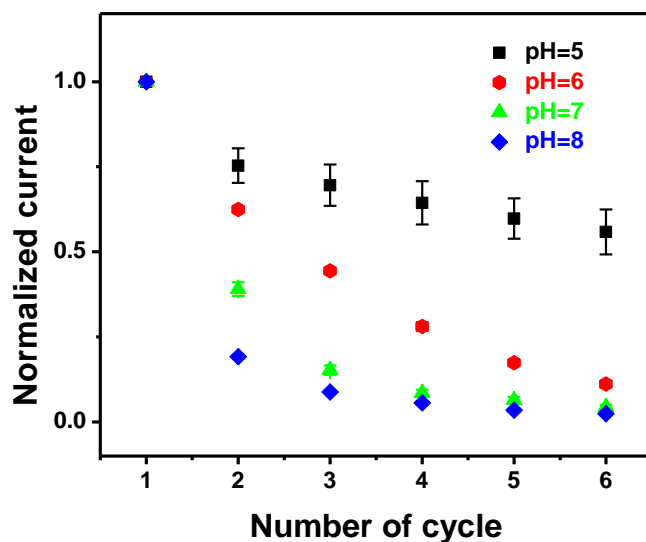


**Figure 2-18** Peak current of six consecutive CVs (obtained by CFE) from  $100 \mu\text{M}$  **I** in PBS solutions at different pH values of 5, 6, 7, and 8. Each point represents an average of triplicate measurements; scan rate:  $100 \text{ mV/s}$ .

The passivation of the electrode presumably due to the electrochemical detection was also considered. Therefore Fig.2-18 depicts peak currents of six consecutive CVs obtained from 100  $\mu\text{M}$  **1** on CFE in PBS solutions over a pH range from 5 to 8. It is evident that the CFE surface was blocked faster and faster as the increase of pH values. Furthermore, taking account to the successive CVs of **1** recorded at different pH values (Fig.2-19), the shape of the oxidation wave of **1** seemed to be modified. Indeed, a plateau was observed at lower pH values ( $\text{pH} \leq \text{p}K_a$ , i.e.  $\text{pH} = 5$  or  $6$ ) while at higher pH values ( $\text{pH} > \text{p}K_a$ , i.e.  $\text{pH} = 7$  or  $8$ ), a peak of current was preferentially obtained. Such pH-dependent shapes suggest that the concentration of the deprotonated phenolate form of **1** plays a role on the passivation phenomenon. Combined to the previous data above, it evidences that the deprotonated phenolate form of **1** is the real species involved during the oxidation process.

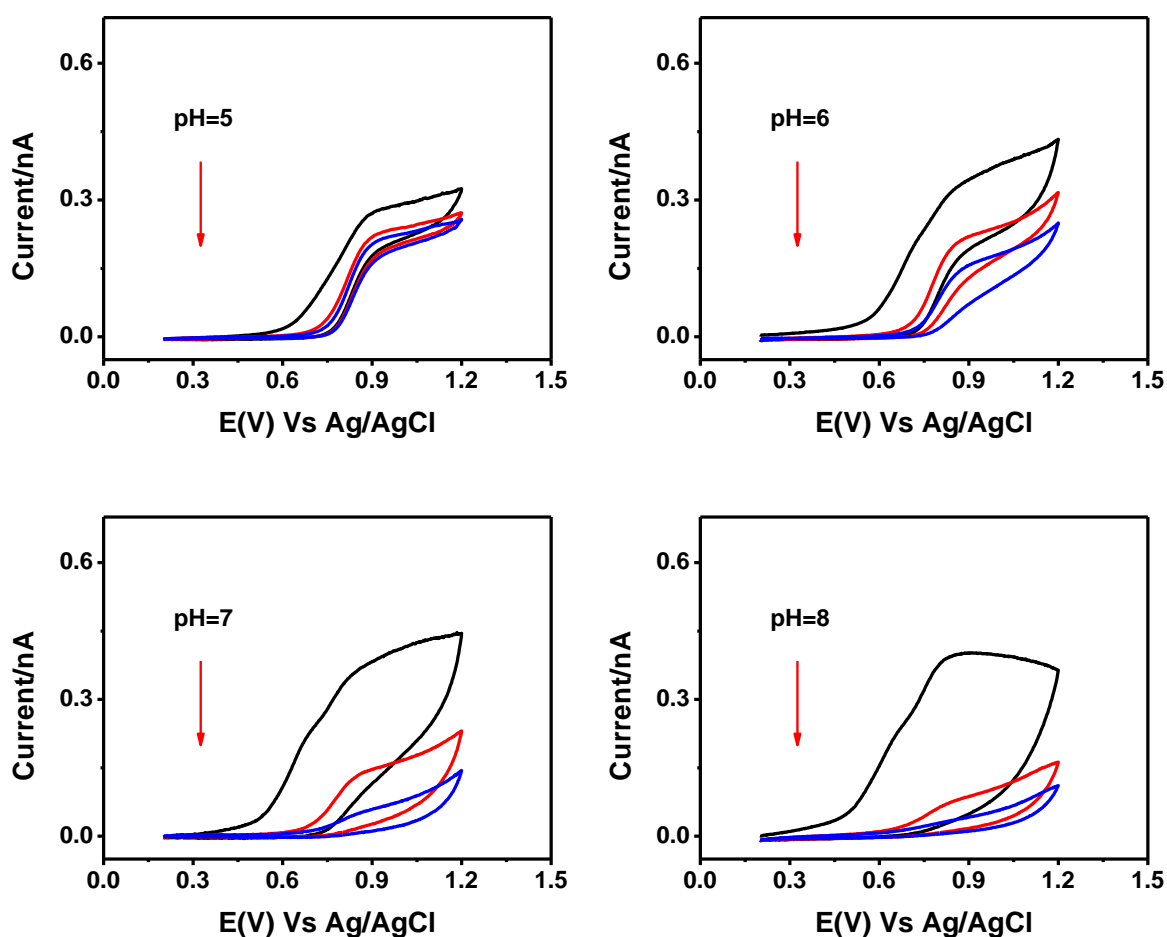


**Figure 2-19** Three consecutive CVs (obtained by CFE) of 100  $\mu\text{M}$  **1** in PBS solutions at different pH values of 5, 6, 7, and 8. Initial potential: +0.2 V (vs. Ag/AgCl); scan rate 100 mV/s. All the CVs presented were background-subtracted.

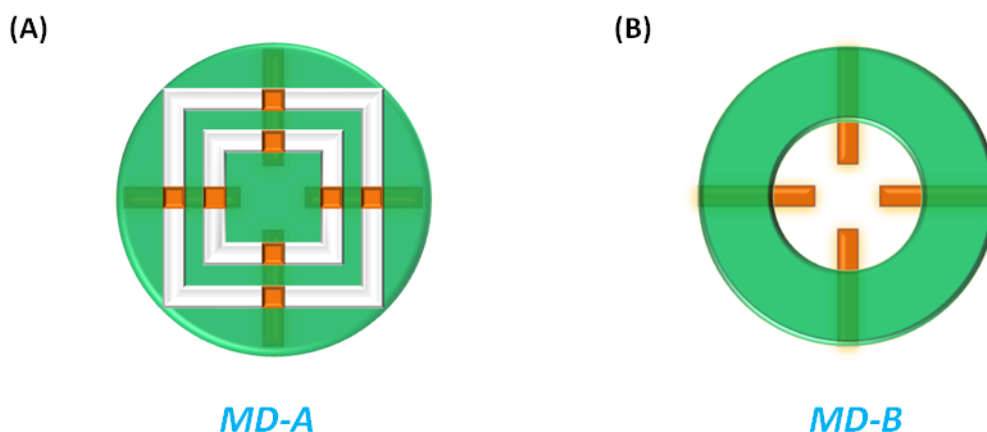
We summarize that **1** was able to be oxidized on CFE surface, showing good electroactivity and its electroactive behavior was highly pH-dependent owing to the phenolic hydroxyl group in the 7-position of the coumarin. CFE was inclined to be passivated by **1** as that we observed on GCE and the passivation rate was faster at basic environment compared with that we observed at acidic environment.

### **2.3.3 Electrochemical test of 1 on ITO microelectrodes**

Different types of microelectrodes have been employed for amperometric detection of electroactive molecules discharged from individual vesicle during exocytosis. Among them, ITO microelectrodes appear to be a good choice owing to their excellent optical transparency, high electrical conductivity as well as their appropriate electrochemical working window for the electroanalysis of biomessengers.<sup>[19, 105, 111, 119, 120]</sup>

In our work, we chose the transparent and conductive ITO microelectrodes as working electrodes to study the cellular exocytosis because they are adapted to a simultaneous combined fluorescence and electrochemical detection at the bottom of living cells. All our ITO microelectrodes were manufactured by photolithographic process and acidic wet etching (see Scheme E-2 in the experimental section for more details).<sup>[218]</sup>

A 150 nm-thick layer of transparent ITO on a quartz slide has been selected here for the microdevices fabrication. In the first step, we patterned four independent ITO microbands (200- $\mu\text{m}$  width, 150-nm thickness) onto the glass substrates by using the positive photoresist AZ9260. The whole surface of the glass slide, including the four ITO band-arrays was then completely insulated with a negative photoresist SU8-3010 and a second photolithographic process was then conducted in order to define specific ITO working areas. Different pre-designed masks were thus employed to produce ITO microdevices with different lengths, shapes and configurations.



**Scheme 2-1** Two representative microfabricated ITO devices for electrochemical test of **1**: (A) microdevice A includes four independent ITO microelectrodes (shown in orange) in total and each electrode embeds with two ITO bands of 200- $\mu\text{m}$  width  $\times$  200- $\mu\text{m}$  length; (B) microdevice B includes four independent ITO microelectrodes (shown in orange) in total and each electrode embeds with an ITO band of 200- $\mu\text{m}$  width  $\times$  600- $\mu\text{m}$  length.

For instance, Scheme 2-1 displays two representative microfabricated ITO devices for electrochemical properties investigation of **1**. For microdevice A (MD-A), the mask was designed to carve a spiral-like microchannel of 200- $\mu\text{m}$  width in the SU8-3010 photoresist layer. This microchannel crossed perpendicularly the four ITO microbands at periodic instances thus exposing a series of squared ITO sections (200  $\mu\text{m}$   $\times$  200  $\mu\text{m}$ ) lying on the glass floor of the spiraling microchannel. For microdevice B (MD-B), a disk area of the SU8-3010 photoresist in the center was removed by the mask through photolithographic process. As a result, the terminal shafts of the four ITO bands with 600- $\mu\text{m}$  lengths were exposed and defined as the working area for this microsystem.

- **Influence of ITO patterns**

Fig.2-20 shows CVs of 100  $\mu\text{M}$  **1** measured on the two microfabricated ITO devices mentioned above (MD-A and MD-B) in PBS solution (pH=7.4). For MD-A, the four CVs acquired on the four identical ITO microbands were well overlapped, indicating the high reproducibility of the four ITO microelectrodes. However, when it comes to MD-B, different oxidation peak currents of **1** were recorded due to the different lengths of ITO microelectrodes which could be attributed to the imperfect alignment during the second step of photolithographic process (i.e. the SU8-3010 isolation process).

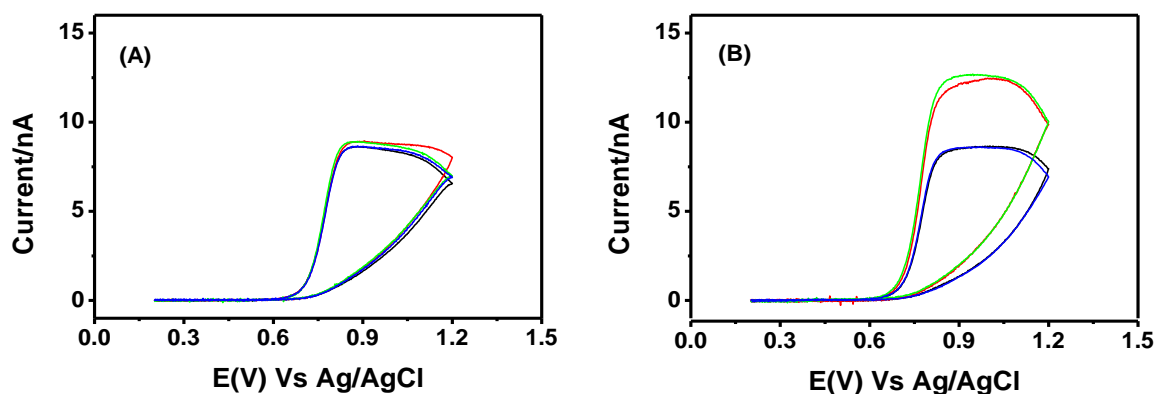


**Figure 2-20** CVs of 100  $\mu\text{M}$  **1** in PBS solution ( $\text{pH}=7.4$ ) obtained from (A) four independent ITO bands in MD-A and (B) Four different ITO bands in MD-B. Initial potential: +0.2 V (vs. Ag/AgCl); scan rate 20 mV/s.

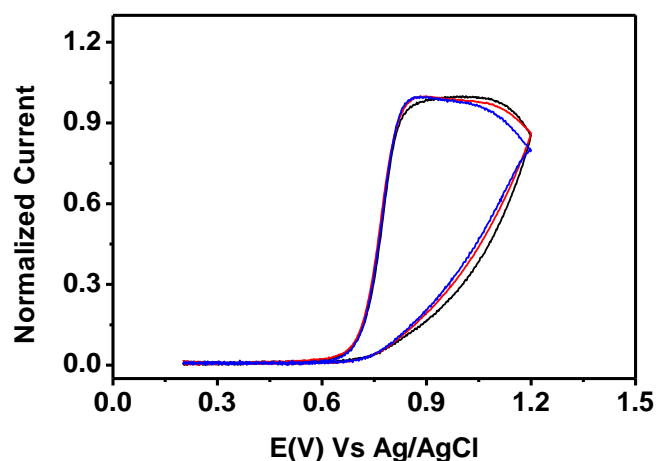


**Figure 2-21** Normalized CVs of 100  $\mu\text{M}$  **1** in PBS solution ( $\text{pH}=7.4$ ) obtained from 400- $\mu\text{m}$  ITO (blank line), 600- $\mu\text{m}$  ITO (blue line) and 200- $\mu\text{m} \times 2$  ITO band (red line). Initial potential: +0.2 V (vs. Ag/AgCl); scan rate 20 mV/s.

Nevertheless, based on CVs, at basic environment ( $\text{pH}=7.4$ ), **1** started to be oxidized at +0.65 V and arrived at a plateau at +0.85 V. The irreversibility of the electrooxidation of **1** on ITO microelectrode was also verified by the appearance of the oxidation peak rather than a plateau.

Moreover, as illustrated in Fig.2-21, the normalized CVs curves recorded from ITO microelectrodes of various configurations were well overlapped with each other, demonstrating that the oxidation of **1** on ITO microelectrode was independent on the patterns we used for their fabrication.

Since it is feasible to get the identical ITO microelectrodes with the spiral mask, we chose MD-A for the electrochemical characterization of **1**.

- **pH influence**

The influence of pH values on CVs of **1** recorded on ITO microelectrodes was in accordance with that we acquired on GCE and CFE. That is to say, the oxidation current peak shifted to more negative position with the pH increasing from 5 to 8 (Fig.2-22).

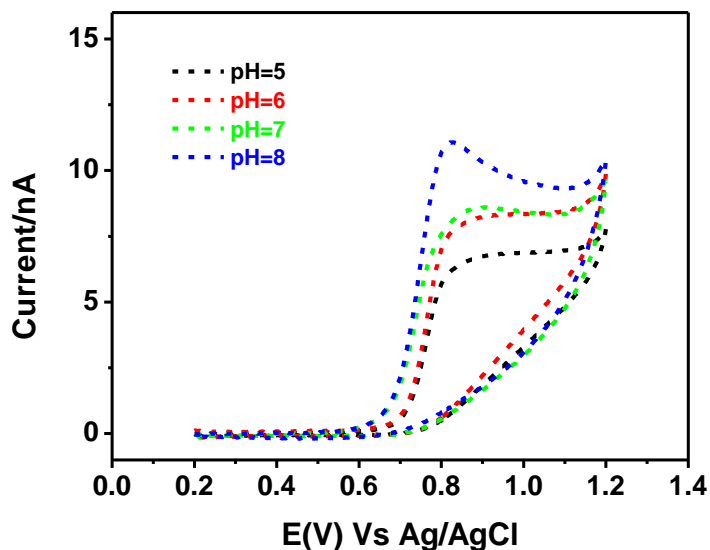


**Figure 2-22** CVs of 100  $\mu\text{M}$  **1** in PBS solutions over a range of pH values on ITO microelectrodes in MD-A: pH=5 (black dashed line), pH=6 (red dashed line), pH=7 (green dashed line), and pH=8 (blue dashed line); initial potential: + 0.2 V (vs. Ag/AgCl); scan rate 20 mV/s.

In addition, since the deprotonated phenolate form is prone to be oxidized, an augmentation of current peak value is predicted to be observed. As presented in Fig.2-23, for triplicate measurements, the mean values of peak currents obtained at pH 5, pH 6, pH 7, and pH 8 were 13.0 nA, 16.0 nA, 17.8 nA as well as 21.7 nA, respectively, confirming our viewpoint described previously.

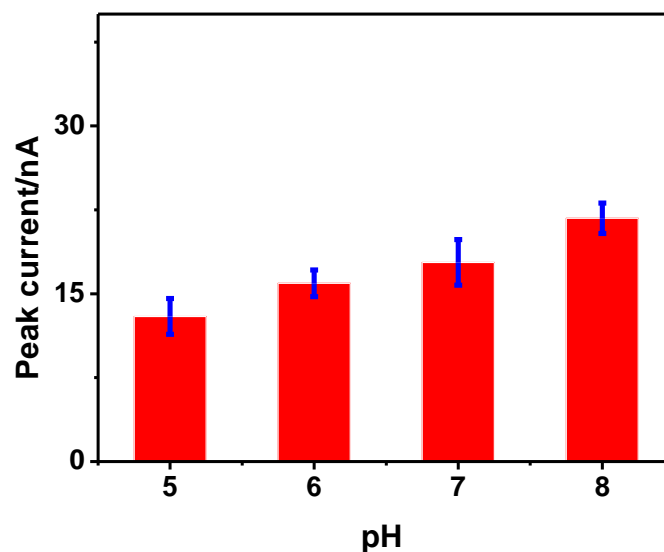


**Figure 2-23** Peak currents of CVs of 100  $\mu\text{M}$  **1** in PBS solutions over a range of pH values on ITO microelectrodes in MD-A. Each point represents an average of triplicate measurements; scan rate: 100 mV/s.

Fig.2-24 shows mean values of peak currents from six consecutive CVs obtained from 100  $\mu\text{M}$  **1** in PBS solutions over a pH range from 5 to 8. The decrease of **1** anodic peak currents upon successive CVs was consistent with the results we acquired on CFE. Specifically, ITO electrode surface was blocked faster and faster as the increase of pH values from 5 to 8. To elucidate the pH influence clearly, we compared the insulating process of the ITO microelectrode surface by **1** oxidation at pH 5 and pH 8. As shown in Fig.2-25, for both conditions, the electrode passivation was highlighted as the film grew on repeated scans. However, during the second cycle, the peak currents decreased by 20% and 50% at pH 5 and pH 8, respectively. As the passivation of ITO surface by **1** electrooxidation was more speedy at basic condition (pH=8), we conclude that the oxidation of deprotonated phenolate favored the formation of uncondutive film on ITO microelectrode surface.

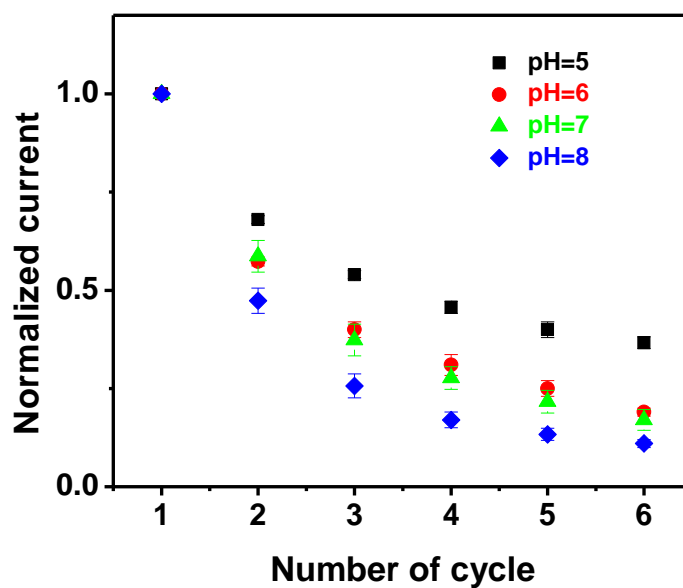


**Figure 2-24** Current-pH diagram of 100  $\mu\text{M}$  **I** in PBS solution. Each point represents an average of triplicate measurements obtained by CVs obtained in MD-A; scan rate: 100 mV/s.

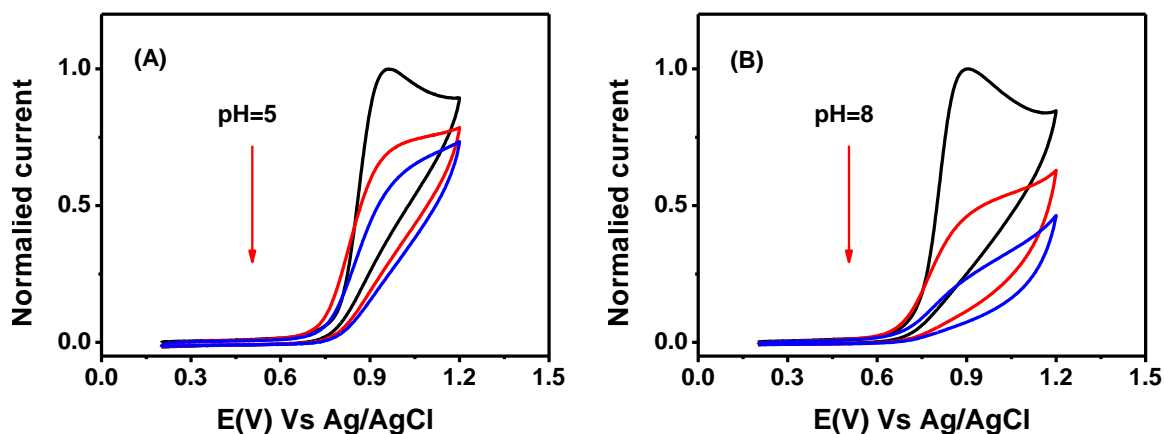


**Figure 2-25** Three consecutive CVs of 100  $\mu\text{M}$  **I** in PBS solutions at pH 5 (A) and pH 8 (B) in MD-A. Initial potential: +0.2 V (vs. Ag/AgCl); scan rate 100 mV/s. All the voltammograms presented were background-subtracted.

- **Influence of **1** concentration**

The concentration influence on the CVs of **1** on ITO microelectrodes was then studied. As illustrated in Fig.2-26, the normalized CVs of **1** from 20  $\mu\text{M}$  to 1mM were overlapped with each other, suggesting that the concentration of **1** did not affect the main feature of its electrooxidation on ITO surface. The lightly imperfect overlap could be attributed to the slight difference between ITO electrode surfaces.

In the meanwhile, oxidation current of **1** augmented from 2.4 nA to 22.4 nA as the increase of its concentration from 20  $\mu\text{M}$  to 1 mM. However, no linear relationship was seen between the recorded peak current value and the concentration of **1**, which was mainly caused by the increase of passivation rate of the ITO electrode surface with the augmentation of **1** concentration at low scan rate of 20 mV/s (Fig.2-27). In other words, the more amount of deprotonated phenolate form of **1** exists, the faster the electrode surface becomes blocked, confirming our previous viewpoint that the real species involved during the oxidation process is the deprotonated phenolate form.

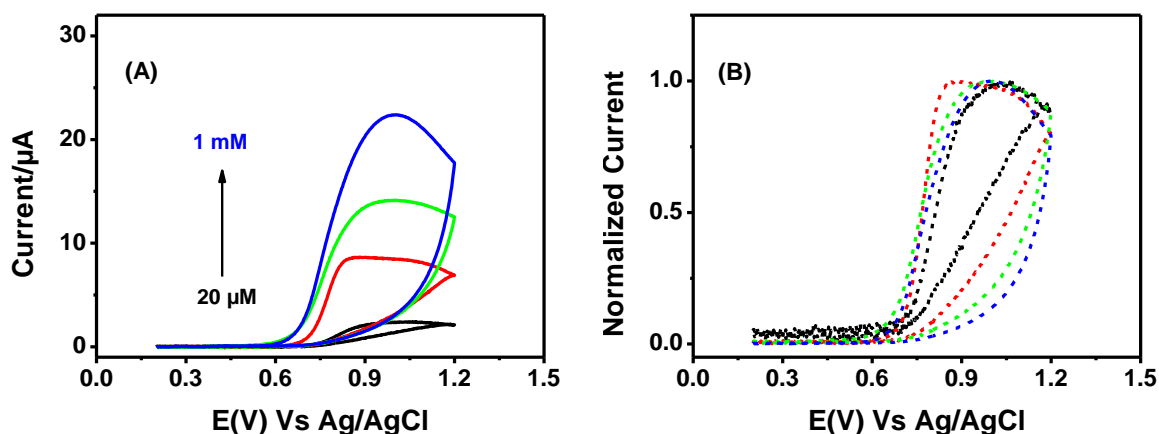


**Figure 2-26** CVs (A) and normalized CVs (B) of **1** at different concentrations in PBS solution (pH=7.4): 20  $\mu\text{M}$  (black line), 100  $\mu\text{M}$  (red line), 300  $\mu\text{M}$  (green line), and 1 mM (blue line); initial potential: +0.2 V (vs. Ag/AgCl); scan rate 20 mV/s. All the voltammograms presented were background-subtracted.

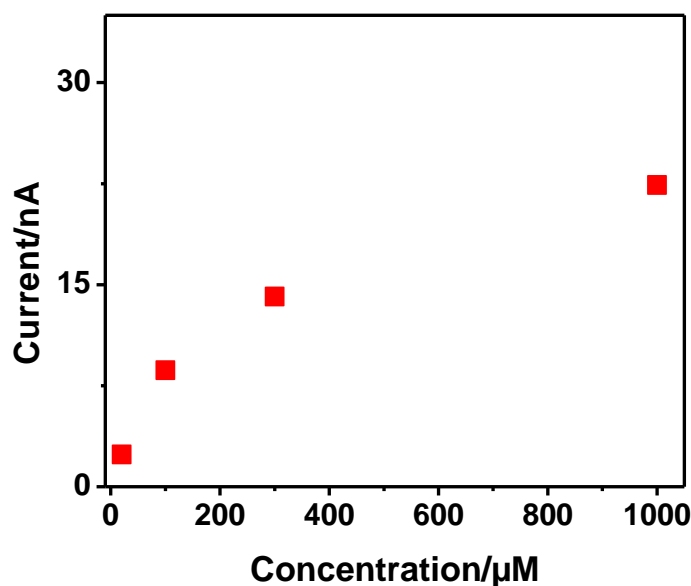


*Figure 2-27* Peak currents of CVs obtained from **1** with various concentration in PBS solution (pH=7.4).

#### 2.3.4 Electrochemical oxidation mechanism of **1**

Taking account to our present results of electrochemical detection, it seems clear that when **1** was oxidized at the interface, a non-conductive product formed and adsorbed onto electrode, leading to the passivation of electrode surface. In order to confirm this phenomenon and figure out the mechanism of electrooxidation of **1**, we compared the CVs of a common redox mediator ferrocenemethanol measured by CFE before and after **1** passivation. We firstly measured CV of 0.5 mM ferrocenemethanol with a freshly polished CFE electrode and a typical reversible CV curve was obtained, as indicated by the black line in Fig.2-28. We then blocked CFE surface by **1** oxidation and rinsed the electrode surface with distilled water before carrying out the second CV measurement in previous ferrocenemethanol solution. As predicted, no proper CV curve of ferrocenemethanol was acquired, as shown the red line in Fig.2-28. We thus believe that the oxidation of **1** could be an electropolymerization process, generating a non-conductive product which could not diffuse away and prefer to adsorb on the electrode surface.

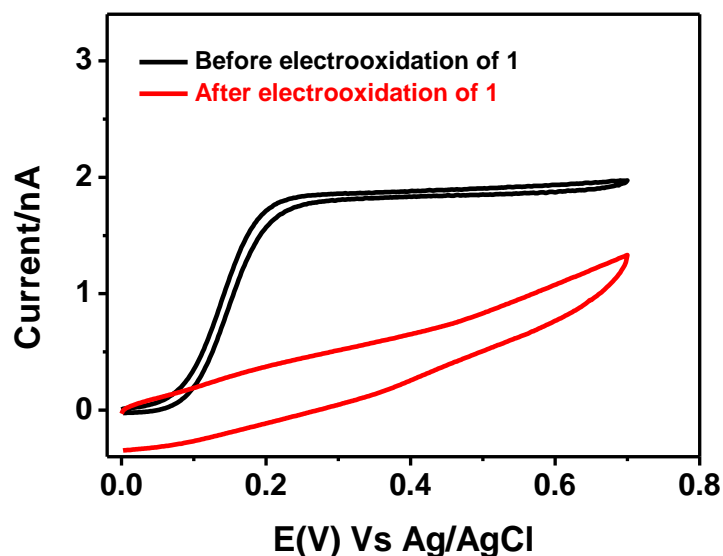


**Figure 2-28** CVs of 0.5 mM ferrocenemethanol in PBS solution (pH=7.4) measured on CFE before (black line) and after (red line) **1** oxidation: CFE surface was blocked after **1** oxidation due to the electropolymerization. Initial potential: 0 V (vs. Ag/AgCl); scan rate 100 mV/s.

On account of our current electrochemical results, we propose a possible explanation for the oxidation mechanism of **1** based on previous publication related to electrooxidation of umbelliferone (molecule **7**).<sup>[208]</sup> At lower pH values ( $\text{pH} \leq \text{pKa}$ , i. e.  $\text{pH} = 5$  or  $6$ ), the oxidation of undissociated **1** molecules is through one-electron one-proton transfer while only one-electron transfer takes place for the oxidation of deprotonated phenolate anions at higher pH values ( $\text{pH} > \text{pKa}$ , i. e.  $\text{pH} = 7$  or  $8$ ). In both cases, a reactive phenoxy radical, the key element for polymerization reaction in the next step, could be generated through the initial proton and electron transfer steps. The reactive phenoxy radical then undergoes a dimerization reaction with another deprotonated phenolate anion to form an alkyl-aryl ether which is likely to induce successive oxidation and polymerization once meeting **1** anion. The polymer chain keeps on extending until the electrode surface is completely covered by the growing non-conductive oligomer, resulting in electrodes surface passivation.

In addition, according to the electrooxidation mechanism we propose, deprotonated phenolate anion participates in the whole polymerization process and plays an important role in electrode surface passivation. We believe that is the reason why electrode surfaces are inclined to be blocked at basic environment, in accordance with the reported publications<sup>[208, 210]</sup>.

## 2.4 Conclusions

In summary, **1**, a synthesized analog of neurotransmitter, exhibits bright, stable, pH-dependant fluorescence as well as electroactivity. It shows promising prospect to be employed as a novel difunctional probe (i.e. optical and electrochemical probe) in the amperometry/TIRFM coupling technique to investigate cellular exocytotic behavior. A phenomenon of electrode passivation was also observed during the electrochemical detection of **1** in voltammetry with CFE or ITO electrode. However, such a passivation does not preclude the amperometric investigations of exocytosis at the single cell level since voltammetry conditions (temporal and spatial scales, non-dynamic solution...) are not necessarily comparable with the artificial synapse configuration. As an example, serotonin release via exocytosis is usually monitored by the mean of CFE at single cells though serotonin is well known to easily passivate carbon surfaces. As a conclusion, the high consistency of optical and electrochemical signals might allow the simultaneously real-time monitoring of complementary aspects of individual exocytotic event at single living cell.

### 3 TIRFM observation of exocytosis in 1-stained BON N13 cells

#### 3.1 Introduction

Vesicular exocytosis is a ubiquitous way for intercellular communication in neurons and neuroendocrine cells. It occurs when an intracellular vesicle fuses with the plasma membrane, releasing its contents (chemical or biochemical messengers) to the extracellular space.<sup>[2, 219-223]</sup> Because of its importance in many processes such as insertion of particular receptors at defined areas of the plasma membrane, release of neurotransmitters, and removal of waste products from the cell, vesicular exocytosis has been extensively investigated by a number of exciting analytical methods (see section 1.3) such as membrane capacitance measurements by patch clamp,<sup>[224, 225]</sup> current detection by amperometry and fluorescence tracking by optical imaging such as confocal microscopy and TIRFM.<sup>[176, 226, 227]</sup> Compared with other techniques, optical methods are particularly attractive because they provide lots of important exocytotic details visually and directly.

So far, among all the optical techniques, TIRFM is the most widely used method to study exocytosis because in this technique, the evanescent field employed to illuminate the fluorophores decays exponentially over a distance that is roughly comparable to the size of a secretory vesicle (~hundreds of nanometers).<sup>[129, 144, 227]</sup> That is, only fluorescent vesicles locating within the decay depth are able to be visualized while signals from those far from the plasma membrane are eliminated, resulting in a high signal-to-noise ratio as well as a distinct spatial resolution (~10 nm).<sup>[143]</sup> These particular characteristics of TIRFM make it a remarkable tool for exocytosis observation.

In TIRFM, visualization of exocytosis is generally realized by labeling vesicular membranes or vesicle contents. For example, the endocytic dyes FM-1-43 are usually employed to visualize recycling membranes during exocytosis while transfection of vesicular proteins by pH-sensitive pHluorin proteins linked to synaptic vesicular proteins has been widely used to track the behaviors of secretory vesicles and the dynamic of exocytotic events, as well as to unravel the processes governing the exocytotic pathway.<sup>[228-231]</sup> Even though application of these probes has advanced understanding of exocytotic process, they do not directly report on the release of non-fluorescent monoamine neurotransmitters such as serotonin, dopamine, epinephrine, as well as norepinephrine. Therefore, the development of fluorescent probes that mimic the behaviors of monoamine neurotransmitter is necessary to directly visualize exocytotic secretions. In recent years, one of the most exciting discoveries in the field of optical probes development for exocytosis investigation is the successful synthesis of a series of fluorescent molecules in the FFNs family which are capable of mimicking the biogenic monoamine neurotransmitters and being selectively taken up into secretory vesicles by cells

expressing VMAT.<sup>[152, 178, 190, 200]</sup> Therefore, we believe the combination of TIRFM with **1** will help us to better understand monoamine neurotransmitter release during exocytosis.

In this chapter, two cell lines, PC-12 cells and BON N13 cells, are employed to characterize the kinetics of uptake and release of **1**. Furthermore, behaviors of **1**-stained vesicles adjacent to the plasma membrane before and during exocytosis are also going to be discussed at TIRFM configuration.

### **3.2 Penetration of 1 into PC-12 cells and BON N13 cells**

#### **3.2.1 PC-12 cells**

PC-12 cell line is a widely used cell model for neurosecretion investigation because of their extreme versatility for pharmacological manipulation, their ease of culture and the large amount of background knowledge on their proliferation and differentiation.<sup>[13, 232]</sup> In addition, **1** has been recently reported to be a favorable fluorescent probe for in situ pH measurement of catecholamine secretory vesicles in PC-12 cells.<sup>[178]</sup> We therefore tested the possibility of employing **1** as the fluorescent reporter for exocytosis investigation of PC-12 cells in the first place.

- **Cellular uptake of 1**

Dynamic viewing of the penetrating process of **1** into the cellular vesicles of PC-12 cells was conducted by time-lapse imaging with a confocal microscope.

PC-12 cells grown on the collagen IV pretreated Petri dish were kept on the platform at a friendly environment (5%  $CO_2$  and 37 °C) and the probe uptake was then initiated by adding 0.1 mL concentrated **1** (final concentration = 20  $\mu$ M) to the cells. Temporal sequential images of PC-12 cells incubated in 20  $\mu$ M **1** were presented in Fig.3-1.

We can see that at the very beginning (i.e. 0 min), cellular outlines were clearly seen thanks to the difference of fluorescence intensity between the non-fluorescent PC-12 cells (black) and the highly fluorescent **1** solution (blue). Interestingly, some small blue spots began to appear inside the cells from 5 min and the number of the bright spots increased with the elapse of time. These small blue spots could be considered as the fluorescent cellular vesicles stained by **1**, as reported in the previous studies.<sup>[178]</sup> Moreover, almost all the PC-12 cells ( $\geq 95\%$ ) in the Petri dish were able to be visualized with the excitation of 405 nm laser after 1 h incubation in solutions supplemented with **1**. Briefly, fluorescent probe **1** was able to be accumulated rapidly (less than 5 min) into the cellular vesicles, showing good affinity to PC-12 cells.

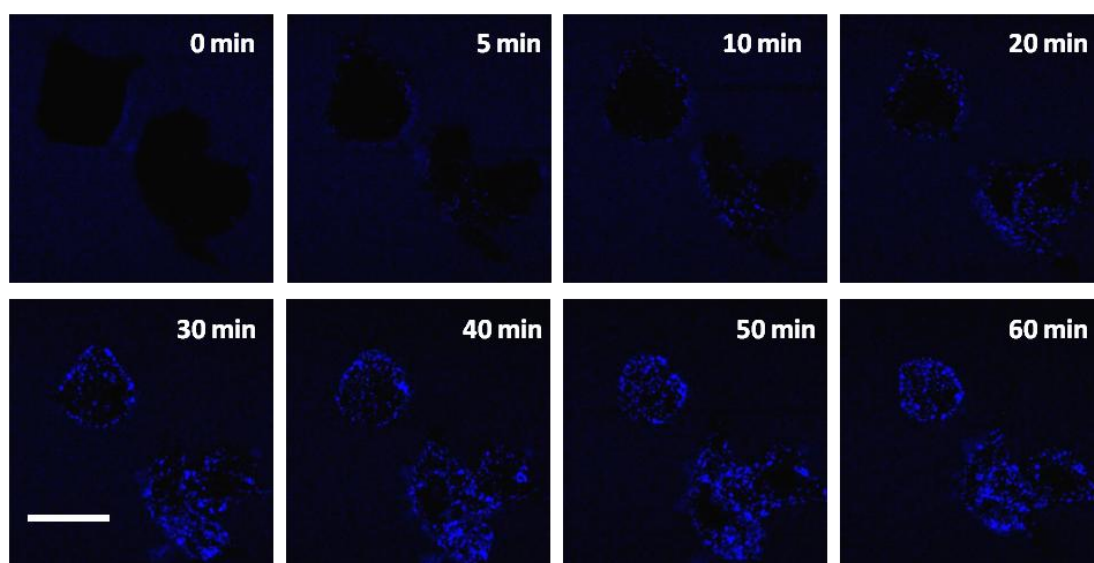


**Figure 3-1** A representative example of the selective uptake of **1** by PC-12 cells. Sequential images of PC-12 cells incubated in 20  $\mu$ M **1** from 0 min to 60 min and the small blue spots were their vesicles stained by **1**; images were acquired by confocal microscope; scale bar: 10  $\mu$ m.

- **Depolarization-induced exocytotic release of 1 from PC-12 cells**

Next we investigated whether **1** accumulated inside the vesicular lumens of PC-12 cells could be released by triggering exocytotic events with KCl solution at high concentration. Cellular vesicles were thus preloaded with **1** in advance, as described previously and 105 mM KCl solution was used to induce membrane depolarization. As shown in Fig.3-2(B), PC-12 cells became fluorescent owing to the internalized **1** stored inside their vesicles and those small blue spots represented the small, fluorescent vesicles of which the radius were typically 75-120 nm.<sup>[13]</sup> After the application of KCl solution (1 min), the fluorescence of PC-12 cells diminished and some blue spots disappeared caused by the diffusion of **1** from the vesicular lumens to the extracellular space, resulting in a significant reduction of fluorescence in Fig.3-2(C).

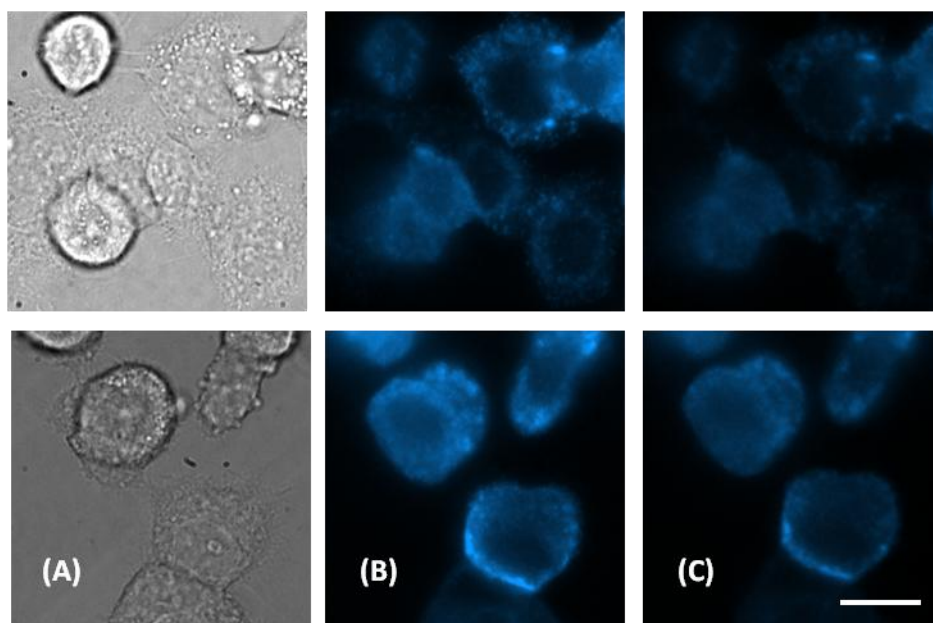


**Figure 3-2** Two representative examples of potassium induced exocytotic release of **1**-stained PC-12 cells: (A) PC-12 cells observed at bright field; (B) and (C) show fluorescent images of cells acquired before and after the application of 1 min stimulation by 105 mM KCl solution, respectively; potassium induced depolarization of PC-12 cells leads to significant fluorescence loss; images were acquired at epi-fluorescence configuration with TIRF microscope; scale bar: 10  $\mu$ m.

The fluorescence differences before and after potassium treatment (Fig.3-3(A)) indicate that **1**-stained cells underwent exocytosis because of the membrane depolarization at high KCl concentration and their fluorescence intensities declined significantly to  $63.1 \pm 2.9\%$  ( $n=6$  cells) as **1** dispersed to the extracellular space (Fig.3-3(B)). So far, we have demonstrated that **1** could be rapidly accumulated and discharged by PC-12 cells, making it a potential optical probe for exocytotic behavior study. Nevertheless, when focusing on single exocytotic events, we found PC-12 cells were not good cell models for exocytosis investigation with the combination of **1** and TIRFM. To be specific, no matter at TIRFM or epi-fluorescence condition, the cellular vesicles were not able to be clearly visualized. Furthermore, most of exocytotic secretions of **1**-stained PC-12 cells were seen as the disappearance of fluorescent spots and only few events appeared as ‘flashes’ with the diffusion of fluorescent dye, making it difficult for the identification of individual exocytotic events.

Generally, to explain the results we obtained, the following reasons could be suggested:

- (1) Vesicles of PC-12 cells are smaller (75~120 nm radius) compared with chromaffin cells (170 nm radius) and BON cells (100~150 nm radius).<sup>[13, 211]</sup> It has been reported that

catecholamines are present in much lower levels in vesicles of PC-12 cells compared with adrenal cell vesicle because of its smaller vesicular size. Therefore, it is logical that PC-12 cells would accumulate less **1** into the vesicular lumens and be less fluorescent compared with those cells with larger vesicles. As a consequence, when exocytosis of **1**-stained PC-12 cells was triggered by 105 mM KCl solution, it mainly occurred as the extinction of fluorescence since there was only a few amount of **1** stored inside the vesicular lumen, not enough to leading to the detectable ‘flash’ of fluorescence.

- (2) As discussed in the second chapter, the optimum excitation wavelength of **1** lies at 331 nm and 371 nm at acidic (pH=5) and basic (pH=7~8) condition, respectively, whereas our TIRFM is equipped with 405 nm laser as the light source. As a result, in our case, a majority of optical signals were lost at TIRFM condition and a relatively high concentration of **1** was thus essential to guarantee the appearance of fluorescent diffusion. Taking account to the few amount of **1** inside the small vesicles of PC-12 cells, it seems reasonable that not many ‘flashes’ took place in this case.

Considering the two main points mentioned above, it sounds hard to track the exocytotic behaviors of PC-12 cells by using **1** at TIRFM configuration. That is the reason why we turn to another cell line, namely BON N13, which has been used more and more for exocytosis studies recently.

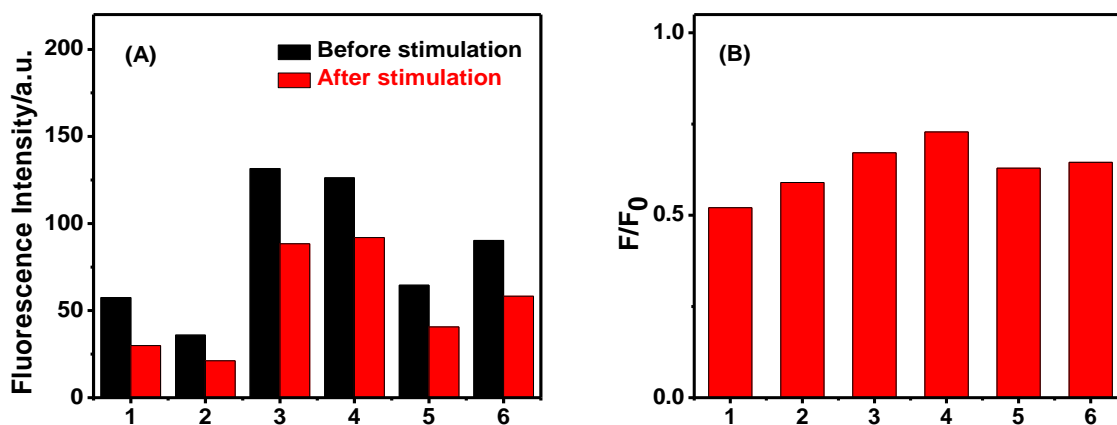


**Figure 3-3** (A) Fluorescence intensity (in arbitrary units) comparison of six **1**-stained PC-12 cells before ( $F_0$ ) and after ( $F$ ) 1 min stimulation of 105 mM KCl solution; images were acquired at epi-fluorescence configuration; (B) Significant loss of fluorescence intensity triggered by potassium induced depolarization ( $n=6$  cells).

### 3.2.2 BON N13 cells

The BON cell line was derived from a metastatic human carcinoid tumor of the pancreas and it displays morphological and biochemical characteristics consistent with the enterochromaffin cell phenotype.<sup>[16, 17, 233, 234]</sup> In recent years, this cell line has been increasingly employed as a convenient model for investigation of calcium-triggered exocytosis of secretory granules.<sup>[18, 19, 105, 211, 235-237]</sup>

- **Cellular uptake of **1****

BON N13 cells displayed similar **1** staining behavior as that observed with PC-12 cells. As shown in the temporal sequential images in Fig.3-4, during the previous 5 min, we observed cellular outlines clearly owing to the fluorescence intensity difference between the non-fluorescent N13 cells (black) and the highly fluorescent environment (blue). Some small blue dots then began to appear inside the cells from 10 min as **1** started to be specifically recognized by BON N13 cells, then more and more blue vesicles were seen with time lapse. Moreover, the cytoplasm of BON N13 cells also became fluorescent after 40 min incubation, indicating that **1** could be accumulated not only inside vesicles but also in cytoplasm. Indeed, according to the time lapse imaging results, not all the BON N13 cells could recognize **1**. As illustrated in Fig.3-4, after being exposed to 20  $\mu$ M **1** for 1 h, among the 7 target cells, only 3 of them owned fluorescent vesicles while the other 4 cells remained non-fluorescent.

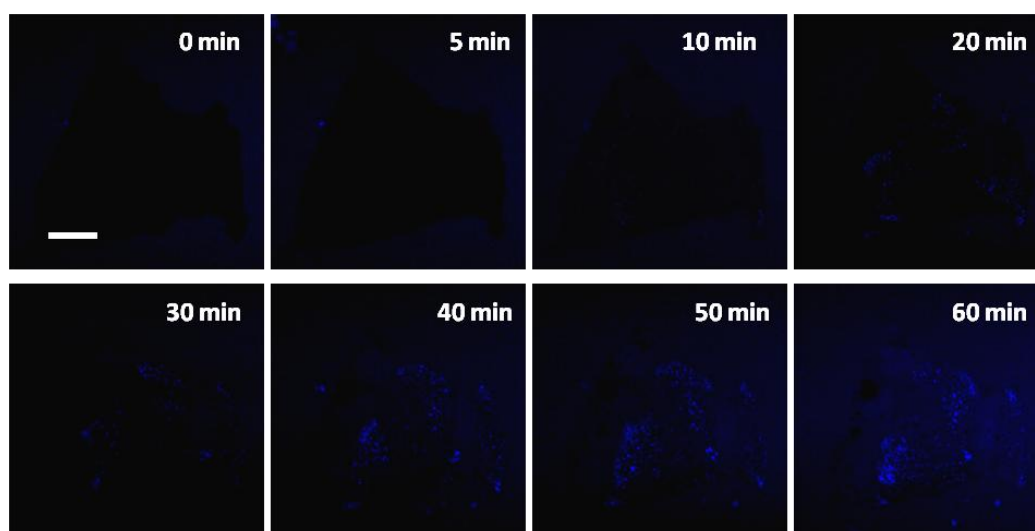


*Figure 3-4* A representative example of the uptake of **1** by BON N13 cells; sequential images of seven aggregated cells incubated in 20  $\mu$ M **1** solution from 0 min to 60 min and only three of them exhibited ability to selectively take up **1**; images were acquired by confocal microscope; scale bar: 10  $\mu$ m.

- **Incubation time**

In order to investigate the influence of incubation time, images of BON N13 cells exposed to 20  $\mu\text{M}$  **1** solution from 1 h to 6 h were taken at epi-fluorescence configuration. As that we observed from confocal microscope, only part of N13 cells selectively took up **1** into their vesicles (Fig.3-4) and no appreciable difference was seen from 1 to 6 h of incubation. More specifically, the percentage of cells with fluorescent vesicles was independent with the exposure time to **1**, always varying from 10 % to 40 % after 1 h incubation, as illustrated in Fig.3-5.

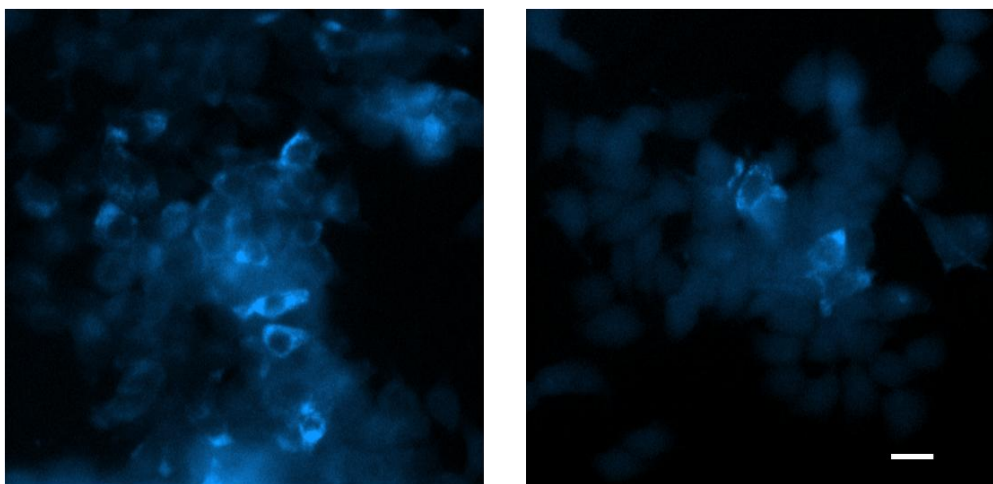


*Figure 3-5* Fluorescence images of BON N13 cells exposed to 20  $\mu\text{M}$  **1** for 1 h; the ratio of **1**-stained cells varying from 10 % (right image) to 40 % (left image) after 1 h of incubation in 20  $\mu\text{M}$  **1** solution; images were acquired at epi-fluorescence configuration by TIRF microscope; scale bar: 20  $\mu\text{m}$ .

- **The aminoethyl group is the key recognition element**

**1** is a fluorescent substrate which closely mimics biogenic monoamine neurotransmitters. Its aminoethyl group was designed as the key element for cell recognition. Fig.3-6 shows fluorescence images of BON N13 cells incubated in 20  $\mu\text{M}$  **9** and **1** solutions for 1 h respectively. As previously described, **1** was able to be accumulated into cellular vesicles. However, for cells pre-incubated in the **9** solution for 1 h, the cell membrane became bright but no fluorescent vesicle was seen. Moreover, the fluorescence resulting from **9** adsorption was totally photobleached after cells being exposed to the light source for 1 min whereas the **1**-labeled vesicles were still quite bright, indicating that the detected fluorescence of cells incubated into **9** solution was resulted from the adsorption of fluorescent **9** onto the cell membrane and aminoethyl group of **1** is the key factor for cell recognition.

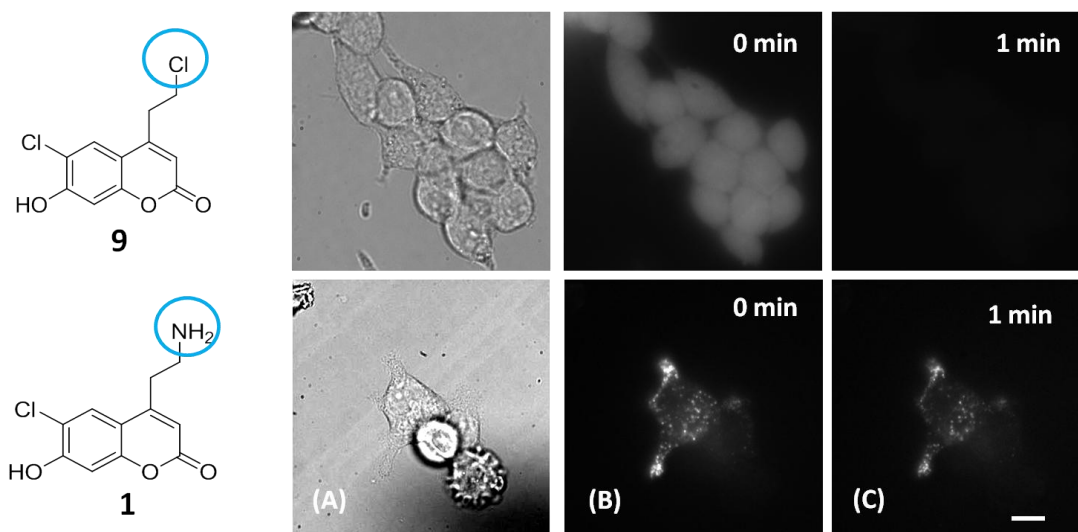


**Figure 3-6** A typical example of BON N13 cells exposed to 20  $\mu\text{M}$  **9** (top) and 20  $\mu\text{M}$  **1** (bottom) for 1 h, respectively: (A) BON N13 cells observed at bright field; (B) and (C) show fluorescent images of cells acquired before and after 1 min exposure to the light source, respectively; no **9** was transported into the cellular vesicles and the fluorescence of plasma membrane caused by **9** adsorption was likely to be photobleached; images were acquired at epi-fluorescence configuration by TIRF microscope; scale bar: 10  $\mu\text{m}$ .

### 3.3 Exocytosis observed by epi-fluorescence and TIRFM

#### 3.3.1 Epi-fluorescence versus TIRFM

As we discussed in the introduction section, TIRFM is the most widely used optical approach to study exocytosis because of its outstanding spatial resolution as well as its high signal-to-noise ratio. In this technique, fluorescence signals were excited by an evanescent wave generated by total internal reflection at the interface and its intensity decays exponentially as a function of distance from the interface, with a characteristic decay depth of the order of hundreds of nanometers. As a consequence, only fluorophores within the decay depth could be excited while those far from the interface blur. Compared with traditional fluorescent microscopy based on epi-fluorescence, TIRFM seems to be a powerful tool for exocytotic process observation, with an outstanding axial resolution of about 10 nm.<sup>[119, 142, 143]</sup>

To illustrate the distinctive advantages of TIRFM for exocytosis investigation, we firstly visualized fluorescent secretory vesicles preloaded with **1** in BON N13 cells with 405 nm laser excitation at two configurations: epi-fluorescence configuration and TIRFM configuration.

Fig.3-7 shows micrographs of three typical examples of single adherent, **1**-stained BON N13 cell viewed in bright field, epi-fluorescence, and evanescent field excitation configurations (TIRFM). In epi-fluorescence configuration, all the vesicles of the entire sample were uniformly illuminated, leading to a blurry visual effect of secretory vesicles. In contrast, in TIRFM configuration, fluorescent signals out of the observation depth were eliminated because only those labeled vesicles adjacent to the cell membrane were able to be illuminated as single fluorescent spots, leading to a low fluorescence background. It is clear that fluorescence vesicles were visualized with a significantly better signal-to-noise ratio at TIRFM configuration compared with that observed at epi-fluorescence configuration.

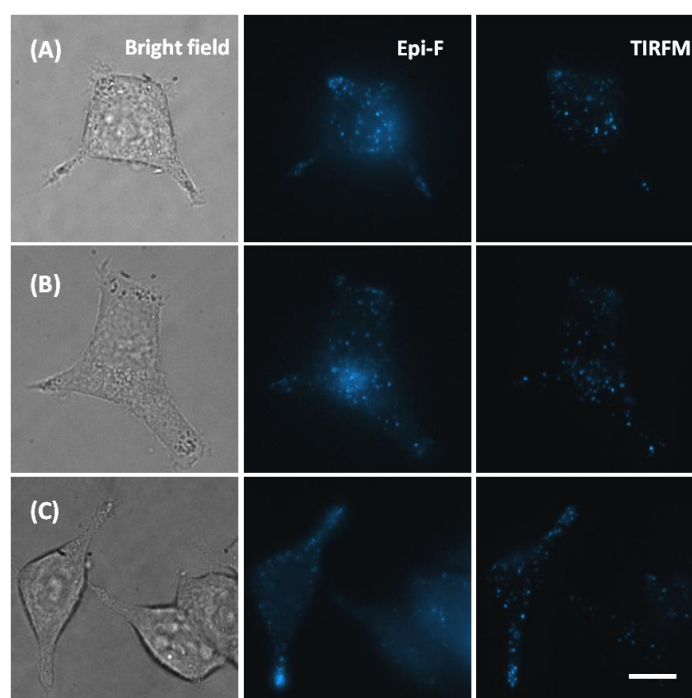


**Figure 3-7** Comparison of images of **1**-labeled cell specimen obtained at bright field, epi-fluorescence and TIRFM. The microscope was focused at the adherent plasma membrane and images were acquired with one of two modes of excitation: epi-fluorescence and TIRFM. In each case, TIRFM clearly eliminates out-of-focus fluorescence and reveals details near the cell membrane; such vesicles appear as diffraction-limited fluorescent spots in the evanescent field, since typical vesicle sizes are 200~300 nm; scale bar: 10  $\mu$ m.

### 3.3.2 Incident angle dependence of TIRFM signals

In TIRFM, optical observation range is defined by the decay depth of evanescent wave which is dependent on the incident angle of the light source. In other words, we can control optical observation range of I-labeled specimen by adjusting the incident angle of the excitation laser.

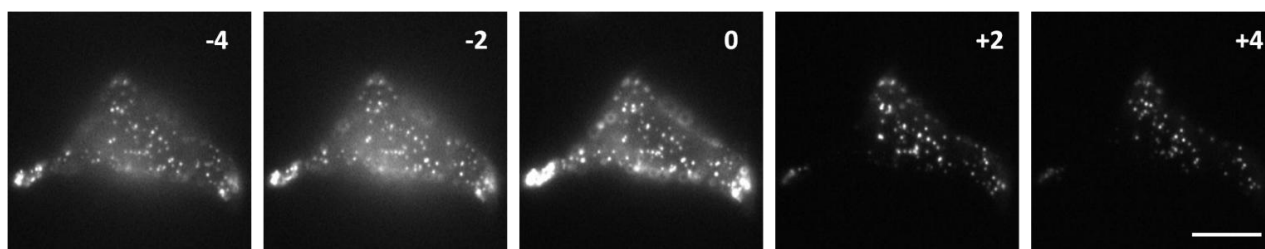


**Figure 3-8** Sequential images of I-labeled BON N13 cells illuminated by 405 nm laser at different incident angles; images were acquired by TIRFM and here 0 represents the critical incident angle in TIRFM; scale bar: 10  $\mu\text{m}$ .

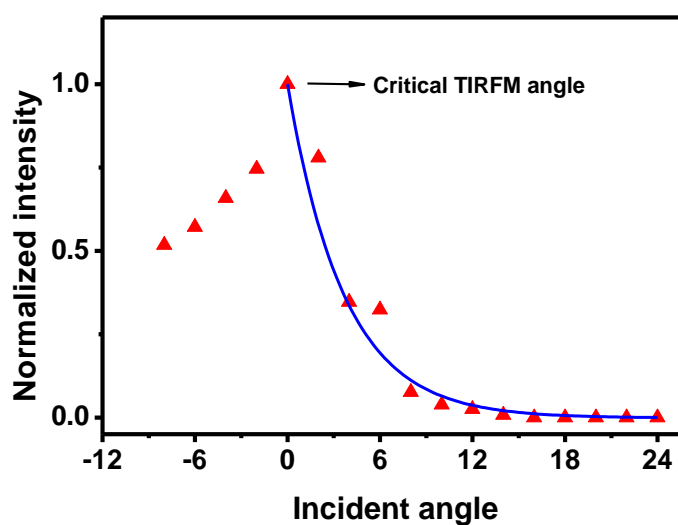


**Figure 3-9** Fluorescence intensities obtained from sequential images of a I-labeled BON N13 cell illuminated by 405 nm laser at different incident angles; the blue curve shows the fitting results of the exponential decay of fluorescent intensities as a function of incident angle ( $y = e^{x/3.67}$ ,  $R^2 = 0.946$ ); here 0 represents the critical incident angle in TIRFM.

An example of a single 1-labeled BON N13 cell illuminated by 405 nm laser at different incident angles is presented in Fig.3-8. We can see that before arriving at the critical incident angle, all the vesicles were uniformly illuminated by the laser whereas at higher incident angle beyond the critical angle, some bright vesicles became invisible because evanescent wave initiated fluorescence was limited to hundreds of nanometers from the coverslip and thus not all vesicles were able to be detected. In other words, the observation depth of TIRFM declined with the increase of incident angle beyond the critical angle. In addition, the fluorescence intensities decayed exponentially after exceeding the critical angle, as illustrated in the blue simulated curve ( $y = e^{x/3.67}$ ,  $R^2 = 0.946$ ) of Fig.3-9.

### 3.3.3 Behaviors of 1-labeled vesicles assessed by TIRFM

Cargo-enriched secretory vesicles must be transported to a site of cell membrane where exocytosis will take place. Transport is thus the first exocytotic behavior which could be visually identified by TIRFM. At TIRFM configuration, we found that in resting cells without stimuli, random displacement of illuminated vesicles in the x-y plane was seen all the time. However, the number and distribution of visualized vesicles were fairly stable even though ‘appearances’ and ‘disappearances’ of fluorescent vesicles were occasionally observed along the z-axis.

- **Vesicle movement in the X-Y trajectories**

Highly organized sub-plasmalemmal structures of living cells are able to direct or transport vesicles to their would-be docking sites, leading to the lateral and axial motility of vesicles. According to our current experimental TIRFM results, we discover that compared with those undocked vesicles, these already-docked vesicles showed a significant decrease in the mobility and tended to undergo exocytosis, in accordance with previous publications.<sup>[145-147, 153]</sup> To well illustrate this viewpoint, a representative example of the lateral motilities of the undocked (A) and already-docked vesicles (B) was shown in Fig.3-10.

Undocked vesicle **A** kept on approaching to vesicle **B** by displacement at the x-y plane and it moved around 2  $\mu\text{m}$  during the first 60 s. On the contrary, docked vesicle **B** was less mobile. It also moved but only within a limited space, showing ‘restricted’ or ‘caged’ movements. Additionally, the content inside vesicle **B** was released (data not shown) upon the application of a secretory stimulus (i.e. 10  $\mu\text{M}$  ionomycin), suggesting that the docked vesicle constituted the readily releasable pool. In brief, the mobility of vesicles is a specific character to distinguish already-docked vesicles from vesicles still seeking their docking sites.

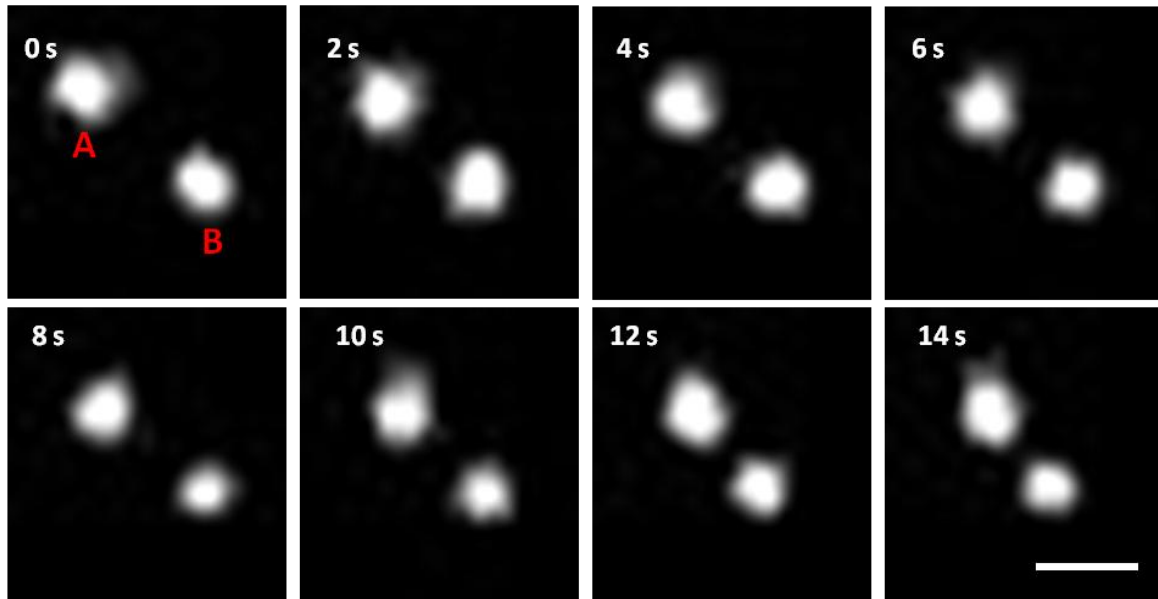


**Figure 3-10** Successive images of two I-labeled vesicles (vesicle A and vesicle B) illuminated at TIRFM configuration; scale bar: 1  $\mu\text{m}$ .

- **Vesicle movement in Z trajectories**

As mentioned above, ‘appearances’ and ‘disappearances’ of fluorescent spots were occasionally seen along the z-axis. Fig.3-11 and Fig.3-12 present two examples of vesicles leaving and approaching the plasma membrane, respectively. As illustrated in Fig.3-11, for the leaving 1-labeled vesicle, its fluorescence gradually dimmed and finally disappeared at 13 s with its diffusion from the cell membrane to the cytoplasm out of the observation range. In contrast, the vesicle approaching the membrane experienced a reversed fluorescence variations. That is, the blurred fluorescence became much clearer with the decrease of distance between the vesicle and the plasma membrane. Moreover, upon arriving at the cell membrane, the vesicle showed little lateral mobility.

It is important to note that disappearances of fluorescent vesicles were also observed when exocytotic events occurred. However, the kinetics of the whole process is much faster (hundreds of milliseconds) compared with the one resulting from vesicle movement along the z-axis (several seconds). We define this kind of exocytotic event as ‘extinction of fluorescence’ and will discuss this viewpoint later.

The behaviors of vesicles in resting cells before the application of the secretory stimulus have been characterized using TIRFM and we then investigated the exocytotic events of BON N13 cells upon 10  $\mu\text{M}$  ionomycin stimulation.

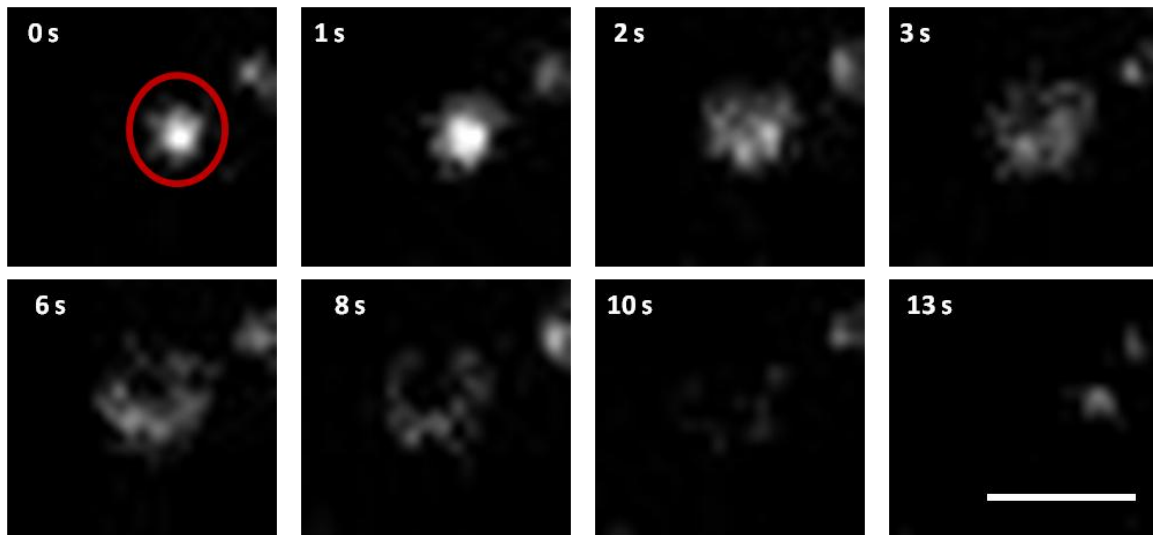


**Figure 3-11** Sequential TIRFM images of a single **I**-labeled vesicle leaving the plasma membrane; scale bar: 2  $\mu$ m.

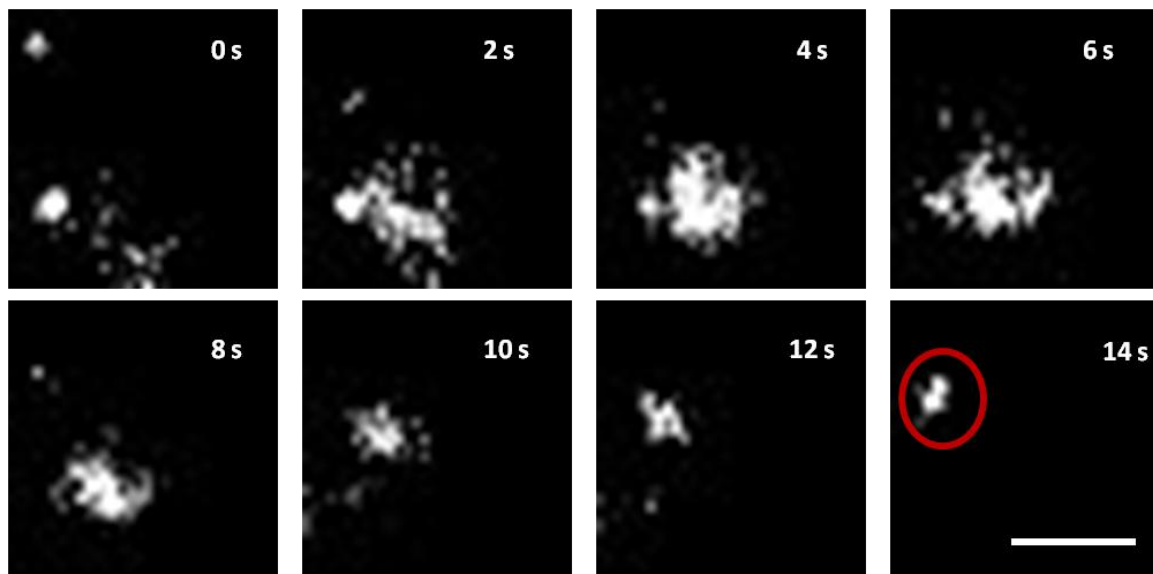


**Figure 3-12** Sequential TIRFM images of a single **I**-labeled vesicle approaching the plasma membrane; scale bar: 2  $\mu$ m.

- **Comparison of fluorescence of **1** inside and outside the cellular vesicles**

On the basis of the results obtained by confocal microscopy (Fig.3-4), both the cytoplasm and cellular vesicles of BON N13 cells were stained after being incubated in 20  $\mu$ M **1** for 1 h. Furthermore, the cell

membrane was also fluorescent because of the adsorption of **1**. Nevertheless, the fluorescence from cytoplasm and membrane adsorption was more likely to be photobleached compared with that from the cellular vesicles. As illustrated in Fig.3-13, the fluorescence intensity of **1** out of cellular vesicles decreased by 90% after cells being exposed to the light source for 30 s, resulting in neglectable optical background. As a result, it did not interfere with the observation of behaviors of **1**-labeled vesicles.

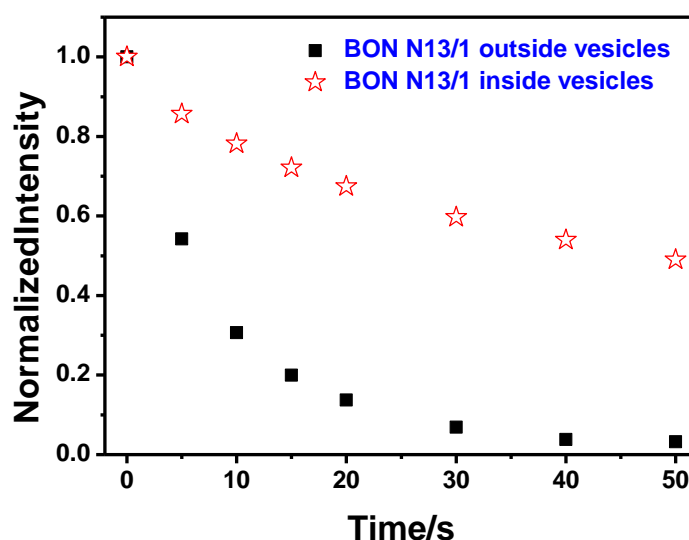


**Figure 3-13** Time course of fluorescence intensities of **1** inside and outside cellular vesicles at epi-fluorescence configuration. The fluorescence background resulting from **1** adsorption is able to be neglected during TIRFM measurement because it is likely to be photobleached.

- **Exocytotic behaviors of 1-labeled vesicles assessed by TIRFM**

Using TIRFM, we have studied the calcium-triggered exocytosis of single, fluorescently **1**-labeled vesicles in BON N13 cells. As shown in Fig.3-14, most of the fluorescent vesicles of the target cells vanished because of exocytosis after the application of a secretory stimulus (i.e. 10  $\mu$ M ionomycin). Fig.3-15 shows the exocytotic frequency of the two individual **1**-stained BON N13 cells presented in Fig.3-14 and time  $t = 0$  corresponds to the first fusion event detected in each cell. It is necessary to note that the exocytotic frequency of an individual cell is dependent on lots of parameters such as cell condition, type of secretory stimulus as well as the amount of internalized dyes. For the two cells in Fig.3-14, their curves of cumulated number of exocytotic events were occasionally quite consistent even though slight variations were observed. Furthermore, most of **1**-stained vesicles responded to ionomycin stimulation in the first 15 seconds and experienced exocytosis, leading to the highest

exocytotic frequency. And then a ‘fading’ effect occurred, resulting in the slower release. Additionally, some blue spots still existed after the whole stimulating process.

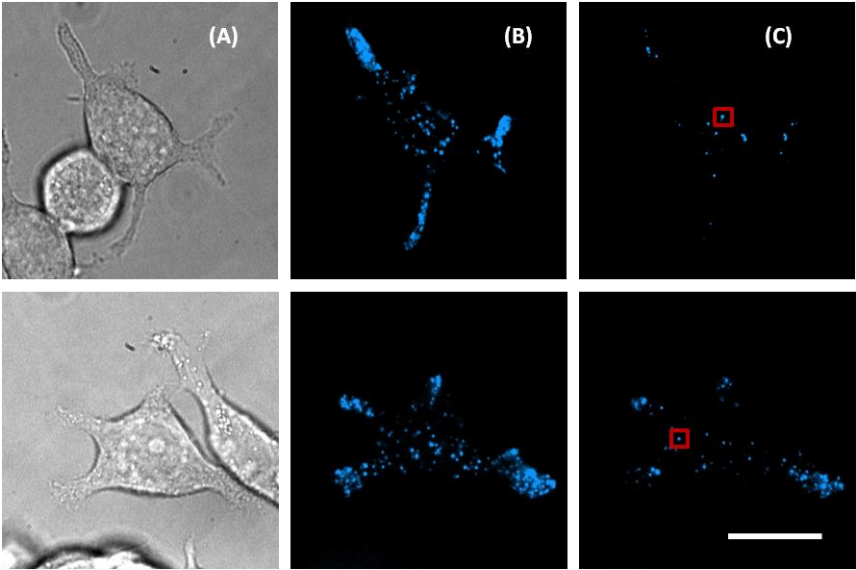


**Figure 3-14** Two typical examples of individual I-stained BON N13 cells observed at bright field (A) and TIRFM configuration (B and C); (B) and (C) show the images of the target cell before and after the application of 10 μM ionomycin, respectively; the blue spots represent I-labeled fluorescent vesicles and an example of such vesicles is indicated in the red rectangular; scale bar: 10 μm.

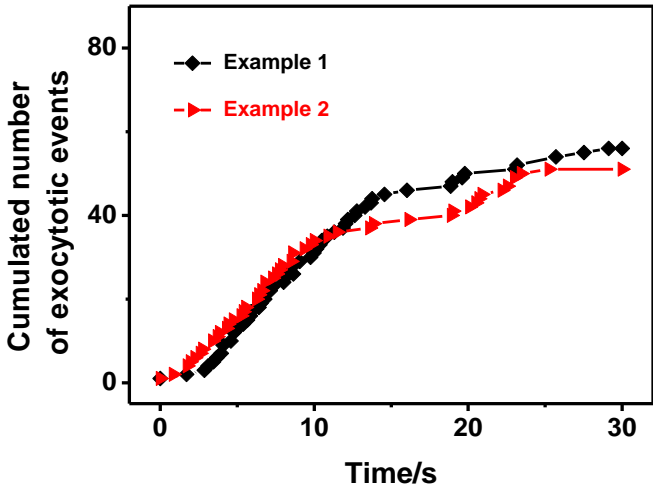


**Figure 3-15** Exocytotic frequency of individual I-stained BON N13 cells (in Fig.3-14) measured by TIRFM; the number of cumulated events is reported in the previous 30 seconds since the first exocytotic event was detected. Time  $t = 0$  corresponds to the first fusion event detected in each cell.

By analyzing the recorded TIRFM movie, we find three main types of single exocytotic events exist in 1-stained BON N13 cells stimulated by 10  $\mu$ M ionomycin.

### (1) The normal ‘flash’

Among the 157 exocytotic events acquired from 1-stained BON N13 cells, 84 of them (~54 %) appeared as the normal ‘flash’ which has been demonstrated to be a typical exocytotic type in many other cell lines such as chromaffin cells and PC-12 cells.<sup>[145, 238]</sup> That is, all the contents stored inside the vesicle were completely expelled to the extracellular medium and the vesicular membrane fully fused with cell membrane. From the standpoint of TIRFM, single exocytotic events were visualized as ‘puffs’ of light which were accompanied by the extinction of fluorescent spots. To be more specific, the fluorescent signal transiently brightened during the release of fluorescent 1 from acidic vesicle to the neutral extracellular medium and then disappeared completely within 100~200 ms as the fluorophores diffuse away, as illustrated in Fig.3-16.

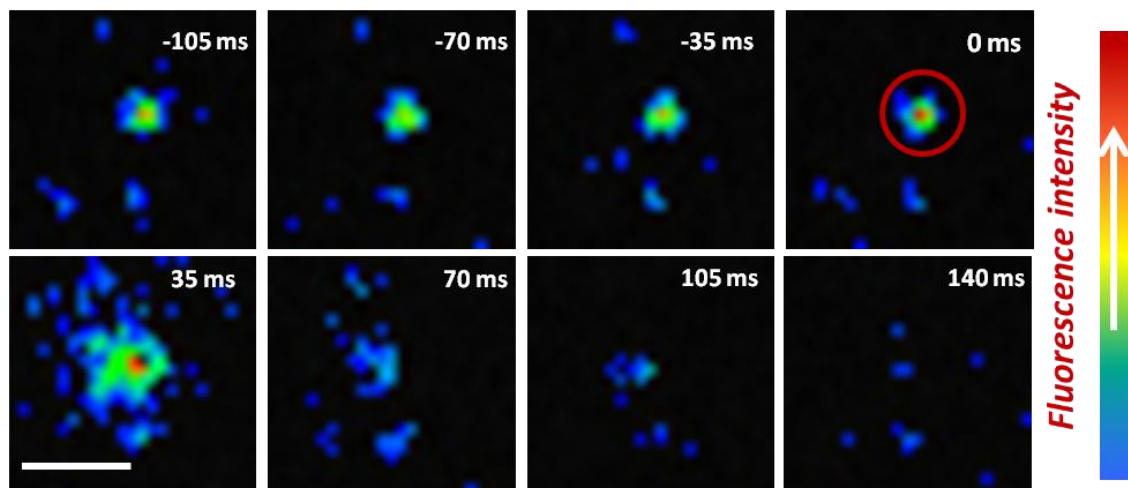


**Figure 3-16** Sequential pseudocolor images of an individual exocytotic event described as a normal ‘flash’ at TIRFM configuration. A fluorescent parent vesicle (indicated by the red ellipse) remained visible for at least several frames (-105 ms, -70 ms and -35 ms). Upon stimulation, it expelled the soluble dyes which dispersed rapidly; scale bar: 1  $\mu$ m.

### (2) The extinction of fluorescent spots

In many other cases (49 among 157 events, ~31%), the whole exocytotic process was observed as the rapid disappearance of fluorescent spots within hundreds of milliseconds (Fig.3-17). That is, the 1-

stained vesicles directly disappeared after a transient augmentation of fluorescence intensity, without the visible diffusion of fluorescent dyes. In fact, this type of exocytosis could be attributed to the low concentration of **1** accumulated inside the vesicle, in accordance with our viewpoint that most exocytotic events of PC-12 cells occurred as the disappearance of fluorescence because of their smaller vesicle size.

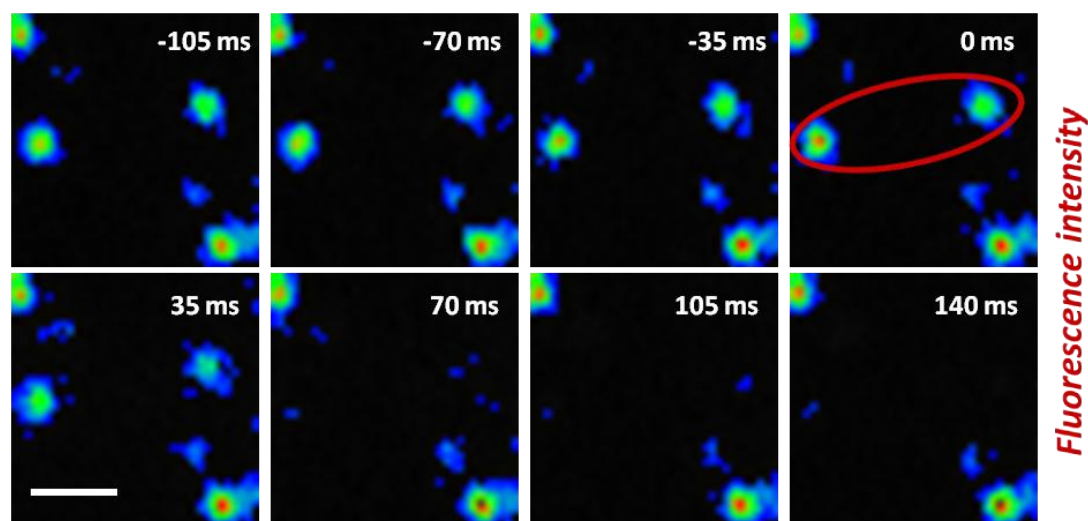


**Figure 3-17** Sequential pseudocolor images of an exocytotic event described as ‘extinction of fluorescence’ at TIRFM configuration. Two fluorescent parent vesicles (indicated by the red ellipse) remained visible for at least several frames (-105 ms, -70 ms and -35 ms) and disappeared immediately without detectable fluorescent diffusion upon stimulation; scale bar: 1  $\mu\text{m}$ .

### (3) The ‘sudden flash’

In some rare cases (24 among 157 events, ~15%), the ‘sudden flash’ took place. Actually, this kind of exocytotic events displayed identical characteristics as the normal ‘flash’ except that no corresponding parent vesicles could be identified in the previous several frames (-105 ms, -70 ms and -35 ms) before the dispersion of **1** into the extracellular medium. In other words, the ‘sudden flash’ was seen as a ‘puff’ of fluorescence appearing suddenly, without a detectable prior fluorescent signal of a parent vesicle, and disappearing by diffusing away rapidly, also within 100~200 ms (Fig.3-18).

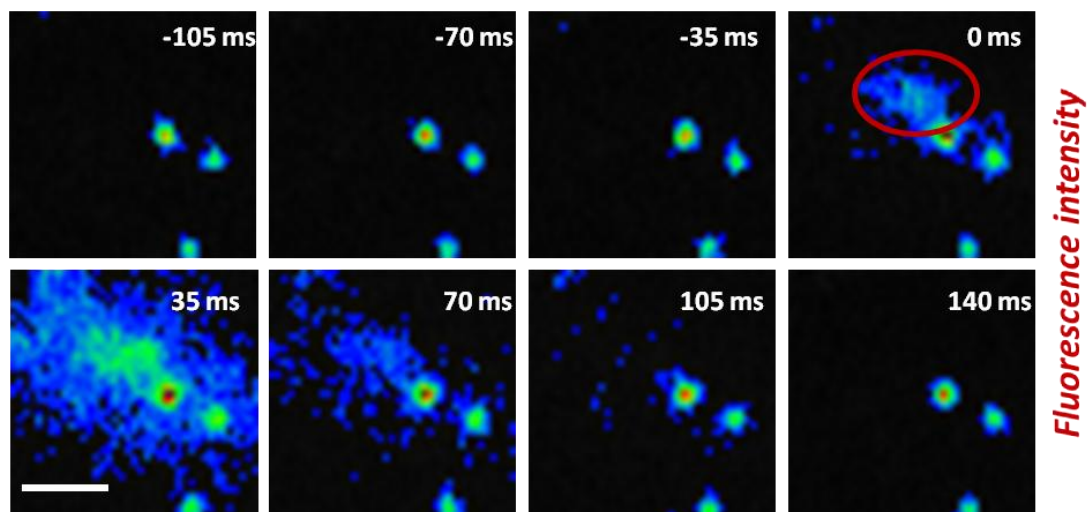


**Figure 3-18** Sequential pseudocolor images of a typical exocytotic event described as ‘sudden flash’ at TIRFM configuration. It displayed the same post-fusion characteristics as ‘normal flash’, yet the parent vesicle somehow escaped detection. The red ellipse indicated the first appearance of fluorescent diffusion; scale bar: 1  $\mu\text{m}$ .

### 3.3.4 Fluorescence intensity investigation of different types of exocytosis

Fluorescence is an important and significant parameter to characterize exocytosis at single vesicle level. We thus analyzed the fluorescence variations of these three types of exocytotic events mentioned above so as to illustrate their features and differences. As discussed previously, BON N13 cells stained by **1** underwent photobleaching with the excitation of 405 nm laser source, leading to the reduction of fluorescence intensity which might interfere with the fluorescence intensity characterization of exocytosis.

Therefore, two reference vesicles showing less motility were chosen to investigate if the photobleaching effect interferes with the fluorescence intensity characterization. Their normalized fluorescence intensities are plotted as a function of time exposed to 405 nm laser at TIRFM configuration, as shown in Fig.3-19. We can see that the fluorescence intensities of these two reference vesicles were quite stable within 1 second even though a slightly random fluctuation caused by the lightly displacements of vesicles was seen. It thus becomes clear that the fluorescence intensity decrease caused by photobleaching at TIRFM configuration seems to be negligible if we only focus on an individual exocytotic event of which the intact duration lasts hundreds of milliseconds.

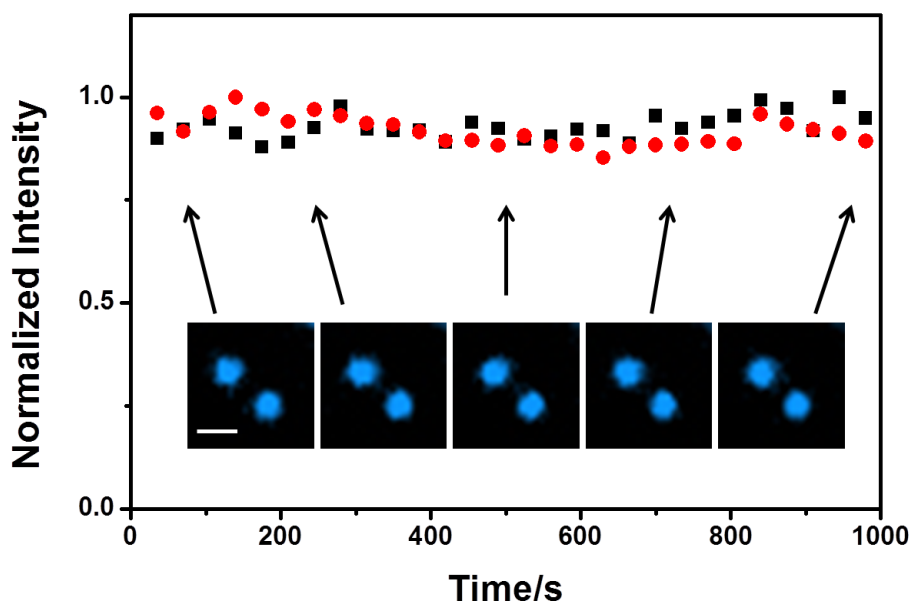


**Figure 3-19** Time course of fluorescence intensities measured from two reference vesicles moving laterally: upper vesicle (black square) and lower vesicle (red dot); insets are TIRFM images of these two vesicles corresponding to different moments; scale bar: 1  $\mu\text{m}$ .

### (1) The normal ‘flash’

According to sequential TIRFM time lapse images, exocytotic event described as a normal ‘flash’ underwent a sudden brightening and rapid spreading of the fluorescence signal, as previously described. The tracking of fluorescence intensity variations of this event was highly consistent with this description. As indicated in Fig.3-20, in the previous 200 ms before releasing, the fluorescence of the active vesicle was quite stable besides some lightly variations because of its displacement. Then an increase of fluorescence intensity was observed when **1** started to diffuse out. It could be attributed to the signal augmentation resulting from pH gradient between the acidic vesicular lumen and neutral extracellular environment since the photophysical properties of our fluorescent probe, **1**, were strongly pH-dependant, as discussed in Chapter 2. Moreover, evanescent excitation was more efficient closer to the interface. After that, an exponential decay of fluorescence intensity was detected because of the brupt spreading of **1** out of exocytotic regions, as indicated by the blue simulated curve ( $y = 25442.5 e^{x/36.1} + 1.8, R^2 = 0.997$ ). Additionally, the fluorescence after exocytosis declined a lot compared with that before release because of the full fuse of cellular vesicle and cell membrane.

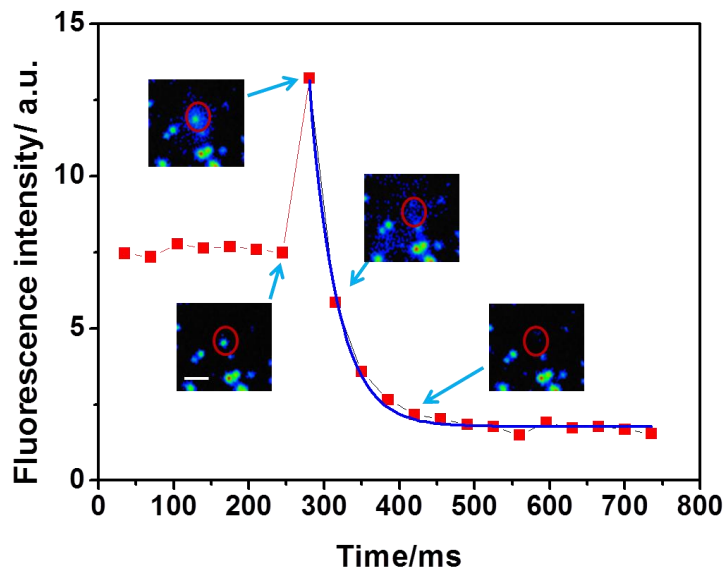


**Figure 3-20** Time course of the fluorescence intensities (in arbitrary units) measured from an individual vesicle indicated by the red circles which experienced a normal ‘flash’ release; insets are TIRFM images corresponding to different moments and the blue curve shows the fitting results of the exponential decay of fluorescent intensities as a function of time ( $y = 25442.5 e^{-x/36.1} + 1.8, R^2 = 0.997$ ); scale bar: 1  $\mu\text{m}$ .

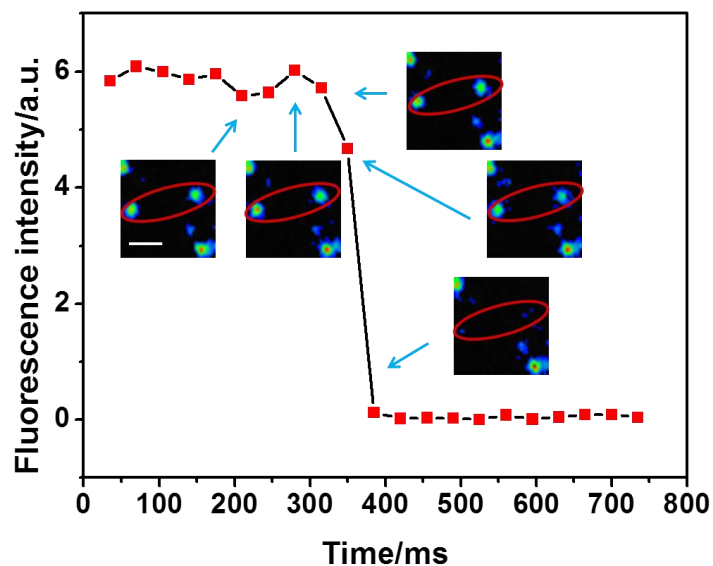
### (2) The extinction of fluorescent spots

Fig.3-21 shows an example of fluorescence intensity changes of two representative vesicles which expelled their contents by the exocytotic type of ‘extinction of fluorescent spots’. Compared with the normal ‘flash’, fluorescent signal arose slightly when **1** release was triggered whereas sudden increase of fluorescence intensity lacked in this type of exocytosis. It confirms our viewpoint that the concentration of **1** inside the vesicles was so low that diffusion of the dye was not able to be tracked by TIRFM.

### (3) The ‘sudden flash’

As mentioned above, the ‘sudden flash’ of BON N13 cells represents a special exocytotic type of which only rapid dye diffusion, but not the parent vesicle could be detected. We can see from Fig.3-22 that fluorescence intensity was pretty low until the arriving of diffusing dye since there was no parent vesicle at first. With the diffusion of the new coming dye, the fluorescent signal experienced a dramatic augmentation followed by a prompt decrease of fluorescence intensity. As all the new

coming dyes dispersed away, the fluorescence intensity went back to zero as that we observed before the 'sudden flash'.



**Figure 3-21** Time course of the fluorescence intensities (in arbitrary units) measured from an individual vesicle indicated by the red ellipses which experienced a 'extinction of fluorescent spot' release; insets are TIRFM images corresponding to different moments; scale bar: 1  $\mu\text{m}$ .

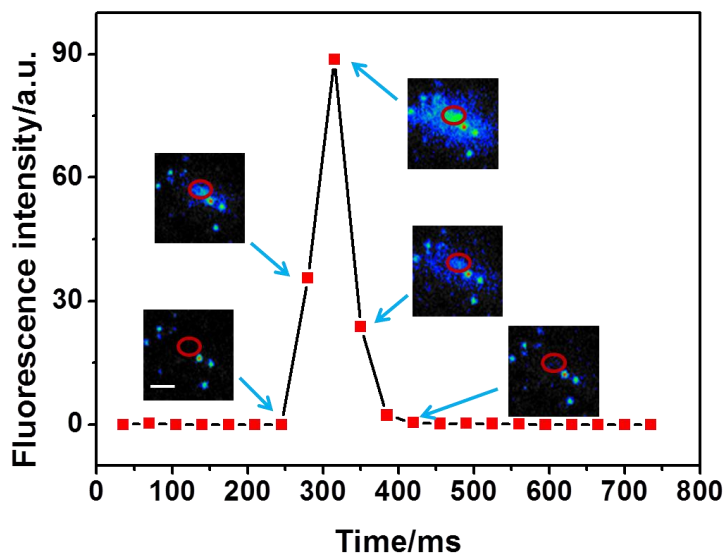


**Figure 3-22** Time course of the fluorescence intensities (in arbitrary units) measured from an individual vesicle indicated by the red ellipses which experienced an 'sudden flash' release; insets are TIRFM images corresponding to different moments; scale bar: 1  $\mu\text{m}$ .

According to our experiments based on **1**-stained BON N13 cells, two forms of ‘sudden flash’ were supposed to take place. One occurred at the borders of cells out of the decay depth of evanescent wave while the other took place at the extracellular space between the adherent cell and the coverslip, within the TIRFM observation range. The former case was accompanied by the lateral diffusion of **1**, indicating that the invisible parent vesicles were located on the lateral cell membrane, outside the evanescent field. When it comes to the latter case, two alternative explanations have been proposed as following:

#### **i. The mechanism of sequential fusion**

Taking advantages of a combination of two-color imaging and TIRFM, Tran et al. showed that around 25% of all exocytotic events in the basal membranes of BON cells (of which vesicles were transfected by fluorescent NPY-GFP) occurred through a specific process defined as ‘sequential fusion’, for which retention of vesicular shape after exocytosis was a prerequisite.<sup>[211]</sup> In sequential fusion, when a primary secretory vesicle firstly fusing with the cell membrane, unlike the full fusion case, its vesicular membrane does not collapse but forms a  $\Omega$ -shaped empty lumen which survives for at least several seconds. Since all its fluorescent contents have been already expelled, it becomes invisible under TIRFM, existing as a ‘ghost’ vesicle. Then, a secondary deep-lying vesicle queuing up behind the primary vesicle comes up to fuse with this ‘ghost’ vesicle. It is important to note that, because of the limited observation depth of TIRFM, deep-lying vesicles located far from the cellular membrane are invisible before fusing with the primary ‘ghost vesicle’. When the fluorophores inside the secondary vesicle is released into the empty  $\Omega$ -shaped lumen of the ‘ghost’ vesicle, the fluorescent labels enter into the evanescent field, resulting in a sudden appearance of fluorescence. Finally, through the  $\Omega$ -shaped lumen, the dyes diffuse away to the extracellular space between the adherent cell and the coverslip. Briefly, shape retention of primary fused vesicle ghosts which became targets for sequential fusions with deeper lying vesicles played a key role in sequential fusion. That is one of the possible explanations why ‘sudden flash’ events are observed.

#### **ii. The existence of ‘ballistic vesicles’**

It has been reported that there exists a particular population of vesicles referred as ‘ballistic vesicles’ considering their distinguish mobility and they are taken as a likely contributor to a fraction of orphan exocytotic events.<sup>[211, 230, 239]</sup> Generally, before fusion, these dye-stained ‘ballistic vesicles’ are located in the deeper cytosol beyond evanescent field and are therefore invisible under TIRFM. Unlike the deep-lying vesicles in sequential fusion, they do not rely on the  $\Omega$ -shaped ‘ghost’ vesicle to accomplish exocytosis. Upon stimulation, they directly travel several hundred nanometers

perpendicularly within a short time (less than ~100 ms) in order to fuse with cellular membrane within evanescent field, generating an orphan event without a detectable parent vesicle.

Even though both mechanisms discussed above are reasonable to explain the observed orphan events, it is still difficult to figure out which is the exact reason when we taking account to an individual orphan exocytosis since we only employ **1** as the optical probe in our case.

### **3.4 Conclusions**

Neurotransmitter secretion through exocytosis is a fundamental process for cell communication. In this chapter, we introduced **1**, a pH-responsive fluorescent false neurotransmitter, as a novel, optical probe to track the calcium-triggered exocytosis at single vesicle level by TIRFM. As expected, **1** was able to be recognized and selectively transferred into the acidic vesicular lumen by both PC-12 cells and BON N13 cells. Nevertheless, we finally employed **1**-stained BON N13 cells as cell models for TIRFM measurements of exocytotic secretions since PC-12 cells were demonstrated not to be appropriate cell models due to their small vesicle size. By the combination of TIRFM and BON N13 cells labeled by **1**, the motility behaviors of vesicles adjacent to plasma membrane before and during exocytosis were studied. Moreover, upon stimulation, three forms of calcium triggered exocytotic events were observed from BON N13 cells stained by **1**: the normal ‘flash’, the extinction of fluorescent spots as well as the ‘sudden flash’. In this work, we demonstrate that at TIRFM configuration, **1** is a proper optical probe to directly visualize and quantify the neurotransmitter release during exocytosis at single vesicle level.



## 4 Amperometric detection of exocytosis in 1-stained BON N13 cells

### 4.1 Introduction

The release of neurotransmitters through exocytosis is one of the most common ways for neuronal communications.<sup>[31, 32]</sup> A unique feature of some well-known monoamine neurotransmitters is their electroactive property which promises the possibility of using an electrochemical technique to detect these molecules so as to quantitatively characterize exocytotic process.<sup>[33-35]</sup> In the 1990s, owing to the electroactivity of catecholamines, their quantal secretion during exocytosis was firstly monitored electrochemically by amperometry and cyclic voltammetry with a CFE placed adjacent to a single chromaffin cell of interest by Wightman and his colleagues.<sup>[36, 37]</sup> After two decades of development, amperometry has become the most widely used electrochemical technique for exocytosis investigation because of its remarkable advantages such as facility to implement, high temporal resolution as well as high sensitivity.<sup>[2, 35, 38]</sup>

CFE is the firstly and mostly used microelectrode in amperometric measurement of exocytosis at single cell level. In this technique, a constant potential that is sufficient to oxidize the released electroactive biomessengers is applied to the CFE positioned gently against the cell of interest and the current is then recorded as a function of time. Upon stimulation, an individual exocytotic event appears as a single current spike resulting from the electrooxidation of released biomessengers and the whole exocytotic process of a single cell is thus observed as a series of oxidation spikes, as illustrated in Fig.4-1.

In the past two decades (especially in recent five years), besides CFE, plenty of other microelectrodes/MEAs have also been developed as the working electrodes for real-time amperometric determination of electroactive molecules discharged from individual vesicle during exocytosis.<sup>[38, 109]</sup> Among them, ITO microelectrodes have attracted more and more attention owing to their excellent optical transparency, high electrical conductivity as well as their appropriate electrochemical working window for the electroanalysis of biomessengers. Our group<sup>[19, 105, 118]</sup> and others<sup>[111, 117, 120, 240, 241]</sup> have been developing microchips based on transparent ITO microelectrodes on a glass substrate in order to facilitate higher throughput measurements of exocytosis as well as to enable fluorescent measurements that are impossible to achieve with traditional CFE.

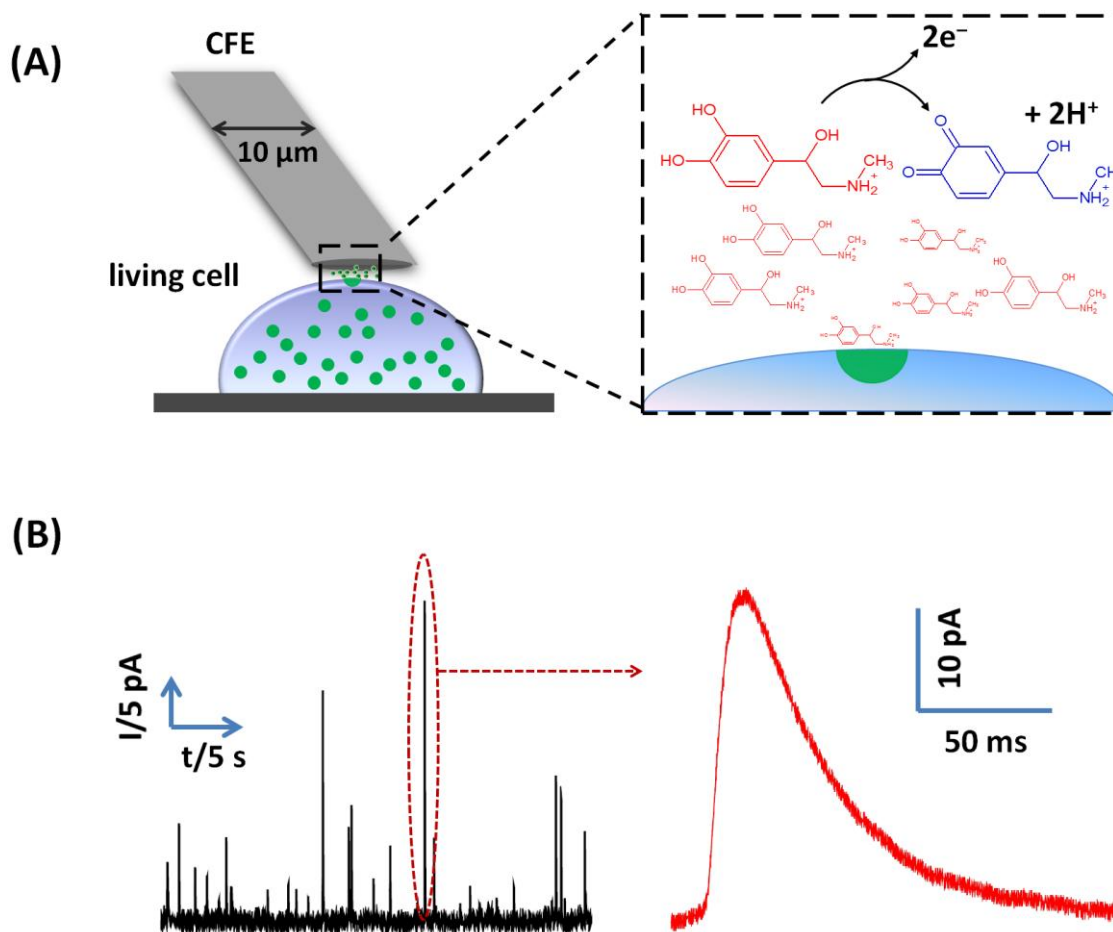


**Figure 4-1** (A) Scheme of the experimental configuration ('artificial synapse' configuration) of amperometric measurements at a constant potential at which the electroactive biochemical messengers released during exocytosis could be oxidized. CFE (10-μm diameter) is positioned gently against the cell of interest and a well-known neurotransmitter, epinephrine, is employed to illustrate the oxidation process on the electrode surface when the cellular vesicle fuses with the cell membrane and discharges its contents; (B) A series of current spikes as a function of time resulting from the oxidation of neurotransmitters at the CFE surface is presented and a representative oxidation spike extracted from the trace corresponds to an individual vesicular release.

So far, chemical biomessengers including serotonin<sup>[18, 168, 197]</sup>, dopamine<sup>[212, 213]</sup>, norepinephrine<sup>[214, 215]</sup> as well as epinephrine have already been employed as the electrochemical reporters for real-time, quantitative characterization of exocytosis by amperometric detection as they can be easily oxidized at the electrode surface. As we have discussed in Chapter 2 (Fig.2-9), electroactivities of **1** and these monoamine neurotransmitters mentioned above are all assigned to the oxidation of their phenolic hydroxyl group. We thus believe certain molecules in the FFNs family, are also capable of being

employed as electroactive reporters for quantitative dynamic assessment of exocytosis in amperometric detection.

In this chapter, the design, fabrication, characterization and comparison of three ITO microdevices will be firstly discussed in detail. And then, the feasibility of the employment of **1** as electrochemical probes for exocytosis investigation is going to be tested with BON N13 cells seeded in the microfabricated ITO chips. Finally, the comparison of the vesicular release detected at different configurations (at the cell apex recorded by CFE positioned against the target cell and at the cell bottom monitored by ITO, respectively) is about to be carried out.

## **4.2 ITO microchips for amperometric measurement**

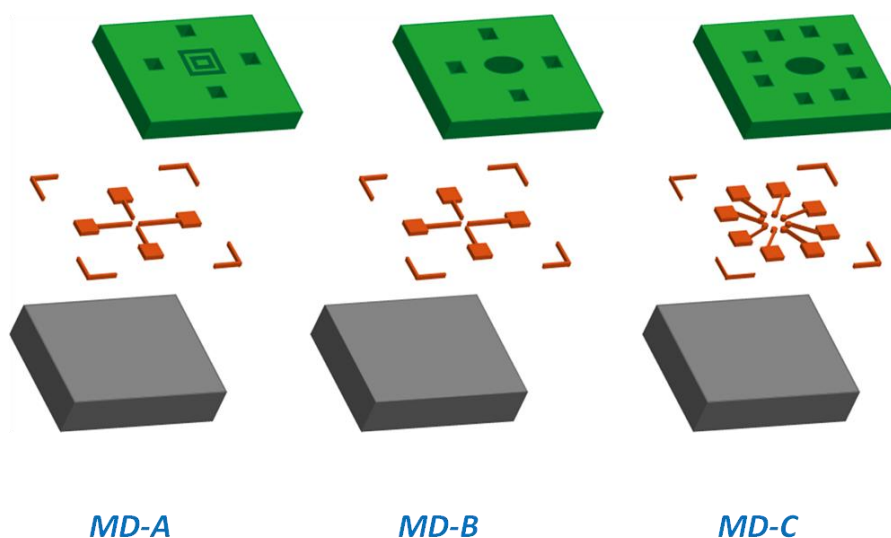
The investigation of exocytosis by fluorescence microscopy such as TIRFM provides dynamic information of the release event with excellent spatial resolution, as we mentioned in Chapter 3, but the application of TIRFM is limited by its relatively low temporal resolution (~35 ms in our case). That is the main reason why people turn to another electrochemical technique called constant-potential amperometry which is able to reveal the kinetic parameters of the exocytotic events with distinct temporal resolution (~ms). Among various materials of microelectrodes applied to electrochemical detections of cellular exocytosis, ITO has attracted increasing attention owing to its characteristic ability for simultaneously optical (transparency) and electrochemical (conductivity) recordings.<sup>[19, 109, 118]</sup>

### **4.2.1 ITO microdevice preparation**

All our ITO microelectrodes used for electrochemical detection in this chapter were carefully fabricated by photolithography and acid etching process. The thickness of ITO on the substrate (quartz slide) is  $150\pm 10$  nm and two representative photoresists (AZ9260 and SU8-3010) were employed alternatively to define the working areas of ITO microelectrodes taking account to their reverse photosensitive features.

- **ITO microelectrodes fabrication**

Three types of ITO microdevices (MD-A, MD-B and MD-C) were designed and constructed in this work. Two of them (MD-A and MD-B) have already been introduced for electrochemical characterization of **1** in Chapter 2 (Scheme 2-2) and the other one is a novel microdevice embedded with 8 ITO microelectrodes (MD-C).



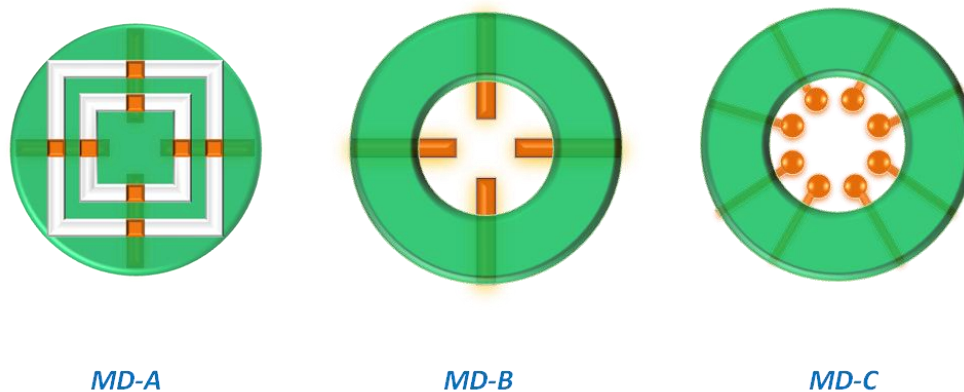
**Scheme 4-2** Illustration of different layers of the three microdevices (MD-A, MD-B and MD-C) obtained by alternatively using the photoresists AZ9260 and SU8-3010, respectively. Bottom: glass coverslip (in gray); middle: ITO microelectrodes (in orange); top: the isolation layer composed of SU8-3010 exposed to UV light (in green).

A series of masks with various patterns were designed and employed to produce the three ITO microchips with different lengths, shapes and configurations. As shown in Scheme 4-2, the microfabricated devices were composed by the following three layers:

- (1) The substrate suitable for fluorescence microscope observation (glass coverslip shown in gray in Scheme 4-2);
- (2) The multiple ITO microelectrodes adaptable to optical/amperometric measurement (displayed in orange in Scheme 4-2). The second layers of MD-A and MD-B are identical, consisting of four independent ITO microbands (200- $\mu\text{m}$  width) while eight independent ITO microbands (50- $\mu\text{m}$  width) with a round disk (200- $\mu\text{m}$  diameter) in the end were patterned to MD-C by the positive photoresist, AZ-9260, through the photolithography and acid etching;
- (3) SU8-3010 isolation layer defining the working area (presented in green in Scheme 4-2). ITO microelectrodes were firstly completely insulated with a nonconductive photoresist SU8-3010. It is worth noting here that, in this step,  $\text{O}_2$  plasma treatment before the deposition of SU8-3010 is highly proposed for the sake of improving the adhesion between the photoresist and the substrate. In fact, the detachment of SU8-3010 layer from the glass/ITO substrates occurred for microdevices exposed to air plasma or even without plasma pre-treatment,

resulting in a high electrical noise background (i.e. low signal-to-noise ratio). A second photolithographic process was then conducted so as to define specific ITO working areas.

In our microfabricated devices, all the small ITO squares over the periphery were designed for electrical contact.



**Scheme 4-3** The defined working areas of three microfabricated ITO devices: ITO microelectrodes are shown in orange and the isolation layers displayed in green are composed of a nonconductive layer of SU8-3010.

Scheme 4-3 displays the working area of the three microfabricated ITO devices. For MD-A, the mask was designed to carve a spiral-like microchannel of 200- $\mu\text{m}$  width in the SU8-3010 photoresist layer. This microchannel crossed perpendicularly the four ITO microbands at periodic instances thus exposing a series of squared ITO sections (200- $\mu\text{m}$  width  $\times$  200- $\mu\text{m}$  length) lying on the glass floor of the spiraling microchannel. For MD-B and MD-C, a disk area of the SU8-3010 photoresist in the center was removed by the mask through photolithographic process. In consequence, four ITO microbands (200- $\mu\text{m}$  width/600- $\mu\text{m}$  length) and eight terminals of ‘lollipop’ shapes were exposed in MD-B and MD-C, respectively. Here, ITO of ‘lollipop’ shape is defined as a narrow microband (50- $\mu\text{m}$  width) connected with a wider round disk (200- $\mu\text{m}$  diameter) at the end.

- **Assembly of microdevice**

To make our microfabricated ITO devices compatible for amperometric measurements as well as living cell culture, they were finally fixed on a Petri dish compatible with the TIRFM set-up and previously holed. Fig.4-2 displayed a typical example of MD-B for electrochemical test. It is necessary to note that, in this work, biocompatible polydimethylsiloxane (PDMS) was used for the fixing step

rather than the silicone rubber (3140 RTV coating, Dow Corning) previously used in our lab<sup>[19]</sup> because some cells became fluorescent with the excitation of 405 nm laser in this work (It is not the case before<sup>[19]</sup>) after being incubated in the devices fixed by silicone rubber.

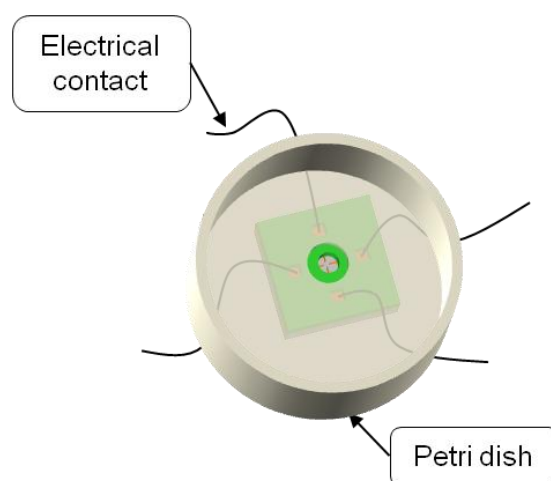


**Figure 4-2** Schematic representation of MD-B with four ITO microbands (shown in orange) used for electrochemical detections.

#### 4.2.2 Characterization of ITO microdevices

In the viewpoint of amperometric measurements, for quantitative investigation of cellular exocytosis, the employed working electrode should not only exhibit electrical conductivity and appropriate electrochemical properties but also be small so as to minimize non-faradic signals such as electrical noise and capacitive currents. However, the size of electrode surfaces needs to avoid being too small to collect all the secretions from the whole cell surface. These two opposite constraints have to be taken into consideration to achieve a compromise when designing the mask. In addition, the bottom surface of the microfabricated devices are composed by ITO, glass as well as the photoresist, showing inhomogeneity, further surface treatment is thus necessary to provide a friendly environment for cells culture. We then characterized the electrochemical properties of the three microdevices mentioned above and studied the influence of surface treatment on their electrochemical characteristics.

- **Electrical noise test**

Current noise is often a significant limitation when using constant-potential amperometry for detection of transmitter release from single cells through exocytosis.<sup>[105, 242-244]</sup> The relationship between the current noise and the surface area of ITO working microelectrode is shown as in Fig.4-3. Because of

the imperfect alignment during the second step of photolithographic process (i.e. the SU8-3010 isolation process), the ITO microelectrodes were not exactly identical for MD-B and MD-C, showing slightly differences of the electrode length. Moreover, the widths of the obtained ITO electrodes were also a little smaller than the sizes of the masks we used due to the fast acid etching process. For instance, in MD-B, the width of an individual ITO band is measured as around 180~190  $\mu\text{m}$  whereas the size of the employed mask was 200  $\mu\text{m}$ . So, the surface areas of ITO microelectrodes in Fig.4-3 were calculated on the basis of their corresponding micrographs.

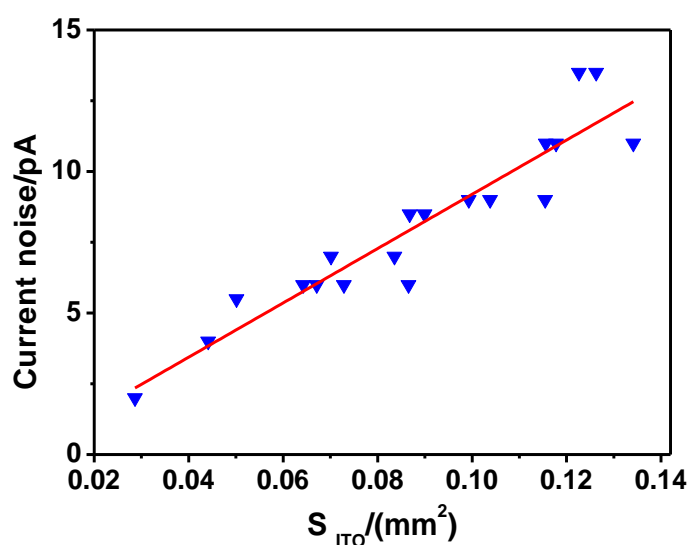


**Figure 4-3** Measurements of the electrical noise of ITO microelectrodes in PBS (pH=7.4) at the potential value required for analyzing the release of **1** ( $E=+900$  mV vs. Ag/AgCl) as a function of electrode dimensions ( $y=95.9x-0.4$ ,  $R^2=0.875$ ).

Globally, the current noise augmented as the increase of the electrode dimension and the red fitting curve in Fig.4-3 depicted a good linear relationship between the electrical noise and the surface areas with a slope of  $0.095 \text{ fA}/\mu\text{m}^2$ . Moreover, the best electrical properties were obtained from MD-C, of which ITO electrodes of ‘lollipop’ shapes with minimum surface area of  $0.03 \text{ mm}^2$  showed a rms noise of typically 2~4 pA, in accordance with our previous work based on ITO microelectrodes.<sup>[105]</sup>

- **Influence of collagen coating and cell seeding on electrical noise**

In order to quantitatively measure exocytosis by amperometry, planar ITO microelectrodes ought to be positioned right against the cell of interest to avoid the rapid dilution of released biomolecules to the extracellular spaces. One of the common ways is to seed the cells onto the planar electrodes and

perform the electrochemical test until cells adhere to the surfaces of electrodes. Taking account to the inhomogeneity of the surfaces of our microdevices (glass/ITO/SU8-3010), we precoated the bottom of microchips with collagen in order to improve its biocompatibility and to promote cell adhesion. Therefore, we take the MD-B as an example to illustrate the effects of collagen coating as well as cell seeding on the current noises obtained from ITO microelectrodes.

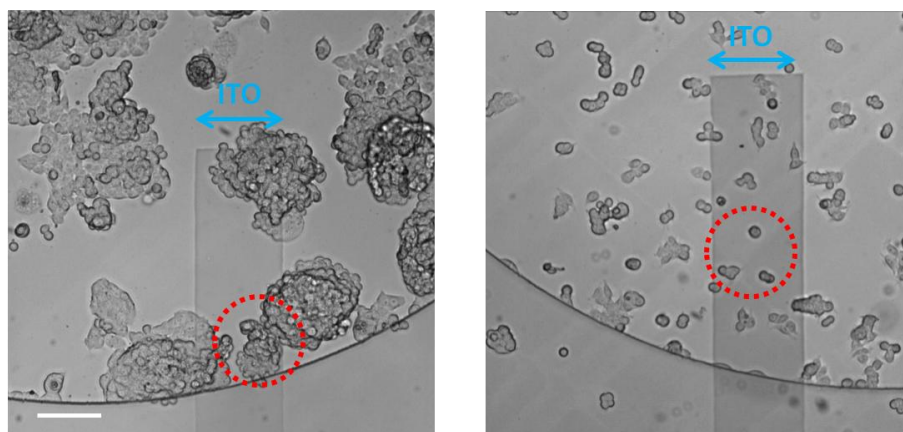


**Figure 4-4** BON N13 cells seeded on ITO microchip without (left) and with (right) collagen pre-treatment; the blue double headed arrow depicts the position of the transparent ITO microelectrodes and the red dashed line circle indicates cells lying on ITO microelectrode; scale bar: 100  $\mu$ m.

Fig.4-4 illustrates the micrographs of BON N13 cells seeded on ITO microchips with and without collagen pre-treatment. We can see that the aggregation of cells took place on naked ITO electrodes, making it impossible for individual cells investigation whereas on collagen-coated microchips, cells were adherent and well dispersed, demonstrating that the collagen treatment was capable of providing a biocompatible environment so as to improve the cell adhesion on ITO microchips.

The comparison of electrical noises before and after collagen treatment demonstrates that collagen coating did not affect the electrical background, as shown in Fig.4-5. In addition, no obvious variation of current noise due to the cell seeding was observed neither, suggesting that cells adjacent to ITO electrodes did not increase the background noise. In brief, the baseline current noise during amperometric measurement of quantal exocytosis from adherent cells was comparable to that of bare ITO microelectrodes without any treatment.

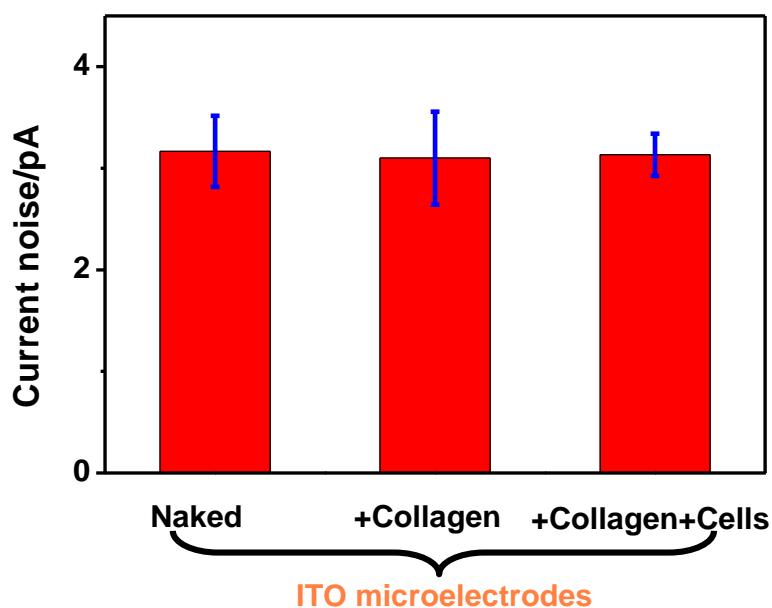


**Figure 4-5** Electrical noises obtained from naked, collagen-coated ITO microelectrodes (75- $\mu\text{m}$  width  $\times$  500- $\mu\text{m}$  length) as well as collagen-coated ITO microelectrodes with BON N13 cells. Collagen coating did not affect the electrical noise and the baseline noise during amperometric measurement of quantal exocytosis from adherent cells is comparable to that of bare microelectrodes.

- **Collagen coating effect**

As discussed previously, we pre-coated our ITO microchips with collagen with the purpose of creating a homogenization of the whole surface friendly to cell growth. It has been reported that some pre-treatments on the exposed surface might alter the electrochemical properties of microelectrodes.<sup>[104, 105]</sup> Voltammetric experiments on a well-characterized redox mediator  $\text{Ru}_3(\text{NH}_3)_6\text{Cl}_3$  (100  $\mu\text{M}$ ) were thus performed to investigate whether electrochemical properties of ITO microelectrodes were affected by collagen coating. CVs of 100  $\mu\text{M}$   $\text{Ru}_3(\text{NH}_3)_6\text{Cl}_3$  were recorded on a naked ITO microelectrode (black curve in Fig.4-6) and collagen-coated ITO band (red curve in Fig.4-6) respectively at the scan rate of 20 mV/s. We can see from Fig.4-6 that CVs of  $\text{Ru}_3(\text{NH}_3)_6\text{Cl}_3$  before and after collagen treatment were well overlapped, suggesting that the surface treatment by collagen did not affect the electrochemical detection at ITO microelectrodes.

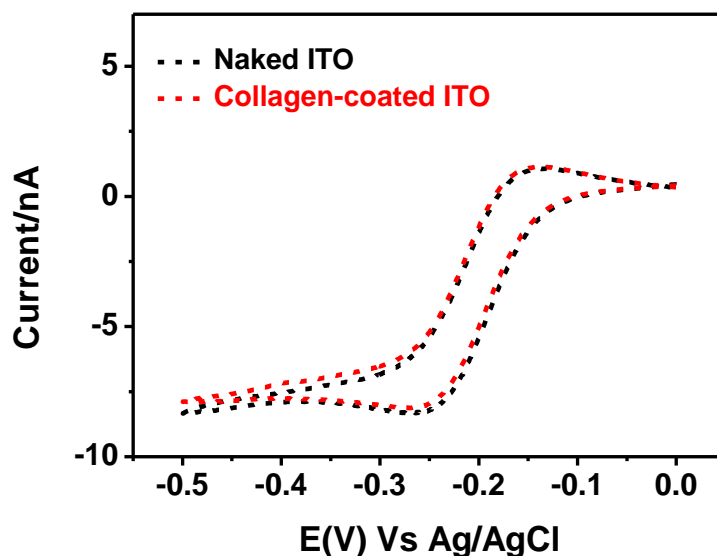


**Figure 4-6** Representative CVs of 100  $\mu\text{M}$   $\text{Ru}(\text{NH}_3)_6\text{Cl}_3$  dissolved in physiological saline (Locke's $\times$ 1, pH=7.4) before (blank curve) and after (red curve) collagen coating to illustrate the effect of collagen coating on the electrochemical properties of ITO microelectrodes; initial potential: 0 V vs. Ag/AgCl; scan rate: 20 mV/s.

- **Fluorescence interference of the insulation layer composed by SU8-3010**

MD-A is the former device used for TIRFM/amperometry coupling measurements in our group (notably during PhD of Anne Meunier).<sup>[19]</sup> However, it is not suitable for the fluorescence observation of **1**-stained cells because the insulation layer composed of SU8-3010 in this microchip was found to be highly fluorescent with the excitation of either the 405 nm laser or the mercury lamp. Fig.4-7 displays the micrographs of a single ITO microelectrode with **1**-stained cells acquired at bright field (Fig.4-7(A)) and epi-fluorescence configuration (Fig.4-7(B)). The border of the coverslip and the photoresist SU8-3010 was clearly observed because of the high contrast between fluorescent insulation layer and the non-fluorescent substrate (ITO/glass), as indicated by the blue arrows in Fig.4-7. In addition, the fluorescence intensity of SU8-3010 was much stronger than that obtained from cells labeled by **1** (Fig.4-7(C)), making it difficult to track the behaviors of adherent cells locating in the vicinity of the ITO/SU8-3010 border. In other words, only cells far from the bright border (100~200  $\mu\text{m}$  away) were appropriate for fluorescence studies. Considering that the electrical background is proportional to the surface area of all the ITO exposed to the electrolyte (i.e. Locke's $\times$ 1 solution), we designed and fabricated a novel microchip (MD-C) of which the individual working electrode looks like a 'lollipop' shape (Fig.4-8).

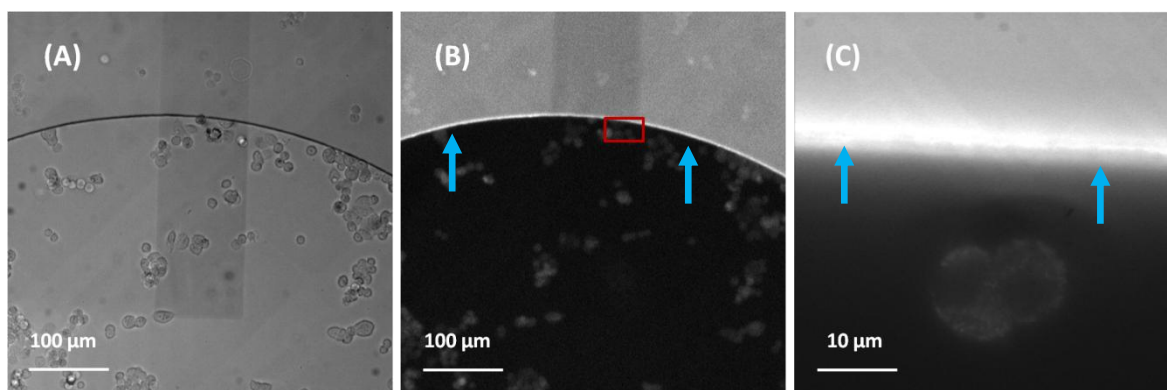


**Figure 4-7** Images of a single ITO microelectrode seeded with **1**-stained cells acquired at bright field (A) and (B) epi-fluorescence configuration (illuminated by the mercury lamp); (C) represents a zoom-in image of the cells inside the red rectangular of (B); the blue arrows indicate the border of the coverslip and highly fluorescent photoresist SU8-3010.

The design of MD-C displays two main advantages for TIRFM/amperometry coupling measurements compared with MD-A and MD-B. Firstly and most importantly, the fluorescence interference caused by the bright insulation layer could be subtly eliminated because only cells on the round disk (far away from the border, indicated by the blue arrow in Fig.4-8) would be taken account to the fluorescence tracking; secondly, in MD-B, it is certain that we are also able to find some **1**-stained cells suitable for fluorescence observation at the end of the ITO band. Nevertheless, in this case, the utilization of ITO as the working electrode is largely ineffective because a large portion of the electrode surface close to the fluorescent border works only as an ‘electrical conductor’, leading to a relatively lower signal-to-noise ratio. On the contrary, for MD-C, the width of the ‘electrical conductor’ is decreased to around 30  $\mu\text{m}$  so as to minimize its contributions to the overall electrical noise background, resulting in a higher sensitivity in amperometric detection.

In addition, MD-C embeds eight individual ITO microelectrodes while the other two devices possess four. The augmentation of the number of applicable working electrode in MD-C would optimize largely the probability to find a decent cell considering the fact that not all the BON N13 cells are able to internalize **1** as optical probes, as we mentioned in the third chapter (Fig.3-5).

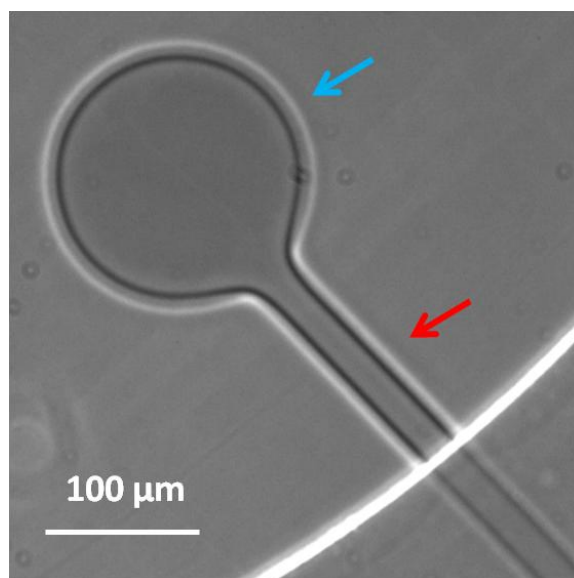


**Figure 4-8** A representative ITO microelectrode ('lollipop' shape) of MD-C: a narrow ITO microband (about 30- $\mu\text{m}$  width, indicated by the red arrow) is designed to electrically connect to the round ITO disk (around 170- $\mu\text{m}$  diameter, marked by the blue arrow) far from the border; scale bar: 100  $\mu\text{m}$ .

#### 4.2.3 Electrical characterization of MD-C

Taking account to its remarkable advantages compared with the other two ITO microchips, we employed MD-C for the following amperometric measurements of exocytotic release. To characterize its electrochemical properties, we measured the current noise of a single ITO microelectrode and studied the oxidation behavior of electroactive **1** on the ITO surface.

Fig.4-9 represents a typical example of the current noise trace recorded when a constant voltage (+900 mV) was applied to the electrochemical cell. Owing to the small size of the 'lollipop' shape ITO microelectrode, the detected current decayed rapidly to a constant value. Moreover, depending on the variation of the lengths of the 'electrical conductor' part caused by the imperfect alignment during photolithographic process, the recorded current noise background varied from 2 to 4 pA (inset of Fig.4-9), comparable to that of the reported devices for exocytosis investigation.<sup>[107, 120, 243, 245]</sup> In addition, the current noises of the naked ITO microelectrodes were identical to those observed from microchips pre-treated by collagen coating and cell seeding, in accordance with our previous results (Fig.4-5).

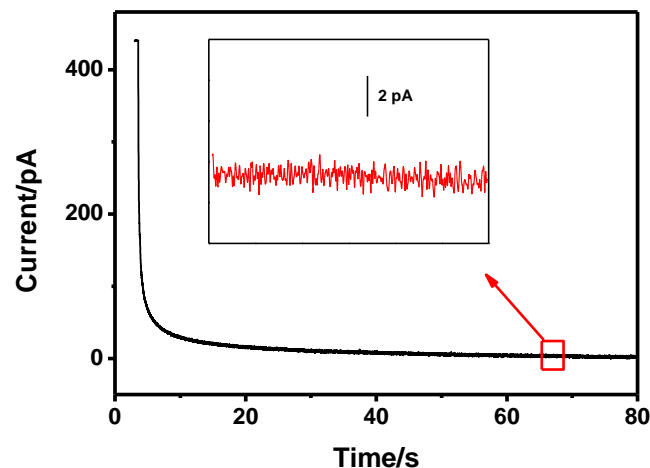


**Figure 4-9** Measurements of the electrical noise of an individual ITO microelectrode (MD-C) obtained in physiological solution (pH=7.4) at a constant potential value corresponded to the **1** release analysis ( $E = +900$  mV vs. Ag/AgCl) and the inset represents the zoom-in graph of noisy current trace at a later time where the current has reached a constant value.

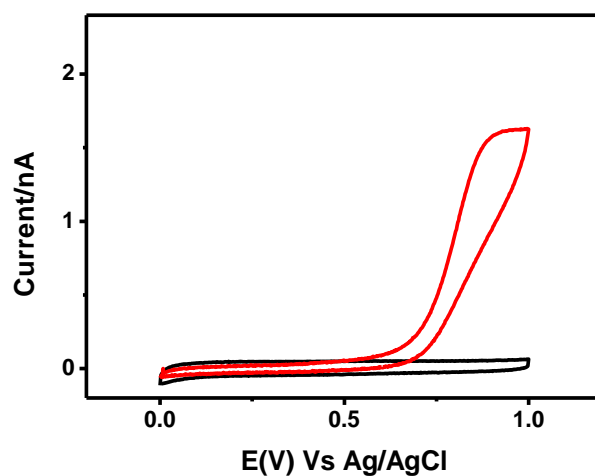


**Figure 4-10** CV of  $25 \mu\text{M}$  **1** in Locke's $\times 1$  solution (pH=7.4) obtained on an individual ITO microelectrode of MD-C: the black trace depicts the background recording from the PBS whereas the red trace illustrates the response of  $25 \mu\text{M}$  **1** dissolved in physiological solution; a clear oxidation peak is noted; initial potential: 0 V vs. Ag/AgCl; scan rate: 100 mV/s.

Next, the electrochemical behavior of **1** on ITO surface of MD-C was studied by cyclic voltammetry. As illustrated in Fig.4-10, for an individual ITO microelectrode, there was no response observed from

0 V to +1.0 V in Locke's×1 solution (pH=7.4), indicating a wide and stable working window (black curve in Fig.4-10). Nevertheless, when 25  $\mu$ M **1** was introduced to the previous Locke's×1 solution, an obvious oxidation peak appeared at around +850 mV (red curve in Fig.4-10), suggesting that MD-C with 'lollipop' shape ITO microelectrodes offered a satisfying active region for the electrochemical oxidation of **1** that had already been demonstrated to be a proper optical probe for the observation of the exocytotic release of BON N13 cells. Therefore, a constant potential of +900 mV was applied to the electrical cell so as to test if **1** discharged during exocytosis could be able to be oxidized on the ITO surface in amperometric detection.

### **4.3 Amperometric test of exocytosis in 1-stained BON N13 cells in MD-C**

#### **4.3.1 Cellular exocytosis assessed by amperometric measurement**

BON cells are easy to culture or to transfect compared with neuron cells and chromaffin cells of which the main disadvantages are the low yield and short survival of cells in culture.<sup>[246-248]</sup> In addition, the secretory vesicles of BON cells are able to be easily labeled by fluorescent probes such as GFP<sup>[19, 143, 211, 235]</sup> and FFNs (**1** in this work), enabling this cell line to be available for optical monitoring of exocytosis. Moreover, the typical size of these vesicles were around 200~300 nm, bigger than that reported for some other cell lines such as PC-12 cells.<sup>[12, 13, 249]</sup> In other words, the contents stored inside the vesicles of BON cells were higher, making it easier to be visualized by fluorescent microscopy (as we mentioned in Chapter 3) and to be detected by electrochemical techniques.

Actually, the exocytotic behaviors of BON cells have been electrochemically studied using CFE (10- $\mu$ m diameter)/ITO microchips (200- $\mu$ m width  $\times$ 200- $\mu$ m length) in our group.<sup>[18, 19, 105, 109]</sup> Before the application of amperometric measurement, the cells were previously preloaded with serotonin (working as the electrochemical probe) to enhance the quantity of release during exocytosis because BON cells lost the ability to secrete a sufficient amount of serotonin to be detected with amperometry at microelectrodes.<sup>[18, 234]</sup> Upon stimulation, the exocytotic events were depicted as a series of amperometric spikes as a function of time because of oxidation of serotonin on the surface of microelectrodes positioned against the cell of interest. Because of their moderate activity in terms of exocytotic frequency and amount of release, BON N13 cells are considered as an appropriate choice exocytosis investigation through TIRFM/Amperometry coupling technique.<sup>[18]</sup> In this work, we are going to try to load BON N13 cells with **1** instead of serotonin to check if their exocytotic released are capable of being electrochemically detected on MD-C.

On the basis of our TIRFM results described in Chapter 3, it is evident that **1** could be specifically recognized by BON N13 cells and be selectively internalized into the acidic cellular vesicles.

Additionally, it is also been able to be expelled back to the extracellular space subsequently with the stimulation of 10  $\mu\text{M}$  ionomycin. Considering the electroactivity of **1** on ITO microelectrode (Fig.4-10), it could be probably adopted as a novel electrochemical probe to investigate cellular exocytotic behavior even though a phenomenon of electrode passivation was observed during the electrochemical detection of **1** in voltammetry with CFE or ITO electrode, as we previously mentioned in Chapter 2.

Indeed, such a passivation does not impede its application in amperometric investigations of exocytosis at the single cell level since voltammetry conditions (temporal and spatial scales, non-dynamic solution...) are not comparable to those of the artificial synapse configuration. For instance, serotonin and dopamine are two widely recognized neurotransmitters which easily foul the working electrodes because of the generation of insoluble polymer-like oxidation products at the electrode surface.<sup>[196, 250-252]</sup> Nevertheless, they are still the most extensively used probes for electrochemical characterizations of cellular exocytosis using amperometric detection at the artificial synapse configuration.<sup>[2, 35, 38, 253-255]</sup> We thus believe that **1** could be also employed as an electrochemical probe for exocytosis investigation of BON N13 cells.

To test the possibility of the application of **1** as the electrochemical probe to study the exocytotic events, a certain amount of BON N13 cells ( $3 \times 10^5$  cells) was firstly plated into the assembled ITO microchip (MD-C with eight ITO microelectrodes precoated with collagen, Fig.4-11(A)) and cells appeared to settle randomly on the glass/ITO surfaces and usually a few cells adhered onto the ITO band after 1~2 days incubation, as shown in Fig.4-11(B). Before the performance of amperometric measurement, cells grown in MD-C were incubated in the medium supplemented with 20  $\mu\text{M}$  **1** for 1 h for purpose of staining a portion of cells with fluorescent **1** and then they were thoroughly rinsed by PBS solution before use.

During the amperometric test, a constant potential of +900 mV vs. Ag/AgCl was applied to the working electrode and a glass capillary (with an opening end of 1~5  $\mu\text{m}$  diameter) filled with a saline solution supplemented with 10  $\mu\text{M}$  ionomycin was placed close to the cell of interest to trigger the release (Fig.4-11(C)). The background current of the ITO microelectrodes measured in the physiological solution (Locke's $\times$ 1, pH=7.4) was typically 2~4 pA, depending on its size. The amperometric current was recorded as a function of time and injection of calcium ionophore (10  $\mu\text{M}$  ionomycin) was implemented once the baseline of the noise current became stable. It is necessary to note that the selections of target cells were carried out with the help of optical microscopy taking advantages of the fluorescent properties of **1**-stained cells.

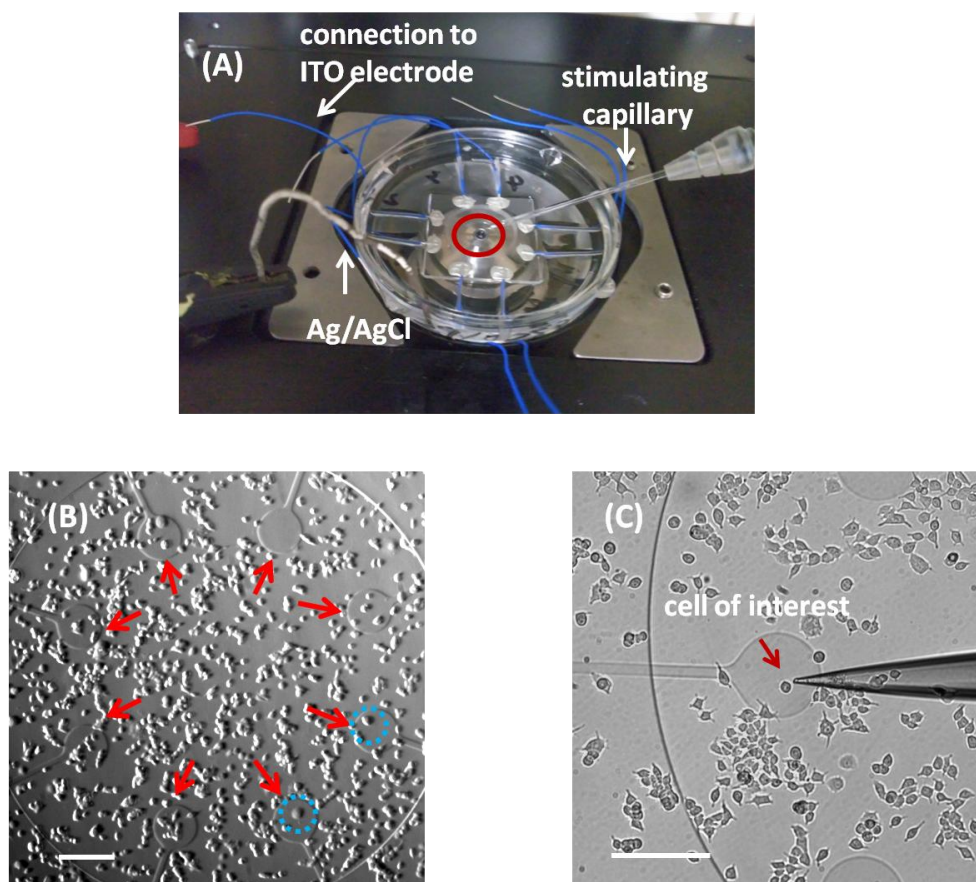


**Figure 4-11** An example of amperometric measurement of cells stained by **1** in MD-C: (A) Photograph of MD-C embedded with eight 'lollipop' shape ITO microelectrodes for exocytosis investigation of BON N13 cells and the glass capillary (1~5  $\mu\text{m}$  diameter) filled with a saline solution supplemented with 10  $\mu\text{M}$  ionomycin was used to trigger the release of cells of interest; (B) A zoom-in micrograph of the area defined by the red ellipse in (A): here the eight ITO microelectrodes were indicated by the red arrows and the blue circles show examples of cells located on the round disk of a single 'lollipop' shape ITO microelectrode; (C) A single cell lying on the ITO; scale bars: 200  $\mu\text{m}$ .

Fig.4-12(A) is a typical amperometric trace representing the exocytotic release of **1**-stained BON N13 cells and the red arrow inside the figure indicates the moment when ionomycin solution was injected by the microinjector. As expected, no oxidation signal was observed before the application of 10  $\mu\text{M}$  ionomycin solution (before the red arrow). A succession of individual amperometric spikes appeared afterwards (several seconds after the injection of stimulation solution), which could be attributed to the calcium-triggered sequential release of **1** followed by its rapid oxidation on ITO microelectrode surface. The slight delay of the effect of stimulation solution was due to the distance between the stimulating capillary and the target cell. In the amperometric trace, each spike was corresponding to an

individual exocytotic event of a single secretory vesicle (Fig.4-12(B)). It is evident that this technique exhibits extremely high temporal resolution since the isolated spikes usually last for less than 100 ms. Significant kinetic and quantitative parameters could be extracted from an amperometric trace to illustrate the specific steps of the whole exocytotic event at single vesicle level, which would be discussed in detail later.

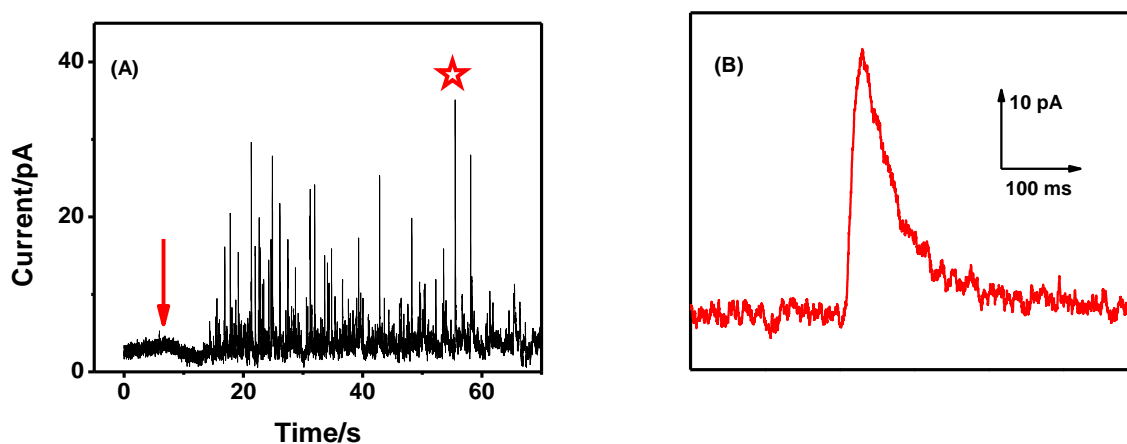


**Figure 4-12** (A) A typical example of amperometric trace obtained from BON N13 cells preloaded with **1** (20  $\mu$ M, 1 h) with the stimulation of a saline solution supplemented with 10  $\mu$ M ionomycin; the red arrow indicates the moment when stimulation solution was injected by the microinjector; (B) Representative single amperometric spike extracted from the left trace (see labeling by red star in (A)) which stands for an individual exocytotic event of a secretory vesicle.

It has been demonstrated so far that **1** is feasible to work as an electrochemical probe to monitor the calcium-triggered exocytotic process. Therefore, it is reasonable that the amperometric traces of **1**-stained BON N13 cells resulting from the oxidation of **1** on the ITO surface ought to closely relate to the number of the stained secretory vesicles as well as the internalized amount of **1** in individual vesicles. Fig.4-13 shows fluorescent images of three individual **1**-stained BON N13 cells excited at epi-fluorescence configuration. We can see that the number of illuminated vesicles varied from cell to cell, suggesting that distinct disparity of the accumulated count of current spikes resulting from **1** oxidation should be predicted for different cells. Additionally, the fluorescence intensities of individual vesicles were not identical, even the ones lying in the same single cell, indicating the variations of the concentration of internalized **1** which was a decisive element for the integral charge of current spikes in amperometric recording.

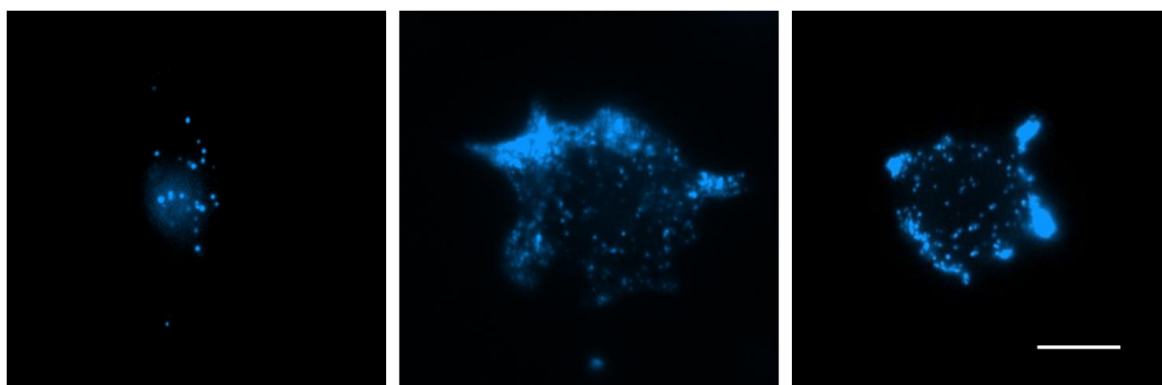


**Figure 4-13** Three examples to illustrate the various abilities of BON N13 cells to take up the fluorescent **1**; images were acquired at epi-fluorescence configuration with TIRF microscope; scale bar: 10  $\mu\text{m}$ .

Two examples of amperometric traces of **1**-stained BON N13 cells were presented in Fig.4-14 and Fig.4-15, respectively and their corresponding fluorescent photographs were compared before and after the electrochemical detection. To be specific, fluorescent images of the cells of interest were firstly taken at the epi-fluorescence configuration (excited by the mercury lamp) exactly right before the electrochemical detection (Fig.4-14(B)) and 10  $\mu\text{M}$  ionomycin was then injected for 1 min to trigger the exocytotic process which was depicted as a session of oxidation spikes in amperometric measurement (Fig.4-14(A)). As soon as the stimulation finished, the other fluorescent images of the cells of interest were acquired at the same condition as the ones obtained before stimulation right after the electrochemical test (Fig.4-14(C)). It is necessary to note the light source was shut off during the amperometric recording in order to avoid the interference of fluorescence decline caused by the photobleaching. In other words, if differences of fluorescent intensities appear before and after ionomycin stimulation, it ought to be ascribed to the diffusion of **1** from the cellular vesicles to the extracellular space during the calcium-triggered exocytosis.

According to the amperometric traces presented in Fig.4-14 and Fig.4-15, the oxidation current spikes obtained in amperometric measurement were accompanied by the extinction of **1**-stained vesicles at epi-fluorescence configuration. We firstly compared the accumulated numbers of current spikes of the two obtained traces and it is evident that the trace in Fig.4-15(A) showed more spikes than that in Fig.4-14(A) in the first 1 min after the stimulation. This declined oxidation spikes in Fig.4-14(A) was likely to be ascribed to less vanished number of stained vesicles by **1**. In addition, the spikes in second trace showed higher amplitudes than that in the first trace. Specifically, in Fig.4-14(A), almost all the

peak currents (28 among 29 events, 1 exceptional spike) were lower than 10 pA whereas in Fig.4-15(A), about 35% of the spikes (19 among 55) possessed the current peak exceeding 10 pA. We thus believe that the internalized amount of **1** in the second cell was probably higher, which was confirmed afterwards by its higher integral charge Q (data not shown).

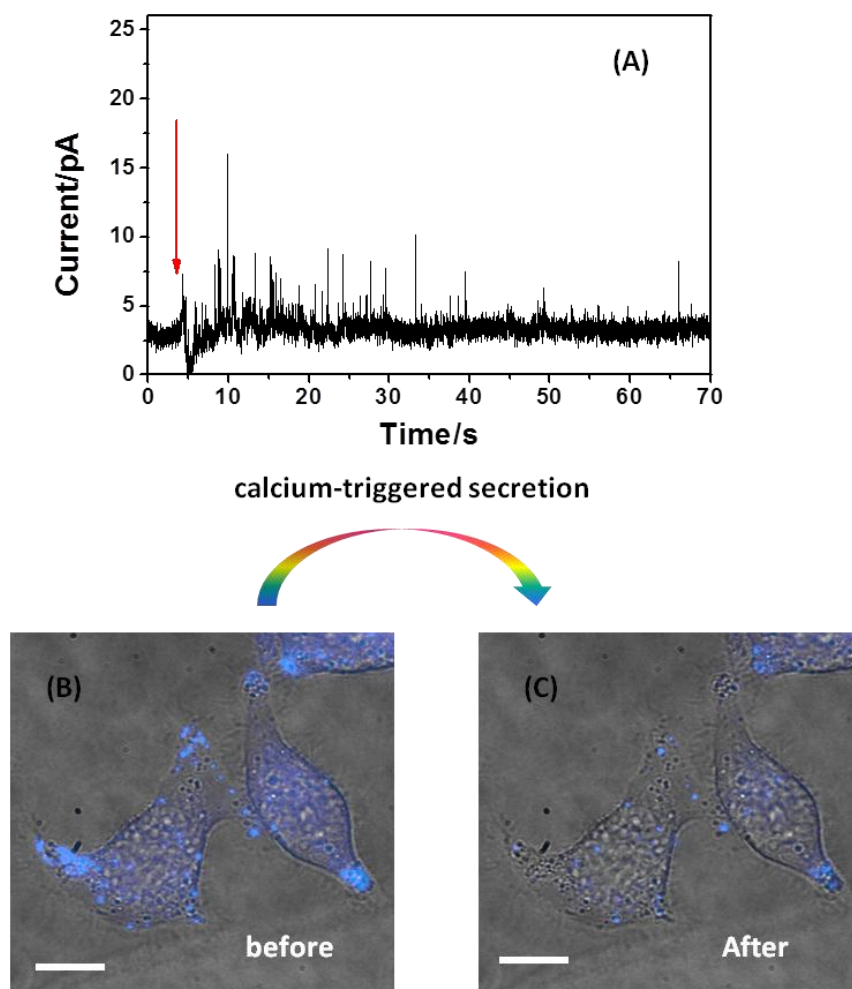


**Figure 4-14** (A) An example of amperometric trace acquired from **1**-stained BON N13 cells with the stimulation of a saline solution supplemented with 10  $\mu\text{M}$  ionomycin; experiments were performed on MD-C and the red arrow indicates the moment when stimulation solution was injected by the microinjector; the fluorescent photographs before (B) and after (C) the application of the stimulation solution.

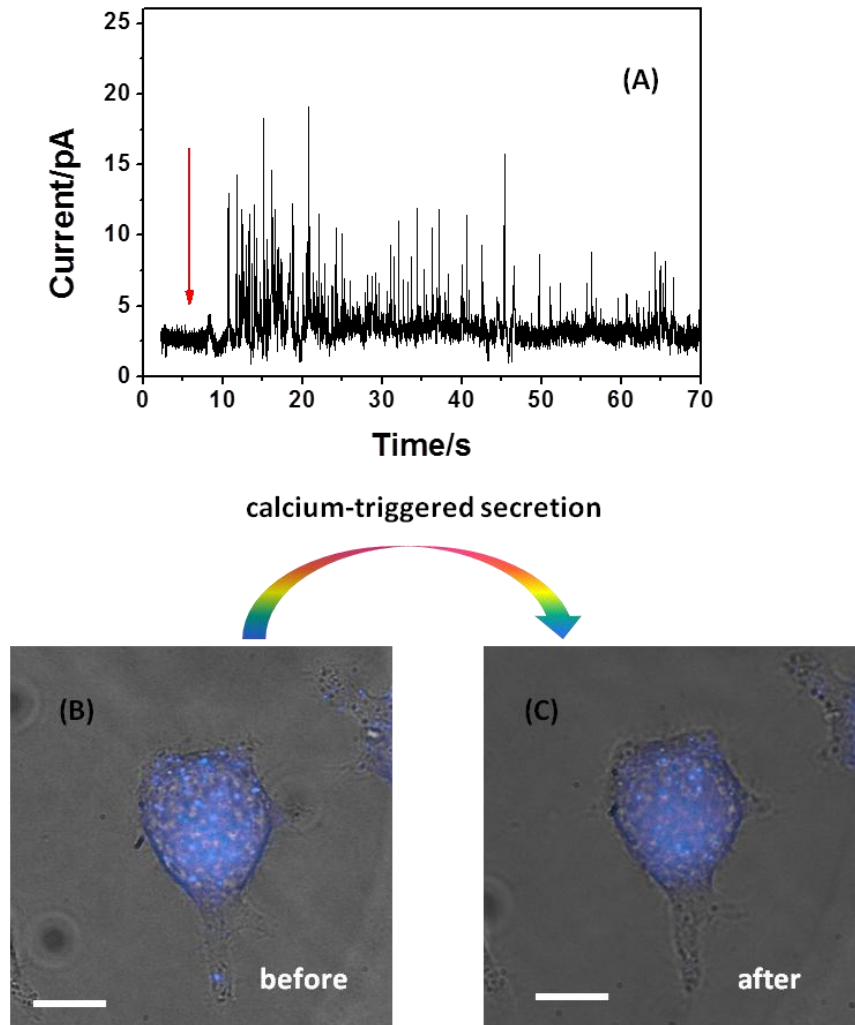


**Figure 4-15** (A) An example of amperometric trace acquired from I-stained BON N13 cells with the stimulation of a saline solution supplemented with  $10\ \mu\text{M}$  ionomycin; experiments were performed on MD-C and the red arrow indicates the moment when stimulation solution was injected by the microinjector; the fluorescent photographs before (B) and after (C) the application of the stimulation solution.

#### 4.3.2 Characterization of exocytotic process

In order to quantitatively illustrate the dynamic of exocytotic process, each isolated spike as shown in Fig.4-12(B) was analyzed on the basis of the method established previously and those overlapped spikes will be not taken into account.<sup>[113, 256, 257]</sup>

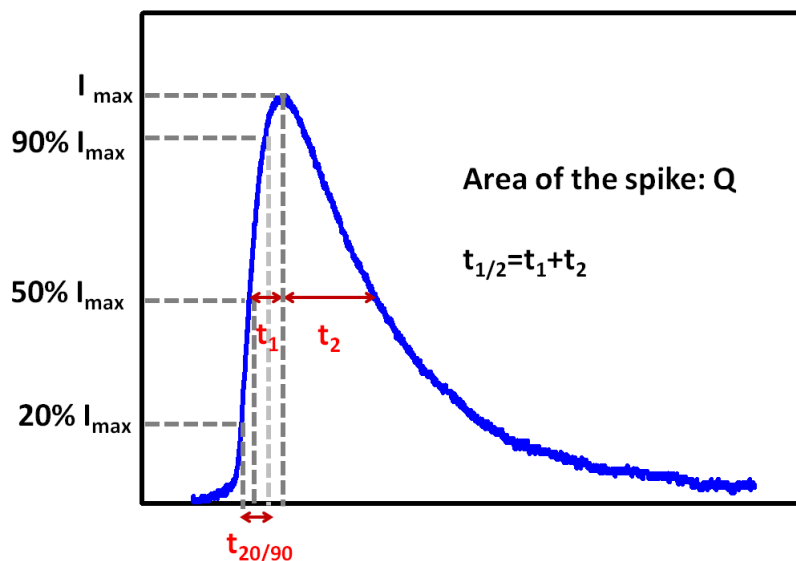


**Figure 4-16** Major relevant quantitative and kinetic parameters (  $Q$ ,  $I_{max}$ ,  $t_1$ ,  $t_2$ ,  $t_{20/90}$  and  $t_{1/2}$  ) extracted from an individual amperometric spike resulting from single exocytotic event.

According to the analysis method, for a given amperometric spike, significant quantitative and temporal parameters could be extracted so as to characterize the feature of an individual exocytotic event, as presented in Fig.4-16:

- (1) The maximum oxidation current  $I_{max}$  (pA) and the total electrical charge  $Q$  (pC) represent the two common quantitative parameters employed for an individual amperometric spike characterization: note that  $I_{max}$  stands for the maximum release flux while the integral charge  $Q$  is used to calculate the precise quantity of molecules released according to Faraday's law;
- (2) Temporal parameters:  $t_1$ ,  $t_2$ ,  $t_{1/2}$  as well as  $t_{20/90}$  (all in ms) corresponding to the different phases of an exocytotic event. Additionally,  $t_{1/2}$  is a common used element to evaluate the time course of an individual secretion event which is defined as the width of the spike where current amplitude equals 50% of  $I_{max}$ .

For BON N13 cells stained by **1**, we analyzed the results from a total of 297 individual events obtained on MD-C. Firstly, the release of **1** from vesicular lumen to the extracellular space was a particular fast process, showing a half-height width ( $t_{1/2}$ ) varying from 8.1 to 56.2 ms, with a mean value of  $16.7 \pm 0.3$  ms; secondly, the detected current peaks  $I_{max}$  varied from 6.7 to 49.6 pA with a mean value of  $15.2 \pm 0.4$  pA; finally, the integral charge  $Q$  changed from 0.12 to 2.95 pC (the mean  $Q$  value is  $0.65 \pm 0.01$  pC).

#### **4.4 Comparison of apex and bottom secretion in BON N13 cells**

In fact, the employment of CFE to build the ‘artificial synapse’ configuration is the traditional and efficient way to study cellular exocytosis and the electrochemical signals thus origin from the release at the cell apex since CFE is gently placed against the top of target cells. Nevertheless, recently, owing to the rapid developments of the utilization of microfluidic chips in this area, more and more studies were performed by positioning the working electrodes in the bottom of cells. Namely, the amperometric spikes come from the electroactive biomolecules expelled from the base of cells. In addition, these microfabricated devices detecting the basal electrochemical signals show distinct advantages in the combined application of fluorescence/amperometry for exocytosis investigation because they provide another way to monitor the fluorescence and electrochemical signals at the same side of the cell. To demonstrate the importance of measuring the combined signals at the same side of cells, we compared the quantitative and kinetic parameters extracted from the amperometric traces obtained by CFE and MD-C, respectively. That is, the employment of MD-C for the fluorescence/amperometry coupling test of BON N13 cells at the bottom is essential to avoid the physiological disparity at the bottom and the top of cells so as to acquire the highly consistent fluorescent/amperometric signals.

##### **4.4.1 Amperometric detection of vesicular exocytosis by CFE**

In the last two decades, CFE is the most widely used UME in amperometry for exocytosis investigation at single cell level since its first introduction for the detection of catecholamines secretion from individual chromaffin cells by Wightman and his colleagues.<sup>[36]</sup> This is mainly owing to its several unique characteristics<sup>[258]</sup> as described in the following:

- (1) Thanks to its small size (usually  $\leq 10 \mu\text{m}$  diameter), it exhibits favorable advantages to sample very small environments, such as a single cell (tens of  $\mu\text{m}$ ) or vesicular volumes (hundreds of nm);
- (2) Amperometric measurement based on CFE shows high temporal resolution ( $\sim$ milliseconds), making it possible to monitor the rapid process such as the neurotransmitter release; moreover, considering its small dimensions, the current noise background ought to be low, resulting in a high signal-to noise ratio as well as a high sensitivity;
- (3) The surface of carbon is suitable for various modifications such as chemical treatment, electrochemical deposition as well as nanomaterial coating so as to meet different research requirements.<sup>[259, 260]</sup>

In this work, the tracking of the exocytotic release from **1**-stained BON N13 cells was achieved by amperometric detection with CFE (10- $\mu\text{m}$  diameter) based on artificial synapse configuration, as shown in Fig.4-17. As the measurements performed in MD-C, the cells of interest were selected with the help of epi-fluorescence excited by mercury lamp so as to make sure that **1** existed inside the vesicles of tested cells. It is important to note that the polymer we used to insulate the carbon fiber surface during the microelectrode fabrication process was particularly sensitive to the UV light that was sent to initiate the fluorescence of **1**. That is, during amperometric measurement, the current noise background caused by the capacitive current augmented gradually with the time lapse when CFE surface was exposed to the excitation light ( $\sim 370\text{ nm}$ ), indicating that the polymer insulation of the microelectrode was destroyed little by little by the UV light irradiation, leading to a larger exposed surface area. In consequence, the excitation light source was kept off during the test so as to avoid the electrode damage.

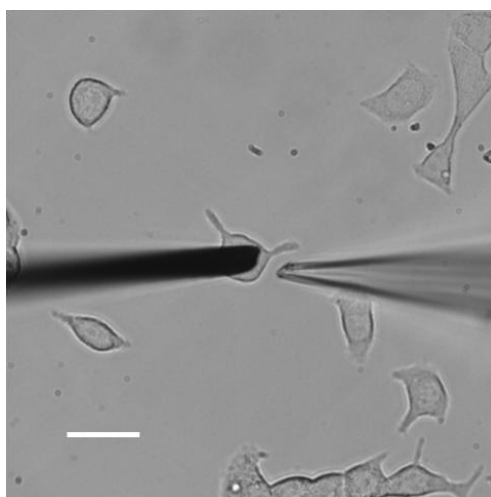


**Figure 4-17** Amperometric detection of cellular exocytosis by CFE and the glass capillary (1~5  $\mu\text{m}$  diameter) filled with a saline solution supplemented with 10  $\mu\text{M}$  ionomycin was used to trigger the release of cells of interest; scale bar: 20  $\mu\text{m}$ .

To study the exocytotic events at single cell level, as shown in Fig.4-17, the CFE was positioned gently against the top surface of the target cell and a specific potential of +900 mV vs Ag/AgCl was hold to the microelectrode in order to oxidize **1** released during exocytosis. When the baseline became stable, ionomycin solution (10  $\mu\text{M}$ ) was injected by the glass capillary to the cell for 1 min to trigger the release of **1** from the cellular vesicles to the electrode surface. The exocytotic release trace thus featured a succession of individual, well separated amperometric spikes due to sequential releasing

events immediately followed by the **1** oxidation at the electrode surface (Fig.4-18). In addition, the comparison of the fluorescent micrographs before and after electrochemical detection demonstrated that the oxidation current spikes were accompanied by the extinction of illuminated cellular vesicles (data not shown), in accordance with the results we obtained by MD-C.

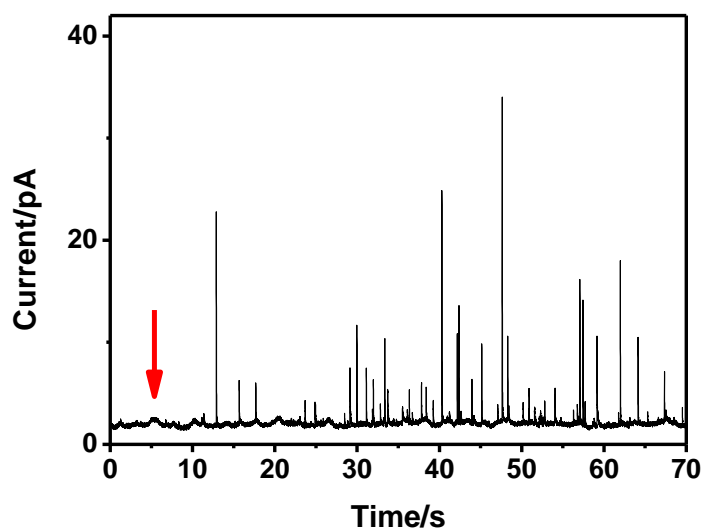


**Figure 4-18** An example of amperometric trace acquired from **I**-stained BON N13 cells with the stimulation of a saline solution supplemented with  $10\ \mu\text{M}$  ionomycin; experiments were performed with CFE and the red arrow indicates the moment when stimulation solution was injected by the microinjector.

#### 4.4.2 Comparison of exocytotic release detected by CFE and ITO microelectrode

As previously discussed, the tracking of vesicular exocytosis is capable to be achieved by performing experiments either on the cell apex by positioning a CFE gently against the cell surface (Fig.4-19, left image) or on the cell bottom by seeding cells on conductive substrate such as Pt<sup>[252, 261]</sup>, Au<sup>[117]</sup> or ITO<sup>[105, 117]</sup> microelectrode (Fig.4-19, right image). In both cases, as soon as the electroactive biomolecules are released from the cellular vesicles to the electrode surfaces, they will be immediately oxidized, forming a current spike lasting hundreds of milliseconds in amperometric recording (Fig.4-19, single spike in red). However, on account of the inconsistent physiological conditions of the two sides of cells as well as the intrinsic differences of employed microelectrodes features, the variations of the extracted quantitative and temporal parameters for characterization of exocytosis of BON N13

cells from the apex analysis and the basal analysis is likely to be predicted, as those already observed from chromaffin cells<sup>[113]</sup> and BON BC21 cells<sup>[105]</sup>.

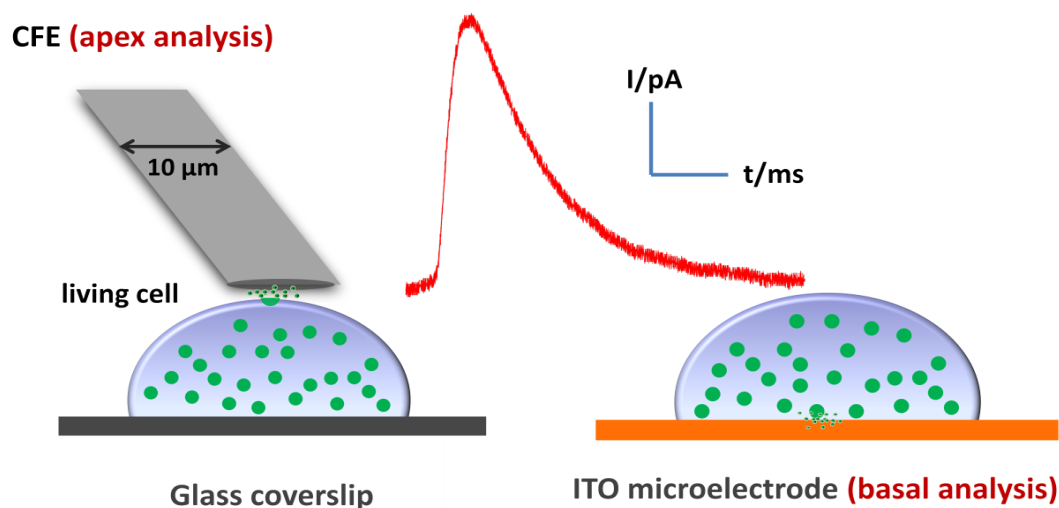


**Figure 4-19** Schematic illustration of the electrochemical detection of vesicular exocytosis by a BON N13 cell as performed at the apical pole (CFE) or at the basal pole (ITO planar electrode). Note that the planar ITO microelectrode is used both as substrate for cell adhesion and to detect oxidation signals.

In this work, the tracking of the exocytotic release of the two different sides of 1-stained BON N13 cells was achieved by 10-µm CFE (electrochemical detection at the cell top) as well as MD-C (electrochemical detection at the cell bottom). Table 1 displays the statistical data obtained in both conditions (CFE: 214 single events; ITO: 297 individual events). It is worth mentioning that only well separated, isolating spikes have been taking account to the comparison whereas those overlapped spikes are manually excluded.

Globally, our results in Table 4-1 demonstrate that characteristics of secretions at the apex differ from those at the cell bottom, displaying various exocytotic behaviors. Furthermore, these variations cannot be attributed to the intrinsic disparities of the employed microelectrodes features since the electrochemical behavior of adrenaline (the main catecholamine released during exocytosis) has been demonstrated to be undistinguishable in vitro at ITO and carbon electrodes.<sup>[113, 118, 120]</sup> In consequence, the detected discrepancies of exocytotic events at the two sides ought to be assigned to the inherent differences of cellular vesicle nature at the top and bottom of cell surface.

	$t_1$ (ms)	$t_2$ (ms)	$t_{20/90}$ (ms)	$t_{1/2}$ (ms)	$I_{max}$ /pA	Q/fC
<b>CFE</b>	6.7±0.4	23.6±0.9	8.3±0.6	30.2±1.2	5.3±0.5	209±15
<b>ITO</b>	7.7±0.2	16.7±0.3	9.6±0.3	24.4±0.4	15.2±0.4	551±19

**Table 4-1** Comparison of vesicular exocytotic events of I-stained BON N13 cells occurring at the apical (detected by CFE) and basal (monitored by ITO microelectrode) poles as monitored by amperometry.

- **Quantitative parameters**

As previously described, the maximum oxidation current  $I_{max}$  and the total electrical charge Q are the two common quantitative parameters employed for an individual amperometric spike characterization.  $I_{max}$  stands for the maximum release flux while Q is used to calculate the precise quantity of molecules released on the basis of Faraday's law. According to Fig.4-20, the maximum oxidation spike obtained from basal pole by ITO ( $I_{max}=15.2\pm0.4$  pA) is 2.9 times as large as that detected from the apical pole by CFE ( $I_{max}=5.3\pm0.5$  pA). From an electrochemical viewpoint, it means a higher maximum flux of electroactive biomolecules onto the ITO surface was taking place compared with that occurred on the CFE surface during exocytosis. Additionally, the amount of the released molecules from individual vesicles detected at basal pole ( $Q=551\pm20$  fC, by ITO) was 2.6 times as high as that monitored at apical pole ( $Q=209\pm15$ fC, by CFE), highly consistent with previous studies on chromaffin cells<sup>[113]</sup> and BON cells<sup>[105]</sup> in our group. In the mean time, the statistical logarithmic distribution of the charge (Q, fC) at the apical pole (CFE, Fig.4-21(A)) also differs from that detected by MD-C at the basal pole (ITO, Fig.4-21(B)).

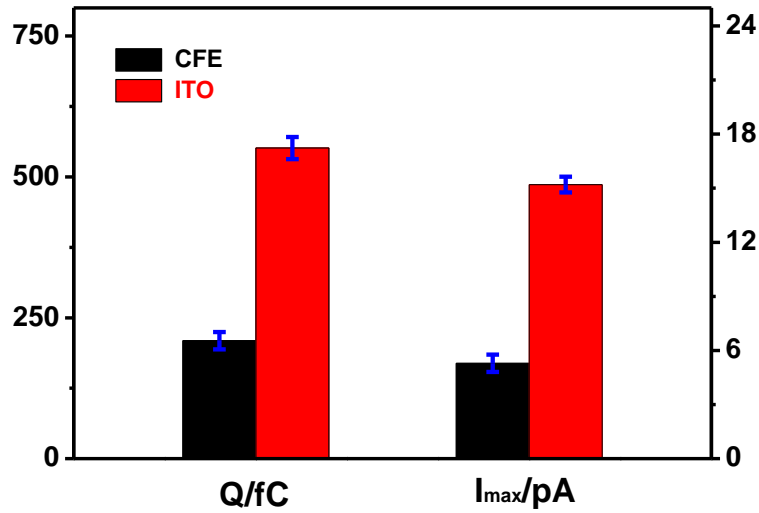


**Figure 4-20** Comparison of main parameters (charge  $Q$  and maximum current  $I_{max}$ ) for quantitative characterization of cellular exocytosis obtained by CFE and ITO; all values are given as mean  $\pm$  standard error of the mean.

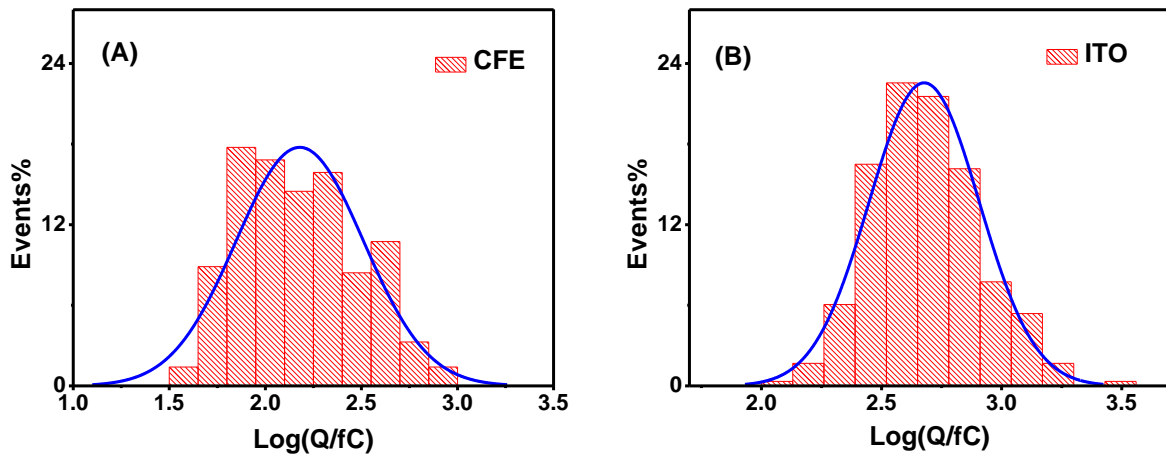


**Figure 4-21** Statistical logarithmic distributions of the charge ( $fC$ ) obtained for each exocytotic event of 1-stained BON N13 cells electrochemically detected by using CFE (A) and ITO (B), respectively.

To illustrate why the quantitative parameters in amperometric recordings varied with the tested locations (at the top and bottom of cells) of 1-stained BON N13 cells, we propose three alternative explanations /hypothesis as following:

(1) The distance between the cell membrane and the electrode surface plays a role

According to the Faraday's law, in amperometry, the oxidation current is directly proportional to the concentration of the released electroactive molecules while their concentration controlled by diffusion is highly dependent on the distance between the cell membrane and the electrode surface. In fact, in basal configuration (ITO electrode), the distance between the microelectrode and cell of interest is probable shorter than that in apical configuration (CFE) since the cells were tightly adherent to the ITO surface, leading to a higher diffused concentration of released species.

(2) Existence of different populations of secretory vesicles

Considering that the composition of the cytoskeleton as well as the natures of vesicle pools near the cell membrane rely on the pole, it is thus rational that the exocytotic releases from two different populations of vesicles vary. That is, the mean size of vesicles that fuse at basal pole are larger than those at the apical pole since they release a larger amount of electroactive content than those that are implied at the apical cell pole.

(3) Intrinsic disparities of the exocytotic events

On the basis of patch clamp measurements on chromaffin cells, it has been reported that 60% of the fusion events which occur at the apical pole stop before full release and undergoes partial releases,<sup>[262]</sup> in accordance with the lower electrical charge detected at the apical pole by amperometry with microelectrodes.<sup>[113]</sup> Assuming that this result remains adaptable for the exocytosis investigation of **1** stained BON N13 cells, it is reasonable that in our experiments, the higher average charge detected at basal pole on MD-C might be attributed to a larger proportion of events undergoing full release.

- **Temporal parameters**

The excellent temporal resolution of amperometry allows its application in real-time analysis of the kinetic processes involved in extrusion of vesicular content into the extracellular space.<sup>[2, 23]</sup> Comparing the exocytotic events electrochemically detected from the two poles of cells, we discover that not only the amount of released content varied but also the exocytotic dynamics altered at single vesicle level. As presented in Fig.4-22, generally speaking, for **1**-stained BON N13 cells, the exocytotic process at the basal pole (detected by ITO) were slightly faster than that occurring at the apical pole (monitored by CFE). It is interesting to note that the temporal parameter comparisons based on chromaffin cells leading to the contrary conclusion. In other word, for chromaffin cells, the kinetics of exocytotic events at the basal pole (detected by ITO) is slightly slower than that taking place at the apical pole (monitored by CFE).<sup>[113]</sup> Since current results based on **1**-stained BON N13

cells in this work are in agreement with the consequences obtained from the BON cell lines preloaded with serotonin,<sup>[105]</sup> we propose that the kinetics of exocytotic events is not only closely related to the factors such as vesicular size, the amount of contents stored inside the cellular vesicles as well as the membrane dynamics, but also highly dependent on the cell lines, of which the time course of exocytosis varies a lot.

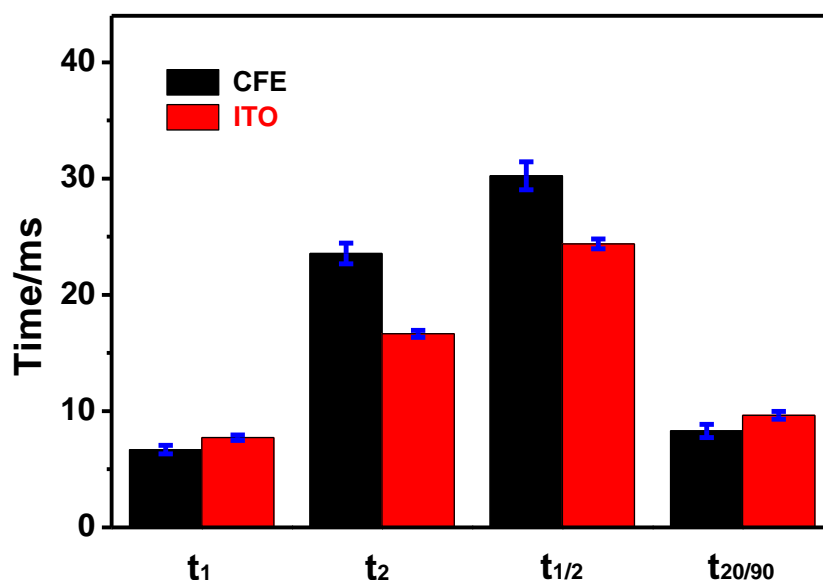


**Figure 4-22** Typical temporal parameters ( $t_1$ ,  $t_2$ ,  $t_{1/2}$ , and  $t_{20/90}$ ) extracted from the amperometric trace obtained from I-stained BON N13 cells by CFE (black column) and ITO (red column), respectively; all values are given as mean $\pm$ standard error of the mean.

So far, an obvious disparity of the exocytotic secretion at the two poles has been demonstrated through the comparison of the temporal and quantitative parameters collected in different geometric configurations although further chemical and biological analysis need to be performed to precisely verify the exact reasons leading to the resulting differences. As a result, it is necessary that the combined application of fluorescence/amperometry for exocytosis investigation have to be performed on the same side rather than the opposite sides. Therefore, those fluorescence/electrochemistry coupling techniques depending on the signals originating from the opposite sides seem to be less meaningful since these two results were not well comparable.<sup>[116, 118]</sup>

## 4.5 Reuse of ITO microdevice

In consideration of the high price of ITO slides as well as the time-consuming microfabrication process, the feasibility of the reuse of the ITO microdevices was tested by removing the attached cells in the microchips. This was achieved by trypsinization process, exactly as what we did for the cell passage (see the experimental part, section I. 1). To be specific, adherent cells in the microchips were detached from the ITO surface by trypsin-EDTA solution treatment for 2 min and then a thorough rinse was conducted with distilled water and 70% ethanol alcohol alternatively in order get rid of the detached cells and to refresh the surface.

To confirm whether the electrochemical properties of ITO microelectrodes were altered by the cell seeding and detachment, the CVs of a well-characterized redox mediator  $\text{Ru}_3(\text{NH}_3)_6\text{Cl}_3$  (100  $\mu\text{M}$ ) before (naked ITO) and after (refreshed ITO surface) trypsinization process were thus recorded respectively at the scan rate of 20 mV/s. As presented in the Fig.4-23, CVs of 100  $\mu\text{M}$   $\text{Ru}_3(\text{NH}_3)_6\text{Cl}_3$  on naked ITO (red line) and refreshed ITO surface (blue line) were globally well overlapped, suggesting that the reused microfabricated ITO chips were suited for electrochemical detection.

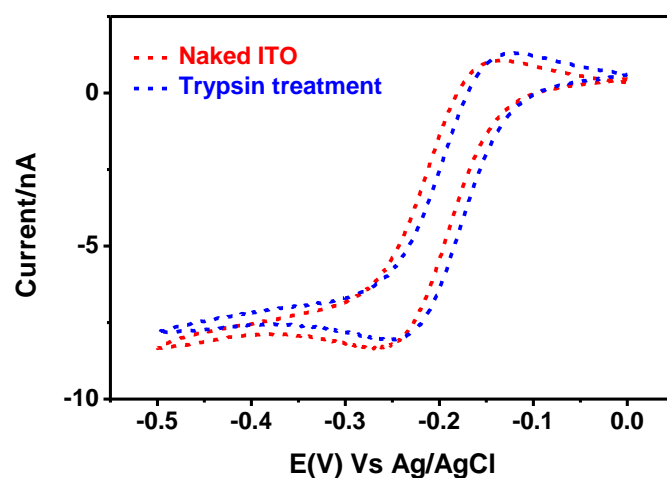


**Figure 4-23** Representative CVs of 100  $\mu\text{M}$   $\text{Ru}(\text{NH}_3)_6\text{Cl}_3$  before (blue) and after (red) collagen coating to illustrate the effect of trypsin treatment on the electrochemical properties of ITO microelectrodes; initial potential: 0 V (vs. Ag/AgCl); scan rate: 20 mV/s.

In addition, no evident difference of the cell behaviors was observed when cells were replated into the renewed ITO microchips. That is, cells were again found adherent and some of them were located on

the ITO substrate. Moreover, cells were still capable of recognizing and taking up **1**. Cellular vesicles appeared thus as blue dots with the excitation of a 405 nm laser and an eligible response of amperometric spikes was subsequently detected upon the stimulation of 10  $\mu$ M ionomycin. Therefore, we consider that our ITO microchips are reusable for electrochemical detection of cellular exocytosis. However, the microdevices have to be sterilized by ethanol, oxygen plasma as well as 30 min UV exposure before cell culture and each ITO device was used no more than three times in this work so as to avoid microelectrodes fouling by accumulated contaminations from abnormal cell metabolism or adherent biological residues.

## 4.6 Conclusions

In this chapter, the design, fabrication, characterization and comparison of three microfabricated ITO devices were presented and MD-C was finally employed to accomplish the amperometric investigation of exocytotic secretion of **1**-stained BON N13 cells owing to its relatively low current noise as well as its multiple microelectrodes of ‘lollipop’ shapes. As expected, upon stimulation of a calcium ionophore (i.e. 10  $\mu$ M ionomycin), a fraction of internalized **1** was expelled from the vesicular lumen to the extracellular space through the fusion pore, leading to an obvious decline of fluorescence intensity. For those cells lying on the ITO microelectrode, the rapid flux of **1** from fusion pore to the electrode surface was depicted as a sharp oxidation current spike and the exocytotic process of an individual cell thus appeared as a session of oxidation current spikes, demonstrating that **1** was highly probable to be able to work as an electrochemical probe for vesicular secretion investigation.

The comparison of the vesicular release detected at different configurations, namely by CFE at the cell apex and by ITO at the cell bottom, displayed that there was a distinct disparity in terms of release dynamics and amounts between the secretions at the two poles. To be more specific, compared with the exocytotic events monitored on CFE, those detected on ITO discharged higher amount of contents ( $\sim$ 2.6 times as high as that of CFE) and their kinetics were also faster. Considering the exocytotic disparity observed at the two poles, it is thus extremely important to monitor the signals at the same side when results are compared for techniques that examine similar phenomena from different geometric setups, such as the coupling of fluorescence and amperometry measurements.

Indeed, taking account to the transparent property of ITO, we believe our microfabricated ITO devices detecting the basal electrochemical signals exhibit distinct advantages in the combined application of fluorescence/amperometry for exocytosis investigation because they provide an approach to simultaneously monitor the fluorescence (TIRFM) and electrochemical signals at the basal pole. Since both the fluorescence and amperometric current are resulting for the same probe (i.e. internalized **1**), we really hope a comprehensive and precise analysis of the whole exocytotic event would be achieved with excellent temporal, spatial resolution as well as high sensitivity owing to the employment of

TIRFM/amperometry coupling technique combining complementary natures of the electrical and optical measurements. The combination of difunctional probe (**1**) and TIRFM/amperometry coupling technique for cellular exocytosis studies would be further discussed in Chapter 5.

## **5 TIRFM/amperometry coupling measurement of exocytosis in 1-stained BON N13 cells**

### **5.1 Introduction**

Over the past 25 years, study of vesicular exocytosis has attracted more and more attention because of its great importance in cell communications and various electrochemical and optical analytical approaches have thus been developed for its investigation.<sup>[2, 22, 109, 176, 263]</sup> Among them, amperometry and TIRFM are commonly considered to be two of the most powerful tools to study the process of exocytotic release. With regard to exocytosis analysis, the major advantages of electrical recording are its excellent time resolution (~ms) as well as its high sensitivity, which allows quantitative studies of the dynamics of the fusion pore at single vesicle level. However, an intrinsic drawback of this technique limits its application in tracking the entire release process. That is, it is completely ‘blind’ to the dynamics of the secretory vesicle itself or any labeled regulatory protein prior to the fusion event since electrical signals can only be detected when the electroactive biomessengers arriving the electrode surface and thus at the stage of the fusion pore aperture. On the contrary, in TIRFM, the whole exocytotic process (before and after the release) is able to be fully visualized owing to the illuminated fluorescence even though its temporal resolution is not expected to be as good as that of amperometric detection. Furthermore, owing to visual fluorescence, TIRFM exhibits remarkable spatial resolution, allowing precise identification of the behaviors of illuminated vesicles such as their displacements, docking locations as well as geometric areas of fusion.<sup>[139, 144, 227]</sup> This specific feature of TIRFM plays a significant role in distinguishing exocytotic releases originating from two/several vesicles concurrently discharging their contents, which would be depicted as an overlapped current spike difficult to analyze in amperometric measurement. In consideration of complementary natures of TIRFM and amperometry, we believe the combination of these two techniques would become a promising approach for comprehensive and precise analysis of the whole exocytotic event (from predocking through fusion steps up to full vesicular release) with high temporal (from amperometry) and spatial (from TIRFM) resolution.

The implementation of TIRFM/amperometry coupling measurement highly relies on the specific property of working electrode which allows both the electrochemical detection and fluorescence imaging. Namely, the material for working electrode fabrication has to be not only transparent, but also electrically conductive so as to record the optical and amperometric signals resulting from same individual vesicles at the same time. In 2006, our group has demonstrated that the employment of transparent/electrical conductive ITO microdevice is capable of accomplishing the recording of fluorescent signals (epi-fluorescence configuration) as well as the amperometric tracking of exocytotic

events from single chromaffin cell. However, at that stage, rather than combined recording, it was two separated detections of independent signals.<sup>[118]</sup> Actually, the first real fluorescence/electrochemical coupling test based on ITO was firstly achieved in 2011, in the PhD work of Anne Meunier in our group, by simultaneously collecting the fluorescence (by TIRFM) and oxidation currents (by amperometry) signals from GFP-transfected BON BC21 cells charged with serotonin.<sup>[19, 264]</sup> In recent years, thanks to the rapid development of microfluidic chip fabrication, besides ITO microsystems<sup>[117, 119]</sup>, some other microdevices based on semi-transparent Au film (12~17 nm), nitrogen-doped diamond-like carbon materials<sup>[117]</sup> have also been applied to fluorescence/electrochemical combined analysis. In this work, the feasibility of microfabricated ITO device (MD-C) embedded multiple electrodes for the TIRFM/amperometry detection was tested.

In our previous work (Chapter 3), **1** has been proved to be a proper optical probe for TIRFM imaging, allowing direct visualization of cellular vesicle behaviors (vesicular displacements in the X-Y/Z trajectories) as well as recognition of different kinds of exocytotic releases ('normal flash', 'extinction of fluorescent spots' and 'sudden flash'). In the meanwhile, its capability of working as an electrochemical probe in amperometry has also been confirmed in Chapter 4. Moreover, the disparity of extracted kinetic and quantitative parameters of **1**-stained BON N13 cells acquired on CFE (exocytotic release at the top of cell) and ITO microelectrode (exocytotic release at the bottom of cell) highlights the significance of measuring the optical signal and amperometric current at the same pole of cell.

Independent optical and amperometric detections of exocytosis have already been evidenced in BON N13 cells by using the difunctional probe (i.e. **1**) previously in this thesis. In order to better understand the exocytotic release process in this chapter, we attempt to simultaneously track the optical (TIRFM observation) and electrochemical (amperometry) signals resulting from exocytotic events of **1**-stained BON N13 cells lying on transparent ITO microelectrodes in MD-C. More detailed and intuitive information about the release events is thus expected to be collected in view of the combination of the two complementary analytical techniques.

## **5.2 TIRFM/amperometry coupling measurement in one set-up**

As previously discussed, MD-C embedded with eight independent ITO microelectrodes shows relatively low electrical noise (2~4 pA) on account of its small size and is suitable for fluorescence observation in spite of the bright fluorescence of SU8-3010 illuminated by the 405 nm laser because of its specific 'lollipop' shape. Therefore, it was employed for the TIRFM/amperometry combined test of vesicular secretion of **1**-stained BON N13 cells.

### 5.2.1 Vesicular release tracked by TIRFM in MD-C

When BON N13 cells were seeded into MD-C, a lot of cells were observed in the central well and some of them lying on the disks of the ‘lollipop’ shape ITO microelectrodes (Fig.5-1). Culture medium supplemented with 20  $\mu\text{M}$  **1** was then used to fluorescently label the cellular vesicles. Cells with **1**-stained vesicles located on the ITO disk were selectively chosen to test the suitability of MD-C for TIRFM tracking of exocytotic events.

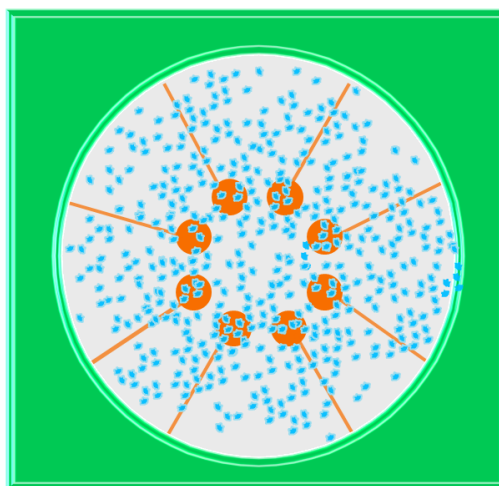


**Figure 5-1** Scheme of cells grown on MD-C device embedded with 8 independent ITO electrodes (top view): ITO microelectrodes were shown in orange; the isolation layers (in green) are composed of a non-conductive layer of SU8-3010; the blue dots represent BON N13 cells seeded into this device.

The thickness of the ITO film we use for electrode microfabrication is of  $150 \pm 10$  nm, of which the transmission efficiency achieves as high as  $\sim 90\%$  across the visible spectrum. We thus believe the existence of ITO will not affect the fluorescence observation of **1**-stained cells. As predicted, for fluorescent cells lying on ITO, the release of **1** from vesicular lumen to extracellular space was able to be clearly visualized at TIRFM configuration with the excitation of 405 nm laser. No visible difference was detected from those acquired on the optical glass substrate. That is, the fluorescence of the insulating layer did not interfere with TIRFM observation of the release of **1** and three different types of exocytotic events were also detected with MD-C (data not shown).

### 5.2.2 Set-up for TIRFM/amperometry coupling measurement

Since the feasibility of MD-C for independent TIRFM/amperometry measurement of exocytotic secretion from **1**-stained BON N13 cells has already been separately confirmed, we then attempt to

concomitantly record the fluorescence/electrochemical signals by virtue of an objective-based TIRF microscope. (Fig.5-2)

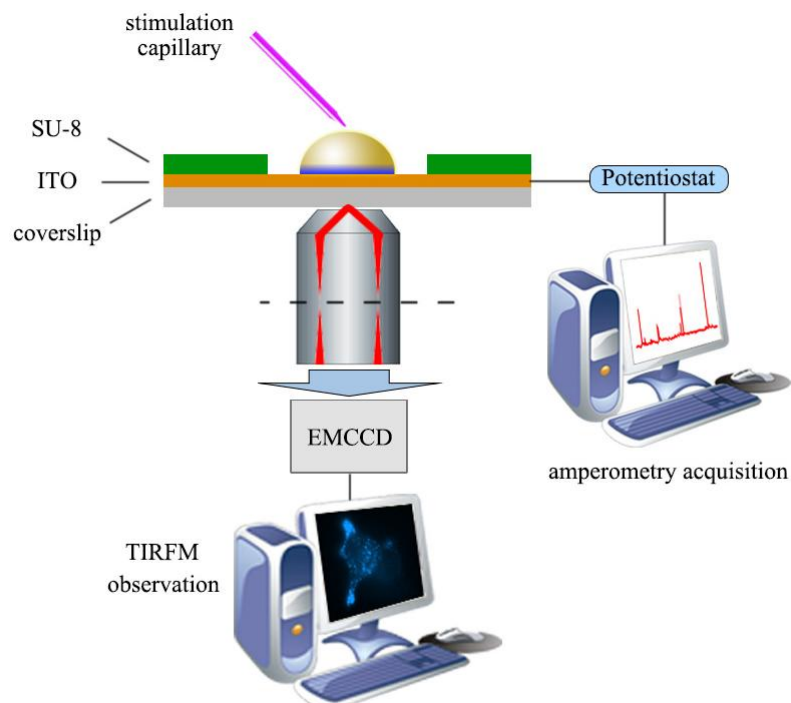


**Figure 5-2** Setup required for TIRFM/amperometry coupling measurements; the fluorescent/electrochemical signals were concurrently collected through the transparent ITO microelectrode.

In order to perform coupling test, MD-C is placed on the platform of the inverted TIRF microscope and only one ITO microelectrode is selectively connected to perform the electrochemical detection. As illustrated in Fig.5-2, for an isolated **1**-labeled BON N13 cell lying on ITO surface, the incident laser (405 nm) is guided into the objective so as to trigger the fluorescence of **1** at TIRFM configuration and the emitted fluorescence is collected by an EMCCD (see experimental section, Scheme E-3). In the meanwhile, for amperometric measurement, a constant potential of +900 mV (vs. Ag/AgCl) is applied to the ITO working electrode so as to monitor the oxidation of electroactive **1** molecules at the surface during exocytotic secretion. Upon stimulation, the ensuing secretory process of cell is expected to be electrochemically (by amperometry) and optically (by TIRFM) tracked at the same time.

### 5.2.3 Influence of 405 nm laser irradiation on amperometric detection

- **Instable baseline caused by 405 nm laser irradiation**

With the irradiation of 405 nm laser to ITO microelectrode, an unexpected sudden increase of current baseline was observed during the amperometric detection, as shown in Fig.5-3(A). In addition, the electrical noise was not as stable as that detected without the 405 nm laser excitation, showing irregular fluctuations (Fig.5-3(B)). Nevertheless, in comparison of rapid dynamic of an individual exocytotic event (~ms), the time course of current baseline variation caused by 405 nm seemed to be relatively slower, making it possible to distinguish the transient current spikes caused by **1** oxidation from electrical noise.

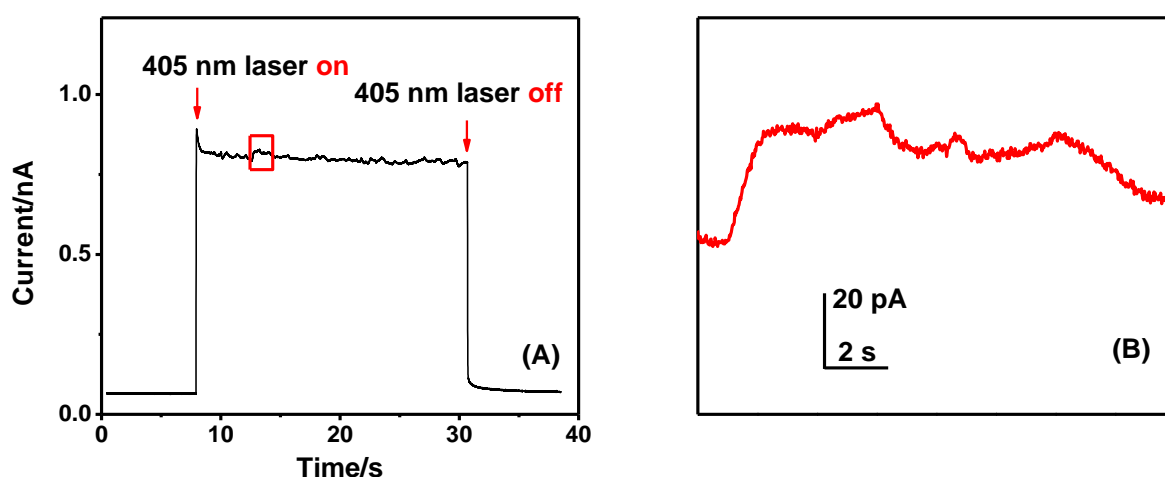


*Figure 5-3 (A) Influence of 405 nm laser irradiation on the current noise of amperometric test with MD-C; (B) The zoom-in graph in (A) as indicated by the red rectangle.*

- **Characterization of 405 nm laser exposure effect on exocytotic response of 1-stained BON N13 cells**

Prior to performing the TIRFM/amperometry coupling measurement of cellular exocytosis, we firstly test whether the irradiation of 405 nm laser (at TIRFM configuration) is likely to modulate the kinetics of individual vesicular release in BON N13 cells assessed by amperometric detection. Table 5-1 presents the general temporal and quantitative parameters extracted from amperometric traces detected from cells with (215 events, ‘laser on’ in Table 5-1) and without (295 events, ‘laser off’ in Table 5-1) 405 nm laser irradiation. The overall responses of cells at the two different conditions

mentioned above showed that 405 nm irradiation slightly decreased the time course of exocytotic processes whereas it did not alter the amount of released **1** according to the two comparable values (524 fC and 551 fC respectively) of the integral charge Q if the respective standard errors of the mean was taken into account.

	$t_1$ (ms)	$t_2$ (ms)	$t_{20/90}$ (ms)	$t_{1/2}$ (ms)	$I_{max}$ (pA)	Q (fC)
<b>laser on</b>	6.7±0.2	13.5±0.4	8.9±0.3	20.3±0.5	19.7±0.7	524±23
<b>laser off</b>	7.7±0.2	16.7±0.3	9.6±0.3	24.4±0.4	15.2±0.4	551±19

**Table 5-1** Illustration of influence of 405 nm laser irradiation on vesicular exocytotic behaviors of **1**-stained BON N13 cells amperometrically detected at the ITO microelectrode surface. 215 (for 405 nm laser irradiation) and 295 (for no 405 nm laser irradiation) individual amperometric spikes were separately analyzed and all values are given as mean±standard error of the mean.

As we previously discussed, in amperometry, the time course of single exocytotic release is characterized by several temporal parameters such as  $t_1$ ,  $t_2$ ,  $t_{20/90}$  and  $t_{1/2}$  (as defined in Fig.4-16). On the basis of comparative results shown in Fig.5-4(A), we discover that 405 nm laser excitation at TIRFM configuration slightly speeded up the exocytotic process of **1**-stained cells as all the temporal parameters were mildly decreased. In the meanwhile, the mean height of the current spikes ( $I_{max}=19.7±0.7$  pA) was also affected by 405 nm-irradiation treatment (Fig.5-4(B)), increasing by few pA compared with the ‘normal’ spikes ( $I_{max}=15.2±0.4$  pA). Nevertheless, the mean charge (area of the amperometric spike,  $Q=524±23$  fC) appeared not to be altered by 405 nm laser excitation, seeming comparable to those acquired at normal conditions ( $Q=551±20$  fC). Furthermore, no obvious difference of the statistical logarithmic distributions of the charge Q was observed from these two different conditions (Fig.5-5), suggesting that the amount of **1** discharged during individual exocytotic events was quite stable and the initiation of 405 nm laser did not affect its released quantity.

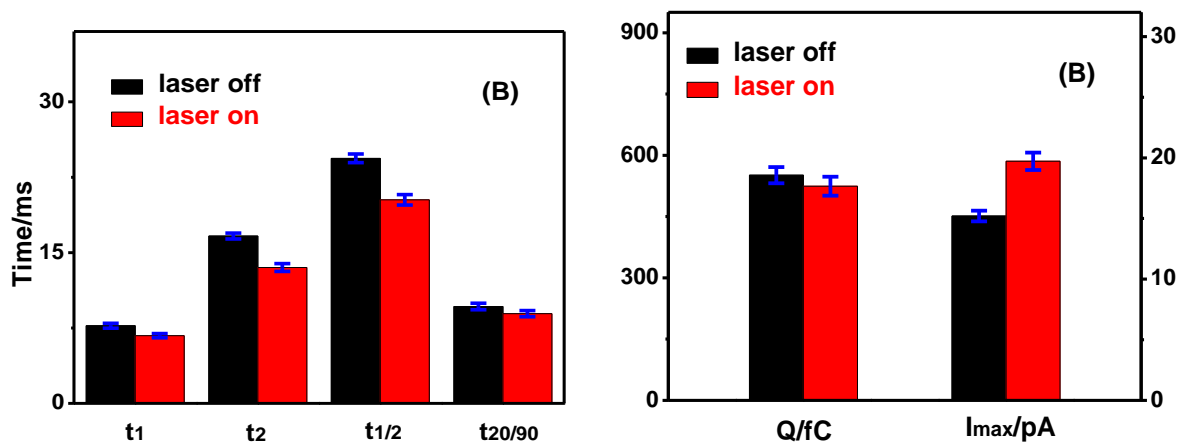


**Figure 5-4** (A) Typical temporal ( $t_1$ ,  $t_2$ ,  $t_{1/2}$ , and  $t_{20/90}$ ) and (B) quantitative parameters ( $I_{max}$  and  $Q$ ) extracted from the amperometric trace obtained from *I*-stained BON N13 cells on ITO microelectrode with (red column) and without (black column) 405 nm laser irradiation, respectively; all values are given as mean  $\pm$  standard error of the mean.

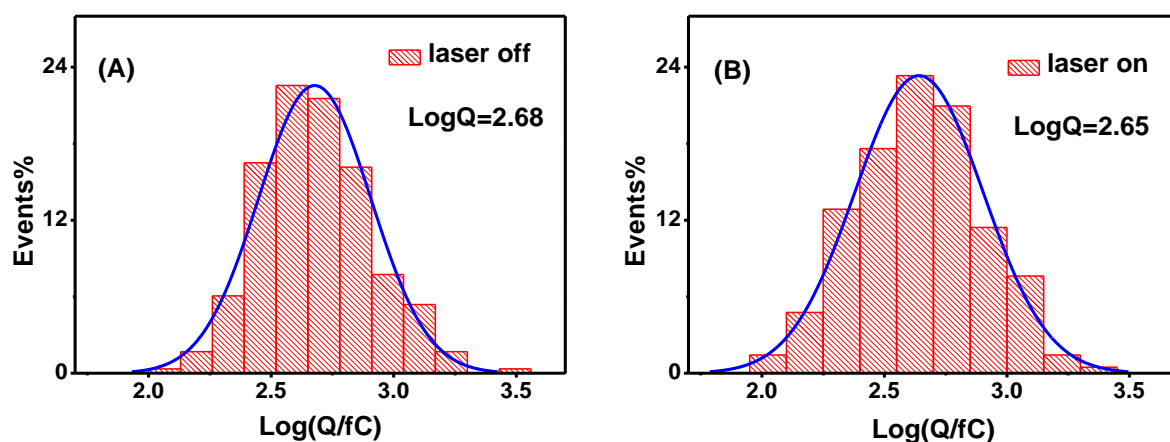


**Figure 5-5** Statistical logarithmic distributions of the charge  $Q$  (fC) obtained for each exocytotic event of *I*-stained BON N13 cells electrochemically detected by ITO microelectrode with (A) and without (B) 405 nm laser irradiation, respectively.

Briefly summarize, the trigger of 405 nm laser led to a variation of the current baseline in amperometric measurement whereas this relatively unstable baseline was demonstrated to be neglectable because of its much slower time course compared with that of the amperometric spike

resulting from the rapid exocytotic release. In addition, the discharge of **1** from single vesicles became faster due to the 405 nm irradiation while the released quantity of **1** was found to be equal. Three alternative explanations are thus deduced to illustrate the decline of detected temporal parameters in view of our current experimental results.

Firstly, it has already been reported that some chemical/biological treatments are able to modulate the exocytotic behaviors of cells.<sup>[69, 265]</sup> The 405 nm laser exposure is likely to be a factor which might alter the way of BON N13 cells to discharge **1**. That is, cells are sensitive to the 405 nm-laser beam, leading to an acceleration of their vesicular exocytosis. As a consequence, the amperometric spikes highly dependent on the temporal course of the exocytotic event appear to become lightly shorter.

Secondly, it is also possible that the 405 nm-laser irradiation speeds up the oxidative process of the expelled **1** on the ITO microelectrode surface. Namely, **1** is expelled as usual from vesicular lumen to the ITO surface while the oxidation course is altered. In fact, it is common knowledge that the employment of different electrode materials (Au, ITO, CFE...) leads to disparities of amperometric results (as the differences of **1** oxidation observed on CFE and ITO shown in Table 4-1), demonstrating that the electrode characteristic plays an important role in electrochemical determination.<sup>[18, 117]</sup> Therefore, it is likely that the irradiation of the 405 nm laser could probably modify the electrical properties of ITO microelectrode, resulting in a faster oxidation process of **1** on its surface.

Last but not least, it can also be considered that **1** exposed to 405 nm laser enhances the electron transfer ability from **1** to the electrode surface, making it easier to be oxidized and that is an acceptable reason why amperometric spikes with shorter time courses were recorded.

Nevertheless, it is worth mentioning that this kinetic distortion of the amperometric spikes under the 405 nm laser exposition does not preclude the possibility of the TIRFM/amperometry coupling measurements. Indeed, the distortion remains moderate since the kinetic parameters stay in the same order of magnitude. Furthermore, the usual work involving real-time amperometric detection of exocytosis is not absolute but relative investigations. In other words, control experiments are commonly compared to peculiar experimental conditions to highlight the effect of a given parameter on the exocytotic release. In that way, the level of reliability on the control release does not need to be perfect because the crucial point is related on the comparison between mean spikes for two series of experiments and not on the analysis of the mean spike for the solely control experiment.

## 5.3 TIRFM/amperometry coupling measurement of vesicular exocytosis

### 5.3.1 Effect of exposure time in TIRFM imaging

Vesicular exocytosis is a rapid process through which various biological and chemical contents are expelled from the emitting cell to extracellular space in order to achieve cell communication. In a large amount of studies of exocytotic release by TIRFM, even in recent five years, exposure time for each acquisition was set as hundreds of milliseconds so as to capture proper fluorescent images with high signal-to-noise ratio.<sup>[19, 266-268]</sup> However, the temporal resolution at hundreds milliseconds level is not adapted to the TIRFM/amperometry coupling real-time tracking of exocytotic release in BON N13 cells as time courses of their individual exocytotic events are usually below 100 ms, especially for these cases with the acceleration of 405 nm laser irradiation.

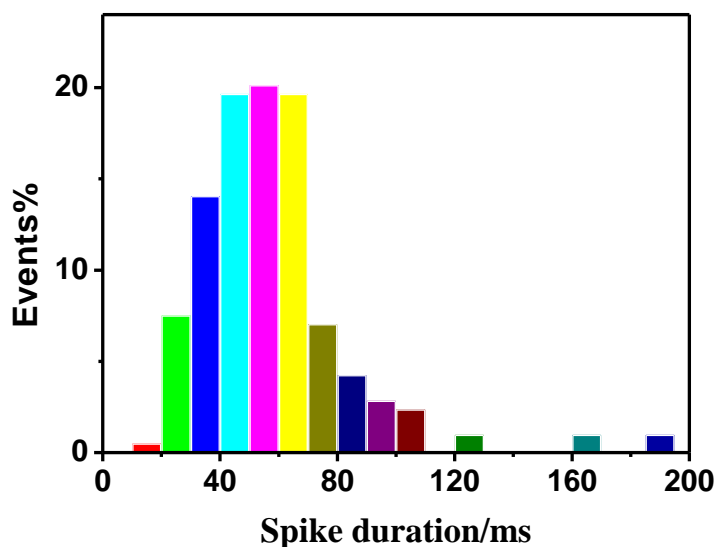


*Figure 5-6 Distributions of the temporal durations of individual amperometric spikes acquired from cells excited by 405 nm laser at TIRFM configuration; the duration for single exocytotic event is defined as the time interval between the initial flux of **1** (onset of current rising) and its complete expansion (current regression to the baseline).*

As displayed in Fig.5-6, on the basis of statistic analysis of 215 individual amperometric spikes detected from **1**-labeled BON N13 cells with the excitation of 405 nm laser, we discover that an overwhelming majority of events (~87% in total) underwent a rapid release of **1** with the temporal duration between 30~100 ms and only about a few of them (~5 % altogether) experienced time courses

longer than 100 ms. As a consequence, in TIRFM, if the exposure time of TIRFM is set at a value exceeding 100 ms, it is predictable that for most exocytotic secretion, observation of their later release phase is going to be lacked. In other words, in TIRFM, most events are prone to appear as fluorescence extinction, without any visual information about the releasing process itself.

Apparently, more release details could be revealed at higher temporal resolution (i.e. lower exposure time for each acquisition) in TIRFM. Nevertheless, in consideration of the image quality as well as the camera resolution limit, in this work, the exposure time of TIRFM acquisition is always set less than 100 ms and mainly around 35 ms in coupling technique depending on the fluorescence variations of cell samples labeled by **1**, to make sure at least one step of an individual content expansion process is able to be directly visualized in TIRFM.

### **5.3.2 TIRFM/amperometry coupling test of vesicular exocytosis**

On microfabricated MD-C, two modes of detection (electrochemical and optical) were concurrently triggered on **1**-stained BON N13 cells lying on the ITO surface. To be more specific, amperometric measurement was firstly conducted by applying a constant potential of +900 mV (vs. Ag/AgCl) to the ITO working electrode and as soon as the current baseline became stable, the 405 nm laser was then turned on in order to illuminate the **1**-labeled cellular vesicles at TIRFM configuration. As a result, the behaviors of the fluorescent vesicles were optically visualized (by TIRFM) and electrically monitored (by amperometry) in the mean time.

Fig.5-7 represents a typical example of such dual measurements based on **1**-stained BON N13 cells. As shown in Fig.5-7(A), the activation of TIRFM light source (405 nm laser) was immediately reflected in the recorded amperometric trace according to the sudden augmentation and relatively unstable current baseline, in accordance with our previous results (Fig.5-3). Meanwhile, vesicles labeled by internalized **1** were depicted as small blue spots in TIRFM (Fig.5-7(C)). Afterwards, 10  $\mu$ M ionomycin was injected through the glass capillary positioned close to the target cells so as to initiate the exocytotic release of illuminated cells, as indicated by the red arrow in Fig.5-7(A). Through cellular exocytosis, **1** was discharged from the vesicular lumens to ITO surface, therefore, some oxidation current spikes (Fig.5-7 (A)) and fluorescence extinctions (Fig.5-7(C) and (D)) were simultaneously detected. According to Fig.5-7(B), an individual oxidation current spike extracted from Fig.5-7(A), it is evident that, regarding to single exocytotic event occurring within a short period (~50 ms), the background variation caused by 405 nm laser irradiation is likely to be neglected.

For the given example in Fig.5-7, with the stimulation of 10  $\mu$ M ionomycin for 1 min, 41 current spikes were detected in amperometry while 53 exocytotic secretions were visualized by TIRFM. Furthermore, 24 among the 41 detected amperometric spikes were associated with a fluorescence

change observed concomitantly by TIRFM. That is, besides the coupled information, we also observed some ‘fluorescence only’ and ‘electrochemical only’ signals which were called ‘optical orphan’ or ‘amperometric orphan’ events in the past.<sup>[19, 264]</sup> We thus compared the ratios of these three types of events obtained from **1**-stained BON N13 cells with those acquired from BON BC 21 cells of which a soluble luminal marker of secretory granules (i.e. NPY-GFP) and electroactive serotonin were employed as fluorescent and electrochemical probes, respectively.

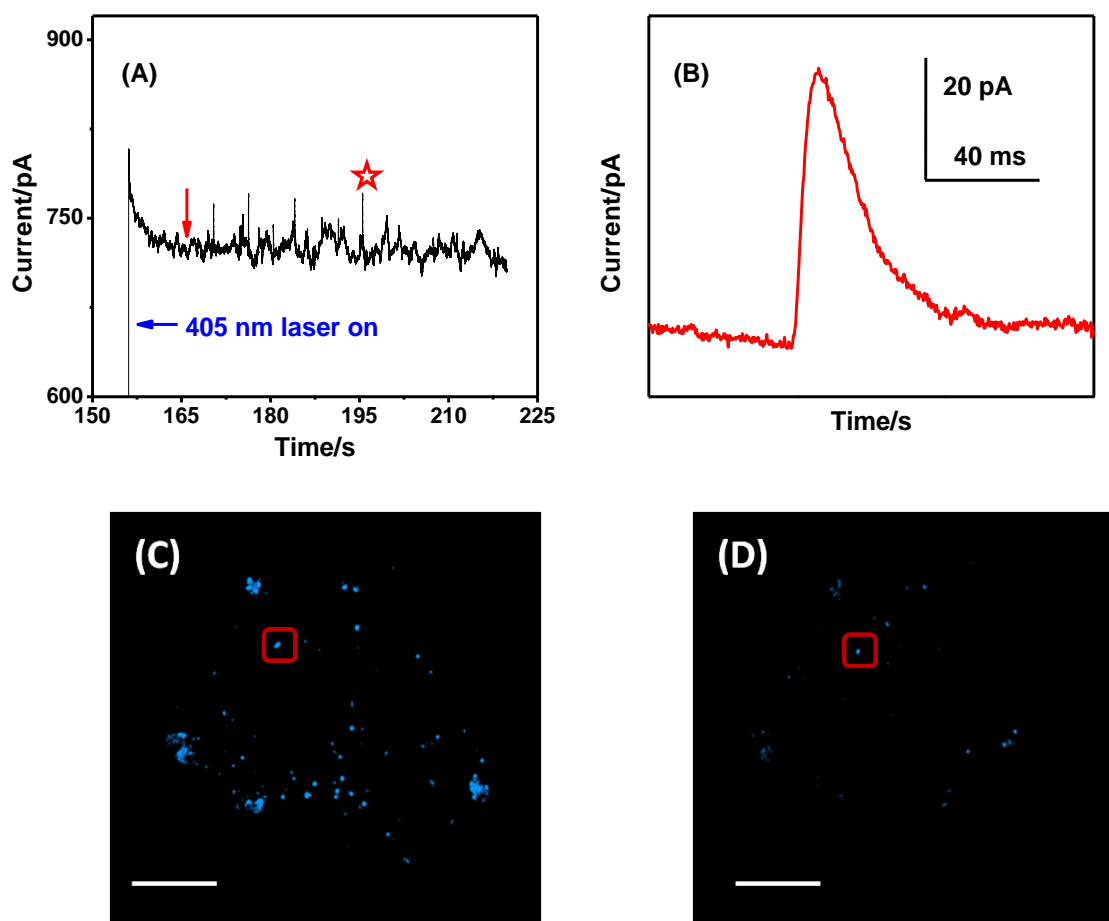


**Figure 5-7** (A) A typical example of amperometric trace obtained from **1**-stained BON N13 cells with the stimulation of a saline solution supplemented with 10  $\mu$ M ionomycin; the red arrow indicates the moment when stimulation solution was injected by the microinjector; the unstable current baseline was caused by 405 nm laser irradiation at TIRFM configuration; (B) Representative current spike extracted from the amperometric trace (see labeling by red star in (A)) which stands for an individual exocytotic event of a secretory vesicle; (C) and (D) are fluorescent micrographs of **1**-stained BON N13 cells illuminated by 405 nm laser at TIRFM configuration before and after the amperometric measurement, respectively; single cellular vesicles appear as blue spots in TIRFM, as indicated by the red rectangle; exposure times were 80 ms; scale bar: 10  $\mu$ m.

As shown in Table 5-2, in similar conditions, the optical/amperometric coupling efficiency obtained is optimized by 12% because of the employment of dual probe **1** to stain vesicles of BON N13 cells. For coupling measurement based on BON BC21 cells with two independent probes, 57% of the events are only TIRFM signals and 21% are solely amperometric spikes. In addition, amperometric spikes in this case ranged from 0.2 to 3.5 pA in magnitude due to the low amount of serotonin accumulated inside the GFP-transfected vesicles. Such a low current signal makes it difficult to really ‘see’ the spikes and a lot of extra data treating process such as filtering is thus necessary. In contrast, the electrochemical signals coming from **1** oxidation seems much better ( $I_{\max}=19.2\pm0.7$  pA, see Table 5-1) because of its successful loading into the vesicles.

	<b>1</b>	<b>GFP+serotonin</b>
<b>Coupled events</b>	34%	22%
<b>Optical ‘orphan’</b>	42%	57%
<b>Amperometric ‘orphan’</b>	24%	21%

**Table 5-2** Comparison of proportions of three kinds of signals (coupled events, optical ‘orphan’ and amperometric ‘orphan’) detected from BON N13 cells labeled by **1** and GFP-transfected BON BC21 cells preloaded with serotonin, respectively.

Another comparison can be done with the work of Kisler and her colleagues which reported on TIRFM/amperometry analysis at chromaffin cells (the probes are endogenous electroactive adrenaline and loaded acridine orange respectively) with thin Au or ITO electrodes.<sup>[117]</sup> While the data analysis were partial, it was established that 20% of the amperometric spikes were accompanied with a fluorescence event at ITO electrodes and 38% of the amperometric spikes were combined with a detectable fluorescence event at gold electrodes. In our case involving **1**, 59% of the electrochemical signals were coupled to their corresponding optical event (42% in our previous work on BON BC21 cells with serotonin-GFP).

Analyzing in details the percentages obtained in Table 5-2 allows us to conclude that the unique loading with dual probe **1** permits an amelioration on the quality and efficiency of the electrochemical

loading. Indeed percentage of coupled events increases from 22% to 34% with a decrease of the optical 'orphan' events percentage from 57% to 42% for 'GFP + serotonin' and **1** loadings, respectively. The fact that optical orphan events are defined as events without any amperometric spikes leads to the conclusion that the molecule **1** has a more favorable affinity of passage within the vesicles than serotonin alone and that working with a unique dual probe is more efficient than with two separated (optical and electrochemical) in the case of GFP and serotonin in BON N13 cells. Furthermore, the percentage of amperometric 'orphan' events remains constant. By comparison with the previous 'GFP + serotonin' work, it means that the enhancement was only due to the electrochemical loading and not to the change of camera temporal resolution. This is consistent with the fact that the time resolution is set at 80 ms in the present work when it was fixed at 100 ms in the case of the past loading strategy. It also means that adjusting this parameter up to 30 ms, which is feasible with our new EMCCD camera, is a tuning parameter which can only bring favorable in reducing the detection of percentage of optical 'orphans' in the future.

Therefore, the strategy of using a unique probe for electrochemical and fluorescent detection of exocytotic release at the single cell and individual event levels looks more adapted than all the previous works involving independent probes.

## **5.4 Fluorescent/amperometric coupled signals of exocytotic events**

As discussed in section 5.2, MD-C is convincingly suitable for the electrochemical/optical coupling detection and exocytotic release of **1** from cellular vesicles to ITO surface leads to detectable amperometric signals as well as intuitional fluorescence intensity variation. Actually, upon the stimulation of **1**-stained BON N13 cells lying on ITO surface, three kinds of signals have been observed by the coupling measurement (see Table 5-2). Besides the coupled events, fluorescence or electrochemical orphan signals were also detected, as that preciously observed in GFP-transfected BON BC21 cells.<sup>[19, 264]</sup> However, when it comes to the investigation of exocytotic behaviors at single vesicle level, this coupling technique based on the difunctional probe **1** allows direct, intuitional and real-time monitoring of exocytotic release. More quantitative and temporal details of the exocytotic process are thus expected to be revealed by electrochemical spikes associated with fluorescence variations at individual vesicle level.

### **5.4.1 Three different modes of exocytotic release**

By tracking the fluorescence variations upon stimulation in TIRFM, three types of exocytotic events were discovered from **1**-stained secretory vesicles, namely 'normal flash', 'extinction of fluorescent spots' as well as 'sudden flash'. Interestingly, these different release modes were also detected by the

coupling detection with MD-C. Examples of these three kinds of exocytotic events were displayed in Fig.5-8, Fig.5-9 and Fig.5-10, separately.

- **The normal ‘flash’**

Fig.5-8 represents a classic exocytotic event defined as the normal ‘flash’ which was detected by the TIRFM/amperometry coupling technique.

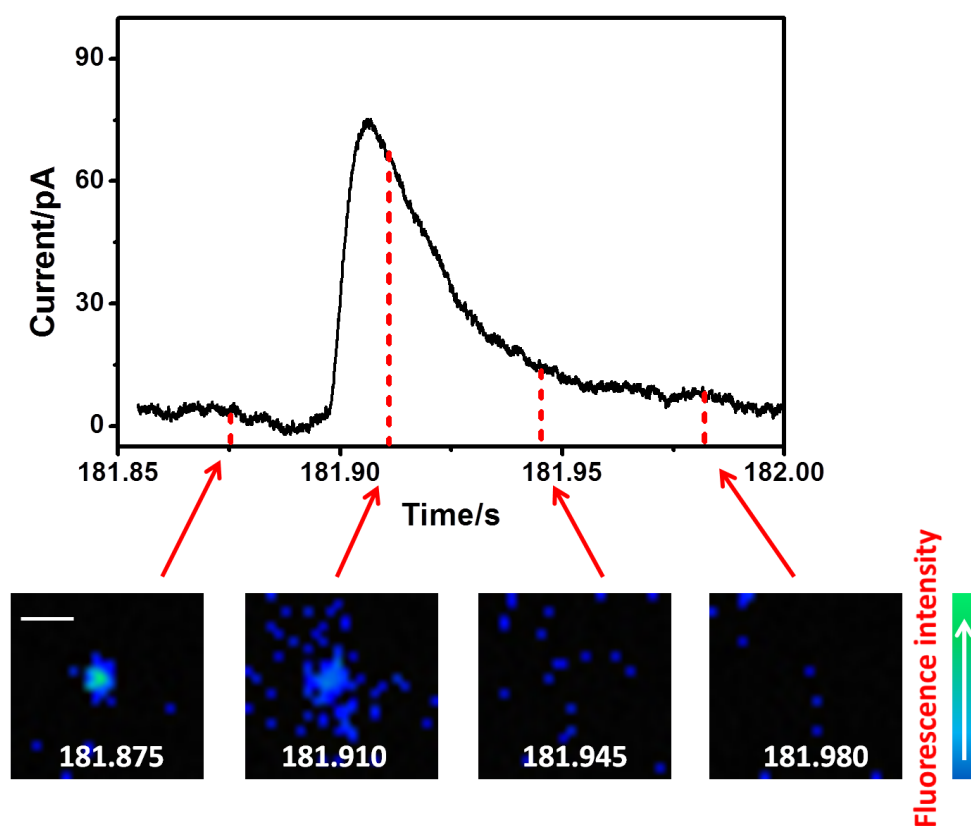


**Figure 5-8** Correlation of amperometric and fluorescent information for a single release event of I-stained BON N13 cells over an ITO microelectrode; top: an exocytotic event on ITO appeared as the current spike in electrochemical detection; bottom: sequential pseudocolor TIRFM images of a single exocytotic event defined as normal ‘flash’ in Chapter 3; 405 nm laser excitation ( $I=1.5$ ); exposure time is set as 35 ms; TIRFM angle 625; the corresponding moments of fluorescent and amperometric signals are precisely indicated by red arrows and the red dashed lines; scale bar: 500 nm.

With respect to the TIRFM sequence imaging (Fig.5-8, bottom), the exocytotic release was indicated as a bright flash. That is, the fluorescent signal transiently brightened during the release of fluorescent **1** from acidic vesicular lumen to the neutral extracellular medium and then disappeared completely within ~100 ms as the fluorophores diffused away, in agreement with our previous result shown in Fig.3-20. On account of the limited temporal resolution of fluorescent signals (35 ms/frame), it is unlikely to real-time monitoring the diffusion of illuminated **1** at every exocytotic step. That is the reason why it is very important to do a coupling detection where amperometry will bring the distinct temporal resolution. In the corresponding amperometric detection (Fig.5-8, top), the oxidation current spike lasted less than 100 ms which was highly comparable to the temporal duration of fluorescence ‘flash’ recorded in TIRFM, but the temporal resolution was greatly improved (~25  $\mu$ s for each acquisition).

The combination of TIRFM with electrochemical detection will thus illuminate the exocytotic mechanisms. The correlation of the optical and amperometric signals demonstrates that the frame (t=181.910 s) in which the initial fluorescence augmentation occurred was accompanied by the steep rise of the amperometric spike, indicating a maximum flux of the fluorescence/electrochemical dual probe **1**. Then, the dispersion of **1** led to a lower concentration of fluorophores/weaker fluorescence (frame, t=181.945 s) on ITO surface, being associated with a slow decrease of the detected current. Finally, the disappearance of fluorescence (frame, t=181.980 s) was testified by the regression of the current to the baseline. Moreover, it is logical to propose that, for vesicles with **1** at higher concentrations, the ‘fading’ time from the ‘current peak’ to the return to baseline is going to take a longer time in comparison of those with **1** at lower concentration, as we will discuss afterwards.

- **The extinction of fluorescent spots**

For some cellular vesicles, because of the low amount of accumulated **1** inside the vesicular lumens, their exocytotic releases were therefore depicted as the rapid disappearance of illuminated vesicles, without visible fluorescence diffusion in TIRFM. For the given example shown in Fig.5-9, the blue spot representing the **1**-stained vesicle (indicated by the red ellipses in the later two frames of TIRFM imaging) suddenly vanished within the time interval between two images (~35 ms). Accordingly, the time course of the corresponded amperometric spike (Fig.5-9, ~31 ms) therefore appeared to be relatively faster, especially in contrast with the duration of the spike caused by the normal ‘flash’ (Fig.5-8, ~75 ms).

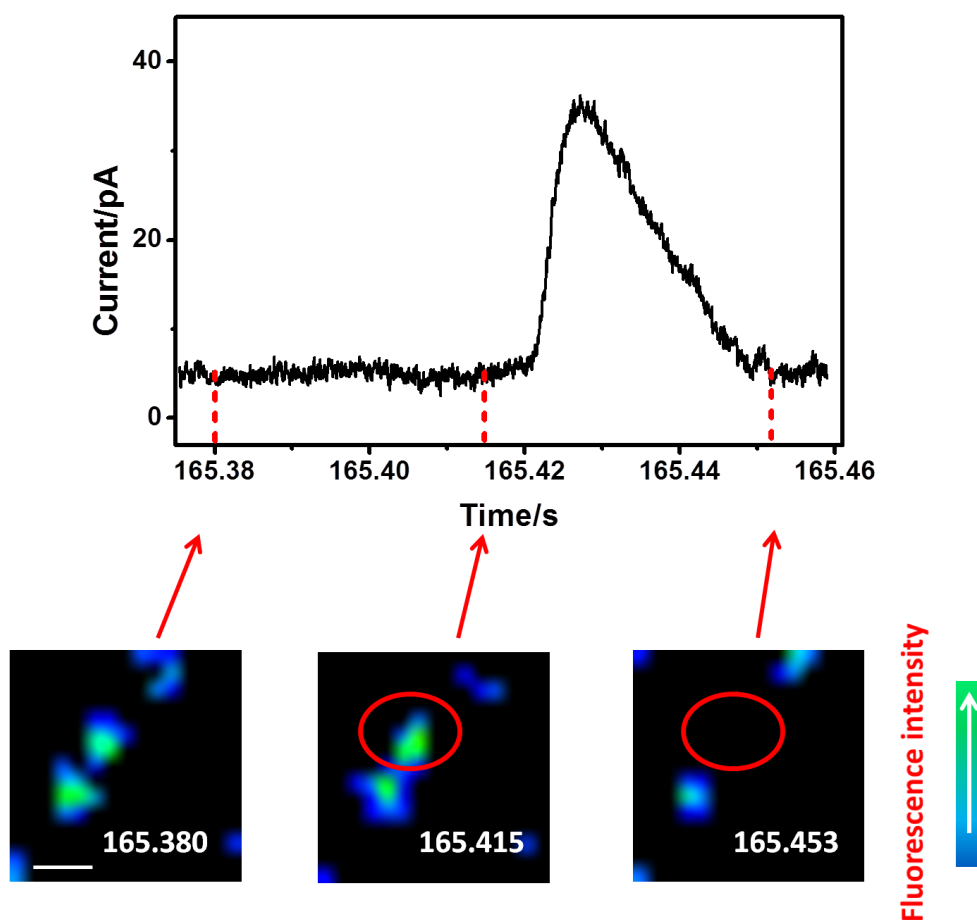


**Figure 5-9** Correlation of amperometric and fluorescent information for a single release event of I-stained BON N13 cells over an ITO microelectrode; top: an exocytotic event on ITO appeared as the current spike in electrochemical detection; bottom: sequential pseudocolor TIRFM images of a single exocytotic event defined as ‘extinction of fluorescence’ in Chapter 3; 405 nm laser excitation ( $I=1.5$ ); exposure time is set as 35 ms; the corresponding moments of fluorescence and amperometric signals are precisely indicated by red arrows and the red dashed lines; scale bar: 500 nm.

- **The ‘sudden flash’**

The ‘sudden flash’ of BON N13 cells represents a special exocytotic type of which only rapid dye diffusion, but not the corresponding secretory vesicle could be detected with the time resolution of our camera. We can see from Fig.5-10 that the fluorescent signals recorded by TIRFM imaging experienced a dramatic augmentation followed by a prompt decrease of fluorescence intensity. As

expected, with the complete expansion of **1**, the fluorescence micrograph went back to be black as that we observed before the ‘sudden flash’.

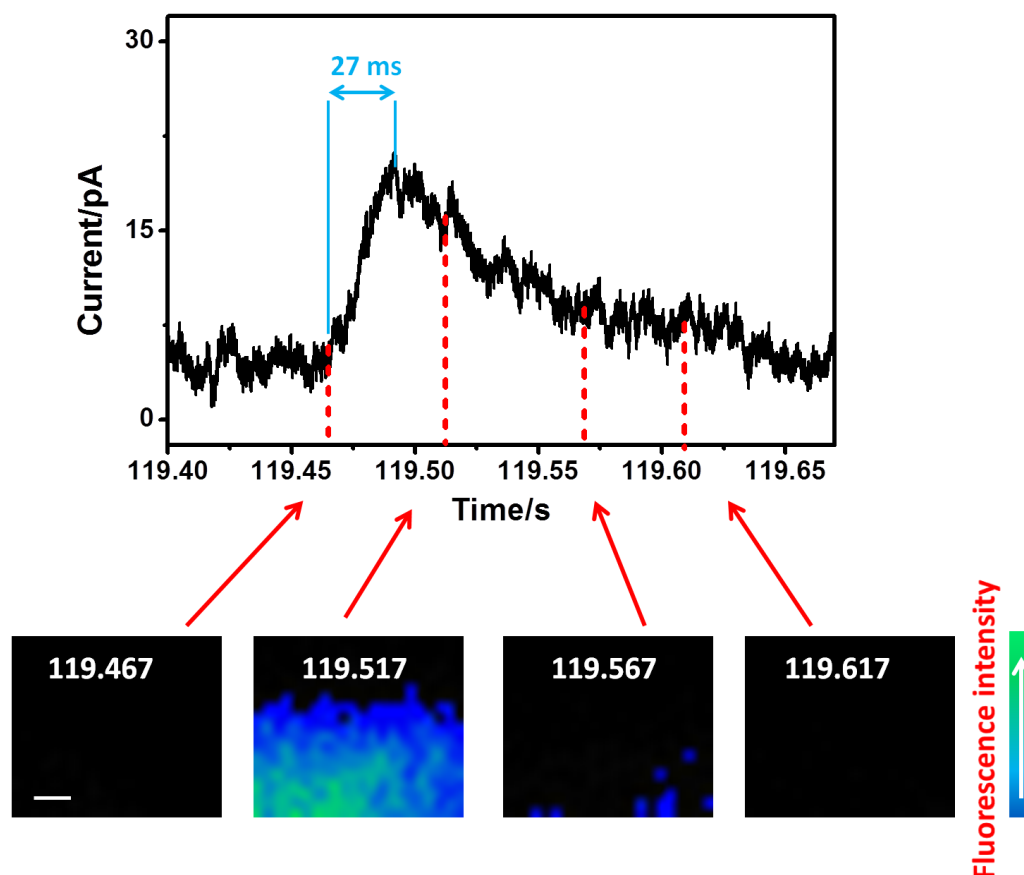


**Figure 5-10** Correlation of amperometric and fluorescent information for a single release event of **1**-stained BON N13 cells over an ITO microelectrode; top: an exocytotic event on ITO appeared as the current spike in electrochemical detection; bottom: sequential pseudocolor TIRFM images of a single exocytotic event defined as ‘sudden flash’ in Chapter 3; 405 nm laser excitation ( $I=2.5$ ); exposure time is set as 50 ms; the corresponding moments of fluorescence and amperometric signals are precisely indicated by red arrows and the red dashed lines; scale bar: 500 nm.

In Chapter 3, we proposed three probable possibilities to illustrate the causes of this particular exocytotic phenomenon, namely, the mechanism of ‘the existence of ballistic vesicles’, ‘the sequential release’ as well as the lateral diffusion of **1** originating from the vesicles lying beyond the TIRFM observation region. However, for the specific example presented in Fig.5-10, from an electrochemical viewpoint, it seems more likely that this particular ‘sudden flash’ probably resulted from the latter two reasons rather than ‘the existence of ballistic vesicles’. In fact, if the ‘sudden flash’ here is considered

to be caused by the ballistic vesicles with extremely fast speed, it seems more reasonable that its corresponding oxidation current spike ought to display high similarity to that of the ‘normal flash’ since the expansion ways of **1** in the two cases are expected to be the same. However, we can see from Fig.5-10 that the rising time ( $t_1$ ) of the associated amperometric spike from the ‘sudden flash’ is around 27 ms, much slower than that detected from the two former types of vesicular release (~8 ms), indicating that the diffusion of **1** from vesicular lumen to ITO surface in this specific event is probably particular. Nevertheless, in order to make sure which is the precise cause of ‘sudden flash’, plenty of statistic analysis on the basis of more fluorescence/electrochemical coupled signals is mandatory.

#### **5.4.2 Continuous secretions monitoring with high temporal/spatial resolution**

Amperometry is completely ‘blind’ to the 3D movements of the secretory vesicle itself or any labeled regulatory protein prior to the fusion event since electrical signals can only be detected after the electroactive biomessengers arrive at the electrode surface. In spite of the high temporal resolution and distinct sensitivity, its low spatial resolution becomes the main constraint of electrochemical methodology for investigations of vesicular secretions. However, the combination of amperometry with TIRFM is likely to solve this problem considering the spatial resolution of this optical technique. That is, the coupling of these two analytical techniques with complementary natures will allow precisely tracking of exocytosis with both high spatial and temporal resolution.

Fig.5-11 shows an example of two continuous exocytotic events of **1**-stained BON N13 cells monitored by the fluorescence/electrochemical combined determination in MD-C. According to the detected amperometric spikes, it is apparent that two independent exocytotic secretions sequentially took place within a very short time, ~200 ms. For sure, their kinetic and quantitative parameters are able to be extracted based on the well-separated current spikes, as presented in Table 5-3, from which we know that in comparison of the latter release (vesicle 2,  $t=176.256$  s), the former secretion (vesicle 1,  $t=176.151$  s) underwent a relatively slower release but larger amount of **1** was discharged from this vesicle in consideration of the higher integral charge.

Moreover, in this coupling measurement, owing to the visual optical signals in TIRFM, the locations and behaviors of these two secretory parent vesicles were precisely identified, as indicated by the red ellipses in Fig.5-11. The manual correlation of optical/electrochemical complementary signals demonstrates the ability of coupling technique for direct, intuitional and real-time monitoring of exocytotic release, revealing more quantitative and temporal secretion details.

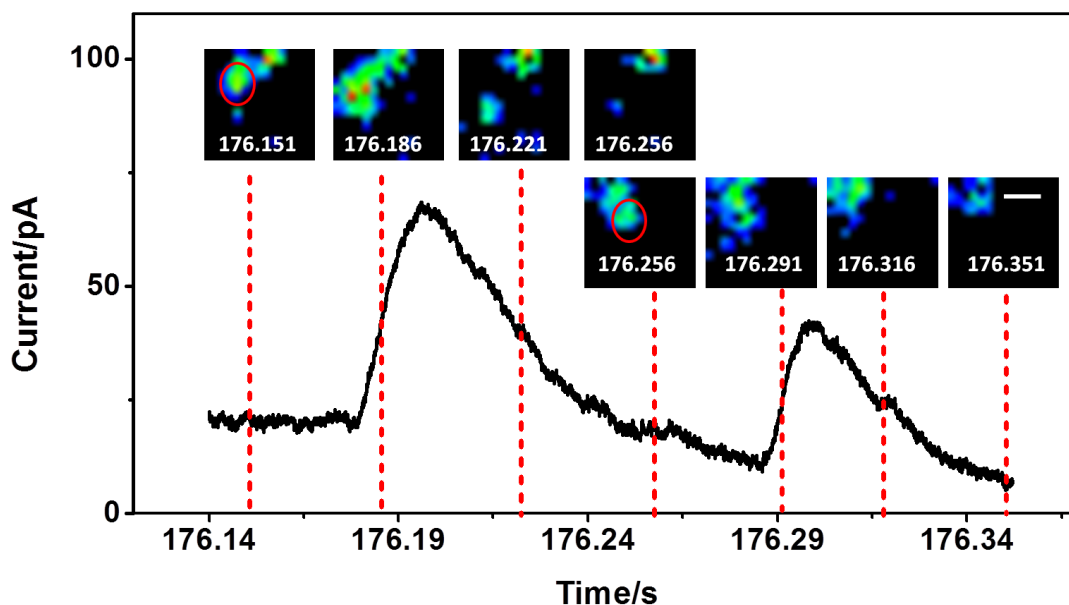


**Figure 5-11** An example of two consecutive exocytotic secretions of I-stained BON N13 cells recorded in MD-C to illustrate the striking spatial/temporal resolution of TIRFM/amperometry coupling methodology; sequential pseudocolor TIRFM images of two individual vesicles (marked by the red ellipse) undergoing exocytotic releases are temporally correlated to the corresponding amperometric spikes at ~ms level, as indicated by the red dashed line; 405 nm laser excitation ( $I=1.5$ ); exposure time is set as 35 ms; scale bar: 500 nm.

	$t_1$ (ms)	$t_2$ (ms)	$t_{20/90}$ (ms)	$t_{1/2}$ (ms)	$I_{\max}$ (pA)	Q (fC)
<b>vesicle 1</b>	10.6	23.4	12.3	34.1	52.5	1920
<b>vesicle 2</b>	6.9	17.0	7.5	24.0	35.2	980

**Table 5-3** The kinetic and quantitative parameters of the two independent vesicular secretions extracted from the corresponding amperometric spikes in Fig.5-11.

Another remarkable advantage of TIRFM/amperometry coupling test is considered to be its application for the analysis of those secretions occurring nearly simultaneously which result in overlapped current spikes in electrochemical detection.

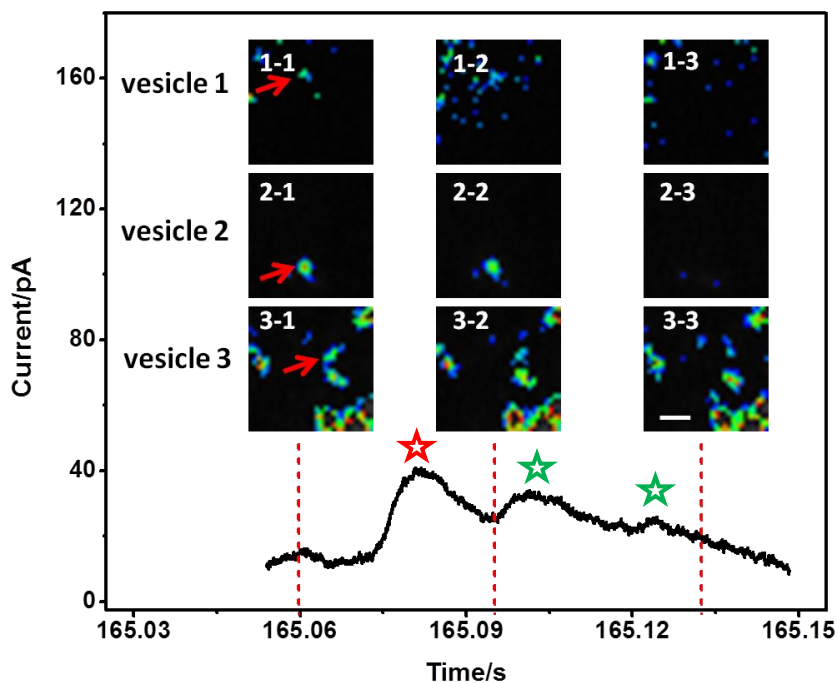


**Figure 5-12** An example of the feasibility of TIRFM/amperometry coupling technique for analysis of overlapped exocytotic events of **1**-stained BON N13 cells recorded in MD-C; sequential pseudocolor TIRFM images of three individual vesicles (vesicle 1, 2 and 3, as indicated by the red arrows) undergoing exocytotic releases are temporally correlated to the corresponding overlapped amperometric spikes (current peaks are marked by red/green stars) at  $\sim$ ms level, as indicated by the red dashed line; 405 nm laser excitation ( $I=1.5$ ); exposure time is set as 35 ms; scale bar: 500 nm.

Fig.5-12 displays a representative example of overlapped amperometric spikes obtained in the coupling detection. By correlating the amperometric trace to the TIRFM sequential images, the overlapped spike was found to be caused by three vesicular releases taking place within tiny time interval ( $\sim$ ms). On the basis of fluorescent signals (Fig.5-12, inset TIRFM images), we discover that the maximum flux of **1** for vesicle 1 appeared between the first two TIRFM frames while that of the latter two vesicles were likely to lie between the last two TIRFM frames. That is, vesicle 1 discharged **1** a little earlier than the two latter vesicles (vesicle 2 and vesicle 3). In consideration of the correlated optical/electrochemical signals, it is highly probable that the first peak (marked by red stars in Fig.5-12)

in amperometric trace ought to be mainly ascribed to the oxidation of **1** expelled by vesicle 1 and in the meanwhile, the onset of exocytotic release was observed from vesicle 2 (frame 2-2 in Fig.5-12); in addition, the full expansion of **1** from the later two vesicles contributed to the two later undistinguishable spikes (marked by green stars in Fig.5-12).

### 5.4.3 Tracking of ITO microelectrode surface passivation by electrooxidation of **1**

As we mentioned in Chapter 4, the electrooxidation of the well-known neurotransmitter, serotonin, is proven to be associated by the generation of hydroxylated products, dimers and other species that can irreversibly adsorb to the working electrode, fouling the surface, with a resulting diminution in the oxidation current.<sup>[196, 252, 269]</sup> Fortunately, in exocytosis investigation by amperometry, owing to the particular artificial synapse configuration as well as few amount of released molecules which temporally and spatially differ from the voltammetry detections based on a large amount of bulk solution, individual exocytotic events are successfully depicted as a series of amperometric current spikes in electrochemical detection, suggesting that the electrooxidation of serotonin resulting from vesicular release generally do not impede the amperometric measurement. Actually, it has been reported that the fouling speed of active electrode surface is closely affected by many decisive factors such as property of electrode material, the concentration of serotonin as well as the experimental configuration.<sup>[196, 252]</sup> We are thus wondering whether there will be some extreme conditions (for instance, a super high quantity of serotonin stored inside a single vesicle) at which the insoluble species generated by the electrooxidation of serotonin quickly occupy and passivate a substantial portion of the electroactive area, interfering with the recording of exocytotic events. It seems impossible to testify this viewpoint on basis of amperometric measurement where electrochemical signal is solely recorded. However, when it comes to cells fluorescently labeled by **1**, the verification of this viewpoint becomes feasible and easier by virtue of the dual signals (optical/electrochemical) concurrently detected in the TIRFM/amperometry coupling technique.

In this work, **1** has been demonstrated to be a decent electrochemical probe for amperometric tracking of exocytotic behaviors of BON N13 cells even though the passivation of electrode surface by its electrooxidation is observed at voltammetry conditions (see Chapter 2), behaving similarly to serotonin.<sup>[18, 19, 33, 105, 270, 271]</sup> We thus attempt to test whether ITO electrode will be blocked by the oxidation of **1** at ITO surface taking advantage of the fluorescence/electrochemical coupling methodology. If yes, the coupling results will conversely help us to better understand how this molecule passivates the active area of electrode and the feature of the resulting products.

Notably, it is extremely important to mention that there is definitely no doubt that **1** is feasible to work as a decent electrochemical reporter of individual exocytotic event and its oxidation on ITO surface

normally leads to a classic amperometric current spike, as we previously described. In this section, we will discuss some very rare cases of electrooxidation of **1** detected by the coupling technique.

In general, for BON N13 cells stained by **1**, their exocytotic events were depicted as an amperometric spike associated with fluorescence extinction, as three previously examples displayed from Fig.5-8 to Fig.5-10. Nevertheless, in some rare cases (less than 5%) during coupling measurement, once **1** arriving at ITO surface, the fouling of the working electrode was immediately observed due to the electrooxidation of this molecule, which was clearly indicated by the fluorescent, insoluble oxidation product remaining on the electrode surface for long time (from several seconds to dozens of seconds).

To clearly elucidate this phenomenon, two typical examples of ITO surface passivation caused by **1** oxidation are shown in Fig.5-13 and their temporal durations were around 1.5 s and 20 s, respectively. We can see that in both cases, before exocytosis, the fluorescence intensity of these two vesicles seemed quite stable, indicating a neglectable photobleaching effect cause by 405 nm laser during the first 0.8 s, in agreement with our previous study (Fig.3-19). Then, **1** started to diffuse to the ITO surface upon stimulation, leading to a sudden augmentation followed by a gradual, slow decline of fluorescence intensity.

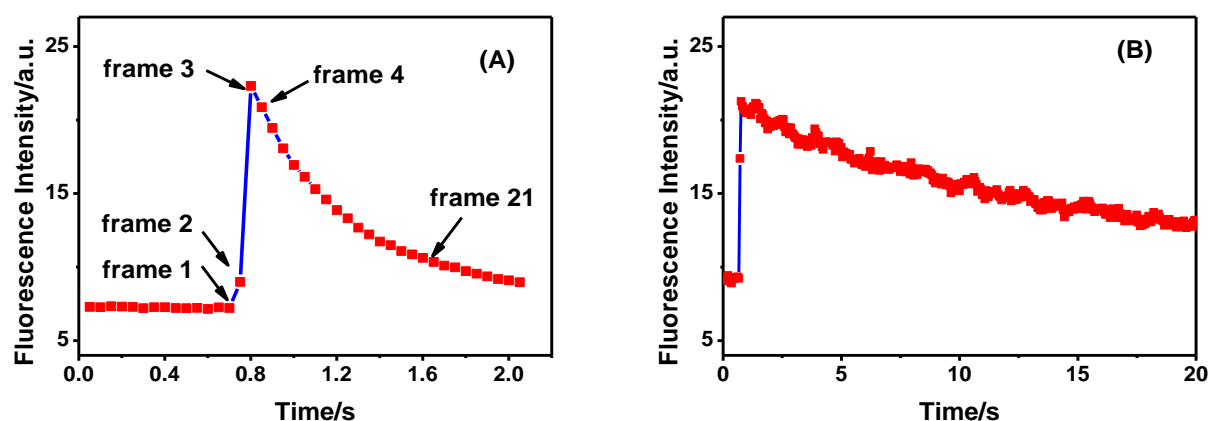


**Figure 5-13** Two representative examples illustrating the time course of fluorescence intensities (TIRFM configuration, in arbitrary units) relate to ITO microelectrode passivation caused by the electrooxidation of **1** on its surface; the corresponding sequential TIRFM images from 'frame 1' to 'frame 21' of (A) are presented in Fig.5-14.

The fluorescence/electrochemical dual signals of the single exocytotic release of **1** presented in Fig.5-13(A) were simultaneously detected by TIRFM/amperometry coupling measurement. The correlation

of these two complementary signals is going to help us to better understand the passivation process of ITO surface because of the electrooxidation of **1**, as displayed in Fig.5-14.

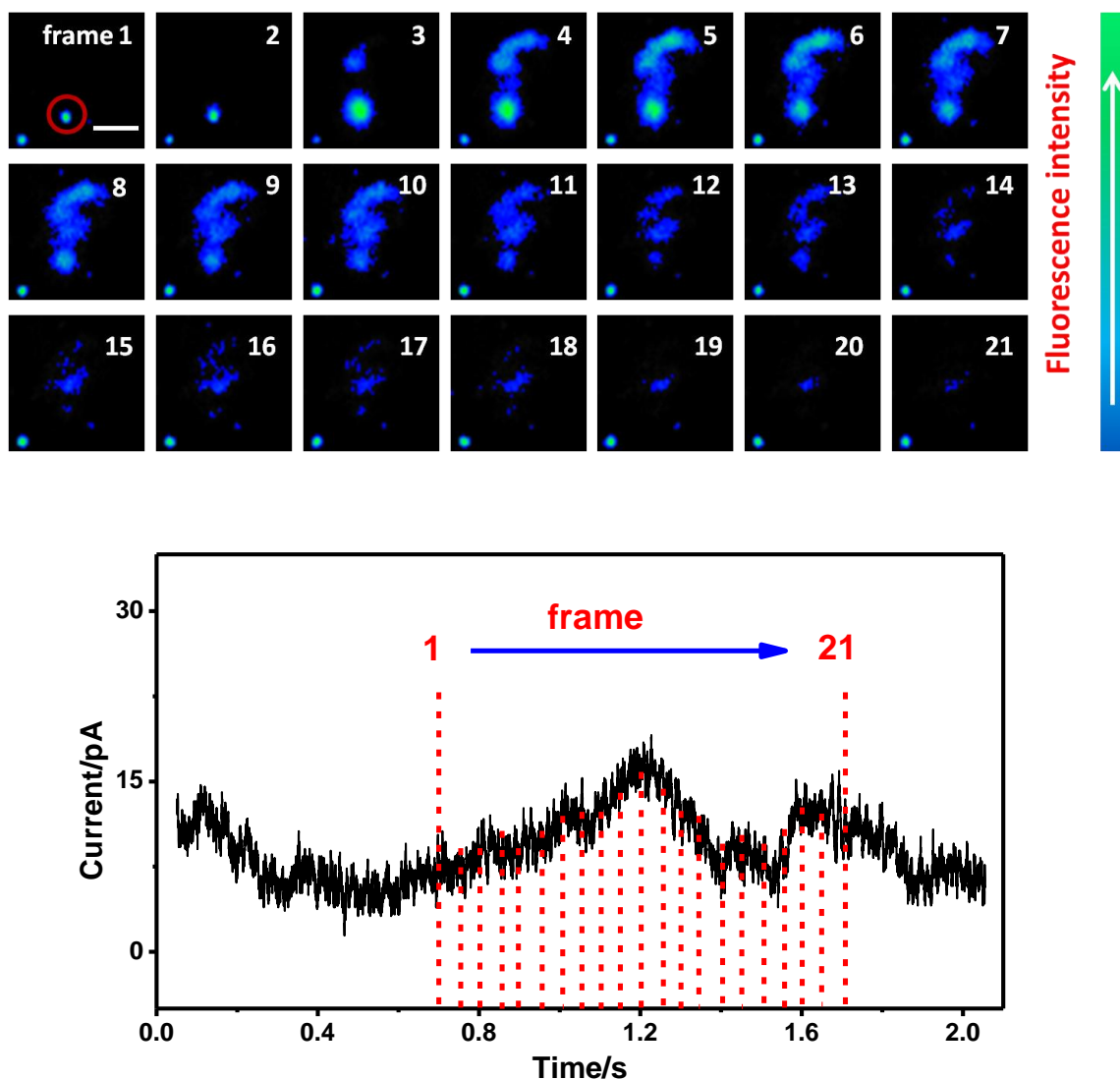


**Fig.5-14** Correlation of amperometric and fluorescent information for an ITO microelectrode passivation event caused by electrooxidation of **1**; top: sequential pseudocolor images acquired at TIRFM configuration; the fluorescent vesicle undergoing exocytosis is indicated by the red ellipse and the time interval between each image is 50 ms; bottom: the corresponding electrochemical signals with red dashed lines indicating the equivalent moments in TIRFM micrographs; scale bar: 2  $\mu$ m.

It has been demonstrated in this work that, for BON N13 cells labeled by **1**, 95% of the exocytotic events were fully accomplished within 100 ms (Fig.5-6), leading to an obvious extinction of visible

fluorescence. However, in these rare cases mentioned in this section, it seems that **1** was instantly oxidized as soon as its arrival on the ITO electrode and the diffusion of its resulting oxidation product was restricted to a limited area, without detectable fluorescent diffusion, especially after the 4<sup>th</sup> frame (according to the sequential TIRFM micrographs in Fig.5-14, top). It is thus evident that the oxidation of **1** on ITO surface generated an insoluble, polymer-like, highly fluorescent product which firmly adsorbed to the microelectrode, probably resulting in the fouling of active surface of ITO. In addition, on the basis of the electrochemical signals acquired during the equivalent moments (Fig.5-14, bottom), we discover that sluggish current variations were observed (which might be attributed to the baseline fluctuation caused by 405 nm laser) whereas no amperometric current spike was detected to correspond to this oxidation process, indicating a prompt block of the electroactive surface by the oxidation products. Briefly, no apparent relationship between these two signals could be drawn and the gradual decrease of fluorescence intensity in TIRFM was considered to be induced by the photobleaching effect of exposure to 405 nm laser.

By using the coupling technique, the passivation process of the ITO working electrode by electrooxidation of **1** is directly visualized and the resulting insoluble, polymer-like oxidation product adsorbed on ITO in these rare cases is confirmed to be strongly fluorescent. Additional experiments need to be performed if we want to figure out the possible decisive factors of the ‘polymerization’ process such as the concentration, the pH as well as electrode properties, etc.

## 5.5 Conclusions

In this Chapter, we have demonstrated the feasibility of **1** functioning as a fluorescent/ electrochemical dual probe in TIRFM/amperometry coupling measurement of vesicular exocytosis in one set-up (MD-C). During the coupling measurement, the trigger of 405 nm laser for **1**-stained vesicles illumination was found to induce a sluggish fluctuation of the amperometric current baseline whereas this effect was likely to be neglectable in consideration of its much slower time course compared with that of the detected current spikes resulting from exocytotic release. In addition, by comparing the amperometric signals measured with and without 405 nm laser illumination, we discovered that the kinetics of individual exocytotic release became faster due to the 405 nm irradiation and the measured current amplitude appeared to be also higher while the discharged amount of **1** was demonstrated to be equal in these two cases. These results indicate that coupling monitoring of vesicular exocytosis with 405 nm laser irradiation is feasible by employing **1** as the fluorescent/amperometric dual probe considering its specific optical/electrochemical characteristic.

TIRFM/amperometry coupling measurement was then successfully conducted on **1** labeled-BON N13 cells grown in MD-C. Upon stimulation, **1** started to diffuse from vesicular lumen to the extracellular

space, leading to the fluorescence and amperometric signals which were able to be simultaneously collected from transparent ITO electrode surface. Moreover, three forms of calcium-triggered exocytotic events are found in the coupled detection by virtue of optical and electrochemical properties of **1**: the normal ‘flash’, the extinction of fluorescent spots as well as the ‘sudden flash’, in accordance with our previous results obtained by TIRFM in Chapter 3.

TIRFM/amperometry measurement combining two powerful analytical tools with complementary natures ensures its high spatial and temporal resolutions. The application of this coupling technique for consecutive exocytotic secretion determination as well as for overlapped events analysis was demonstrated by using the electrochemical/optical difunctional probe **1**. In addition, some rare cases of the electrode passivation caused by electrooxidation of **1** were also directly visualized and discussed with the help of the dual signals showing complementary features. Relying on the coupling measurement, we discovered that electrooxidation product of **1** seemed to be hydrophobic, fluorescent, polymer-like film which adsorbed tightly to the ITO surface, resulting in an electrode surface fouling.

In summary, we have presented a microfabricated ITO device that allows coupling of two complementary analytical techniques for the direct and real-time analysis of exocytotic phenomena. The ability of **1** working as an optical/electrochemical dual probe in TIRFM/amperometry coupling measurement of vesicular exocytosis of BON N13 cells has been demonstrated and gives promising and better results than the previous strategies involving independent electrochemical and fluorescent probes. Future studies will relate the visible vesicle pool to the functional states of secretory vesicles, perhaps shedding light on the roles of specific roles of regulatory proteins.



## General conclusions and perspectives

This work took place in the context of monitoring exocytosis by combination of two analytical methods (TIRFM/amperometry) with complementary features. To the best of our knowledge, the optical and electrochemical probes were usually independently loaded so as to satisfy simultaneously optical imaging and amperometric detection. Our objective in this work was thus to develop a unique probe with dual fluorescent/electrochemical characteristics for investigation of exocytotic process in one set-up by TIRFM/amperometry coupling technique. This is why an analog of biogenic monoamine neurotransmitters, 4-(2-aminoethyl)-6-chloro-7-hydroxy-2H-1-benzopyran-2-one hydrochloride (named as **1** in this thesis) was synthesized considering its specific optical and electrochemical properties.

**1** exhibited bright, stable, pH-dependant fluorescence. When excited at 405 nm, its fluorescence intensity was almost doubled with the increase of pH values from 5 (similar to that in the vesicular lumen) to 7 (similar to the extracellular medium). Furthermore, in voltammetry, **1** was demonstrated to be easily electrooxidized on GCE, CFE and ITO electrodes surfaces, showing good electroactivity. A phenomenon of electrode passivation was also observed during the electrooxidation of **1** on these electrode surfaces. However, such a passivation does not preclude the amperometric investigations of exocytosis at single vesicle level since voltammetry conditions (temporal and spatial scales, non-dynamic solution...) are not comparable to those at artificial synapse configuration (the millisecond scale time course and nanometric secretory vesicles in which limited number of electroactive molecules are stored). **1** thus emerges as a dual probe with a promising future in the TIRFM/amperometry combined method.

The capability of **1** to be a convenient fluorescent reporter in TIRFM measurement of exocytosis was proven. By optical imaging, **1** was found to be able to be specifically recognized and selectively transferred into the acidic vesicular lumens by both PC-12 cells and BON N13 cells. As secretory vesicles of PC-12 cells were too small to be clearly observed at our TIRFM configuration, we finally chose **1**-stained BON N13 cells as cell model for exocytosis studies. The motility behaviors of vesicles adjacent to plasma membrane before and during exocytosis were directly visualized owing to the bright fluorescence of **1**. Upon stimulation, three different forms of calcium triggered exocytotic events were observed from BON N13 cells labeled by **1**: the normal 'flash', the extinction of fluorescent spots as well as the 'sudden flash'. **1** thus demonstrated its favorable ability of working as a novel, fluorescent probe to directly visualize and quantify the exocytotic release at single vesicle level.

The feasibility of **1** functioning as an electrochemical reporter in amperometric detection of exocytosis was also testified. The design, fabrication, characterization and comparison of three ITO microdevices were presented and the third one, called ‘MD-C’ was finally employed to accomplish the amperometric investigation of exocytotic secretions of **1**-stained BON N13 cells owing to its relatively low current noise as well as its multiple microelectrodes of ‘lollipop’ shapes. The rapid flux of **1** from a vesicular lumen to the electrode surface resulted in a sharp oxidation current spike and the exocytotic process of individual cells were thus depicted as a session of oxidation current spikes, suggesting that **1** was capable of working as an electrochemical reporter for vesicular secretion investigation. The comparison of the vesicular secretions detected at different configurations, namely by CFE at the cell apex and by ITO at the cell bottom, displayed that there was a distinct disparity in terms of release dynamics and amounts between the secretions at the two poles.

Since independent optical and electrochemical measurements of exocytotic releases were successfully achieved by using **1** as reporters, we then characterized the feasibility of **1** working as the fluorescent/electrochemical dual probe to monitor vesicular exocytosis in one set-up (MD-C). Three different forms of exocytotic events were detected in TIRFM/amperometry coupling measurement, in agreement with our former results already obtained by TIRFM alone. 405 nm laser illumination during the test was found to slightly alter the kinetics of individual exocytotic release while the discharged amount ( $Q$ ) of **1** was quite stable. Indeed, fluorescent/amperometric coupled signals (34%) resulting from the released dual probe **1** were acquired whereas some ‘optical orphan’ (42%) and ‘amperometric orphan’ (24%) events were also detected. Nevertheless, the coupled efficiency (34%) was improved by 12% compared with our former work on BON BC21 cells of which the fluorescent (GFP) and electrochemical (serotonin) probes were separately loaded. This favorable improvement ought to be attributed to the unique probe functioning simultaneously as electrochemical and optical reporters in our present work. Considering the high spatial and temporal resolution of this combined method, we then applied it to analyze consecutive exocytotic secretions as well as overlapped events of **1**-stained cells. In addition, in coupling measurements, some rare cases of the electrode passivation caused by electrooxidation of **1** were directly visualized and discussed with the help of the dual signals showing complementary features.

In summary, in this work, we used a unique probe with dual fluorescent/electrochemical characteristics to investigate cellular exocytosis in one set-up by TIRFM/amperometry coupling technique. With this specific probe, exocytotic secretions of BON N13 cells were simultaneously detected by optical imaging and electrochemical measurement. The analysis of these two signals with complementary information allows the correlation of the fusion pore behavior (opening/closure dynamics, stability, measured by amperometry) with the motion of a vesicle in three dimensions (tethering, docking, fusion and retrieval, detected by TIRFM).

This work offers an innovative idea to develop other novel probes capable of functioning as fluorescent/electrochemical dual reporters for quantitative, temporally and spatially resolved monitoring of single-vesicle motions and exocytosis by the coupling method, especially those with similar structures to **1** but with longer excitation/emission wavelengths. In this way, baseline variations resulting from 405 nm laser irradiation in amperometric detection could be avoided, making it easier to distinguish small current spikes and the coupled efficiency is thus expected to be further improved.

The combination of dual probes with TIRFM/amperometry coupling method provides information that could not be obtained with amperometry or fluorescence imaging alone, showing a promising prospect for investigation of other physiological process related to exocytosis. (i) Further studies will perhaps shed light on the specific roles of some regulatory proteins (such as SNAREs proteins, actin and other functional proteins interacting with them) involved in the fusion mechanism before, during and after fusion. (ii) It allows observation of the recruitment of fluorescently tagged molecules into secretory vesicles (using dual-color TIRFM). (iii) It is capable of revealing whether vesicular content/size (measured by amperometry) depends on the secretion area of the plasma membrane (by TIRFM) or whether there are specific spatial zones or hotspots of exocytotic secretion at single cell level. (iiii) It enables the study of differential release of various non-electroactive fluorescent vesicle markers in relation to the amperometrically detected release, which will contribute a lot to the understanding of various regulating factors of exocytotic secretion owing to the specificity of these fluorescent markers.



## **Experimental section**

### **I Cell culture**

#### **I. 1 BON N13 cells culture**

The BON cell line was derived from a metastatic human carcinoid tumor of the pancreas. BON N13 cells for all our experiments were kindly provided by C.M. Townsend (University of Texas Medical Branch, Galveston, TX) and F. Darchen, I. Fanget (UMR 8250, Université Paris-Descartes).

- **Culture media**

##### Complete growth medium

The base medium for BON N13 cell line is DMEM/F12 (Dulbecco's modified eagle medium: nutrient mixture F-12). DMEM/ F-12 medium supplemented with 10% heat-inactivated fetal bovine serum as well as 1% penicillin/streptomycin solution were employed as complete growth medium. For the preparation, 44.5 mL DMEM/F-12 medium, 5 mL heat-inactivated fetal bovine serum and 0.5 mL penicillin/streptomycin solution were mixed in a 50 mL sterile centrifuge tube, filtered by 0.22  $\mu\text{m}$  filtration membrane before use.

##### Freezing medium

To minimize damage to cells at low temperature, a cryoprotectant such as DMSO should be added to the freeze medium. Generally, we used complete growth medium supplemented with 10% (v/v) DMSO (cell culture grade) for cryopreservation of BON N13 cells and it was stored at +4 °C before use.

- **Routine culture**

BON N13 cells were maintained in complete growth medium in a 37 °C incubator with a humidified atmosphere of 5% CO<sub>2</sub>. Cells were grown on 75 cm<sup>2</sup> cell culture flasks (Nunc, Roskilde, Denmark) and culture medium was renewed every 2-3 days. Subculture of BON N13 cells were conducted weekly by trypsinization when cell confluence reaching approximately 90%, namely 30-40 millions cells per flask. The whole process of trypsinization included the following four steps: (1) Cell pre-washing by sterile PBS (pH=7.4); (2) Trypsin-EDTA solution treatment; (3) Inactivation of trypsin effect and (4) Cell splitting. Specifically, after aspirating the culture medium out of the culture flask, these confluent BON N13 cells were firstly rinsed twice with 5 mL sterile PBS solution in order to completely remove serum-containing culture medium which contained trypsin inhibitors. Then, 1 mL

trypsin-EDTA solution, a widely-used cell dissociation reagent, was employed to gently dissociate cells from the flask bottom. After being incubated in 37 °C incubator for about 2-3 min, almost all the cells were detached from the flask bottom by trypsin treatment. Over-treatment by trypsin might damage the cell membrane and cause cell death. To inhibit the trypsin effect, the trypsinized cells were thus re-suspended in 9 mL fresh serum containing complete culture medium and were gently pipetted so as to dissociate all cell clumps into single cell. Finally, 1 mL cell suspension was added into a new culture flask with 14 mL fresh medium, resulting in a 1:15 dilution factor.

- **Cryopreservation and thawing**

#### Cryopreservation

BON N13 cells' cryopreservation was executed when its confluence reached around 90%, indicating cells were in exponential growth. In general, cells were detached by trypsin-EDTA solution treatment, harvested by centrifugation at 1000 rpm for 5 min, resuspended in precooled freezing medium at a final concentration of viable cells in the range between  $10^6$  and  $10^7$  cells per mL and transferred into 1.5 mL sterile cryovials (1 mL cell suspension per cryovial). Before being stored in the -80 °C freezer, all the cryovials were placed inside a commercial freezing container (Thermo Scientific™ Mr. Frosty™) for the purpose of gradually cooling down the cells to -80 °C at an optimum rate of cooling very close to -1 °C per minute.

#### Thawing

One cryovial containing BON N13 cells was taken out of -80 °C freezer, placed into a prewarmed water bath (37 °C) and swirled gently until a small bit of ice left in the cryovial. Afterwards, cells were transferred into a 50 mL sterile centrifuge tube with 9 mL prewarmed complete growth medium and the cryovial was rinsed by another 10 mL culture medium in order to remove all the cells. Since DMSO in freezing medium was toxic to cells, these previous operations must be performed as quickly as possible to obtain the best cell viability. Cells were collected by centrifugation at 1000 rpm for 5 min, resuspended in 6 mL prewarmed culture medium and removed to a new 75 cm<sup>2</sup> flask with 6 mL culture medium. Fresh thawing cells were fragile, so we kept the flask in the 37 °C, 5% CO<sub>2</sub> incubator for two days without any touch before verifying under an inverted microscope, to avoid physical damage.

## **I.2 PC-12 cells culture**

The PC-12 cell line was derived from a transplantable rat pheochromocytoma. Our PC-12 cells were purchased from American Type Culture Collection (ATCC, CRL-1721).

- **Culture media**

**Complete growth medium**

RPMI-1640 medium supplemented with 10% heat-inactivated horse serum, 5% heat-inactivated fetal bovine serum and 1% penicillin/streptomycin solution was the complete growth medium for PC-12 cells recommended by ATCC. In a 50 mL sterile centrifuge tube, we mixed 42 mL RPMI-1640 base medium with 5 mL heat-inactivated horse serum, 2.5 mL heat-inactivated fetal bovine serum and 0.5 mL penicillin/streptomycin solution. The complete growth medium was filtered by 0.22 µm filtration membrane before use.

**Freezing medium**

Complete growth medium supplemented with 10% (v/v) DMSO was prepared and stored at +4 °C before use for cryopreservation.

- **Routine culture**

PC-12 cells were cultured in complete growth medium as described above in a 37°C incubator with a humidified atmosphere of 5% CO<sub>2</sub> and culture medium was renewed every 2-3 days, as suggested by ATCC. Cells cultured on 75 cm<sup>2</sup> flasks (Nunc, Roskilde, Denmark) appeared as floating clusters as well as few scattered lightly attached cells. Subculture was carried out when cell density achieved around 2 to 4 million cells per mL. Briefly, cell suspension was transferred into a 50 mL centrifuge tube and harvested by centrifugation at 1500 rpm for 12 min at room temperature. After removing and discarding supernatant, cell pellet was resuspended in 5 mL fresh medium. In order to break up cell clusters, 5 ml aliquot of cells was gently aspirated 4 or 5 times with a 20 ml sterile syringe outfitted with a 22g (1½ in.) needle. Finally, 1.5 mL cell suspension was added into a new culture flask with 13.5 mL fresh medium, leading to a 1:3 dilution factor.

- **Cryopreservation and thawing**

**Cryopreservation**

We froze PC-12 cells when they were in exponential growth where the cell density arrived at approximately 2 to 4 million cells per mL. All the operations were the same as that we did for BON N13 cells cryopreservation except that here PC-12 cells were gathered by centrifugation at 1500 rpm for 12 min, without the pre-treatment of trypsin-EDTA solution.

## Thawing

All the experimental procedures for PC-12 cells' thawing were identical to that we described previously for thawing of N13 cells apart from that, PC-12 cells clusters were broken up for 4 or 5 times with a 20 ml sterile syringe outfitted with a 22g (1½ in.) needle before being added into new culture flask with prewarmed medium.

## **II Fabrication of microelectrodes and microsystems**

### **II.1 CFE construction**

CFE has been mainly used for exocytosis investigation at single cell level since they display a very stable, low background current in biological media. In this thesis, all CFEs were fabricated by sealing individual carbon fibers into pulled-glass capillaries, a traditional method previously described.<sup>[272]</sup> Specifically, we firstly aspirated individual carbon fibers (10-µm diameter, Thornel P-55S, Cytec) into glass capillary tubing (GC120F-10, Clark Electromedical Instruments), then through a vertical micropuller (PB-7; Narishige), the capillary was separated into two identical tubes with a short length of protruding carbon fiber at the tapered end and then a drop of mercury was back-filled into the capillary tubes to make an electrical contact.

In order to limit a specific working area at the tip, an insulating layer of poly(oxyphenylene) was electrochemically deposited onto the protruding carbon fiber according to a published method.<sup>[273]</sup> A mixed solution containing 0.40 M allylamine, 0.23 M 2-allylphenol, and 0.23 M 2-butoxyethanol in 1:1 (v/v) water-methanol was made up as electrolyte. To achieve polymer deposition, a potential of +4 V was applied to carbon fiber electrode for 3 min with a platinum counter electrode. After being thoroughly washed by distilled water, the polymer insulated electrodes were cured for 3 h at 150 °C to completely evaporate the solvent as well as to strengthen the insulation. Finally, all these glass capillary tubes with insulated carbon fiber were stored in well-sealed boxes until use.

To perform amperometric test, polymer insulated carbon fiber tip was cut to an appropriate length (c.a. 0.8 cm) under a bifocal microscope (Stemi 2000; Zeiss) and was polished on a diamond particle whetstone microgrinder (EG-4; Narishige) at an angle of 45° for 6 min to produce a fresh, clean, elliptical and conductive surface, as presented in Fig.E-1(A). Nichrome wire was finally inserted into conductive mercury to make an electrical contact. For exocytosis investigation, CFE was positioned right against an individual cell during amperometric test, as shown in Fig.E-1(B).

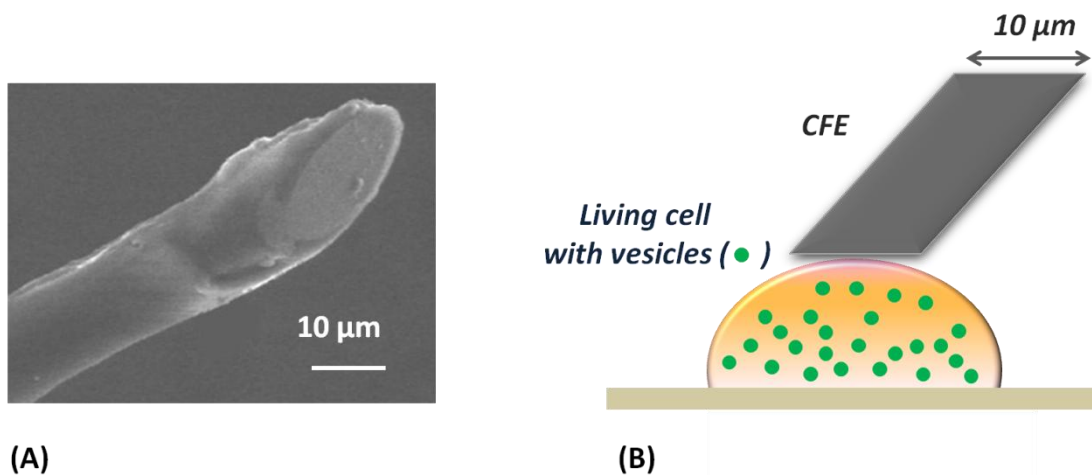


**Figure E-1** (A) Scanning electron microscopy image of a CFE (10- $\mu\text{m}$  diameter) tip; (B) Principle of the artificial synapse configuration, in which a CFE microelectrode is positioned against a living cell that releases electroactive species.

## II.2 Fabrication of ITO microelectrodes

So far, CFE has been extensively used for amperometric monitoring of quantal exocytosis but it couldn't meet the requirements of simultaneously cell observation and amperometric measurement. To achieve this goal, we employed transparent ITO microelectrodes on a glass substrate as the working electrode. In the microfabrication, photolithography is one of the most commonly used lithography technology to define the original microstructures. It has many advantages like high resolution, convenience in transferring entire design at once, and feasibility of multi-layer structure. ITO microelectrodes with different patterns in our work were manufactured by photolithography and wet acid etching.

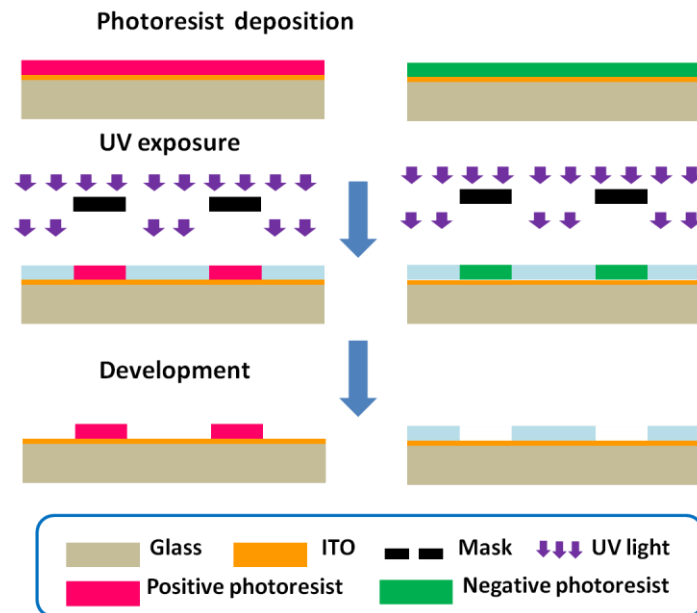
### II.2.1 Photolithographic process

Generally, photolithography includes the following steps: substrate cleaning, photoresist coating, soft baking, UV exposure, hard baking (not always, it depends on the character of used photoresist) and development.

- **Photoresists**

Photoresists are organic polymers both photosensitive and acid-resistant. Once exposed to UV light at a certain time, they change their chemical structures, resulting in the image transfer from predesigned

mask onto the substrate. According to their distinct properties, photoresists are mainly defined as two categories: positive photoresist and negative photoresist.



*Scheme E-1 Behaviors of positive and negative photoresists in photolithography.*

As illustrated in Scheme E-1, for positive photoresist, exposure to UV light makes it more soluble in the developer. As a consequence, exposed photoresist could be easily washed away by developer and unexposed part remains with the exact pattern of mask. In the contrast, negative photoresist becomes more difficult to dissolve in the developer due to the polymerization reactions caused by UV light exposure. A negative photographic of the mask's pattern is thus left on the substrate since the unexposed photoresist can be thoroughly removed by developer. In our experiments, two well-known photoresists, AZ9260 (positive, with high resolution) and SU-8 3010 (negative, permanent epoxy) were employed for ITO microdevices fabrication.

- **Substrate cleaning and photoresist spin-coating**

To improve photoresist-to-substrate adhesion force, substrates must be thoroughly cleaned by various solvents, oxygen plasma treatment, and dehydrated at high temperature before photoresist deposition. Moreover, the thickness of spin-coated photoresist can be adjusted by altering the spinning speed and time in accordance with different requirements.

- **Soft baking and UV exposure**

After spin-coating, photoresist on top of substrate is sticky and soft baking on a hotplate is a common way to evaporate the volatile solvent components before UV light exposure. A thin, non-sticky, compacted film forms after soft-baking and the thickness of photoresist film is thus decreased. To create both exposed and unexposed portions of photoresist on the substrate, we use UV spot light source Hamamatsu LC5 (radiation wavelength ranging from 300 nm to 450 nm) and its power intensity at 365 nm is about 12 mW. The exposure time varies from thickness as well as nature of photoresists, and proper exposure degree guarantee the high resolution of photolithographic process.

- **Hard baking and development**

Hard baking after UV light exposure is not recommended in most application for positive photoresist. For instance, AZ9260 could be directly developed in mixture of AK400 solution and distilled water. However, when it comes to SU-8 3010, hard baking is obligatory to be performed because the exposed area of SU-8 film is able to be selectively cross linked via this operation, resulting in the appearance of an exact image of pre-designed mask in the SU-8 3010 photoresist coating film. Finally, the unexposed part of photoresist was removed by SU-8 developer, followed by isopropyl alcohol (IPA) cleaning for 10 seconds. The appearance of a white film during IPA rinse indicates underdevelopment of the unexposed SU-8 photoresist.

All the substrates should be dried by clean compressed air or nitrogen before use.

### ***II.2.2 Manufacture of ITO microdevices***

A thin film of ITO (90% In<sub>2</sub>O<sub>3</sub> 10% SnO<sub>2</sub>; 150±10 nm thickness; ACM, Villiers Saint Frédéric, France) was previously sputtered onto optical glass slides (22 mm × 22 mm × 0.13 mm) in order to afford a material of low electrical resistance ( $\leq 20$  ohms per square) and transparency.

- **Multiple ITO microelectrodes pattern transfer**

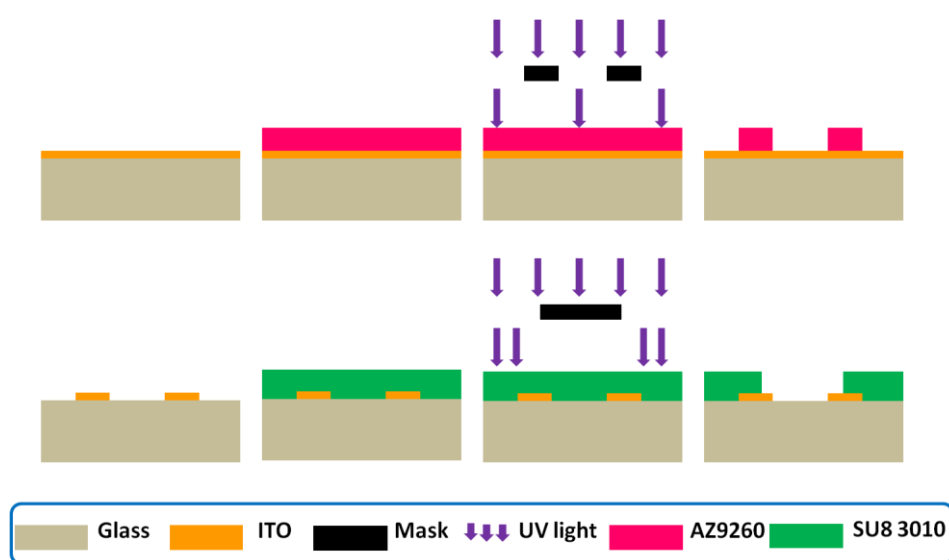
ITO substrate was thoroughly cleaned by distilled water, ethanol and isopropyl alcohol in order. After 2 min of oxygen plasma treatment at 400 mTorr, an insulating positive photoresist (AZ9260, Clariant GmbH, Germany) was patterned onto the ITO/glass slides, as illustrated in Scheme E-2:

(a) AZ9260 deposition: A positive photoresist, AZ9260, was firstly deposited onto an ITO substrate with a pipette to cover the entire surface without any bubble. In order to produce a homogeneous thin layer (10- $\mu$ m thickness) of AZ9260 on ITO surface, photoresist-covered ITO substrate was spun at 2000 rpm for 60 s with acceleration of 300 rpm/s;

(b) UV exposure: Before being exposed to UV light for 70 s through a specific mask design, AZ9260-covered ITO substrate was firstly prebaked on a hotplate at 110 °C for 160 s to get rid of volatile solvents;

(c) Development: The substrate was agitated in 1:4 (v/v) AZ 400K-H<sub>2</sub>O mixture to remove exposed AZ9260. After complete development, unexposed part was reserved on ITO surface, leading to the exact pattern transfer of pre-designed mask to the substrate;

(d) Wet etching: To achieve acid etching, the substrate was immersed inside commercial HCl solution for 6-8 min, followed by H<sub>2</sub>O rinsing. Since the transferred mask pattern was protected by acid-resistant AZ9260, only ITO without ‘photoresist protective layer’ was chemically dislodged by acid corrosion. Moreover, photoresist covering multiple ITO microelectrodes was removed by acetone. This ‘wet etching’ step left multiple microelectrodes on the glass surface.



*Scheme E-2 Experimental steps for the fabrication of ITO multiple microelectrodes.*

- **Isolation of ITO multiple microelectrodes**

The value of electrical noise of ITO microelectrodes observed from amperometric measurement is proportional to surface area of microelectrode.<sup>[105]</sup> For the sake of current noise optimization, photoresist SU-8 3010 was employed to insulate the ITO so as to obtain a specific working region. The whole insulation process is shown in Scheme E-2:

(e) SU-8 3010 deposition: Deposition of negative photoresist SU-8 3010 thin film onto substrate was carried out by two-step spin-coating as the photoresist is too viscous. Firstly, SU-8 3010 was dispensed to cover the entire surface of ITO-embedded glass substrate. Then it was spin-coated at 500 rpm for 10 s with acceleration of 100 rpm/s, followed by a faster spin-coating step at 3000 rpm for 30s with acceleration of 500 rpm/s. A thin SU8-3010 film of 10- $\mu$ m thickness thus appeared on the surface after soft-baking at 110 °C for 4 min;

(f) UV exposure: SU-8 3010 covered ITO substrate was then exposed to 365 nm UV light for 17 s, followed by post-baking at 65 °C for 1 min and 95 °C for 2 min. An image of the mask thus occurred after post baking;

(g) Development: SU-8 3010 was developed within SU-8 developer. As a result, the ITO-embedded microchip with a specific working region emerged. Several masks with different motifs were utilized throughout the course of this work.

- **Chamber assembly and pre-treatment**

To build an appropriate living environment for cells, we prepared a Petri dish with 1.5 cm diameter hole in the center (P50G-1.5-14-F, MatTek Cultureware, Ashland, MA) in advance and the multiple ITO microelectrodes chip was fixed onto the Petri dish by polydimethylsiloxane (PDMS), a biocompatible silicone elastomer. Prior to introducing cells, the assembled microdevice was exposed to 400 mTorr plasma for 2 min and precoated with 300  $\mu$ L collagen IV (0.1 mg/mL). After 6 hours incubation at 37 °C, dishes were washed 3 times by PBS solution. Our microfabricated ITO devices described above are able to hold 4 mL culture medium and feasible to TIRFM/amperometry coupling measurement.

### **II.3 Construction of other electrodes**

- **Glassy carbon electrode**

GCE for electrochemical characterization of **1** was fabricated from a 1 mm diameter glassy carbon rod press-fitted into a Teflon covering to provide a planar, circular electrode with an area of 0.79 mm<sup>2</sup>. GCE was polished on a MasterTex (Buehler) polishing pad before each use.

- **Silver/silver chloride reference electrode**

We used Ag/AgCl as a reference electrode for electrochemical measurement considering its favorable advantages such as small size, flexible form as well as easy-to-make property. It consists of a metallic

Ag wire (Goodfellow, reference AG005160/22, Lille, France, 1-mm diameter) covered by electrochemical deposited AgCl. In our lab, an easy experiment was conducted to construct all the Ag/AgCl reference electrodes. To be specific, 1 M NaCl solution was electrolyzed when we applied a potential of +15 V between the Ag wire (anode) and a platinum wire (cathode) for a few seconds. The metallic Ag was thus oxidized to Ag<sup>+</sup> ions on the anodic surface (i.e. Ag) and they formed AgCl solid precipitates with the Cl<sup>-</sup> ions in solution. After being rinsed by distilled water, Ag/AgCl reference electrodes were able to be used for electrochemical performance and the potential of this reference electrode was constant during measurement.

### **III Analytical methods**

#### **III.1 Electrochemical techniques**

##### ***III.1.1 Cyclic voltammetry***

Cyclic voltammetry is one of the most useful voltammetric techniques for the characterization of electrochemical reaction. It is carried out by applying triangular voltage ramps (towards both directions by switching at a preset potential) to the working electrode at a certain scan rate, and resulting current is plotted versus corresponding potential to establish a voltammogram. Single or multiple cycles can be operated varying from different experimental requirements.

At a normal planar electrode inside static solution, cyclic voltammetry is conducted under assumption of semi-infinite diffusion and the electrochemical reaction is able to be characterized by the feature of the resulting voltammogram. For instance, Fig.E-2(B) presents a classic CV of a well-known redox mediator K<sub>3</sub>Fe(CN)<sub>6</sub> (100 μM) in PBS solution (pH=7.4) obtained on an ITO working electrode. In order to reduce Fe<sup>3+</sup> ion, we started CV scanning from +600 mV, a distant potential from the electroactive field of the analyte where background mainly came from the capacitive current (Fig.E-2(A)). We can see from Fig.E-2(B) that Fe<sup>3+</sup> ions began to be reduced to Fe<sup>2+</sup> from +250 mV and the reduction peak located at +105 mV. As the scanning direction was inversed, the Fe<sup>2+</sup> freshly generated by the reduction of Fe<sup>3+</sup> was immediately oxidized, resulting in an oxidation peak at +136 mV. Since the anodic and cathodic current peaks exhibited equal currents and the hysteresis of the anodic and cathodic potential peaks was less than +59 mV, demonstrating it is a well-behaved reversible system. Typically, from an established voltammogram, diverse qualitative and quantitative information such as concentration, diffusion coefficient, reaction thermodynamics, adsorption processes, and electron transfer kinetics are able to be extracted.

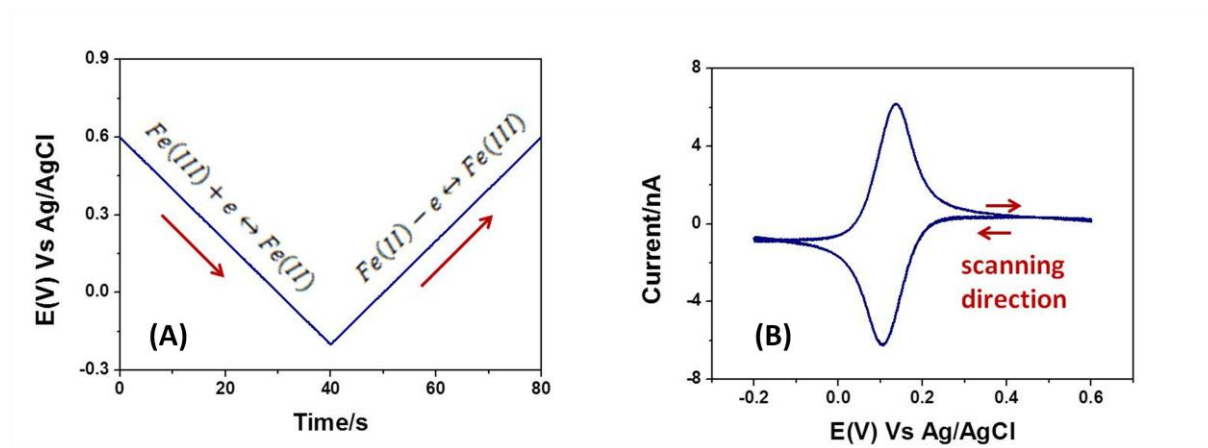


**Figure E-2** (A) Triangular voltage ramps applied to the ITO planar working electrode (320- $\mu\text{m}$  length  $\times$  200- $\mu\text{m}$  width), scan rate 20 mV/s; (B) Resulting CV of 100  $\mu\text{M}$   $\text{K}_3\text{Fe}(\text{CN})_6$  in PBS (pH=7.4).

Voltammogram with a peak as described above is frequently seen because diffusion layer keeps increasing over time. However, when an UME such as CFE is used as the working electrode, current is more likely to reach a limiting value due to the fast establishment of steady state.

### III.1.2 Amperometry

Amperometry is a common technique used for exocytosis investigation by means of monitoring electroactive biomolecules released at the surface of an electrode during exocytosis. So far, many researches with this approach have been carried out yielding important information about exocytosis and neurobiology. Generally, to perform amperometric measurement, an electrode is positioned in the close vicinity of a single cell, either on the top (with CFE electrode) or at the bottom (with ITO electrode), and a constant potential that is sufficient to oxidize the electroactive analyte is applied to the working electrode and the current is recorded as a function of time.

As illustrated in Fig.E-3(A), when CFE is employed as the working electrode, cells are seeded in a glass-bottom Petri dish and CFE is placed on the right top of the targeting cell to detect all the secretion. However, when it comes to ITO microdevice, cells are directly cultured on the transparent, pretreated ITO microelectrode which allows simultaneously cell observation and amperometric measurement of exocytosis (Fig.E-3(B)). No matter which microelectrode we choose, exocytotic events are always depicted as a series of oxidation spikes in amperometric measurement and each spike represent an individual exocytotic event, as presented in Fig.E-4.

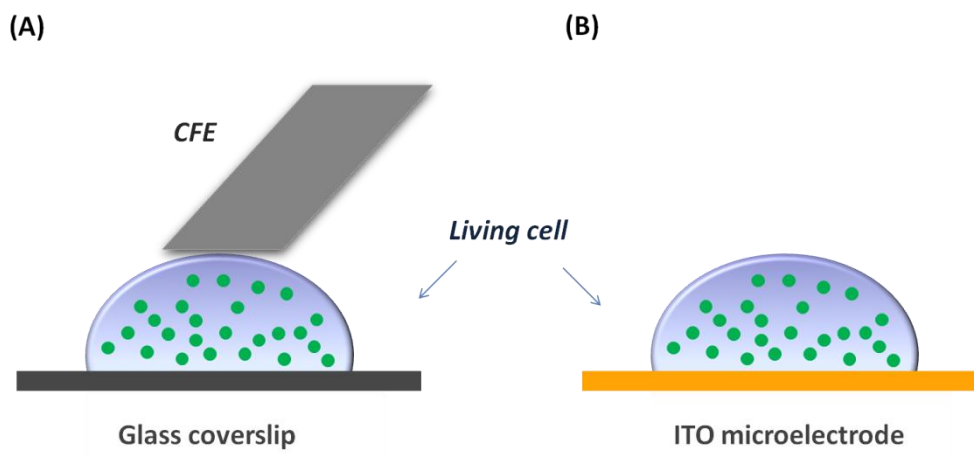


**Figure E-3** Amperometric detection of vesicular exocytosis of a single cell as performed at the apical pole with CFE (A) or at the basal pole with ITO planar microelectrode (B).

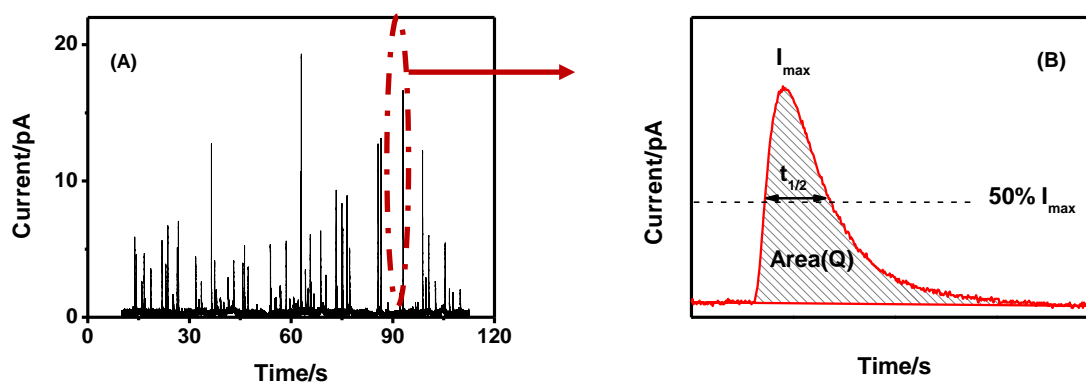
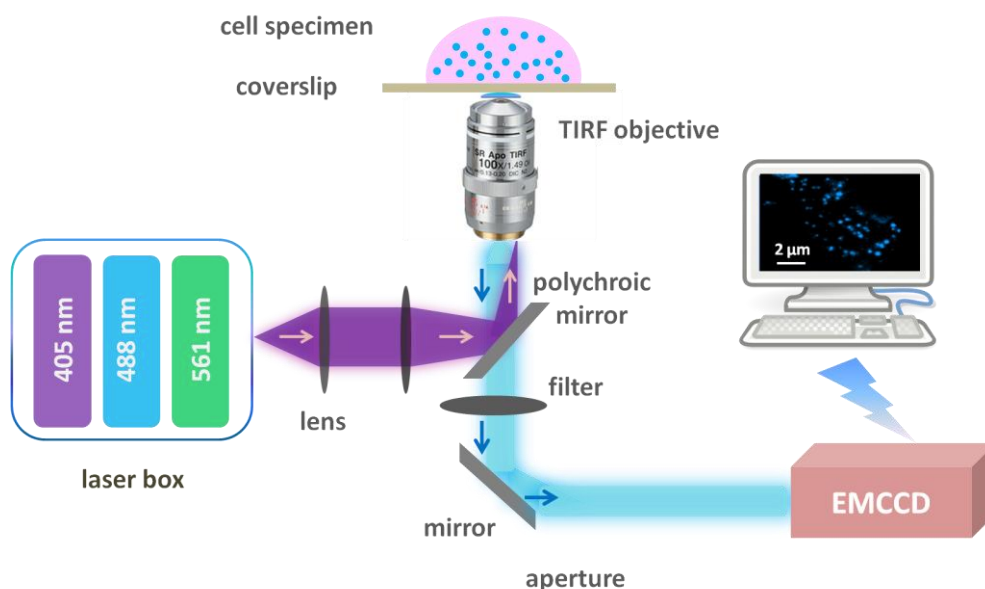


**Figure E-4** (A) Representative amperometric trace of exocytosis from single cell; (B) A typical individual spike extracted from the trace, with indicated characteristic parameters.

All the amperometric performances were carried out using a picoamperometer (model AMU-130, Radiometer Analytical Instruments, Copenhagen, DK) at a constant potential  $E = + 900$  mV vs. a Ag/AgCl reference electrode. The time course of the amperometric current was monitored (output digitized at 40 kHz) and stored on a computer (Latitude D600, Dell) through a D/A converter (Powerlab 4SP, AD Instruments) and its software interface (Chart version 4.2 for Windows, AD Instruments).

### III.2 TIRFM

There are two basic configurations to set up an instrument for TIRFM: the prism-based configuration and the objective-based configuration. In the prism-based method, a prism is attached to the coverslip surface to enable the achievement of critical angle when a focused laser beam is introduced to excite the fluorophores. The sample is therefore located in a narrow space between the objective and the prism, making it difficult to carry out manipulations on the cell specimen such as medium injection and physiological measurements. Considering these disadvantages of prism-based method, we built an objective-based TIRFM by using a high numerical aperture (NA) objective to simultaneously refract incident light beyond critical angle for illumination and collect fluorescence emission. This microscope can be used to acquire bright field, phase contrast, epi-fluorescent and TIRFM images of the same specimen (Scheme E-3).



*Scheme E-3 Schematic representation of experimental set-up for objective-based TIRFM configuration.*

All our TIRFM measurement were performed on the inverted Zeiss microscope (Zeiss, Tokyo, Japan) with a high numerical aperture 100× oil-immersion TIRF objective (1.45 NA, PlanApo, Zeiss), as presented in Scheme E-3. For the sake of the adaptation of various applications, we equipped multiline laser systems with different wavelengths at 405 nm, 488 nm and 561 nm as light sources to illuminate the fluorescence. The coupling of the laser to the microscope is achieved through a flexible optical fiber. The sample coverslip is placed above the 100× TIRFM objective with immersion oil ( $n=1.52$ ,

Nonfluorescence, Olympus) during test. When the laser is guided into the high aperture 100× TIRF objective at an angle beyond the critical angle  $\theta_c$ , a thin evanescent field is generated by the TIR of laser beam inside the objective. As a result, the targeting fluorophores are able to be excited within a defined distance by the evanescent wave and the resulting fluorescence is thus limited to a very thin layer at the interface. The fluorescence emission signal is firstly filtered by a band-pass emission filter (D460/40 nm Chroma Technology) and then collected by a scientific digital camera system called ‘electron multiplying charge coupled device’ (EMCCD), allowing image acquisition with optimal resolution, speed and sensitivity. Images and films with extremely high contrast and resolution could be acquired with the HCIImage software provided by Hamamatsu Company.

### **III.3 Time-lapse imaging**

Time-lapse imaging is a powerful technique whereby serial images are taken at regular time points to visualize cellular events and morphology over an extended period of time. Combining fluorescent probes and time-lapse imaging provides important information to analyze cellular processes in real time.

In order to identify the optimal incubation time of **1** in BON N13 or PC-12 cells for TIRFM experiments, time-lapse imaging experiments were performed on a Zeiss LSM 710 Laser Scanning Microscope equipped with a Plan Apochromat 63×/1.4 NA oil immersion objective and a heated incubation chamber with CO<sub>2</sub> supply. We controlled the CO<sub>2</sub> concentration (5%) as well as the temperature (37 °C) to create a friendly environment for living cell imaging. To follow traces of fluorescent **1** penetrating into the cellular vesicles, we used a 405 nm laser to excite its blue fluorescence. Dynamic viewing of this penetration process was then monitored over a period of 1 hour with a time interval of 2 min. ZEN software was used to collect the data.

## **IV Solution preparation**

### **IV.1 Buffer solutions**

All buffer solutions were made using ultrapure water from a Millipore purification system (resistivity of 18.2 MΩ cm at 25 °C) and unless stated, all the chemicals of analytical grade, were obtained from Sigma-Aldrich.

#### **Phosphate buffer saline**

Phosphate buffer saline (PBS, pH=7.4) containing 10 mM Na<sub>2</sub>HPO<sub>4</sub>, 2.68 mM KCl and 140 mM NaCl was used throughout in vitro experiments as well as BON N13 cells splitting. It was prepared by dissolving one PBS tablet (5g; Gibco) in 500 mL ultrapure water (Millipore) and stored at +4 °C.

### Locke's ×1 physiological saline

The Locke's ×1 physiological saline was used as buffer throughout the ex vivo experiments of BON N13 cells. It was diluted 10 times from Locke's×10 mother solution (pH=7.4) which was composed of 56 mM glucose, 1540 mM NaCl, 56 mM KCl, 50 mM Hepes and 36 mM NaHCO<sub>3</sub> and the solution pH was adjusted to 7.4 with concentrated NaOH solution (1M). For amperometric test of BON N13 cells, 2.5 mM CaCl<sub>2</sub> and 1.2 mM MgCl<sub>2</sub> were supplemented into Locke's×1 physiological saline. All the Locke's solutions were stored in -20 °C freezer after being filtered by vacuum driven sterile cup with 0.22 µm filter.

### HEPES physiological saline

The HEPES physiological saline was used as buffer throughout the ex vivo experiments of PC-12 cells. It consisted of 150 mM NaCl, 5 mM KCl, 1.2 mM MgCl<sub>2</sub>, 5 mM glucose, 10 mM HEPES and 2 mM CaCl<sub>2</sub> and was also filtered by vacuum driven sterile cup with 0.22 µm filter before being stored in -20 °C freezer.

## **IV.2 Solutions for experiments in vitro**

- **Stimulation solutions**

### Ionomycin solution

Ionomycin is an ionophore produced by the bacterium *Streptomyces conglobatus*. In this work, ionomycin solution was used to raise the intracellular level of calcium (Ca<sup>2+</sup>) so as to trigger the exocytosis of BON N13 cells. 10 µM ionomycin solution was diluted from 1 mM mother solution with Locke's ×1 physiological saline supplemented with 2.5 mM CaCl<sub>2</sub> and 1.2 mM MgCl<sub>2</sub>.

### K<sup>+</sup> solution

The concentrated K<sup>+</sup> stimulating solution was used to trigger the exocytosis of PC-12 cells. It consists of 55 mM NaCl, 100 mM KCl, 1.2 mM MgCl<sub>2</sub>, 5 mM glucose, 10 mM HEPES, and 2 mM CaCl<sub>2</sub>.

- **Collagen IV solution**

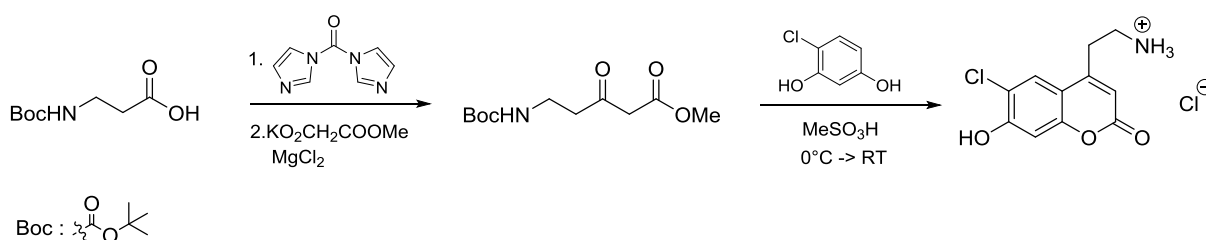
Collagen type IV (Sigma C5533) solution was prepared according to the protocol recommended by Sigma Company. In detail, 5 mg collagen was added into 50 mL 0.1 M glacial acetic acid and stirred at room temperature for 1-3 hours to obtain a 0.01% collagen solution (0.1 mg/mL). We then sterilized the solution by transferring it to a screw capped glass bottle and carefully added 10 mL chloroform which formed a layer beneath the collagen solution. After overnight incubation at +4 °C, the top layer of collagen was aseptically removed and stored in sterile tubes at +4 °C.

## V Sample preparation and measurement

### V. 1 Synthesis of **1**

As shown in Scheme E-4, the desired aminocoumarin, **1**, was synthesized within three steps from the commercially available BOC-protected  $\beta$ -alanine and the 4-chlororesorcinol by the organic chemists (Alexandra Savy, Sylvie Maurin and Laurence Grimaud) in our group according to the procedure reported by Sames and co-workers.<sup>[178]</sup>

To be specific, N-Boc- $\beta$ -alanine (2.5 g, 13.2 mmol, 1 equiv) was added in one portion to a suspension of 1,1'-carbonyldiimidazole (2.6 g, 15.8 mmol, 1.2 equiv) in 36 mL of THF. The resulting suspension was stirred under 4 h under argon. To the resulting yellow solution was added magnesium chloride (1.26 g, 13.2 mmol, 1 equiv) and methyl potassium malonate (4.1 g, 26.4 mmol, 2 equiv). The suspension was stirred overnight under argon. The reaction mixture was quenched with water (25 mL) and a 1M HCl (15 mL). The aqueous phase was extracted with ethyl acetate (3x100 mL). The organic layer was washed with 1M HCl (15 mL) and brine (15 mL), dried over  $\text{MgSO}_4$ , filtered and concentrated under reduce pressure to give the desired product as a yellow liquid (1.8 g, 57 %). After removing the solvent by aspiration, the residual orange solid was dried under high vacuum.



*Scheme E-4 Synthetic route of **1**.*

### V. 2 Optical and electrochemical characterization of **1**

- **Optical properties of **1****

#### Absorption spectra

UV-vis absorbance of **1** was measured at room temperature on an UV-vis spectrophotometer (Lambda 45; Perkin Elmer). To test the pH influence on absorption properties of **1**, we added 100  $\mu\text{L}$  **1** stock solution (10 mM in DMSO) into 9.9 mL phosphate buffer solution with different pH values

varying from pH 3 to pH 10 ( final concentration of **1**: 10  $\mu$ M). Their UV-vis absorption spectra were recorded from 250 nm to 456 nm with an interval of 1 nm and the scan rate was set at 1000 nm/min.

#### Excitation and emission spectra

Fluorescence measurements of **1** were performed on a fluorescence spectrofluorometer and a Xenon lamp was used as the light source. For emission scans, the excitation wavelength was set to the maximum absorption wavelength on the basis of UV-vis spectra and the emission wavelengths were scanned from 400 nm to 650 nm with an interval of 0.2 nm at a scan rate of 1000 nm/min to produce the emission spectrum. In reverse, we fixed the emission wavelength at 456 nm to record the excitation spectra of **1**. The excitation and emission band width were both preset at 2.5 nm. For pH influence studies, a final concentration of 10  $\mu$ M **1** diluted from 10 mM mother solution in DMSO was used.

- **Electrochemical properties investigation of 1**

#### CV based on GCE

Electrochemical measurements of **1** were carried out inside a Faraday cage, using a potentiostat (Autolab PGSTAT 30; Eco Chemie) controlled by GPES 4.9 software. As illustrated in Fig.E-5, a three-electrode system was built for CVs recording. 1 mm diameter GCE was employed as working electrode (WE) and the reference electrode (RE) was a commercial saturated calomel electrode (SCE, Radiometer Analytical) equipped with a bridge compartment filled with the same solvent/supporting electrolyte solution as in the electrolytic cell. 1-cm length platinum net was chosen as the counter electrode.

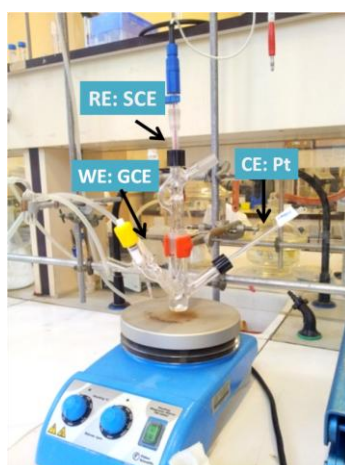


*Figure E-5 Experimental setup for CVs measurement of **1** with 1-mm GCE electrode.*

### CV based on CFE and ITO microelectrodes

As presented in Fig.E-6, all the voltammetric analyses based on ITO microelectrodes or CFE were performed with an EA162 Picostat (eDAQ, Australia) through an e-corder 401 system associated with EChem software inside a Faraday cage. The reference electrode was a Ag/AgCl reference electrode.

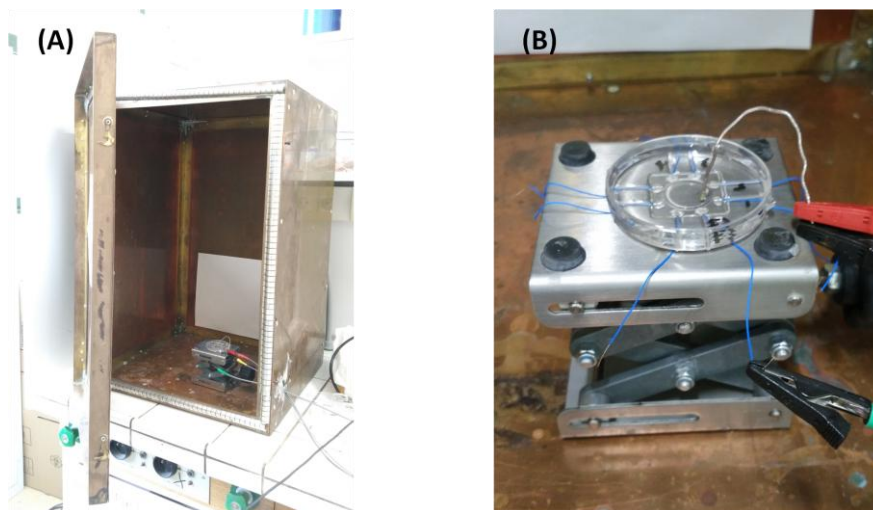


**Figure E-6** Experimental setup for CVs measurement of **1** with ITO microelectrode in a Faraday cage.

## V. 3 Experiments on living cells

### V.3.1 Preparations before cell seeding

- **Substrate treatment**

All the glass bottom Petri dishes (P50G-1.5-14-F, MatTek Cultureware, Ashland, MA) and ITO microdevices were pretreated by collagen IV (0.1 mg/mL) solution prior to cell seeding. 300  $\mu$ L collagen IV was added to cover the substrate surface and was kept for 6 hours in the incubator. Excess fluid was then removed and the microdevices were rinsed three times with PBS before use.

- **Stimulating capillary construction**

Glass capillary tubing (GC 120-10, Clark Electromedical Instruments) was divided into two identical capillaries with an internal diameter of 0.7 mm and outer diameter of 1.2 mm by the same vertical micropuller used for CFE fabrication. Once separated, their tips were polished on the diamond whetstone microgrinder for about 15~20 s to create a small tapered opening whose diameter varied

from 2~10  $\mu\text{m}$  at the end, as shown in Fig.E-7. These capillaries with small openings were checked under a microscope before cell stimulation.

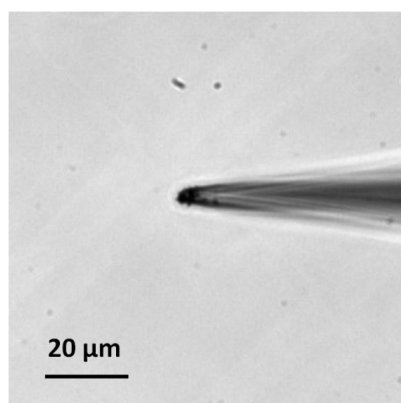


*Figure E-7* A typical glassy capillary with an opening end.

### ***V.3.2 Cell sample preparation***

In 75  $\text{cm}^2$  culture flask, confluent BON N13 cells and PC-12 cells were harvested by trypsinization process and centrifugation respectively, as previously described. In order to seed cells on the surface of our microdevices, both glass-bottom Petri dishes and ITO microchips, concentrated BON N13 or PC-12 cells were counted and resuspended in fresh culture medium at certain volume to reach a concentration of  $10^5$  cells per mL. 3 mL of cell suspension (c.a.  $3 \times 10^5$  cells) were immediately introduced into a microdevice precoated by collagen IV. To allow cells to well adhere and recover at the dish surface, microdevices with cells were maintained inside the incubator for 24~36 h. All the optical cell observations and electrochemical measurements were then performed in isotonic physiological saline (i.e. Locke's  $\times 1$  solution,  $\text{pH}=7.4$ ).

### ***V.3.3 TIRFM measurement***

In glass-bottom Petri dishes/our microfabricated ITO devices, cells were incubated in complete culture medium supplemented with 20  $\mu\text{M}$  **1** to let it penetrating into cellular vesicles. Before fluorescence measurements, cells were rinsed 3 times by PBS to get rid of excessive **1** and were then incubated in 3 mL Locke's  $\times 1$  solution during test. For investigation of single exocytotic event using **1** as fluorescent probe, in TIRFM, a 405 nm laser (50 mW, CMA1-01983, Newport, NJ) was employed as the light source to initiate the fluorescence and the emission light was filtered by an optical filter (band-pass: D460/40) before being detected by EMCCD. Once choosing a region of interest typically encompassing a single cell, the observation depth was controlled by changing the incident angle of

405 nm laser. The quality of fluorescent images could be also optimized by the adjustment of gain, sensitivity as well as the exposure time (i.e. the frame rate). We then put a stimulating capillary at a distance of 10~20  $\mu\text{m}$  from the cell to trigger exocytosis and an image series containing sequential frames were recorded for 1 to 2 min upon stimulation.

#### ***V.3.4 Amperometric detection by CFE***

The amperometric detection of cellular exocytosis by CFE was conducted with cells grown on glass-bottom Petri dishes. CFE was pre-polished at an angle of  $45^\circ$  for 6 min on a diamond particle whetstone microgrinder (EG-4; Narishige) before each test to create the reproducible, fresh electrode surface.

After 24~36 h incubation, cells were firstly rinsed by PBS solution and cell culture medium was then replaced by Locke's $\times$ 1 solution. Electrochemical detection based on individual cell was carried out on the platform of an inverted microscope (Axiovert-135, Carl Zeiss, Germany), as shown in Fig.E-8.

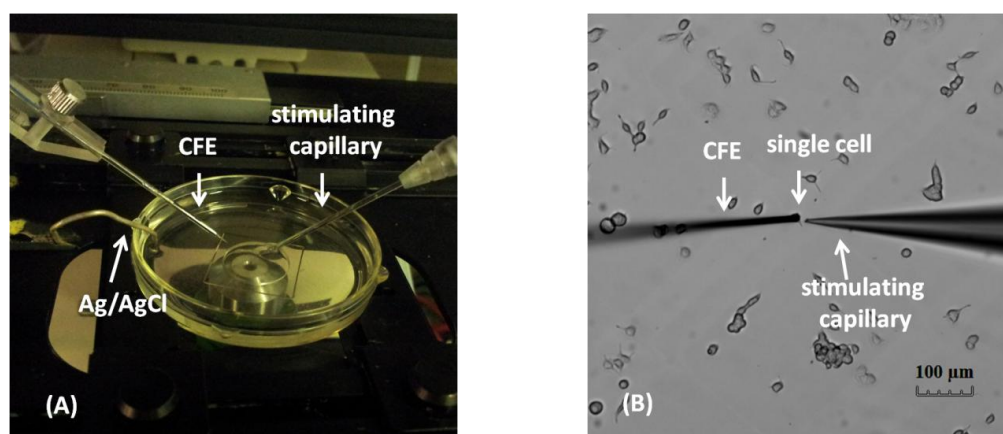


**Figure E-8** (A) Amperometric measurement by CFE performed on the platform of inverted microscope inside a Faraday cage. (B) Two-electrode configuration during single-cell monitoring,  $10\times$  objective. Position of working electrode and stimulating capillary were controlled by micromanipulator.

After finding the target isolated cell, CFE was brought against the cell membrane with the help of a micromanipulator (Model MHW-103, Narishige Co., London, UK). The close proximity of the electrode surface to the cell surface was confirmed by a slight deformation in the outline of the cell. Then, with a second micromanipulator, a glass microcapillary (2~10  $\mu\text{m}$  diameter) filled with stimulating solution was placed at a distance of 10~20  $\mu\text{m}$  from the cell so as to trigger the exocytosis

for a certain time through a micro-injector (Femtojet injector, Eppendorf Inc., Hamburg, Germany). A constant potential of +900 mV Vs Ag/AgCl reference electrode was applied to the CFE working electrode by a potentiostat AMU-130 and current was recorded as function of time.

### ***V.3.5 Amperometric detection by ITO microelectrode***

Amperometric measurement of exocytosis by microfabricated ITO device was carried out on the platform of an inverted microscope inside a Faraday cage, as shown in Fig.E-9. Cells were firstly seeded into the ITO microdevice (Fig.E-10(A) and (B)). A constant potential of +900 mV Vs Ag/AgCl reference electrode was applied to a single ITO working electrode by a potentiostat AMU-130 and current was recorded as function of time. Individual cells grown on ITO microelectrode were selected for detection and a microcapillary filled with stimulating solution was positioned against the cell.

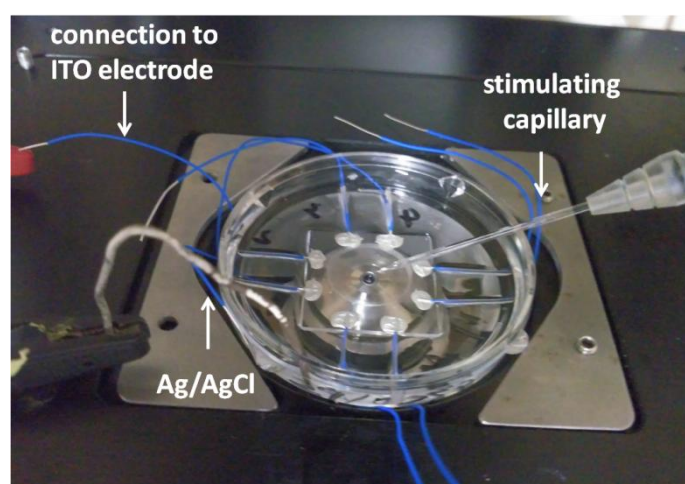


**Figure E-9** Amperometric measurement by microfabricated ITO device performed on the platform of inverted microscope inside a Faraday cage.

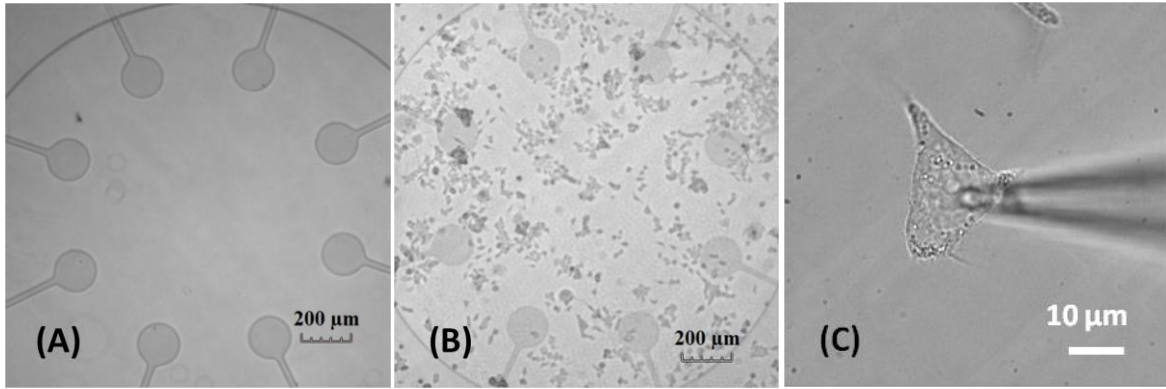


**Figure E-10** A microfabricated device embedded with 8 ITO microelectrodes before (A) and after (B) cell seeding; A single cell on ITO microelectrode (not seen in the image) with a stimulating capillary on the top (C).

### V.3.6 TIRFM/amperometry coupling test on ITO microdevice

TIRFM/amperometry coupling test for exocytosis investigation was also performed on a microfabricated ITO device (Fig.E-11). These two modes of detection were triggered at the same time on a single cell and the corresponding of oxidation current and fluorescent release of each detected exocytotic event was manually correlated.

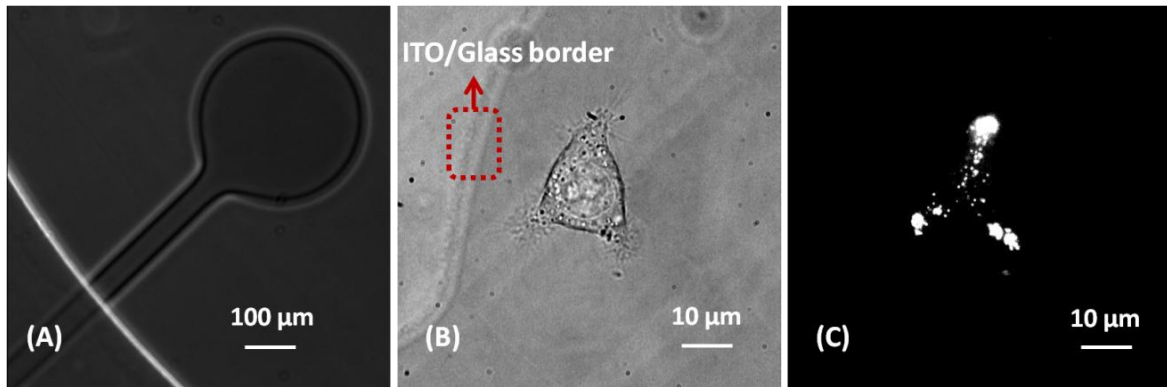


**Figure E-11** (A) Photograph of an individual ITO electrode before cell seeding; (B) A single BON N13 cell extracted from left image: vertical dashed lines depict the position of the border between transparent ITO electrode and glass; (C) The fluorescent single BON N13 cell marked by 1.

## Appendix

In parallel with this thesis on the employment of fluorescent/electroactive dual probe **1** in TIRFM/amperometry coupling measurement of exocytosis in BON N13 cells at ITO microelectrodes, we started another related project with Drs. Ana-Maria Lennon-Duménil and Marine Bretou in Institut Curie during the renovating work in ENS. The main objective was indeed to develop an analytical ITO microdevice adapted to the detection of exocytotic secretions of migratory dendritic cells (DCs) in the 3D confined PDMS channels. (Fig.appendix-1)

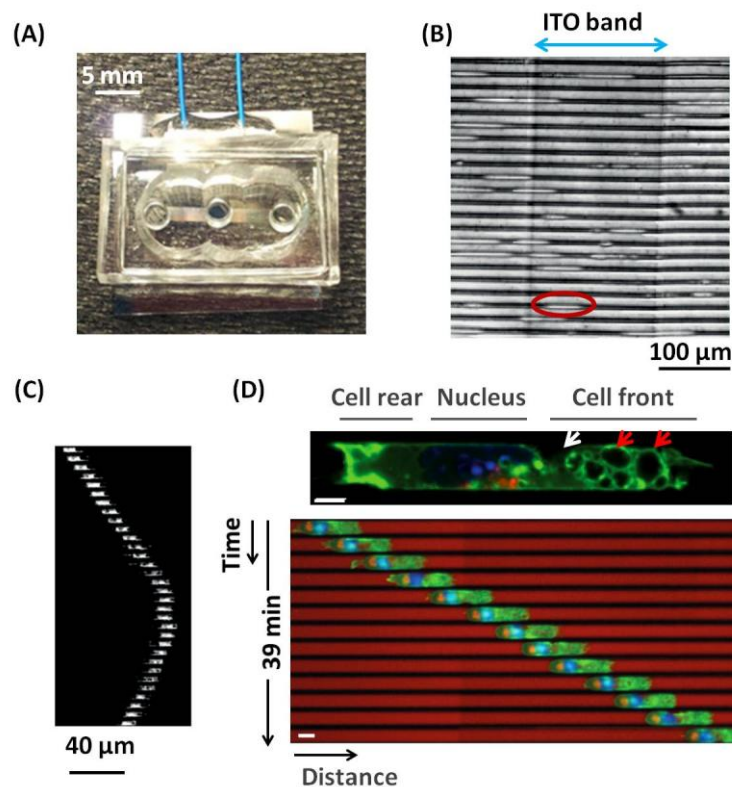


**Figure appendix-1** (A) ITO microdevice for amperometric detection; (B) DCs migrating to ITO/glass substrate; the red ellipse indicates the single migratory DC lying on ITO band; (C) A typical example of an individual DC migrating in PDMS microchannels. Sequential images (time interval: 2 min) were processed to remove the channels so that only the cells are visible (white) (D) Top: A Life-act-GFP DC in microchannel; Bottom: sequential images (time interval: 3 min; scale bar: 5 μm) of the life-act-GFP DC migrating in microchannels filled with OVA AF-647 (in red).

Our ITO microchip (Fig.appendix-1(A)) embedded multiple parallel PDMS channels (around 80 3D confined channels per chamber) that mimic their natural constrained environment of tissues for patrolling in search of danger associated antigens through an endocytotic process called macropinocytosis and the transparent property of ITO facilitated the observation of DCs' behaviors through high-resolution microscopy. As shown in Fig.appendix-1(B-C), after overnight incubation, DCs previously loaded into the entry plug of the ITO microdevice spontaneously entered into PDMS microchannels and were able to move across the ITO electrode, without any mechanical or chemical stimulation. In order to coordinate membrane trafficking and prevent cell volume increment, DCs will release part of their contents back to the extracellular medium while migrating (Fig.appendix-1(D)). Through electrochemical measurements, we demonstrated that exocytotic events of migratory DCs could be properly monitored by our ITO microdevice.

An article on the topic has been accepted by Electroanalysis (DOI: 10.1002/elan.201600360) and the article is attached below.

# Indium Tin Oxide Microsystem for Electrochemical Detection of Exocytosis of Migratory Dendritic Cells

Xiaoqing Liu,<sup>a,b</sup> Marine Bretou,<sup>c</sup> Ana-Maria Lennon-Duménil,<sup>c</sup> Frédéric Lemaître,<sup>a,b</sup> Manon Guille-Collignon<sup>a,b\*</sup>

<sup>a</sup> Ecole normale supérieure, PSL Research University, UPMC Univ Paris 06, CNRS, Département de Chimie, PASTEUR, 24, rue Lhomond, 75005 Paris, France

<sup>b</sup> Sorbonne Universités, UPMC Univ Paris 06, ENS, CNRS, PASTEUR, 75005 Paris, France

<sup>c</sup> INSERM U932, Inst Curie, 12, rue Lhomond, 75005 Paris, France

\* e-mail: manon.guille@ens.fr

## Abstract

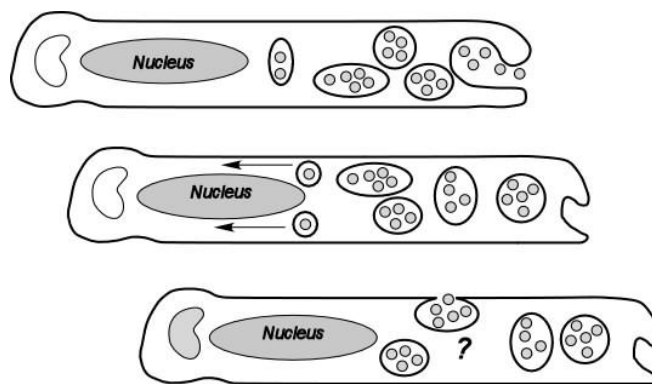
The design, fabrication and test of an indium tin oxide (ITO) microdevice to investigate exocytotic behaviors of migratory dendritic cells (DCs) in confined three-dimensional environment were reported in this work. Indeed, immature DCs were able to migrate into micro-fabricated biocompatible polydimethylsiloxane (PDMS) channels that mimic their natural constrained environment of tissues for patrolling in search of danger associated antigens through an endocytotic process called macropinocytosis. In order to coordinate membrane trafficking and prevent cell volume increment, DCs will release part of their contents back to the extracellular medium while migrating. Through electrochemical measurements, we demonstrated that exocytotic events of migratory DCs could be monitored by our ITO microdevice. In addition, the transparency of ITO electrode should facilitate future combining assays of exocytosis with other fluorescence-based measurements of cell physiology.

**Keywords:** Electrochemical detection; Exocytosis; ITO microsystem; Dendritic cells; Cell migration

Dendritic cells (DCs), the most potent antigen (AG) presenting cells, are the sentinels of the immune system.<sup>[1-3]</sup> They effectively patrol peripheral tissues in search of danger associated AG through a biological phenomenon called “macropinocytosis”. This process constitutes the first step of the adaptive immune response and significantly relies on specific DCs properties, including their high endocytic capacity<sup>[4, 5]</sup> as well as their efficient motility<sup>[6]</sup> in confined three-dimensional (3D) environments. Macropinocytosis represents a distinct pathway of endocytosis in mammalian cells (Scheme 1).<sup>[7-9]</sup> It includes the uptake of cargo from the extracellular medium by macropinosomes, the preservation of the surface membrane area, and the regulation of membrane traffic along the intracellular pathway. Interestingly, previous study<sup>[7]</sup> shows that macropinosome traffic is not unidirectional (endocytic), but bidirectional (endocytic and exocytotic), indicating that DCs macropinocytosis is accompanied by exocytotic events. Recently, high resolution time-lapse imaging confirms that exocytosis is taking place when DCs migrate in the confined 3D microchannels.<sup>[10]</sup> Such secretory events might favor matrix remodeling and membrane recycling required for cell migration. Moreover, this exocytotic process taking place in DCs plays an important role in proper cell communication/activation, and need to be tightly controlled in order to allow either an efficient clearance of pathogens, or the maintenance of immune homeostasis. Characterization of exocytosis of migratory DCs is thus significant to better understand the cellular trafficking in 3D-confinement.

In this context, secretion coupled to cell migration has been poorly addressed. This is why we considered to use amperometry in 3D-confined microchannels that mimics the confined environment in which DCs migrate. Indeed, amperometry is a routine analytical technique for quantitative, real-time monitoring of exocytosis at single cell level.<sup>[11, 12]</sup> In general, a microelectrode is positioned in the close vicinity of a target cell during amperometric measurement, either on the top or at the bottom, and a constant potential is applied to the working electrode at which electrochemical biomolecules (mainly catecholamines) released during exocytosis could be oxidized. As a consequence, the exocytotic fluxes are depicted as a series of amperometric current spikes and each single spike results from an individual exocytotic event.<sup>[13]</sup> The frequency and shapes of amperometric spikes elucidate particular information about the dynamics of the release process while their integrals give the exact quantity of electroactive molecules released. Different microelectrodes (carbon fiber<sup>[11, 13-15]</sup>, Au<sup>[16]</sup>,

Pt<sup>[17]</sup>...) have been employed for amperometric detection of electroactive molecules discharged from individual vesicle during exocytosis. Among them, indium tin oxide (ITO) microelectrodes appear to be a good choice due to their excellent optical transparency, high electrical conductivity as well as their appropriate electrochemical working window for the electroanalysis of biomessengers. Our group and others have been developing microchips based on transparent ITO microelectrodes on a glass substrate in order to facilitate higher throughput measurements of exocytosis as well as to enable fluorescent measurements that are not possible with usual carbon-fiber electrodes.<sup>[18-22]</sup>



Scheme 1. Schematic view of macropinocytosis process. Top : Formation of macropinosomes at the front of the migrating dendritic cell while it is moving. Middle : Antigen presentation towards the back of the cell, behind the nucleus. Vesicles undergo series of morphological changes to concentrate the internalized antigen. Bottom: Possible exocytotic event towards the extracellular medium so as to achieve the membrane retrieval and excessive fluid discharge.

To the best of our knowledge, there have been so far few researches focusing on studies of exocytotic behaviors of DCs. In 2006, by means of fluorescent microscopy, macropinocytosis of DCs was found to be a regulated coordination of endocytic and exocytotic membrane traffic events.<sup>[7]</sup> The membrane release of serotonin from DCs upon ATP stimulation was also confirmed by amperometric measurement with carbon fiber microelectrode.<sup>[23]</sup> However, these studies have been mainly performed *ex vivo* on flat two-dimensional (2D) surfaces and such substrates rarely apply to *in vivo* cell migration, which mainly occurs in 3D confined environment. Exocytotic behaviors of migratory DCs in 3D confinement, as *in vivo*, were investigated in this article by designing and fabrication of a PDMS microchannels/ITO microsystem (Fig.1(A)) allowing

simultaneous observation of cells and amperometric detection of exocytosis as described herein. (The details concerning ITO microdevice assembly are shown as supporting information in Fig.S-1)

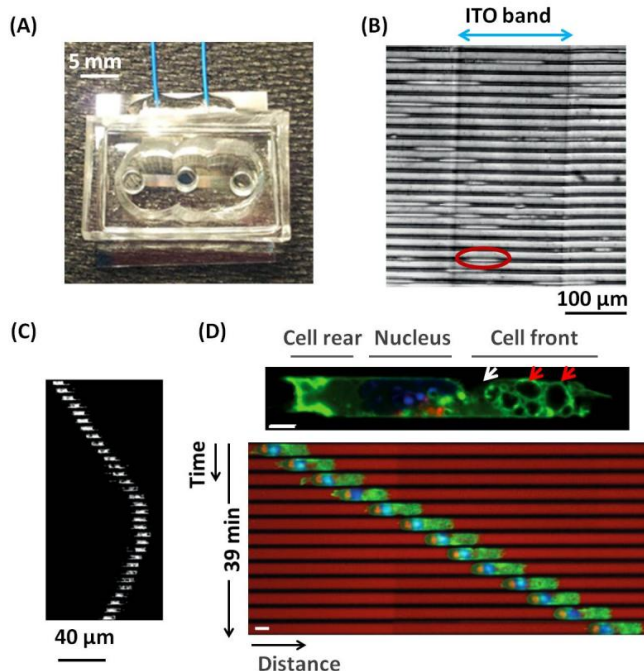


Figure 1. (A) ITO microdevice for amperometric detection; (B) DCs migrating to the fibronectin coated ITO/glass substrate; the blue double headed arrow depicts the position of the transparent ITO microelectrode and the red ellipse indicates the single migratory DC lying on ITO band; (C) A typical example of an individual DC migrating in 4.5- $\mu\text{m}$  width\*5- $\mu\text{m}$  height fibronectin-coated microchannels. Sequential images were processed to remove the channels so that only the cells are visible (white). Temporal sequences were put one below the other (Magnification 10 $\times$ , the interval between two images is 2 min, scale bar 40  $\mu\text{m}$ ). (D) Top: A representative Life-act-GFP DC in 8- $\mu\text{m}$  width\*5- $\mu\text{m}$  height fibronectin-coated microchannels: the nucleus was stained with Hoechst (in blue); lysosomes in red were tagged with WGA-AF647 and macropinosomes of the migrating DC were indicated by the white arrows at the cell front (Magnification 60 $\times$ ); Sequential images of the life-act-GFP DC migrating in microchannels filled with OVA AF-647 (in red). Temporal sequences were put one below the other (Magnification 20 $\times$ , one image every 3 min, scale bar: 5  $\mu\text{m}$ ). DC was able to internalize the OVA-647 in the channels and it was finally accumulated into the lysosomes at the cell rear during migration Several events of secretions might be envisioned for a single DC.<sup>[23]</sup> For instance, a vesicle formed at the cell front could be exocytosed (indicated by the red arrow in the top image).

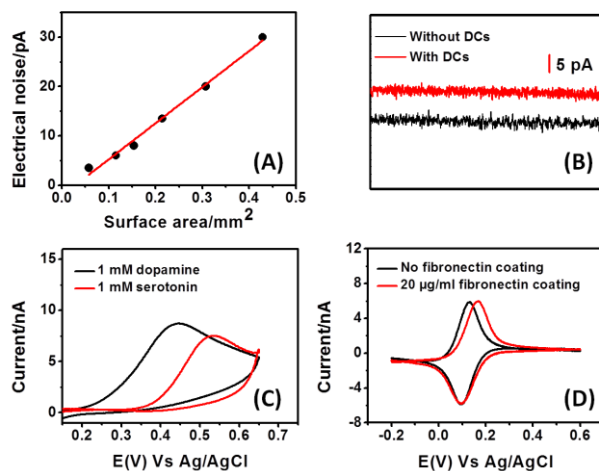


Figure 2. (A) Measurements of the electrical noise in PBS (pH=7.4) at a constant potential value ( $E=+650$  mV vs. Ag/AgCl) as a function of electrodes dimensions ( $y=70x-2$ ,  $R^2=0.948$ ); (B) Electrical noise of ITO microelectrode with and without DCs and its dimension is of 200  $\mu\text{m}$  by 320  $\mu\text{m}$ ; (C) Cyclic voltammograms of 1 mM serotonin and 1 mM dopamine in PBS solution (pH=7.4) respectively, scan rate 20 mV/s. (D) Cyclic voltammograms of 100  $\mu\text{M}$   $\text{K}_3\text{Fe}(\text{CN})_6$  in PBS (pH=7.4) on ITO electrode with and without fibronectin treatment, scan rate 20 mV/s.

3D-confined microchannels made of PDMS, a biocompatible silicone elastomer, have been demonstrated to be able to induce DCs to move inside the microchannels at speeds similar to those observed *in vivo*.<sup>[6, 10, 24, 25]</sup> In our case, the transparent property of the bottom ITO-embedded glass slide allowed us to observe DCs' behaviors through high-resolution microscopy. Additionally, multiple parallel channels in each device (around 80 channels per chamber), enabled an easy recording of many cells' behaviors at low magnification. As shown in Fig.1 (B), after overnight incubation, DCs previously loaded into the entry plug of the ITO microdevice spontaneously entered into PDMS microchannels and were able to move across the ITO electrode, without any mechanical or chemical stimulation. By tracking DCs' migration along PDMS microchannels with time-lapse imaging, we noticed that not all the cells acted at the same way inside the microchannels (see movie 1 shown in supporting information). Firstly, there were big differences of cell sizes; secondly, most cells underwent important speed fluctuations during motion, resulting in different migration distances; finally, some cells showed changes in direction during migration (Fig.1 (C)). However, after overnight incubation, we always saw DCs moving on ITO electrode.

As shown in Fig.1(D), by staining the different compartments of DCs with specific dyes, we found that while migrating along the microchannels, DCs could

form lots of macropinosomes (as indicated by the white arrows in Fig.1(D)) in front of the nucleus to sample the microenvironment so as to take up extracellular antigens and the internalized antigens were accumulated in lysosomes at the cell rear (Fig.1(D)). We thus believe that migrating DCs are able to expel part of their contents to the extracellular space so as to achieve the coordination of endocytic and exocytotic membrane trafficking. That is, exocytotic events are properly taking place during migration. Previous studies have shown that DCs are able to not only accumulate neurotransmitters but also synthesize, store and degrade them. Since neurotransmitters play important roles in immune response of DCs,<sup>[26, 27]</sup> we try to figure out if there are electroactive neurotransmitters, like serotonin or dopamine, expelled by DCs during migration with amperometric detection.<sup>[23, 28-30]</sup> This is different from what have been shown before in the literature in the way that secretion is monitored here while the DCs are confined in 3D microdevices and are migrating into the ITO microsystem channels assembly.

Fig.2(A) presents the relationship between the current noise and the surface area of ITO working electrode of which the band widths varied from 200  $\mu\text{m}$  to 1000  $\mu\text{m}$ . Globally the line depicts a good linear fit with a slope of 0.07  $\text{fA}/\mu\text{m}^2$ . Moreover, the best electrical properties were obtained from 200  $\mu\text{m}$  ITO band with minimum surface area of 0.06  $\text{mm}^2$ , with a rms noise of typically 2 to 4 pA, which is consistent with our previous work based on ITO microelectrodes.<sup>[21]</sup> We also compared the current noises obtained from ITO microelectrodes with and without DCs. As illustrated in Fig.2 (B), migratory DCs adjacent to ITO electrodes didn't increase the background noise for amperometric recordings. All measurements were performed in PBS (phosphate buffer saline) solution and no obvious difference was seen for the two parallel ITO microelectrodes in the same microdevice.

Fig.2(C) shows cyclic voltammograms of two well-known neurotransmitters (1 mM serotonin and 1 mM dopamine) inside the 3D-confined microchannels collected on ITO microelectrode at a scan rate of 20 mV/s. We can see that dopamine started to be oxidized at about +200 mV while the oxidation of serotonin occurred at +400 mV, and their oxidation peaks were located at around +450 mV and +550 mV, respectively. According to the results mentioned above, our ITO microdevice is adequate from an electrochemical point of view for amperometric detection of these electroactive neurotransmitters release. Therefore, in the following experiments, we applied a potential of +650 mV to track neurotransmitter release from DCs on ITO electrode by

amperometric measurement, this value being identical with the one we used to detect serotonin discharged from cells by carbon-fiber and ITO electrodes in previous references.<sup>[21, 22, 31]</sup>

In our microdevice, the bottom surface for DCs' migration is composed by both ITO and glass, showing inhomogeneity, further surface treatment is thus necessary to let DCs adhere and spread in PDMS microchannels. For the sake of creating a homogenization of the whole surface, we pre-coated the microchannels with 20  $\mu\text{g}/\text{mL}$  fibronectin solution for one hour. To investigate whether electrochemical properties of ITO electrodes were affected by fibronectin treatment, we compared cyclic voltammogram of a well characterized redox mediator  $\text{K}_3\text{Fe}(\text{CN})_6$  (100  $\mu\text{M}$ ) acquired on naked ITO microelectrode with that obtained from 20  $\mu\text{g}/\text{mL}$ -fibronectin precoated ITO band. As shown in Fig.2 (B), besides the slightly shift of the oxidation peak, fibronectin coating did not alter the electrochemical detection at ITO microelectrodes.

In our 3D-confined PDMS microchannels that mimic the natural constrained environment of tissues, DCs were able to migrate through the ITO microelectrode (Fig.1(B)). Previous study shows that for migrating DCs, exocytosis was taking place so as to empty part of the ingested fluid as well as to recycle the internalized membrane during macropinocytosis (Fig.1(D)).<sup>[10]</sup> In this present work, based on ITO microelectrode, we tried to investigate the spontaneous exocytotic events of migratory DCs by amperometric detection, which provides the accurate amount of released biomolecules and precise kinetic characteristics with high sensitivity and sub-millisecond temporal resolution.

We applied a +650 mV constant potential at the ITO electrode vs. Ag/AgCl and recorded the current as a function of time. The exocytotic release trace from migratory DCs in 3D-confined PDMS microchannels thus appeared as a succession of individual, well separated amperometric spikes, as presented in Fig.3(A). At a potential at the foot of the oxidation waves of dopamine or serotonin (see Fig.2(C), respectively, 100 and 300 mV vs. Ag/AgCl, no spikes were detected (data not shown). The current spikes suggested electroactive biomolecules were discharged by migratory DCs and then immediately oxidized at ITO surface, confirming the viewpoint that macropinocytosis of migratory DCs is accompanied by exocytotic events, resulting in the coordination of endocytic and exocytotic membrane trafficking. It is important to note that this secretion is detected in the absence of any stimulation/secretagogue nor prior loading of the cells with any neurotransmitter or electroactive molecule, pointing out the facts that the

DCs have endogenous electroactive neurotransmitters<sup>[27]</sup> and that the spontaneous secretion is probably triggered by confinement. Indeed the same experiments performed in Petri dishes with the technique of carbon fiber microelectrodes used by amperometry showed no secretion in the absence of stimulation or prior loading of the cells (data not shown).

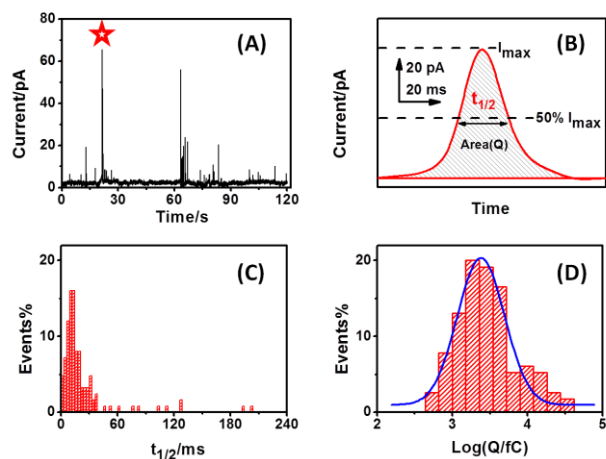


Figure 3. (A) Representative amperometric trace monitored on the 3D-confined ITO microdevice from migratory DCs; (B) A typical amperometric spike extracted from amperometric trace (indicated by the red star); (C) Histogram of half-height width ( $t_{1/2}$ ); (D) Statistical logarithmic distributions ( $y = 0.2e^{-5.6(x-3.4)^2}$ ,  $R^2 = 0.932$ ) of the charge  $Q$  obtained for each exocytotic event electrochemically detected on the 3D-confined ITO microdevice for DCs.

Fig.3(B) displays a typical single oxidative spike on expanded time scale extracted from Fig.3(A), which is corresponding to an individual exocytotic event. In amperometric measurement, maximum current amplitude  $I_{max}$  (pA), half-height width  $t_{1/2}$  (ms) and area  $Q$  (pC) are typical characteristics for a single spike analysis. Note that  $I_{max}$  represents the maximum release flux,  $t_{1/2}$  is defined as the time interval where current amplitude exceeds 50% of  $I_{max}$  while the integral charge  $Q$  was employed to calculate the precise release amount on the base of Faraday's law. For migratory DCs, we analyzed the results from a total of 125 events with a wide range of amplitudes varying from 5 to 120 pA (mean value,  $21.9 \pm 3.4$  pA) and histograms of  $t_{1/2}$  and integral  $Q$  were presented separately in Fig.3(C) and Fig.3(D). The distribution of  $t_{1/2}$  values shows a half-height width of a few milliseconds, with a mean value of  $25.05 \pm 3.44$  ms and the mean  $Q$  value is  $0.74 \pm 0.16$  pC. However, larger, more irregularly shaped events also occurred (see Fig.S-2

shown in supporting information). These spikes may come from sites further from ITO microelectrode or represent multiple releases or another type/size of vesicles.

We have designed and manufactured an effective 3D-confined ITO/PDMS microdevice which allows simultaneously cell observation and amperometric measurement of exocytosis from migratory DCs. The phenomenon that macropinocytosis of migratory DCs is accompanied by exocytotic events was monitored by amperometric detection. We propose that our experiments will identify specific modes of exocytosis and will display the mutual interaction of endocytic and exocytotic trafficking of DCs as well as will quantitatively analyzing exocytosis during cell migration. In addition, further optimization of our microdevice based on transparent ITO microelectrode should facilitate future real-time combining assays of DCs' exocytotic behaviors with other fluorescence technology.<sup>[22, 32, 33]</sup> By doing so, correlations between place (on the DC surface, rear or front) or size of vesicles (lysosomes, macropinosomes etc...) and quantitative parameters of secretion could be drawn.

### Experimental

ITO microelectrodes were manufactured by photolithographic process and acidic wet etching (see Fig.S-1(A) shown in supporting information). A thin film of ITO (90%  $In_2O_3$ /10%  $SnO_2$ ; 150 nm thickness; ACM, Villiers Saint Frédéric, France) was previously sputtered onto optical glass slides (22 mm  $\times$  22 mm  $\times$  0.13 mm) in order to afford a material of low electrical resistance ( $\leq 20$  ohms per square) and transparency. To be specific, firstly, an insulating photoresist (AZ 9260, Clariant GmbH, Germany) was patterned onto the ITO/glass slides by the following steps: (a) spin-coating (b), prebaking on a hotplate at 110°C, exposure to UV light through a specific mask design (c) and development (AZ 400K+  $H_2O$ ) (d). Then, the ITO with no "photoresist protective layer" was chemically etched by commercial HCl solution and the photoresist remaining on ITO band was removed with acetone. This 'wet etching' step left two identical ITO microelectrodes of about 200- $\mu$ m width respectively on the glass slide.

Biocompatible PDMS microchannels with the inlet and outlet ports were prepared as previously described.<sup>[24, 25]</sup> In brief, microchannels were fabricated in PDMS using rapid prototyping and soft lithography. As a result, for each PDMS chamber (see Fig.S-1(B) shown in

supporting information), multiple microchannels are run in parallel which makes it suitable for multiple cells observation. Moreover, we fixed a homemade PDMS gasket with diameter of 1.5 cm onto the top of the PDMS microchannels so as to hold the culture medium, making the chamber an appropriate environment for cells ((see Fig.S-1(C) shown in supporting information)). PDMS chamber and the ITO-embedded glass slide were then activated in a plasma cleaner (PDC-32G Harrick) for 1 min at 400 mTorr and were stuck together. One hour incubation in 60 °C oven was used to strengthen the binding. The upper surface of the microchip was then activated by plasma treatment for 2 min at 400 mTorr to produce hydrophilic inlet which enabled 20 µg/mL fibronectin (fibronectin from bovine plasma 0.1% solution) to fill into the microchannels. After one hour coating at room temperature, the microchip was rinsed 3 times with PBS. The system could be used immediately or stored up to 3 days at +4 °C. Before loading cells, microchannels were washed twice with cell culture medium and kept in the incubator while collecting cells.

Amperometric detection of exocytosis at ITO microelectrodes was carried out using a picoamperometer (model AMU-130, Radiometer Analytical Instruments, Copenhagen, DK) at a constant potential  $E = + 650$  mV vs. a silver/silver chloride reference electrode (Ag/AgCl, a 1-mm diameter wire). The time course of the amperometric current was monitored (output digitized at 40 kHz) and stored on a computer (Latitude D600, Dell) through a D/A converter (Powerlab 4SP, AD Instruments) and its software interface (Chart version 4.2 for Windows, ADInstruments). The significant parameters of an amperometric spike are the maximum oxidation current  $I_{max}$  (pA), the half-height width  $t_{1/2}$  (ms) and the total electrical charge  $Q$  (pC). All the values are presented as the mean  $\pm$  s.e.m. (standard error of the mean = standard deviation/ $\sqrt{n}$ , where  $n$  is the number of spikes analyzed). Voltammetric analyses were performed with an EA162 Picostat (eDAQ, Australia) through an e-corder 401 system associated with EChem software. The reference electrode was also Ag/AgCl.

## References

- [1] M. F. Lipscomb, B. J. Masten, *Physiol. Rev.* **2002**, *82*, 97-130.
- [2] J. Banchereau, R. M. Steinman, *Nature* **1998**, *392*, 245-252.
- [3] J. Banchereau, F. Briere, C. Caux, J. Davoust, S. Lebecque, Y. T. Liu, B. Pulendran, K. Palucka, *Annu. Rev. Immunol.* **2000**, *18*, 767-+.
- [4] A. E. Morelli, A. T. Larregina, W. J. Shufesky, M. L. G. Sullivan, D. B. Stolz, G. D. Papworth, A. F. Zahorchak, A. J. Logar, Z. L. Wang, S. C. Watkins, L. D. Faló, A. W. Thomson, *Blood* **2004**, *104*, 3257-3266.
- [5] W. S. Garrett, L. M. Chen, R. Kroschewski, M. Ebersold, S. Turley, S. Trombetta, J. E. Galan, I. Mellman, *Cell* **2000**, *102*, 325-334.
- [6] M. L. Heuze, P. Vargas, M. Chabaud, M. Le Berre, Y.-J. Liu, O. Collin, P. Solanes, R. Voituriez, M. Piel, A.-M. Lennon-Dumenil, *Immunol. Rev.* **2013**, *256*, 240-254.
- [7] S. Falcone, E. Cocucci, P. Podini, T. Kirchhausen, E. Clementi, J. Meldolesi, *Journal of Cell Science* **2006**, *119*, 4758-4769.
- [8] A. T. Jones, *Journal of Cellular and Molecular Medicine* **2007**, *11*, 670-684.
- [9] M. C. Kerr, R. D. Teasdale, *Traffic* **2009**, *10*, 364-371.
- [10] M. Chabaud, M. L. Heuzé, M. Bretou, P. Vargas, P. Maiuri, P. Solanes, M. Maurin, E. Terriac, M. Le Berre, D. Lankar, T. Pilot, R. S. Adelstein, Y. Zhang, M. Sixt, J. Jacobelli, O. Bénichou, R. Voituriez, M. Piel, A.-M. Lennon-Duménil, *Nature Communications* **2015**, *6*, 7526.
- [11] C. Amatore, S. Arbault, M. Guille, F. Lemaître, *Chemical Reviews* **2008**, *108*, 2585-2621.
- [12] A.-S. Cans, A. G. Ewing, *J. Solid State Electrochem.* **2011**, *15*, 1437-1450.
- [13] R. M. Wightman, J. A. Jankowski, R. T. Kennedy, K. T. Kawagoe, T. J. Schroeder, D. J. Leszczyszyn, J. A. Near, E. J. Diliberto, O. H. Viveros, *Proceedings of the National Academy of Sciences of the United States of America* **1991**, *88*, 10754-10758.
- [14] M. L. Huffman, B. J. Venton, *Analyst* **2009**, *134*, 18-24.
- [15] T. J. Schroeder, J. A. Jankowski, K. T. Kawagoe, R. M. Wightman, C. Lefrou, C. Amatore, *Analytical Chemistry* **1992**, *64*, 3077-3083.
- [16] P. Chen, B. Xu, N. Tokranova, X. J. Feng, J. Castracane, K. D. Gillis, *Analytical Chemistry* **2003**, *75*, 518-524.
- [17] A. F. Dias, G. Dernick, V. Valero, M. G. Yong, C. D. James, H. G. Craighead, M. Lindau, *Nanotechnology* **2002**, *13*, 285-289.
- [18] X. H. Chen, Y. F. Gao, M. Hossain, S. Gangopadhyay, K. D. Gillis, *Lab Chip* **2008**, *8*, 161-169.
- [19] C. L. Gao, X. H. Sun, K. D. Gillis, *Biomed. Microdevices* **2013**, *15*, 445-451.
- [20] X. H. Sun, K. D. Gillis, *Analytical Chemistry* **2006**, *78*, 2521-2525.
- [21] A. Meunier, R. Fulcrand, F. Darchen, M. Guille Collignon, F. Lemaître, C. Amatore, *Biophysical Chemistry* **2012**, *162*, 14-21.
- [22] A. Meunier, O. Jouannot, R. Fulcrand, I. Fanget, M. Bretou, E. Karatekin, S. Arbault, M. Guille, F. Darchen, F. Lemaître, C. Amatore, *Angewandte Chemie-International Edition* **2011**, *50*, 5081-5084.
- [23] P. J. O'Connell, X. B. Wang, M. Leon-Ponte, C. Griffiths, S. C. Pingle, G. P. Ahern, *Blood* **2006**, *107*, 1010-1017.
- [24] M. L. Heuze, O. Collin, E. Terriac, A.-M. Lennon-Dumenil, M. Piel, *Methods in molecular biology (Clifton, N.J.)* **2011**, *769*, 415-434.
- [25] G. Faure-Andre, P. Vargas, M.-I. Yuseff, M. Heuze, J. Diaz, D. Lankar, V. Steri, J. Manry, S. Hugues, F. Vascotto, J. Boulanger, G. Raposo, M.-R. Bono, M.

- Roseblatt, M. Piel, A.-M. Lennon-Dumenil, *Science* **2008**, 322, 1705-1710.
- [26] T. Mueller, T. Duerk, B. Blumenthal, M. Grimm, S. Cicko, E. Panther, S. Sorichter, Y. Herouy, F. Di Virgilio, D. Ferrari, J. Norgauer, M. Idzko, *PLoS One* **2009**, 4.
- [27] R. Pacheco, C. E. Prado, M. J. Barrientos, S. Bernales, *Journal of Neuroimmunology* **2009**, 216, 8-19.
- [28] C. Prado, F. Contreras, H. Gonzalez, P. Diaz, D. Elgueta, M. Barrientos, A. A. Herrada, A. Lladser, S. Bernales, R. Pacheco, *J. Immunol.* **2012**, 188, 3062-3070.
- [29] K. Nakano, T. Higashi, R. Takagi, K. Hashimoto, Y. Tanaka, S. Matsushita, *International Immunology* **2009**, 21, 645-654.
- [30] S. Axelsson, R. Elofsson, B. Falck, S. Sjoborg, *Acta Dermato-Venereologica* **1978**, 58, 31-35.
- [31] A. Meunier, M. Bretou, F. Darchen, M. Guille Collignon, F. Lemaître, C. Amatore, *Electrochimica Acta* **2014**, 126, 74-80.
- [32] C. Amatore, S. Arbault, Y. Chen, C. Crozatier, F. Lemaitre, Y. Verchier, *Angewandte Chemie-International Edition* **2006**, 45, 4000-4003.
- [33] C. Amatore, J. Delacotte, M. Guille-Collignon, F. Lemaitre, *Analyst* **2015**, 140, 3687-3695.



## References

- [1] A. I. Ivanov, *Exocytosis and endocytosis*, Springer, **2008**.
- [2] C. Amatore, S. Arbault, M. Guille, F. Lemaître, *Chemical Reviews* **2008**, *108*, 2585-2621.
- [3] A. A. Alabi, R. W. Tsien, in *Annu. Rev. Physiol.*, *75*, **2013**, 393-422.
- [4] R. M. Wightman, C. L. Haynes, *Nat Neurosci* **2004**, *7*, 321-322.
- [5] D. Fasshauer, H. Otto, W. K. Eliason, R. Jahn, A. T. Brünger, *J. Biol. Chem.* **1997**, *272*, 28036-28041.
- [6] T. Xu, B. Rammner, M. Margittai, A. R. Artalejo, E. Neher, R. Jahn, *Cell* **1999**, *99*, 713-722.
- [7] R. B. Sutton, D. Fasshauer, R. Jahn, A. T. Brünger, *Nature* **1998**, *395*, 347-353.
- [8] K. J. K. Elliott, Thesis, Cornell University (New York), **2009**.
- [9] C. Montecucco, G. Schiavo, *Mol Microbiol* **1994**, *13*, 1-8.
- [10] M. F. Bader, R. W. Holz, K. Kumakura, N. Vitale, *Ann N Y Acad Sci* **2002**, *971*, 178-183.
- [11] R. E. Coupland, *Nature* **1968**, *217*, 384-388.
- [12] L. A. Greene, A. S. Tischler, *Proceedings of the National Academy of Sciences* **1976**, *73*, 2424-2428.
- [13] R. H. S. Westerink, A. G. Ewing, *Acta Physiologica* **2008**, *192*, 273-285.
- [14] L. Orci, F. Malaisse-Lagae, M. Ravazzola, M. Amherdt, A. E. Renold, *Science* **1973**, *181*, 561-562.
- [15] T. Kishimoto, T. T. Liu, H. Hatakeyama, T. Nemoto, N. Takahashi, H. Kasai, *Journal of Physiology-London* **2005**, *568*, 905-915.
- [16] B. M. Evers, J. Ishizuka, C. M. Townsend, J. C. Thompson, in *Molecular and Cell Biological Aspects of Gastroenteropancreatic Neuroendocrine Tumor Disease*, 733, New York Acad Sciences, **1994**, 393-406.
- [17] D. Parekh, J. Ishizuka, C. M. J. Townsend, B. Haber, R. D. Beauchamp, G. Karp, S. W. Kim, S. Rajaraman, G. J. Greeley, J. C. Thompson, *Pancreas* **1994**, *9*, 83-90.
- [18] A. Meunier, M. Bretou, F. Darchen, M. Guille Collignon, F. Lemaître, C. Amatore, *Electrochimica Acta* **2014**, *126*, 74-80.
- [19] A. Meunier, O. Jouannot, R. Fulcrand, I. Fanget, M. Bretou, E. Karatekin, S. Arbault, M. Guille, F. Darchen, F. Lemaître, C. Amatore, *Angewandte Chemie-International Edition* **2011**, *50*, 5081-5084.
- [20] C. G. Zoski, *Electroanalysis* **2002**, *14*, 1041-1051.
- [21] R. J. Forster, *Chemical Society Reviews* **1994**, *23*, 289-297.
- [22] C. Amatore, M. G. Collignon, F. Lemaître, in *Electrochemical Biosensors, Vol. 3*, PAN STANFORD, **2015**.
- [23] E. R. Travis, R. M. Wightman, *Annual Review of Biophysics and Biomolecular Structure* **1998**, *27*, 77-103.
- [24] E. Neher, B. Sakmann, *Nature* **1976**, *260*, 799-802.
- [25] E. Neher, A. Marty, *Proceedings of the National Academy of Sciences* **1982**, *79*, 6712-6716.
- [26] O. P. Hamill, A. Marty, E. Neher, B. Sakmann, F. J. Sigworth, *Pflügers Archiv* **1981**, *391*, 85-100.
- [27] J. Zimmerberg, M. Curran, F. S. Cohen, M. Brodwick, *Proceedings of the National Academy of Sciences of the United States of America* **1987**, *84*, 1585-1589.
- [28] R. Heidelberger, C. Heinemann, E. Neher, G. Matthews, *Nature* **1994**, *371*, 513-515.
- [29] C. Heinemann, R. H. Chow, E. Neher, R. S. Zucker, *Biophysical Journal* **1994**, *67*, 2546-2557.
- [30] J. M. Fernandez, E. Neher, B. D. Gomperts, *Nature* **1984**, *312*, 453-455.
- [31] T. C. Südhof, *Handbook of experimental pharmacology* **2008**, 1-21.
- [32] J. G. Eguiagaray, J. Egea, J. J. Bravo-Cordero, A. G. Garcia, *Neurocirugia* **2004**, *15*, 109-118.
- [33] E. S. Bucher, R. M. Wightman, in *Annual Review of Analytical Chemistry, Vol 8*, *8*, Annual Reviews, **2015**, 239-261.

- [34] M. L. Mundroff, R. M. Wightman, *Current protocols in neuroscience / editorial board, Jacqueline N. Crawley ... [et al.]* **2002**, Chapter 6, Unit 6.14.
- [35] A.-S. Cans, A. G. Ewing, *J. Solid State Electrochem.* **2011**, *15*, 1437-1450.
- [36] R. M. Wightman, J. A. Jankowski, R. T. Kennedy, K. T. Kawagoe, T. J. Schroeder, D. J. Leszczyszyn, J. A. Near, E. J. Diliberto, O. H. Viveros, *Proceedings of the National Academy of Sciences of the United States of America* **1991**, *88*, 10754-10758.
- [37] R. M. Wightman, T. J. Schroeder, J. M. Finnegan, E. L. Ciolkowski, K. Pihel, *Biophysical Journal* **1995**, *68*, 383-390.
- [38] F. Lemaitre, M. G. Collignon, C. Amatore, *Electrochimica Acta* **2014**, *140*, 457-466.
- [39] W. Wang, S.-H. Zhang, L.-M. Li, Z.-L. Wang, J.-K. Cheng, W.-H. Huang, *Analytical and Bioanalytical Chemistry* **2009**, *394*, 17-32.
- [40] I. M. Robinson, M. Yamada, M. Carrion-Vazquez, V. A. Lennon, J. M. Fernandez, *Cell Calcium* **1996**, *20*, 181-201.
- [41] C. P. Grabner, S. D. Price, A. Lysakowski, A. P. Fox, *Journal of Neurophysiology* **2005**, *94*, 2093-2104.
- [42] K. S. Tang, A. Tse, F. W. Tse, *J. Neurochem.* **2005**, *92*, 1126-1139.
- [43] C. Amatore, S. Arbault, I. Bonifas, F. Lemaitre, Y. Verchier, *Chemphyschem* **2007**, *8*, 578-585.
- [44] R. H. S. Westerink, A. de Groot, H. P. M. Vijverberg, *Biochemical and Biophysical Research Communications* **2000**, *270*, 625-630.
- [45] D. Bruns, R. Jahn, *Nature* **1995**, *377*, 62-65.
- [46] D. Bruns, D. Riedel, J. Klingauf, R. Jahn, *Neuron* **2000**, *28*, 205-220.
- [47] D. Bruns, *Methods* **2004**, *33*, 312-321.
- [48] B. B. Anderson, G. Chen, D. A. Gutman, A. G. Ewing, *Brain Research* **1998**, *788*, 294-301.
- [49] G. Chen, P. F. Gavin, G. Luo, A. G. Ewing, *The Journal of Neuroscience* **1995**, *15*, 7747-7755.
- [50] B. B. Anderson, A. G. Ewing, *Journal of pharmaceutical and biomedical analysis* **1999**, *19*, 15-32.
- [51] B. B. Anderson, G. Chen, D. A. Gutman, A. G. Ewing, *Journal of Neuroscience Methods* **1999**, *88*, 153-161.
- [52] R. Borges, D. Pereda, B. Beltran, M. Prunell, M. Rodriguez, J. D. Machado, *Cellular and Molecular Neurobiology* **2010**, *30*, 1359-1364.
- [53] C. Amatore, S. Arbault, Y. Bouret, M. Guille, F. Lemaitre, *Chemphyschem* **2010**, *11*, 2931-2941.
- [54] M. Camacho, J. D. Machado, M. S. Montesinos, M. Criado, R. Borges, *Journal of Neurochemistry* **2006**, *96*, 324-334.
- [55] C. A. Aspinwall, S. A. Brooks, R. T. Kennedy, J. R. T. Lakey, *J. Biol. Chem.* **1997**, *272*, 31308-31314.
- [56] K. Pihel, E. R. Travis, R. Borges, R. M. Wightman, *Biophysical Journal* **1996**, *71*, 1633-1640.
- [57] A. Gil, S. Viniegra, L. M. Gutiérrez, *Eur. J. Neurosci.* **2001**, *13*, 1380-1386.
- [58] S. C. Ge, J. G. White, C. L. Haynes, *Analytical Chemistry* **2009**, *81*, 2935-2943.
- [59] L. A. Sombers, N. J. Wittenberg, M. M. Maxson, K. L. Adams, A. G. Ewing, *Chemphyschem* **2007**, *8*, 2471-2477.
- [60] C. Amatore, S. Arbault, I. Bonifas, Y. Bouret, M. Erard, M. Guille, *Chemphyschem* **2003**, *4*, 147-154.
- [61] J. D. Machado, M. Camacho, J. Alvarez, R. Borges, *Communicative & integrative biology* **2009**, *2*, 71-73.
- [62] J.-P. Henry, C. Sagné, C. Bedet, B. Gasnier, *Neurochemistry international* **1998**, *32*, 227-246.
- [63] J. A. Jankowski, J. M. Finnegan, R. M. Wightman, *J. Neurochem.* **1994**, *63*, 1739-1747.
- [64] J. A. Jankowski, T. J. Schroeder, E. L. Ciolkowski, R. M. Wightman, *J. Biol. Chem.* **1993**, *268*, 14694-14700.
- [65] C. Amatore, M. G. Collignon, F. Lemaitre, *Electrochemical Biosensors* **2015**, *1*.
- [66] S. Taylor, M. L. Roberts, C. Peers, *The Journal of physiology* **1999**, *519*, 765-774.
- [67] R. T. Kennedy, L. Huang, C. A. Aspinwall, *Journal of the American Chemical Society* **1996**, *118*, 1795-1796.

- [68] M. Borisovska, Y. Zhao, Y. Tsytsyura, N. Glyvuk, S. Takamori, U. Matti, J. Rettig, T. Sudhof, D. Bruns, *The Embo Journal* **2005**, *24*, 2114-2126.
- [69] M. E. Graham, R. J. Fisher, R. D. Burgoyne, *Biochimie* **2000**, *82*, 469-479.
- [70] T. Xu, U. Ashery, R. D. Burgoyne, E. Neher, *The EMBO Journal* **1999**, *18*, 3293-3304.
- [71] D. A. Archer, M. E. Graham, R. D. Burgoyne, *J. Biol. Chem.* **2002**, *277*, 18249-18252.
- [72] R. D. Burgoyne, J. W. Barclay, L. F. Ciufu, M. E. Graham, M. T. W. Handley, A. Morgan, *Annals of the New York Academy of Sciences* **2009**, *1152*, 76-86.
- [73] A. Gulyas-Kovacs, H. de Wit, I. Milosevic, O. Kochubey, R. Toonen, J. Klingauf, M. Verhage, J. B. Sorensen, *Journal of Neuroscience* **2007**, *27*, 8676-8686.
- [74] M. E. Graham, G. R. Prescott, J. R. Johnson, M. Jones, A. Walmesley, L. P. Haynes, A. Morgan, R. D. Burgoyne, J. W. Barclay, *PLoS One* **2011**, *6*.
- [75] A. Gil, J. Rueda, S. Viniegra, L. M. Gutierrez, *Neuroscience* **2000**, *98*, 605-614.
- [76] S. C. Ge, J. G. White, C. L. Haynes, *Platelets* **2012**, *23*, 259-263.
- [77] P. Neco, O. Rossetto, A. Gil, C. Montecucco, L. M. Gutiérrez, *J. Neurochem.* **2003**, *85*, 329-337.
- [78] M. Malacombe, M.-F. Bader, S. Gasman, *Biochimica et Biophysica Acta (BBA) - Molecular Cell Research* **2006**, *1763*, 1175-1183.
- [79] A. M. Gonzalez-Jamett, F. Momboisse, M. J. Guerra, S. Ory, X. Baez-Matus, N. Barraza, V. Calco, S. Houy, E. Couve, A. Neely, A. D. Martinez, S. Gasman, A. M. Cardenas, *PLoS One* **2013**, *8*.
- [80] K. Berberian, A. J. Torres, Q. H. Fang, K. Kisler, M. Lindau, *Journal of Neuroscience* **2009**, *29*, 863-870.
- [81] R. Trouillon, A. G. Ewing, *ACS chemical biology* **2014**, *9*, 812-820.
- [82] M. Gabel, F. Delavoie, V. Demais, C. Royer, Y. Bailly, N. Vitale, M. F. Bader, S. Chasserot-Golaz, *J. Cell Biol.* **2015**, *210*, 785-800.
- [83] T. J. Schroeder, J. A. Jankowski, J. Senyshyn, R. W. Holz, R. M. Wightman, *J. Biol. Chem.* **1994**, *269*, 17215-17220.
- [84] I. Hafez, K. Kisler, K. Berberian, G. Dernick, V. Valero, M. G. Yong, H. G. Craighead, M. Lindau, *Proceedings of the National Academy of Sciences of the United States of America* **2005**, *102*, 13879-13884.
- [85] J. Wang, R. Trouillon, Y. Lin, M. I. Svensson, A. G. Ewing, *Analytical Chemistry* **2013**, *85*, 5600-5608.
- [86] J. Wang, R. Trouillon, J. Dunevall, A. G. Ewing, *Analytical Chemistry* **2014**, *86*, 4515-4520.
- [87] J. Wang, A. G. Ewing, *Analyst* **2014**, *139*, 3290-3295.
- [88] J. Wigstrom, J. Dunevall, N. Najafinobar, J. Lovric, J. Wang, A. G. Ewing, A. S. Cans, *Analytical Chemistry* **2016**, *88*, 2080-2087.
- [89] R. Jahn, T. Lang, T. C. Südhof, *Cell*, *112*, 519-533.
- [90] M. B. Jackson, E. R. Chapman, *Nat Struct Mol Biol* **2008**, *15*, 684-689.
- [91] R. H. Chow, L. Von Rueden, E. Neher, *Nature* **1992**, *356*, 60-63.
- [92] Z. Zhou, S. Mislser, R. H. Chow, *Biophys. J.* **1996**, *70*, 1543-1552.
- [93] G. A. de Toledo, R. Fernandez-Chacon, J. M. Fernandez, *Nature* **1993**, *363*, 554-558.
- [94] C. Amatore, S. Arbault, I. Bonifas, M. Guille, F. Lemaître, Y. Verchier, *Biophysical Chemistry* **2007**, *129*, 181-189.
- [95] C. Amatore, S. Arbault, Y. Bouret, M. Guille, F. Lemaître, Y. Verchier, *ChemBioChem* **2006**, *7*, 1998-2003.
- [96] L. A. Sombers, H. J. Hanchar, T. L. Colliver, N. Wittenberg, A. Cans, S. Arbault, C. Amatore, A. G. Ewing, *The Journal of Neuroscience* **2004**, *24*, 303-309.
- [97] P. Chen, B. Xu, N. Tokranova, X. Feng, J. Castracane, K. D. Gillis, *Analytical Chemistry* **2003**, *75*, 518-524.
- [98] C. Spiegel, A. Heiskanen, L. H. D. Skjolding, J. Emneus, *Electroanalysis* **2008**, *20*, 680-702.
- [99] S.-A. Chan, C. Smith, *The Journal of physiology* **2001**, *537*, 871-885.
- [100] B. Zhang, K. L. Adams, S. J. Lubner, D. J. Eves, M. L. Heien, A. G. Ewing, *Analytical Chemistry* **2008**, *80*, 1394-1400.

- [101] Y. Lin, R. Trouillon, M. I. Svensson, J. D. Keighron, A.-S. Cans, A. G. Ewing, *Analytical Chemistry* **2012**, *84*, 2949-2954.
- [102] A. F. Dias, G. Dernick, V. Valero, M. G. Yong, C. D. James, H. G. Craighead, M. Lindau, *Nanotechnology* **2002**, *13*, 285.
- [103] H.-F. Cui, J.-S. Ye, Y. Chen, S.-C. Chong, X. Liu, T.-M. Lim, F.-S. Sheu, *Sensors and Actuators B: Chemical* **2006**, *115*, 634-641.
- [104] H.-F. Cui, J.-S. Ye, Y. Chen, S.-C. Chong, F.-S. Sheu, *Analytical Chemistry* **2006**, *78*, 6347-6355.
- [105] A. Meunier, R. Fulcrand, F. Darchen, M. Guille Collignon, F. Lemaître, C. Amatore, *Biophysical Chemistry* **2012**, *162*, 14-21.
- [106] B.-X. Shi, Y. Wang, K. Zhang, T.-L. Lam, H. L.-W. Chan, *Biosensors and Bioelectronics* **2011**, *26*, 2917-2921.
- [107] H. Zhao, L. Li, H. J. Fan, F. Wang, L. M. Jiang, P. G. He, Y. Z. Fang, *Mol. Cell. Biochem.* **2012**, *363*, 309-313.
- [108] S. Y. Yang, B. N. Kim, A. A. Zakhidov, P. G. Taylor, J.-K. Lee, C. K. Ober, M. Lindau, G. G. Malliaras, *Advanced Materials* **2011**, *23*, 184-188.
- [109] C. Amatore, J. Delacotte, M. Guille-Collignon, F. Lemaître, *Analyst* **2015**, *140*, 3687-3695.
- [110] Y. Gao, S. Bhattacharya, X. Chen, S. Barizuddin, S. Gangopadhyay, K. D. Gillis, *Lab Chip* **2009**, *9*, 3442-3446.
- [111] C. Gao, X. Sun, K. D. Gillis, *Biomed. Microdevices* **2013**, *15*, 445-451.
- [112] I. A. Ges, R. L. Brindley, K. P. M. Currie, F. J. Baudenbacher, *Lab Chip* **2013**, *13*, 4663-4673.
- [113] C. Amatore, S. Arbault, F. Lemaître, Y. Verchier, *Biophysical Chemistry* **2007**, *127*, 165-171.
- [114] X. Liu, S. Barizuddin, W. Shin, C. J. Mathai, S. Gangopadhyay, K. D. Gillis, *Analytical Chemistry* **2011**, *83*, 2445-2451.
- [115] H. G. Sudibya, J. Ma, X. Dong, S. Ng, L. J. Li, X. W. Liu, P. Chen, *Angewandte Chemie International Edition* **2009**, *48*, 2723-2726.
- [116] B.-X. Shi, Y. Wang, T.-L. Lam, W.-H. Huang, K. Zhang, Y.-C. Leung, H. L. W. Chan, *Biomicrofluidics* **2010**, *4*, 043009.
- [117] K. Kisler, B. N. Kim, X. Liu, K. Berberian, Q. Fang, C. J. Mathai, S. Gangopadhyay, K. D. Gillis, M. Lindau, *Journal of biomaterials and nanobiotechnology* **2012**, *3*, 243-253.
- [118] C. Amatore, S. Arbault, Y. Chen, C. Crozatier, F. Lemaître, Y. Verchier, *Angewandte Chemie-International Edition* **2006**, *45*, 4000-4003.
- [119] X. H. Chen, Y. F. Gao, M. Hossain, S. Gangopadhyay, K. D. Gillis, *Lab Chip* **2008**, *8*, 161-169.
- [120] X. H. Sun, K. D. Gillis, *Analytical Chemistry* **2006**, *78*, 2521-2525.
- [121] N. Takahashi, *Biological and Pharmaceutical Bulletin* **2015**, *38*, 656-662.
- [122] H. Kasai, T. Kishimoto, T. Nemoto, H. Hatakeyama, T.-T. Liu, N. Takahashi, *Advanced Drug Delivery Reviews* **2006**, *58*, 850-877.
- [123] N. Takahashi, H. Kasai, in *Pancreatic Beta Cell in Health and Disease*, Springer Japan, **2008**, 195-211.
- [124] I. Cuchillo-Ibanez, P. Michelena, A. Albillos, A. G. Garcia, *Febs Letters* **1999**, *459*, 22-26.
- [125] J. Panyam, V. Labhasetwar, *Pharm. Res.* **2003**, *20*, 212-220.
- [126] M. Krzan, M. Stenovec, M. Kreft, T. Pangrsic, S. Grilc, P. G. Haydon, R. Zorec, *Journal of Neuroscience* **2003**, *23*, 1580-1583.
- [127] R. W. Holz, D. Axelrod, *Acta Physiologica* **2008**, *192*, 303-307.
- [128] R. W. Holz, *Cellular and Molecular Neurobiology* **2006**, *26*, 439-447.
- [129] N. S. Poulter, W. T. E. Pitkeathly, P. J. Smith, J. Z. Rappoport, in *Advanced Fluorescence Microscopy: Methods and Protocols*, 1251, Humana Press Inc, **2015**, 1-23.
- [130] H.-C. Chiang, W. Shin, W.-D. Zhao, E. Hamid, J. Sheng, M. Baydyuk, P. J. Wen, A. Jin, F. Momboisse, L.-G. Wu, *Nature Communications* **2014**, *5*.
- [131] K. I. Willig, S. O. Rizzoli, V. Westphal, R. Jahn, S. W. Hell, *Nature* **2006**, *440*, 935-939.
- [132] Y. Sun, J. Jaldin-Fincati, Z. Liu, P. J. Bilan, A. Klip, *Molecular Biology of the Cell* **2016**, *27*, 75-89.
- [133] H. Tanaka, S. Fujii, T. Hirano, *Nat. Protoc.* **2014**, *9*, 76-89.

- [134] B. Huang, W. Wang, M. Bates, X. Zhuang, *Science* **2008**, *319*, 810-813.
- [135] L. Schermelleh, R. Heintzmann, H. Leonhardt, *The Journal of Cell Biology* **2010**, *190*, 165-175.
- [136] A. Graczyk, C. Rickman, *Frontiers in endocrinology* **2013**, *4*, 147-147.
- [137] B. Huang, M. Bates, X. Zhuang, *Annual Review of Biochemistry* **2009**, *78*, 993.
- [138] D. Axelrod, T. P. Burghardt, N. L. Thompson, *Annual Review of Biophysics and Bioengineering* **1984**, *13*, 247-268.
- [139] A. L. Mattheyses, S. M. Simon, J. Z. Rappoport, *Journal of Cell Science* **2010**, *123*, 3621-3628.
- [140] K. N. Fish, *Current protocols in cytometry / editorial board, J. Paul Robinson, managing editor ... [et al.]* **2009**, Chapter 12, Unit12.18-Unit12.18.
- [141] M. Oheim, *Lasers in Medical Science* **2001**, *16*, 149-158.
- [142] C. Desnos, S. Huet, I. Fanget, C. Chapuis, C. Boerttger, V. Racine, J.-B. Sibarita, J.-P. Henry, F. Darchen, *Journal of Neuroscience* **2007**, *27*, 10636-10645.
- [143] E. Karatekin, V. S. Tran, S. Huet, I. Fanget, S. Cribier, J. P. Henry, *Biophysical Journal* **2008**, *94*, 2891-2905.
- [144] A. Yildiz, R. D. Vale, *Cold Spring Harbor protocols* **2015**, *2015*, pdb.top086348-pdb.top086348.
- [145] J. A. Steyer, H. Horstmann, W. Almers, *Nature* **1997**, *388*, 474-478.
- [146] J. A. Steyer, W. Almers, *Biophysical Journal* **1999**, *76*, 2262-2271.
- [147] M. Oheim, D. Loerke, W. Stuhmer, R. H. Chow, *European Biophysics Journal with Biophysics Letters* **1998**, *27*, 83-98.
- [148] W. Betz, G. Bewick, *Science* **1992**, *255*, 200-203.
- [149] D. A. Richards, J. H. Bai, E. R. Chapman, *J. Cell Biol.* **2005**, *168*, 929-939.
- [150] G. Miesenbock, D. A. De Angelis, J. E. Rothman, *Nature* **1998**, *394*, 192-195.
- [151] Y.-P. Chang, F. Pinaud, J. Antelman, S. Weiss, *Journal of Biophotonics* **2008**, *1*, 287-298.
- [152] N. G. Gubernator, H. Zhang, R. G. W. Staal, E. V. Mosharov, D. B. Pereira, M. Yue, V. Balsanek, P. A. Vadola, B. Mukherjee, R. H. Edwards, D. Sulzer, D. Sames, *Science* **2009**, *324*, 1441-1444.
- [153] J. G. Burchfield, J. A. Lopez, K. Mele, P. Vallotton, W. E. Hughes, *Traffic* **2010**, *11*, 429-439.
- [154] J. Schmoranzner, M. Goulian, D. Axelrod, S. M. Simon, *J. Cell Biol.* **2000**, *149*, 23-31.
- [155] D. R. Passmore, T. Rao, A. Anantharam, in *Exocytosis and Endocytosis*, Springer New York, **2014**, 263-273.
- [156] T. Tsuboi, H. T. McMahon, G. A. Rutter, *J. Biol. Chem.* **2004**, *279*, 47115-47124.
- [157] D. N. Bowser, B. S. Khakh, *Proceedings of the National Academy of Sciences of the United States of America* **2007**, *104*, 4212-4217.
- [158] J. W. Taraska, D. Perrais, M. Ohara-Imaizumi, S. Nagamatsu, W. Almers, *Proceedings of the National Academy of Sciences* **2003**, *100*, 2070-2075.
- [159] L. Ma, V. P. Bindokas, A. Kuznetsov, C. Rhodes, L. Hays, J. M. Edwardson, K. Ueda, D. F. Steiner, L. H. Philipson, *Proceedings of the National Academy of Sciences of the United States of America* **2004**, *101*, 9266-9271.
- [160] L. M. Johns, E. S. Levitan, E. A. Shelden, R. W. Holz, D. Axelrod, *J. Cell Biol.* **2001**, *153*, 177-190.
- [161] M. Ohara-Imaizumi, C. Nishiwaki, Y. Nakamichi, T. Kikuta, S. Nagai, S. Nagamatsu, *Diabetologia* **2004**, *47*, 2200-2207.
- [162] M. Ohara-Imaizumi, C. Nishiwaki, T. Kikuta, K. Kumakura, Y. Nakamichi, S. Nagamatsu, *J. Biol. Chem.* **2004**, *279*, 8403-8408.
- [163] Y. Wu, Y. W. Gu, M. K. Morphew, J. Yao, F. L. Yeh, M. Dong, E. R. Chapman, *J. Cell Biol.* **2012**, *198*, 323-330.
- [164] M. Oheim, W. Stuhmer, *European Biophysics Journal with Biophysics Letters* **2000**, *29*, 67-89.
- [165] T. Lang, I. Wacker, I. Wunderlich, A. Rohrbach, G. Giese, T. Soldati, W. Almers, *Biophysical Journal* **2000**, *78*, 2863-2877.

- [166] A. Papadopoulos, S. Martin, V. M. Tomatis, R. S. Gormal, F. A. Meunier, *The Journal of Neuroscience* **2013**, *33*, 19143-19153.
- [167] A. Albillos, G. Dernick, H. Horstmann, W. Almers, G. A. de Toledo, M. Lindau, *Nature* **1997**, *389*, 509-512.
- [168] Z. Zhou, S. Misler, *J. Biol. Chem.* **1996**, *271*, 270-277.
- [169] A. F. Oberhauser, I. M. Robinson, J. M. Fernandez, *Biophysical Journal* **1996**, *71*, 1131-1139.
- [170] E. Ales, L. Tabares, J. M. Poyato, V. Valero, M. Lindau, G. A. de Toledo, *Nature Cell Biology* **1999**, *1*, 40-44.
- [171] U. Becherer, M. Pasche, S. Nofal, D. Hof, U. Matti, J. Rettig, *PLoS One* **2007**, *2*, e505.
- [172] C. Joselevitch, D. Zenisek, *Journal of visualized experiments : JoVE* **2009**.
- [173] M. Okamoto, M. Ohara-Imaizumi, N. Kubota, S. Hashimoto, K. Eto, T. Kanno, T. Kubota, M. Wakui, R. Nagai, M. Noda, S. Nagamatsu, T. Kadowaki, *Diabetologia* **2008**, *51*, 827-835.
- [174] V. Pattu, M. Halimani, M. Ming, C. Schirra, U. Hahn, H. Bzeih, H.-F. Chang, L. Weins, E. Krause, J. Rettig, *Frontiers in Immunology* **2013**, *4*.
- [175] M. Pasche, U. Matti, D. Hof, J. Rettig, U. Becherer, *PLoS One* **2012**, *7*.
- [176] J. D. Keighron, A. G. Ewing, A. S. Cans, *Analyst* **2012**, *137*, 1755-1763.
- [177] P. Schloss, F. Matthäus, T. Lau, *Neural Regeneration Research* **2015**, *10*, 1383-1385.
- [178] M. Lee, N. G. Gubernator, D. Sulzer, D. Sames, *Journal of the American Chemical Society* **2010**, *132*, 8828-8830.
- [179] S. M. Bagale, Thesis, University of Miami (Florida), **2011**.
- [180] H. Zimmer, *Clinical cardiology* **2006**, *29*, 135.
- [181] O. Loewi, *Pflüger's Archiv für die gesamte Physiologie des Menschen und der Tiere* **1921**, *189*, 239-242.
- [182] D. Peter, Y. Liu, C. Sternini, R. de Giorgio, N. Brecha, R. H. Edwards, *J Neurosci* **1995**, *15*, 6179-6188.
- [183] M. Anlauf, R. Eissele, M. K.-H. Schäfer, L. E. Eiden, R. Arnold, U. Pauser, G. Klöppel, E. Weihe, *J. Histochem. Cytochem.* **2003**, *51*, 1027-1040.
- [184] E. Weihe, M. K.-H. Schäfer, J. D. Erickson, L. E. Eiden, *Journal of Molecular Neuroscience* **1994**, *5*, 149-164.
- [185] J. D. Erickson, M. Schafer, T. I. Bonner, L. E. Eiden, E. Weihe, *Proceedings of the National Academy of Sciences* **1996**, *93*, 5166-5171.
- [186] K. Wimalasena, *Medicinal research reviews* **2011**, *31*, 483-519.
- [187] I. J. Kopin, *Annual review of pharmacology* **1968**, *8*, 377-394.
- [188] J. S. Partilla, A. G. Dempsey, A. S. Nagpal, B. E. Blough, M. H. Baumann, R. B. Rothman, *Journal of Pharmacology and Experimental Therapeutics* **2006**, *319*, 237-246.
- [189] B. Sarkar, A. Banerjee, A. K. Das, S. Nag, S. K. Kaushalya, U. Tripathy, M. Shameem, S. Shukla, S. Maiti, *ACS Chemical Neuroscience* **2014**, *5*, 329-334.
- [190] T. Lau, V. Proissl, J. Ziegler, P. Schloss, *Journal of Neuroscience Methods* **2015**, *241*, 10-17.
- [191] S. J. Lillard, E. S. Yeung, *Journal of Neuroscience Methods* **1997**, *75*, 103-109.
- [192] W. Tan, V. Parpura, P. G. Haydon, E. S. Yeung, *Analytical Chemistry* **1995**, *67*, 2575-2579.
- [193] L. Mellander, A. S. Cans, A. G. Ewing, *Chemphyschem* **2010**, *11*, 2756-2763.
- [194] R. M. Wightman, *ACS Chemical Neuroscience* **2014**, *6*, 5-7.
- [195] M. Berger, J. A. Gray, B. L. Roth, *Annual Review of Medicine* **2009**, *60*, 355-366.
- [196] A. N. Patel, P. R. Unwin, J. V. Macpherson, *Physical Chemistry Chemical Physics* **2013**, *15*, 18085-18092.
- [197] P. A. Smith, M. R. Duchon, F. M. Ashcroft, *Pflugers Arch.* **1995**, *430*, 808-818.
- [198] P. A. Vadola, D. Sames, *Journal of Organic Chemistry* **2012**, *77*, 7804-7814.
- [199] H. Zhang, N. G. Gubernator, M. Yue, R. G. W. Staal, E. V. Mosharov, D. Pereira, V. Balsanek, P. A. Vadola, B. Mukherjee, R. H. Edwards, D. Sulzer, D. Sames, *Journal of Visualized Experiments* **2009**.
- [200] P. C. Rodriguez, D. B. Pereira, A. Borgkvist, M. Y. Wong, C. Barnard, M. S. Sonders, H. Zhang, D. Sames, D. Sulzer, *Proceedings of the National Academy of Sciences of the United States of America* **2013**, *110*, 870-875.

- [201] D. Sames, M. Dunn, R. J. Karpowicz, D. Sulzer, *ACS Chemical Neuroscience* **2013**, *4*, 648-651.
- [202] P. Merchant, D. Sulzer, D. Sames, *Neuropharmacology* **2015**, *98*, 90-94.
- [203] G. Hu, A. Henke, R. J. Karpowicz, M. S. Sonders, F. Farrimond, R. Edwards, D. Sulzer, D. Sames, *ACS chemical biology* **2013**, *8*, 1947-1954.
- [204] Z. Freyberg, M. S. Sonders, J. I. Aguilar, T. Hiranita, C. S. Karam, J. Flores, A. B. Pizzo, Y. Zhang, Z. J. Farino, A. Chen, C. A. Martin, T. A. Kopajtic, H. Fei, G. Hu, Y.-Y. Lin, E. V. Mosharov, B. D. McCabe, R. Freyberg, K. Wimalasena, L.-W. Hsin, D. Sames, D. E. Krantz, J. L. Katz, D. Sulzer, J. A. Javitch, *Nature Communications* **2016**, *7*, article number: 10652.
- [205] D. B. Pereira, Y. Schmitz, J. Meszaros, P. Merchant, G. Hu, S. Li, A. Henke, J. Lizardi-Ortiz, R. J. Karpowicz, T. J. Morgenstern, M. S. Sonders, E. Kanter, P. C. Rodriguez, E. V. Mosharov, D. Sames, D. Sulzer, *Nature Neuroscience* **2016**, *19*, 578-586.
- [206] D. Markov, E. V. Mosharov, W. Setlik, M. D. Gershon, D. Sulzer, *J. Neurochem.* **2008**, *107*, 1709-1721.
- [207] M. M. Wu, M. Grabe, S. Adams, R. Y. Tsien, H. P. H. Moore, T. E. Machen, *J. Biol. Chem.* **2001**, *276*, 33027-33035.
- [208] X.-R. Hu, J.-B. He, Y. Wang, Y.-W. Zhu, J.-J. Tian, *Electrochimica Acta* **2011**, *56*, 2919-2925.
- [209] K. C. D. Leite, L. Torres, L. F. Garcia, S. G. Rezende, J. R. de Oliveira-Neto, F. M. Lopes, T. A. Garcia, R. M. Verly, W. T. P. dos Santos, E. D. Gil, *International Journal of Electrochemical Science* **2015**, *10*, 5714-5725.
- [210] Q. S. Wu, H. D. Dewald, *Electroanalysis* **2001**, *13*, 45-48.
- [211] V. S. Tran, S. Huet, I. Fanget, S. Cribier, J.-P. Henry, E. Karatekin, *European Biophysics Journal with Biophysics Letters* **2007**, *37*, 55-69.
- [212] N. Sasakawa, N. Murayama, K. Kumakura, *Cellular and Molecular Neurobiology* **2005**, *25*, 777-787.
- [213] T. K. Chen, G. O. Luo, A. G. Ewing, *Analytical Chemistry* **1994**, *66*, 3031-3035.
- [214] A. Galli, R. D. Blakely, L. J. DeFelice, *Proceedings of the National Academy of Sciences of the United States of America* **1998**, *95*, 13260-13265.
- [215] C. T. Wang, R. Grishanin, C. A. Earles, P. Y. Chang, T. F. J. Martin, E. R. Chapman, M. B. Jackson, *Science* **2001**, *294*, 1111-1115.
- [216] O. L. Zaika, O. M. Pochinyuk, E. A. Lukyanetz, *Neurophysiology* **2000**, *32*, 174-176.
- [217] C. Amatore, A. I. Oleinick, I. Svir, *Chemphyschem* **2010**, *11*, 159-174.
- [218] D. Bratton, D. Yang, J. Y. Dai, C. K. Ober, *Polymers for Advanced Technologies* **2006**, *17*, 94-103.
- [219] R. Jahn, T. C. Sudhof, *Annual Review of Neuroscience* **1994**, *17*, 219-246.
- [220] N. Vardjan, J. Jorgacevski, R. Zorec, *Neuroscientist* **2013**, *19*, 160-174.
- [221] Z. P. P. Pang, T. C. Sudhof, *Current Opinion in Cell Biology* **2010**, *22*, 496-505.
- [222] T. C. Normann, *Int.Rev.Cytol.* **1976**, *46*, 1-77.
- [223] R. D. Burgoyne, A. Morgan, *Physiol. Rev.* **2003**, *83*, 581-632.
- [224] M. Lindau, *Biochim. Biophys. Acta-Gen. Subj.* **2012**, *1820*, 1234-1242.
- [225] A. V. Kibble, R. J. O. Barnard, R. D. Burgoyne, *Journal of Cell Science* **1996**, *109*, 2417-2422.
- [226] A. Segawa, S. Terakawa, S. Yamashina, C. R. Hopkins, *Eur. J. Cell Biol.* **1991**, *54*, 322-330.
- [227] D. Axelrod, *Traffic* **2001**, *2*, 764-774.
- [228] M. A. Gaffield, W. J. Betz, *Nat. Protoc.* **2006**, *1*, 2916-2921.
- [229] D. M. Yang, C. C. Huang, H. Y. Lin, D. P. Tsai, L. S. Kao, C. W. Chi, C. C. Lin, *Journal of Microscopy-Oxford* **2003**, *209*, 223-227.
- [230] M. W. Allersma, L. Wang, D. Axelrod, R. W. Holz, *Molecular Biology of the Cell* **2004**, *15*, 4658-4668.
- [231] S. Xia, L. Xu, L. Bai, Z. Q. D. Xua, T. Xu, *Brain Research* **2004**, *997*, 159-164.
- [232] T. F. J. Martin, R. N. Grishanin, *Neurons: Methods and Applications for the Cell Biologist* **2003**, *71*, 267-286.
- [233] B. M. Evers, J. I. N. Ishizuka, C. M. Townsend, J. C. Thompson, *Annals of the New York Academy of Sciences* **1994**, *733*, 393-406.

- [234] V. S. Tran, A. M. Marion-Audibert, E. Karatekin, S. Huet, S. Cribier, K. Guillaumie, C. Chapuis, C. Desnos, F. Darchen, J. P. Henry, in *Gastroenteropancreatic Neuroendocrine Tumor Disease: Molecular and Cell Biological Aspects*, 1014, **2004**, 179-188.
- [235] S. Huet, E. Karatekin, V. S. Tran, I. Fanget, S. Cribier, J.-P. Henry, *Biophysical Journal* **2006**, 91, 3542-3559.
- [236] Z. L. Siddique, I. Drozdov, J. Floch, B. I. Gustafsson, K. Stunes, R. Pfragner, M. Kidd, I. M. Modlin, *Neuroendocrinology* **2009**, 89, 458-470.
- [237] L. Sun, L. M. Morris, J. Luo, L. V. Mackey, J. S. Leslie, L. G. Franko-Tobin, J. A. Fuselier, K. T. LePage, D. H. Coy, *Journal of Drug Targeting* **2011**, 19, 666-674.
- [238] S. An, D. Zenisek, *Current Opinion in Neurobiology* **2004**, 14, 522-530.
- [239] M. W. Allersma, M. A. Bittner, D. Axelrod, R. W. Holz, *Molecular Biology of the Cell* **2006**, 17, 2424-2438.
- [240] T. Aoki, M. Tanino, K. Sanui, N. Ogata, K. Kumakura, *Biomaterials* **1996**, 17, 1971-1974.
- [241] R. Tanamoto, Y. Shindo, N. Miki, Y. Matsumoto, K. Hotta, K. Oka, *Journal of Neuroscience Methods* **2015**, 253, 272-278.
- [242] S. T. Larsen, M. L. Heien, R. Taboryski, *Analytical Chemistry* **2012**, 84, 7744-7749.
- [243] J. Yao, X. A. Liu, K. D. Gillis, *Analytical Methods* **2015**, 7, 5760-5766.
- [244] J. Yao, K. D. Gillis, *Analyst* **2012**, 137, 2674-2681.
- [245] H. Zhao, F. Zhang, L. Li, P. G. He, Y. Z. Fang, *Biocell* **2013**, 37, 77-83.
- [246] F. Konings, W. Depotter, *Febs Letters* **1981**, 126, 103-106.
- [247] B. G. Livett, *Physiol. Rev.* **1984**, 64, 1103-1161.
- [248] A. S. Tischler, L. A. Ruzicka, R. A. Delellis, *Neuroscience* **1991**, 43, 671-678.
- [249] L. A. Sombers, H. J. Hanchar, T. L. Colliver, N. Wittenberg, A. Cans, S. Arbault, C. Amatore, A. G. Ewing, *Journal of Neuroscience* **2004**, 24, 303-309.
- [250] A. G. Guell, K. E. Meadows, P. R. Unwin, J. V. Macpherson, *Physical Chemistry Chemical Physics* **2010**, 12, 10108-10114.
- [251] R. Trouillon, D. O'Hare, *Electrochimica Acta* **2010**, 55, 6586-6595.
- [252] D. P. Manica, Y. Mitsumori, A. G. Ewing, *Analytical Chemistry* **2003**, 75, 4572-4577.
- [253] R. Trouillon, A. G. Ewing, *Anal. Chem.* **2013**, 85, 4822-4828.
- [254] G. Y. Chen, A. G. Ewing, *Crit. Rev. Neurobiol.* **1997**, 11, 59-90.
- [255] M. L. Heien, A. G. Ewing, *Methods in molecular biology (Clifton, N.J.)* **2009**, 544, 153-162.
- [256] C. Amatore, S. Arbault, I. Bonifas, Y. Bouret, M. Erard, A. G. Ewing, L. A. Sombers, *Biophysical Journal* **2005**, 88, 4411-4420.
- [257] E. V. Mosharov, D. Sulzer, *Nat Meth* **2005**, 2, 651-658.
- [258] M. L. Huffman, B. J. Venton, *The Analyst* **2009**, 134, 18-24.
- [259] R. Mohammadzadeh Kakhki, *Arabian Journal of Chemistry* **2014** (<http://dx.doi.org/10.1016/j.arabjc.2014.11.058>).
- [260] L. Wang, H. R. Xu, Y. L. Song, J. P. Luo, S. W. Xu, S. Zhang, J. T. Liu, X. X. Cai, *Sensors* **2015**, 15, 868-879.
- [261] K. Berberian, K. Kisler, Q. Fang, M. Lindau, *Analytical Chemistry* **2009**, 81, 8734-8740.
- [262] A. Elhamdani, F. Azizi, C. R. Artalejo, *The Journal of Neuroscience* **2006**, 26, 3030-3036.
- [263] S. Ge, S. Koseoglu, C. L. Haynes, *Analytical and Bioanalytical Chemistry* **2010**, 397, 3281-3304.
- [264] A. Meunier, Thesis, Université Pierre et Marie Curie (Paris) **2012**.
- [265] J. D. Machado, A. Morales, J. F. Gomez, R. Borges, *Molecular Pharmacology* **2001**, 60, 514-520.
- [266] K. Kisler, R. H. Chow, R. Dominguez, *Journal of steroids & hormonal science* **2013**, Suppl 12, 10.4172/2157-7536.S4112-4002.
- [267] T. Yuan, J. Lu, J. Zhang, Y. Zhang, L. Chen, *Biophysical Journal* **2015**, 108, 251-260.
- [268] M. K. Loder, T. Tsuboi, G. A. Rutter, *Methods in molecular biology (Clifton, N.J.)* **2013**, 950, 13-26.
- [269] B. E. K. Swamy, B. J. Venton, *Analyst* **2007**, 132, 876-884.
- [270] B. J. Venton, R. M. Wightman, *Analytical Chemistry* **2003**, 75, 414-421

- [271] K. L. Adams, M. Puchades, A. G. Ewing, *Annual review of analytical chemistry (Palo Alto, Calif.)* **2008**, *1*, 329-329.
- [272] S. Arbault, P. Pantano, J. A. Jankowski, M. Vuillaume, C. Amatore, *Analytical Chemistry* **1995**, *67*, 3382-3390.
- [273] K. T. Kawagoe, J. A. Jankowski, R. M. Wightman, *Analytical Chemistry* **1991**, *63*, 1589-1594.



## Abstract

Vesicular exocytosis is a ubiquitous way for intercellular communications. TIRFM (total internal reflection fluorescence microscopy) and amperometry are nowadays the two most frequently used analytical methods with complementary features for its investigation. The combination of these two analytical techniques to track exocytotic secretions was firstly achieved by our group in 2011 and this new technique was demonstrated to show both high temporal and spatial resolutions by simultaneously recording the fluorescent and amperometric signals. The major disadvantage of this former work was the independent loading of optical and electrochemical probes to the secretory vesicles, which resulted in 'sightless' amperometric or optical signals as well as low coupling efficiency. Therefore, in this thesis, we attempted to develop a unique probe with dual fluorescent/electrochemical characteristics to track exocytotic process by TIRFM/amperometry coupling technique. This is why an analog of biogenic monoamine neurotransmitters, 4-(2-aminoethyl)-6-chloro-7-hydroxy-2H-1-benzopyran-2-one hydrochloride (named as **1** in this work) was synthesized.

**1** exhibited bright, stable, pH-dependent fluorescence. When excited at 405 nm, its fluorescence intensity was almost doubled with the increase of pH values from 5 (similar to that in the vesicular lumen) to 7 (similar to the extracellular medium). Furthermore, in voltammetry, **1** was demonstrated to be easily electrooxidized on GCE (glassy carbon electrode), CFE (carbon fiber electrode) and ITO (indium tin oxide) electrodes surfaces, showing good electroactivity. **1** was also shown to penetrate easily into the vesicles of BON N13 cells within 1 hour incubation, testifying its specific affinity with these VMAT-equipped (vesicular monoamine transporter) vesicles. The applications of **1** as optical and electrochemical probes for exocytosis monitoring were then separately validated in BON N13 cells by TIRFM and amperometry measurements, respectively. Simultaneous recording of fluorescent and amperometric information by using **1** dual probes loaded cells was subsequently acquired in a microfabricated device constituted by conductive and transparent ITO electrodes. Our results based on the unique probe **1** for electrochemical and fluorescent detection of exocytotic release seemed more adapted than all the previous works involving independent probes. The high spatial and temporal resolutions of this combined method also allowed analyzing consecutive exocytotic secretions as well as overlapped events in **1**-stained cells. Further analysis of these two signals with complementary information will shed more light on the correlation of the fusion pore behavior (opening/closure dynamics, stability...) measured by amperometry and the motion of a secretory vesicle in three dimensions (tethering, docking, fusion and retrieval) detected by TIRFM.

## Résumé

L'exocytose vésiculaire est une voie physiologique majeure de la communication intercellulaire. Dans ce contexte, le TIRFM (microscopie de fluorescence par réflexion totale interne) et l'ampérométrie sont aujourd'hui les deux méthodes analytiques les plus fréquemment utilisées dans l'étude de l'exocytose. En raison de la complémentarité de ces deux techniques d'analyse pour le suivi de la sécrétion exocytotique, leur combinaison pour suivre la sécrétion exocytotique a d'abord été réalisée par notre groupe en 2011. Ce couplage a permis un enregistrement simultané des signaux fluorescents et ampérométriques avec une bonne résolution spatiale et temporelle. L'inconvénient majeur de ce travail reste le chargement indépendant des sondes optique et électrochimique dans les vésicules de sécrétion, ce qui entraîne la détection d'évènements « orphelins » ampérométriques ou optiques ainsi que la faible efficacité de détection des évènements couplés. Par conséquent, dans cette thèse, nous avons tenté de mettre à profit une sonde unique à la fois fluorescente et électroactive pour suivre l'exocytose par la méthodologie couplée TIRFM/ampérométrie. Ainsi, un analogue de neurotransmetteurs monoamine primaire, la 4-(2-amino-éthyl)-6-chloro-7-hydroxy-2H-1-benzopyran-2-one (nommé **1** dans ce travail), a été synthétisé.

**1** présente une fluorescence forte, stable et pH-dépendante. Lorsque cette entité est excitée à 405 nm, son intensité de fluorescence est presque doublée de pH 5 (valeur intra-vésiculaire) à 7 (valeur milieu extracellulaire). De plus, des études en voltammétrie ont pu mettre en évidence que **1** est oxydable sur électrode de carbone vitreux, microélectrode à fibre de carbone et ITO (oxyde d'indium dopé à l'étain), montrant ainsi une bonne électroactivité. La pénétration cellulaire dans les vésicules de cellules BON N13 a également été démontrée, prouvant la spécificité de l'interaction entre **1** et ces vésicules équipées d'un transporteur de monoamines primaires (VMAT). L'utilisation de **1** comme sonde unique optique et électrochimique pour le suivi de l'exocytose a ensuite été validée séparément dans des cellules BON N13 par TIRFM et ampérométrie. L'enregistrement simultané par fluorescence et électrochimie en utilisant **1** comme sonde double a ensuite été réalisé dans un microdispositif constitué d'électrodes ITO conductrice et transparente. Nos résultats basés sur la sonde unique **1** montrent qu'elle semble plus adaptée que toutes les stratégies antérieures impliquant deux sondes indépendantes. Les résolutions spatiale et temporelle de cette méthode combinée ont permis d'analyser des sécrétions d'exocytose de cellules marquées par **1**. Une analyse ultérieure de ces signaux couplés optique et électrochimique sera à même d'étudier la corrélation entre le comportement du pore de fusion (dynamique d'ouverture/de fermeture, stabilité..) détecté par ampérométrie et le mouvement d'une vésicule en trois dimensions (ancrage, amarrage, fusion puis retrait dans le cytoplasme) détecté par TIRFM.